

**FUNCTIONAL ANALYSIS OF THE ATP-RELEASE
CHANNEL PANNEXIN1 IN MOUSE AND ZEBRAFISH
MODELS: IMPLICATIONS FOR HEALTH AND
DISEASE**

Paige Alexandra Whyte-Fagundes

A DISSERTATION SUBMITTED TO
THE FACULTY OF GRADUATE STUDIES
IN PARTIAL FULFILLMENT OF THE REQUIREMENTS FOR THE DEGREE OF

DOCTOR OF PHILOSOPHY

GRADUATE PROGRAM IN BIOLOGY

YORK UNIVERSITY
TORONTO, ONTARIO

August 2021

© Paige Alexandra Whyte-Fagundes, 2021

EXECUTIVE SUMMARY

Pannexin1 (Panx1) is a large membrane channel protein with complex gating mechanisms permeable to ions, glutamate, and ATP. Panx1 is ubiquitously expressed throughout the central nervous system, exposing the channel to dynamic molecular, structural, ionic, and electrical changes in neurons or glial cells. The release of signaling molecules from Panx1 channels has been linked to synaptic plasticity, learning and memory, and sensory system function. Evidence also supports purinergic signaling via Panx1 in pathophysiological conditions like epilepsy, ischemia, inflammation, and pain. Here, conflicts in the literature regarding (patho)physiological roles of Panx1 using an interdisciplinary approach are addressed. The motivation for each step, moving from *in vitro* cell models with overexpression of Panx1 to networks or whole system levels in Panx1^{-/-} mice and *Panx1*^{-/-} zebrafish, is to prove how Panx1 and ATP mediated signaling affects olfaction, visual processing, and seizures. A key finding dismisses the role of mouse Panx1 in olfaction but leads to the identification of a compensatory mechanism. The global loss of Panx1 (Panx1^{-/-}) in mice is compensated by the upregulation of Panx3. The roles of Panx1 in the processing of visual stimuli are investigated in the intact retinotectal pathway of the zebrafish. The loss of the zebrafish *panx1* ohnologs, *panx1a* and *panx1b*, leads to distinct responses to light stimuli. The results suggest that each pannexin type contributes differently to primary vision, most likely based on the localization of the channels in the retinotectal network and differences in channel properties. Finally, the conflict in the literature about pro- and anti-convulsant properties of Panx1 is addressed in the zebrafish. Prior investigations demonstrated pro-convulsant roles of Panx1 in the mouse. The principal outcome of the study in the zebrafish model demonstrates that *Panx1a* channels have pro-convulsant properties *in vivo* that *p2rx7* and ATP signaling mediate. However, *Panx1b* channels in the absence of *Panx1a* improves seizure outcomes. The discovery of dual roles of Panx1 channels in the zebrafish provides unique opportunities to study the molecular basis of seizures from genes to organisms and to use it as an anti-convulsant drug discovery model. In summary, the findings in this thesis are a multifaceted approach towards resolving fundamental neurobiological questions from the perspective of Panx1 in health and disease.

DEDICATION

In loving memory of my father Zeke,

*For my mother,
My sisters,
The Tufa family*

*&
For Uilki.*

You do not just wake up and become the butterfly
- *growth is a process, rupi kaur*

ACKNOWLEDGEMENTS

“What you do makes a difference, and you have to decide what kind of difference you want to make.”

- Jane Goodall

Paraphrasing the eloquent statement by Jane Goodall, the individuals that surround you have a great deal of impact. This has been especially evident to me throughout the journey of my Ph.D, and the work presented in this thesis could not have been made possible without a number of individuals around me to whom I extend my sincerest gratitude.

First and foremost, a special thank you is required for my supervisor Dr. Georg R. Zoidl. For always providing constant support, mentorship and guidance both in and out of the lab. I would not be where I am today without you. Under his leadership I have developed as an independent scientist, eager to keep pushing the envelope. For constantly believing in me and always reminding me to see the finish line like a true champion. Here's to a cheers with some ice cold German beers! Christiane Zoidl, your work alongside us in the lab is truly the pillar that supports our successes. Beyond the hard work mentioned in the contributions section, you keep everything organized and in tip-top shape the German way, which I hope I adapt moving forward in my professional life. But I am most thankful for your willingness to thrift some lab supplies and furniture to help with redecorating the electrophysiology room when needed. Thank you to both of the Zoidl's for making the lab environment extremely warm and welcoming.

Dr. Peter Carlen for welcoming me into your lab and providing me the tools and resources to learn electrophysiology and begin my epilepsy research. Your energy is infectious and I hope to continue to see research as exciting as you do after all these years.

My supervisory committee, past (Dr. Thilo Whomelsdorf) and present (Dr. Mark Bayfield and Dr. Steven Connor), for being supportive of my timelines, providing valuable discussions during progress meetings and challenging me to continuously try and poke holes into my own research.

Thank you to my colleagues, in particular 'Club Zoidl,' and my fellow senior PhDs that have trudged this journey with me. Your moral support was invaluable. A special mention to Daria for suffering through remote thesis writing with me and for always being eager to complete more experiments to answer all of my crazy questions for our project. To my lab twin Cherie, I cannot believe our PhDs are ending. Not getting to work by your side anymore is a tough reality but I am so grateful for our friendship and I appreciate you always being my cheerleader when I needed it.

To my close network of friends, my family and the Tufa family. Thank you all for always encouraging me throughout this process, for understanding when I said 'I can't I have too much work to do,' and providing help when I needed it along the way. To my dad, although your body has departed this earth, your spirit remains a constant motivator for me to keep striving for better.

My sincerest acknowledgement is owed to my partner Uilki Tufa for always coming through with the utmost support in and out of the lab when you knew I needed it most. I am unable to properly articulate in words the amount you have done for me throughout my PhD, despite having your own PhD deadlines and stresses, but know that I appreciate you more than anything. You have always challenged my ways of thinking, and taught me so much along the way. Beyond the academic support you have provided me, the love and understanding you have shown me during this time is more than I could have ever imagined. I am unsure of how I can repay your selflessness over all of these years, I am extremely fortunate and blessed to have you by my side.

STATEMENT OF CONTRIBUTIONS

Paige Whyte-Fagundes (author), prepared all aspects of this thesis. Versions or adaptations of chapters 1-5 have been published in peer reviewed journals or have been submitted for peer review:

Chapter 1: Whyte-Fagundes, P., & Zoidl, G. (2018). Mechanisms of pannxin1 channel gating and regulation. *Biochimica Et Biophysica Acta (BBA) - Biomembranes*. 1860(1), 65-71. Doi:10.1016/j.bbamem.2017.07.009

Chapter 1: Whyte-Fagundes, P., Siu, R., Brown, C., & Zoidl, G. (2019). Pannexins in vision, hearing, olfaction and taste. *Neuroscience Letters*. 1-8. Doi.org/10.1016/j.neulet.2017.05.010

Chapter 1: Aquilino, M*., Whyte-Fagundes, P*., Zoidl, G., & Carlen, P. (2019). Pannexin-1 channels in epilepsy. *Neuroscience Letters*. 1-5. Doi.org/10.1016/j.neulet.2017.09.004

* = equal contributions by authors

Chapter 3: Whyte-Fagundes, P., Kurtenbach, S., Zoidl, C., Shestopalov, V., Carlen, P & Zoidl, G. (2018). A potential compensatory role of Panx3 in the VNO of a Panx1 knock out mouse model. *Frontiers in Molecular Neuroscience*. 11(135). 1-16. Doi: 10.3389/fnmol.2018.00135

Chapter 4: Aquilino, M., Whyte-Fagundes, P., Lukewich, M., Zhang, L., Bardakjian, B., Zoidl, G., & Carlen, P. (2020). Pannexin-1 deficiency decreases epileptic activity in mice. *International Journal of Molecular Sciences*. 21(20):7510. Doi: 10.3390/ijms21207510.

Chapter 4: Safarian, N., Whyte-Fagundes, P., Zoidl, C., Grigull J., & Zoidl, G. (2020). Visuomotor deficiency of *panx1a* knockout zebrafish is linked to dopaminergic signalling. *Scientific Reports*. 9538(10). Doi.org/10.1038/s41598-020-66378-y

Chapter 5: Whyte-Fagundes, P., Taskina, D., Safarian, N., Zoidl, C., Carlen, P., Donaldson, L & Zoidl, G. (2021). Panx1 channels promote both anti- and pro- seizure-like activities in the zebrafish via p2rx7 receptors and ATP signaling. bioRxiv. doi:https://doi.org/10.1101/2021.06.03.446992

Several co-authors have contributed directly in performing experiments or collecting data, and/or assisting in interpretation and analysis:

Dr. Georg Zoidl (Thesis Supervisor) provided mentorship in planning experiments as well as manuscript preparation.

Christiane Zoidl provided support in the laboratory, including but not limited to; maintenance and seeding cell culture colonies required for chapter 3, maintenance and breeding of zebrafish for the project outlined in chapter 4 & 5, as well as assisting with ATP assay development and execution for Fig 5.7.

Dr. Stefan Kurtenbach assisted in developing the objective for chapter 3. He performed *in situ* hybridizations and qPCR for Fig 3.1, the intruder assay for Fig 3.6.

Dr. Peter Carlen was essential for starting my career in electrophysiology by providing me a training opportunity in his laboratory, which also began my investigations into epilepsy.

Mark Aquilino contributed to collecting *in vitro* whole-cell patch clamp electrophysiological recordings from brain slices and generated adapted versions of Figs 4.2-4.3 & 6.1. He also provided data analysis techniques for phase amplitude coupling.

Dr. Nickie Safarian generated the three panx1 zebrafish knockout models that were required to carry out investigations in chapters 4 & 5.

Daria Taskina performed and analyzed behavioural and RT-qPCR assays, under my counsel, that were necessary for the investigation of panx1 in seizures presented in chapter 5. She also contributed to generating components of Figs 5.4, 5.5, 5.7 & 5.8.

Dr. Logan Donaldson generated structural imaging and modelling for the zebrafish panx1 ohnologs presented in chapter 5, providing invaluable council regarding channel dynamics and functional properties. He was responsible for generating Fig 5.9 and providing components for Supplementary Fig. 5.7.

Uilki Tufa was pivotal aid and counsel for the development of themes presented in chapter 4 part III for this thesis and publications forming chapters 3 & 5. He provided assistance with coding theory and practice, debugging, as well as improving runtime efficiency.

All other experiments were performed by me, and I was responsible for writing each of the first author manuscripts, or providing written components to second author publications based upon my contributions. Figures were produced by me, unless otherwise credited.

Additional contributions that were made throughout my PhD that are not included in this dissertation include:

Whyte-Fagundes, P., Zoidl, C, Donaldson, L., & Zoidl, G. Decoding unique gating mechanisms by resolving the Panx1 pH sensor. Publication in process

Collaboration with Dr. Ifa (York University) evaluating the alterations to the phospholipid content of white and grey matter in a mouse model for fetal alcohol syndrome.

Collaboration with Dr. Peter Carlen and Dr. Christopher Barden (Krembil, Toronto Western Hospital, UHN), along with Dr. Georg Zoidl, a submission was made to MARS innovation and Evotec for the Lab150 partnership. Lab150 is designed to accelerate drug development by bringing together scientists, investors and company building expertise to rapidly deliver research concepts to the marketplace. Our proposal included repurposing the FDA approved drug Probenecid with the hopes of bringing it to clinical trials as a novel anti-epileptic drug.

TABLE OF CONTENTS

<i>EXECUTIVE SUMMARY</i>	<i>ii</i>
<i>DEDICATION</i>	<i>iii</i>
<i>ACKNOWLEDGEMENTS</i>	<i>iv</i>
<i>STATEMENT OF CONTRIBUTIONS</i>	<i>v</i>
<i>TABLE OF CONTENTS</i>	<i>vii</i>
<i>LIST OF FIGURES</i>	<i>xi</i>
<i>LIST OF TABLES</i>	<i>xiii</i>
<i>LIST OF SUPPLEMENTARY FIGURES</i>	<i>xiv</i>
<i>LIST OF SUPPLEMENTARY TABLES</i>	<i>xv</i>
<i>LIST OF ABBREVIATIONS</i>	<i>xvi</i>
Chapter 1. Introduction	1
1.1. Background.....	1
1.2. Pannexin Overview	1
1.2.1. Structure.....	3
1.2.2. Gating mechanisms.....	6
1.2.2.1. Brief description of mechanisms for Panx1 channel activation.....	7
1.2.2.2. Brief description of mechanisms for Panx1 channel inhibition.....	8
1.2.3. Expression.....	8
1.3. Purinergic receptors and signalling	9
1.4. Pannexin1 in health and disease	10
1.4.1. Olfaction	13
1.4.1.1. Physiological relevance of Panx1 in the olfactory system.....	15
1.4.2. Physiological relevance of Panx1 in the visual system	16
1.4.3. Epilepsy	17
1.4.3.1. Proposed involvement of Panx1 in epilepsy	18
1.5. Hypothesis and research objectives.....	20
1.5.1.1. Determine the involvement of Panx1 in accessory olfaction (Chapter 3)	20
1.5.1.2. Establish electrophysiological markers of epilepsy linked to Panx1 (Chapter 4)	21
1.5.1.3. Uncover functional roles of Panx1 in the retinotectal pathway (Chapter 4).....	22
1.5.1.4. Resolve conflicts regarding pro- or anti-convulsant actions of Panx1 (Chapter 5).....	23
Chapter 2. Experimental materials and methods	25
2.1. Part I: Materials and methods used to investigate the role of Panx1 in physiology: Olfaction.....	25
2.1.1. Panx1 ^{-/-} mouse generation.....	25
2.1.2. Quantitative real-time PCR (qRT-PCR).....	25
2.1.3. <i>In Situ</i> hybridization (ISH)	26
2.1.4. Immunohistochemistry (IHC).....	27
2.1.5. Acute <i>ex vivo</i> VNO preparation for ATP release assay	27
2.1.6. Behavioural test: Modified resident-intruder assay	28
2.1.7. Plasmid constructs	28
2.1.8. Cell culture and transient transfection	29
2.1.9. Western blot.....	29
2.1.10. Confocal imaging.....	29
2.1.11. Fluorescent dye uptake assay.....	29
2.1.12. <i>In vitro</i> luciferase assay for ATP determination.....	31
2.1.13. Blocker pharmacology and stimulants.....	32

2.1.14. Statistical analysis.....	32
2.2. Part II: Materials and methods used for technical development: a multi-part Panx1 series	32
2.2.1. <i>In vitro</i> field potentials under 4-AP	32
2.2.2. Whole-cell patch clamp and field recording.....	33
2.2.3. <i>In vitro</i> field potentials under 4-AP: Electrographic classifier	33
2.2.4. Analysis of Phase-Amplitude Cross-Frequency Coupling	34
2.2.5. Pharmacology	35
2.2.6. Electrophysiological and Statistical Analysis.....	35
2.3. Part III: Materials and Methods used to investigate the role of Panx1 in pathology: Epilepsy	35
2.3.1. Fish husbandry and embryo collection	35
2.3.2. TALEN design.....	36
2.3.3. TALEN constructs.....	38
2.3.4. TALEN microinjection and genotyping	38
2.3.5. Generation of <i>panx1</i> ^{-/-} zebrafish lines	38
2.3.6. <i>In vivo</i> electrophysiology.....	39
2.3.7. Seizure-like event detection and power spectral density	40
2.3.8. Behavioural locomotor assays	41
2.3.9. Stage II and III seizure-associated behaviour scoring	42
2.3.10. Survival assessment.....	43
2.3.11. Extracellular ATP assay	43
2.3.12. Protein quantification.....	45
2.3.13. RNA-seq Analysis	45
2.3.14. Transcriptome analysis	46
2.3.15. RNA extraction and RT-qPCR on immediate-early genes (IEGs).....	47
2.3.16. Molecular modelling.....	47
2.3.17. Pharmacology	47
2.3.18. Statistical analysis.....	48
2.4. Part IV: General materials and methods used	48
2.4.1. Biosafety	48
2.4.2. Organisms	48
2.4.2.1. Bacterial strains.....	49
2.4.2.2. Eukaryotic cells.....	49
2.4.2.3. Mice	49
2.4.2.4. Zebrafish	50
2.4.3. Antibodies.....	50
2.4.4. Commercial kits.....	51
2.4.5. Media and Solutions	51
2.4.6. Genes and Primers used.....	53
2.4.7. Software	57
2.5. References	57

Chapter 3. Loss of Panx1 does not affect primary and secondary olfaction.....61

A potential compensatory role of Panx3 in the VNO of a Panx1 knock out mouse model. 62

3.1. Abstract.....	63
3.2. Introduction	64
3.3. Results	65
3.3.1. Pannexin3 mRNA expression is upregulated in the vomeronasal organ of <i>panx1</i> ^{-/-} mice	65
3.3.2. Localization of pannexin proteins in the VNO of wild-type and <i>Panx1</i> ^{-/-} mice	67
3.3.3. ATP release in the VNO of wild-type and <i>Panx1</i> ^{-/-} mice	71
3.3.4. Aggression and defensive behaviour in wild-type and <i>Panx1</i> ^{-/-} mice.....	73
3.3.5. Expression properties of <i>panx1</i> and <i>panx3</i> in neuro2a cells are similar.....	74
3.3.6. Mouse <i>Panx1</i> and <i>panx3</i> release ATP <i>in vitro</i>	74
3.3.7. Dye uptake properties of <i>Panx1</i> and <i>Panx3</i> in neuro2a cells are similar.....	76
3.4. Discussion.....	79
3.4.1. Pannexins in the mouse VNO.....	79
3.4.2. What is the evidence that ATP release plays a critical role in VNO function?	80

3.4.3. Is Panx3 a channel that can compensate for Panx1?	81
3.4.4. Compensatory regulations of pannexins: Why and how?	83
3.5. Supplementary Data – Included in published manuscript	84
3.6. Supplementary Data – Not included in published manuscript	87
3.7. References	88
Chapter 4. Panx1 is implicated in seizure activity and visual processing	93
4.1. Part I: Electrophysiological markers of epilepsy associated with Pannexin1	94
4.1.1. Introduction	94
4.1.2. Results	95
4.1.2.1. Single cell recordings reveal that targeting Panx1 results in a hyperpolarized membrane potential	95
4.1.2.2. Recordings of LFPs from cortical slices exposed to 4-AP reveal anti-convulsant properties of Panx1	96
4.1.2.3. Cross-Frequency coupling <i>in vitro</i> is absent in Panx1 KOs	99
4.1.3. Conclusion	100
4.2. Part II: Pannexin1 investigations in seizure generation and visual processing using electrophysiology in zebrafish	101
4.2.1. Introduction to epilepsy in zebrafish larvae	101
4.2.1.1. Electrode placement impacts LFP recordings <i>in vivo</i>	106
4.2.2. The role of <i>Panx1</i> in visually processing light stimuli	108
4.2.3. Results	109
4.2.3.1. Recordings of LFPs reveal <i>Panx1</i> dependent alterations in visual system processing	109
4.2.3.2. Loss of <i>Panx1a</i> modifies transitions in brain wave frequencies in response to light	111
4.2.4. Conclusion	113
4.3. Part III: Utilizing automated data analysis tools to address gaps in Panx1 research	114
4.3.1. Automated cell detection for dye uptake analysis Data	114
4.3.2. Spectral EEG analysis	116
4.3.3. Automated seizure-like event detection	118
4.4. References	122
Chapter 5. Loss of <i>Panx1</i> in zebrafish reveal novel seizure outcomes.....	134
<i>Panx1</i> channels promote both anti- and pro-seizure-like activities in the zebrafish via p2rx7 receptors and ATP signaling	135
5.1. Abstract	136
5.2. Introduction	137
5.3. Results	138
5.3.1. Panx1 genotypes determine evoked seizure-like events	138
5.3.2. Loss of Panx1 caused local network differences in the optic tectum of PTZ treated larvae	141
5.3.3. DKO and <i>panx1a</i> ^{-/-} larvae have reduced interictal-like activity in the optic tectum	142
5.3.4. Targeting Panx1 improves PTZ-induced seizure locomotion and molecular responses	143
5.3.5. Acute pharmacological blocking of <i>Panx1</i> suppresses seizure-like activities	147
5.3.6. Seizure phenotypes are linked to transcriptome changes	150
5.3.7. Evidence for an ATP-dependent mechanism contributing to seizure-like activity	153
5.3.8. P2rx7 affects seizure-like activities but does not supersede <i>Panx1a</i>	155
5.3.9. Molecular modeling of fish and human pannexins	156
5.4. Discussion	160
5.5. Supplementary Data – Included in published manuscript	163
5.6. Supplementary Data – Not included in published manuscript	178
5.7. References	180
Chapter 6. Discussion.....	184
CONCLUSION	187
SIGNIFICANCE AND FUTURE DIRECTIONS	188

<i>BIBLIOGRAPHY</i>	190
<i>APPENDICES</i>	197
Table 6: Multialignment sequencing showing residues of conservation for the entire Panx1 sequence.	199
<i>PUBLICATIONS, PRESENTATIONS & CONFERENCES</i>	202

LIST OF FIGURES

Figure 1.1. Transmembrane topology of pannexin family members	2
Figure 1.2. Pannexin1 heptameric structure	5
Figure 1.3. Schematic of the complex gating dynamics involved in the inhibition and activation of the pannexin1 channel.....	6
Figure 1.4. Purinergic signaling.....	10
Figure 1.5. Panx1 in rodent sensory systems.....	12
Figure 1.6. Mammalian olfactory system schematic.....	14
Figure 1.7. Cross section of the eye with an enlarged schematic of the retina.....	17
Figure 1.8. Schematic of speculated mechanisms involving Panx1 in epilepsy including initiation and termination of seizure activity.....	19
Figure 2.1. Summary of protocol for dye uptake assays.....	30
Figure 2.2. Linear correlation analysis of fluorescent reporter expression and uptake of ethidium bromide	31
Figure 2.3. Depiction of methodology for ATP detecting luciferase assays	32
Figure 2.4. TALEN design	37
Figure 2.5. In vitro electrophysiology schematic.....	40
Figure 2.6. Concentration dependent reduction of PTZ-related hyperactivity in TL larvae by Probenecid.....	42
Figure 2.7. Workflow for behavioral locomotor assessments in zebrafish larvae	42
Figure 2.8. Method workflow for molecular assessments in zebrafish larvae	44
Figure 2.9. Linear correlation of larval weight and protein concentration.....	45
Figure 3.1. Pannexin mRNA expression in the mouse VNO	66
Figure 3.2. Panx1 protein expression in the NSE of the juvenile mouse VNO	67
Figure 3.3. Localization of mPanx2 and mPanx3 proteins showing upregulation of mPanx3 in the NSE of juvenile Panx1 ^{-/-} mice.....	68
Figure 3.4. Panx1 and Panx3 localization in the VNO of adult mice	70
Figure 3.5. Quantification of extracellular ATP after mechanical stimulation of the VNO.....	72
Figure 3.6. Behavioural comparison of Panx1 ^{+/+} and Panx1 ^{-/-} mice	73
Figure 3.7. Panx1 and Panx3 localization in Neuro2A cells	74
Figure 3.8. Panx3 has ATP releasing properties like Panx1	76
Figure 3.9. Panx1 and Panx3 dye uptake properties.....	78
Figure 4.1. The resting membrane potential of Panx1 ^{-/-} cells is hyperpolarized	96

<i>Figure 4.2. Seizure-like events in vitro in WT, KO, BB (Brilliant Blue-FCF-treated) and Pb (probenecid-treated) groups</i>	98
<i>Figure 4.3. Frequency-based analysis of the extracellular recordings of WT and Panx1 KO mice</i>	100
<i>Figure 4.4. Images of electrode placement and corresponding sample recordings from 7dpf zebrafish larvae</i>	107
<i>Figure 4.5. Panx1b does not modulate local field potentials in the optic tectum upon light stimulation</i>	110
<i>Figure 4.6. Panx1a modulates local field potentials in the optic tectum upon light stimulation</i>	112
<i>Figure 4.7. Panx1 and Panx3 dye uptake properties</i>	116
<i>Figure 4.8. Spectral EEG analysis</i>	118
<i>Figure 4.9. Automated seizure detection overview</i>	121
<i>Figure 5.1. Panx1 knock out larvae showed distinct seizure-like activities in vivo</i>	140
<i>Figure 5.2. Spectral Analysis of LFPs revealed differences in larvae</i>	142
<i>Figure 5.3. Interictal-like activity was decreased in the optic tectum of DKO and panx1a^{-/-} larvae</i>	143
<i>Figure 5.4. Behavioural and molecular outcomes of genetically targeting panx1</i>	146
<i>Figure 5.5. Acute blocking of Panx1 with Pb is effective for preventing seizure-like activity</i>	149
<i>Figure 5.6. Loss of Panx1a affects biological processes related to metabolism and transport</i>	152
<i>Figure 5.7. Extracellular ATP is associated with propensity for seizure-like activity</i>	154
<i>Figure 5.8. Blocking of p2rx7 with A-438079 improves seizure-like behavior</i>	156
<i>Figure 5.9. Sequence and structural attributes of the zebrafish pannexins</i>	159
<i>Figure 6.1. Median phase-amplitude cross frequency coupling comodulograms for the in vitro 4-AP slice model following z-score normalization to baseline conditions</i>	198

LIST OF TABLES

<i>Table 2.1. Summary of primers for RT-qPCR used in VNO publication.....</i>	<i>26</i>
<i>Table 2.2. Program tools used for thesis and publication completion.</i>	<i>57</i>
<i>Table 4.1. Incidence of seizure-like events (SLEs) in vitro following perfusion of cortical slices with 100μM 4-AP. 12 slices from 7 KO mice had fewer 4-AP-induced SLEs than in the 9 slices from 6 of their WT counterparts ($p = 0.0051$, Chi-squared). Mice treated with Brilliant Blue-FCF (7 mice, 10 slices) or probenecid (8 mice, 13 slices) before 4-AP exposure also had fewer instances of at least one SLE as compared to untreated slices of WT mice (BB $p = 0.0028$; PB $p = 0.0008$, Chi-squared).....</i>	<i>98</i>
<i>Table 4.2. Summary of experimental seizure models and main conclusions from the Panx1 literature.</i>	<i>102</i>
<i>Table 5.1. Proposed gates for panx1 structure.</i>	<i>160</i>

LIST OF SUPPLEMENTARY FIGURES

<i>Supplementary Figure 3.1. Secondary antibody control for Immunohistochemistry (IHC)</i>	<i>84</i>
<i>Supplementary Figure 3.2. Quantitative PCR analysis of total RNA isolated from Neuro2a cells</i>	<i>85</i>
<i>Supplementary Figure 3.3. Expression of pannexin mRNAs in transiently transfected Neuro2a cells</i>	<i>85</i>
<i>Supplementary Figure 3.4. Linear correlation analysis of fluorescent reporter expression and uptake of ethidium bromide</i>	<i>86</i>
<i>Supplementary Figure 3.5. Panx1 and Panx3 expression in the mouse olfactory system of WT mice.....</i>	<i>87</i>
<i>Supplementary Figure 5.1. Comparison of PTZ treatment to baseline activity is indistinguishable</i>	<i>163</i>
<i>Supplementary Figure 5.2. Comparison of TL with and without Pb treatment only</i>	<i>163</i>
<i>Supplementary Figure 5.3. Venn diagrams of differentially regulated genes and biological processes.....</i>	<i>164</i>
<i>Supplementary Figure 5.4. Concentration dependent reduction of PTZ-related hyperactivity in TL larvae by probenecid</i>	<i>165</i>
<i>Supplementary Figure 5.5. Linear correlation of larval weight and protein content</i>	<i>165</i>
<i>Supplementary Figure 5.6. Comparison of TL and DKO seizure-like event detection and spectral analysis</i>	<i>178</i>
<i>Supplementary Figure 5.7. Structural models of W74 substitutions.....</i>	<i>179</i>

LIST OF SUPPLEMENTARY TABLES

<i>Supplementary Table 2.1. Description of the primary (top) and secondary (bottom) antibodies used for completion of western blot and IHC for Panx1 localization experimentation in the olfactory system.</i>	50
<i>Supplementary Table 2.2. List of kits utilized for various laboratory applications.</i>	51
<i>Supplementary Table 2.3. Solutions used for cell culture.</i>	51
<i>Supplementary Table 2.4. Composition of solutions used for biological protocols.</i>	52
<i>Supplementary Table 2.5. Summary of genes and primers.</i>	53
<i>Supplementary Table 5.1. RT-qPCR values for Immediate early genes regulation in TL and panx1 knockout larvae treated with PTZ for one hour (Figure 5.4f). Expression values, respective to non-treated controls are >1 for upregulated IEGs and <1 for downregulated IEGs. P-values in bold = $p < 0.05$.</i>	166
<i>Supplementary Table 5.2. RT-qPCR values for Immediate early genes regulation in TL larvae treated with PTZ for one hour (+PTZ) or treated with Pb 30min prior to the PTZ treatment (Pb+PTZ; Figure 5.5i). Expression values, respective to non-treated controls are >1 for upregulated IEGs and <1 for downregulated IEGs. P-values in bold = $p < 0.05$.</i>	166
<i>Supplementary Table 5.3. Gene ontology enriched biological processes from FishEnrichR.</i>	167
<i>Supplementary Table 5.4. Clustergram genes according to each category and associated regulation values.</i>	173
<i>Supplementary Table 5.5. RT-qPCR values for gene regulation in PTZ treated (one hour) TL, DKO and Pb treated TL larvae compared to their respective controls (Figure 5.7c). Expression values are >1 for upregulated genes and <1 for downregulated genes. P-values in bold = $P < 0.05$.</i>	176
<i>Supplementary Table 5.6. Primers for RT-qPCR.</i>	177

LIST OF ABBREVIATIONS

Symbol	Definition
4-AP	4-Aminopyridine
ATP	adenosine-5'-triphosphate
CL	Cytoplasmic loop
CNS	Central nervous system
Cx	Connexin
EGFP	Enhanced green fluorescent protein
EL	Extracellular loop
EtBr	Ethidium bromide
GABA	Gama amino butyric acid
HC	Horizontal cell
IHC	Immunohistochemistry
ILED	Interictal-like epileptiform discharge
INL	Inner nuclear layer
K ⁺	Potassium ion
KO, -/-	Knockout
LFP	Local field potential
mM	Millimolar
mV	Millivolt
N2a	Neuroblastoma 2a or Neuro2a
OPL	Outer plexiform layer
P2XR	P2X receptor
P2YR	P2Y receptor
PBS	Phosphate buffered saline
PCR	Polymerase chain reaction
PTZ	Pentylentetrazol
ROI	Region of interest
s	Second
SEM	Standard error of the mean
SLE	Seizure-like event
TALEN	Transcription activator-like effector technology
TL	Topfel longfin
WT	Wild-type
μL	Microlitre
μM	Micromolar
μm	Micrometer
VNO	Vomer nasal organ

Extended Abbreviations for species-specific-Pannexin-1 annotation

Abbreviation	Species	Type
PANX1	<i>Homo sapiens</i> (Human)	Gene
PANX1	<i>Homo sapiens</i> (Human)	Protein
Panx1	<i>Mus musculus</i> (Mouse)	Gene
Panx1	<i>Mus musculus</i> (Mouse)	Protein
<i>panx1a</i>	<i>Danio rerio</i> (Zebrafish)	Gene
<i>Panx1a</i>	<i>Danio rerio</i> (Zebrafish)	Protein
<i>panx1b</i>	<i>Danio rerio</i> (Zebrafish)	Gene
<i>Panx1b</i>	<i>Danio rerio</i> (Zebrafish)	Protein
Panxs or Panx1	General	Gene or Protein

Chapter 1. Introduction

“Science makes people reach selflessly for truth and objectivity; it teaches people to accept reality, with wonder and admiration, not to mention the deep awe and joy that the natural order of things brings to the true scientist.”

- Lise Meitner

1.1. Background

Pannexins (Panx), in particular Panx1, play a key role in intercellular communications as they are capable of forming functional plasma membrane channels that are highly permeable to adenosine 5'-triphosphate (ATP) and other important signaling molecules. It is this property, coupled with their vast expression profile, that implicates the protein in a wide range of physiologically and medically significant processes that have yet to be fully elucidated. The work done in this thesis has uncovered a novel safeguarding relationship between Panx1 and Panx3 and provides greater insight into distinct properties of the two zebrafish *panx1* ohnologs in vision and epilepsy that can provide guided investigations in higher vertebrates.

This literature review is designed to highlight the most recent updates to the Panx field and provide a brief overview of topics covered in this thesis, as each chapter includes relevant and sufficient background information required to interpret results. Therefore, readers are encouraged to quench any further curiosities related to mechanisms of Panx1 channel gating and regulation, roles in sensory systems, or the in-depth analysis of Panx1 involvement in epilepsy by referring to these primary authored publications:

Whyte-Fagundes, P., & Zoidl, G. (2018). Mechanisms of pannxin1 channel gating and regulation. *Biochimica Et Biophysica Acta (BBA) - Biomembranes*. 1860(1), 65-71. Doi:10.1016/j.bbamem.2017.07.009

Whyte-Fagundes, P., Siu, R., Brown, C., & Zoidl, G. (2019). Pannexins in vision, hearing, olfaction and taste. *Neuroscience Letters*. 1-8. Doi.org/10.1016/j.neulet.2017.05.010

Aquilino, M*, **Whyte-Fagundes, P***, Zoidl, G., & Carlen, P. (2019). Pannexin-1 channels in epilepsy. *Neuroscience Letters*. 1-5. Doi.org/10.1016/j.neulet.2017.09.004

* = equal contributions by authors

1.2. Pannexin Overview

The pannexin (Panx) genes (Panx, Greek: *pan* = complete, everywhere and *nexus* = junction) were initially described as a second family of gap junction proteins in vertebrates, sharing a predicted

topology similar to connexins (Cxs) (Panchin et al., 2000). However, due to variances in sequence homology and unique glycosylation of the Panx proteins, they soon became known as an independent family of channel-forming integral membrane proteins with three members (Panx1, 2, 3) (Baranova et al., 2004; Bruzzone et al., 2003). They each share a similar topology, with four transmembrane regions, an amino (NT) and carboxy terminus (CT) and two extracellular loops that each contain unique glycosylation sites (**Figure 1.1**). Panx1 and Panx3 share the most structural homology, and Panx2 has the largest CT domain of the protein family. While channel functions of Panx2 and Panx3 have not been unambiguously demonstrated (Whyte-Fagundes et al., 2019), Panx1 functions primarily as a large-conductance channel regulated by post-translational modifications, channel intermixing, sub-cellular localization and tissue distribution, with both physiological and pathophysiological roles in health and disease (Boassa et al., 2008; Penuela et al., 2007; Sosinsky et al., 2011).

Panax1 is the best-characterized family member as it is ubiquitously expressed and is widely accepted as a leading adenosine 5'-triphosphate (ATP) release channel (Dahl, 2015). In contrast, Panx2 expression in humans is presumably brain specific and it is more difficult to study due to its localized intracellular expression (Baranova et al., 2004). However, the channel has been demonstrated to play a role in maintaining rates of neuronal differentiation (Swayne et al., 2010). On the other hand, Panx3 is found primarily in cartilage, bone and skin where it has been shown to switch properties of chondrocytes from proliferation to differentiation (Penuela et al., 2007).

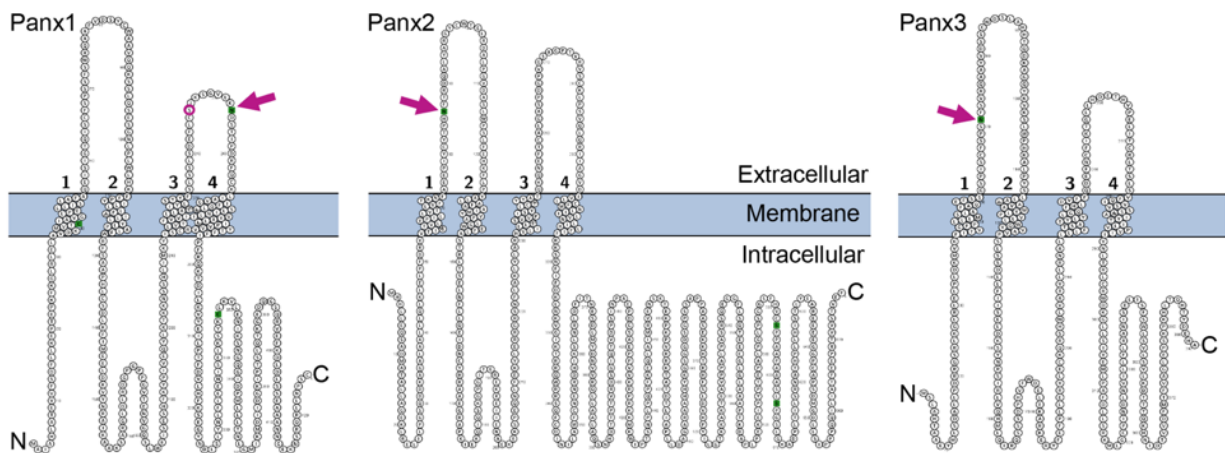


Figure 1.1. Transmembrane topology of pannexin family members. Panx1 (426), Panx2 (677), and Panx3 (392) of varying amino acid lengths are tetra-spanning integral membrane proteins with N-glycosylation sites highlighted in green with a pink arrow at amino acids 254 (Panx1), 86 (Panx2), and 71 (Panx3). The pink circle on Panx1 highlights the glycosylation site (246) for zebrafish ohnologs panx1a (417 amino acids long) and panx1b (354 amino acids long). Panx1 and Panx3 share the most sequence homology and Panx2 is the largest member. Numbers indicate the position of transmembrane domains. Panx1 proteins oligomerize to form single-

membrane channels, connecting the cytoplasm to the extracellular milieu. The predicted sequence features of three Panx proteins were visualized using the Protter open-source tool.

1.2.1. Structure

Since the initial discovery of the pannexins, the oligomeric state of Panx1 was assumed to be hexameric like the connexins (Dahl, 2015; Penuela et al., 2013). Up until recently, no structural resolution of the channel existed to contest this idea. However, six research groups have now independently published similar cryo-EM structures of the Panx1 membrane channel (Deng et al., 2020; Michalski et al., 2020; Mou et al., 2020; Qu et al., 2020; Ruan et al., 2020), opening the field up to many more research opportunities.

The novel finding shared amongst all of the Panx1 structures is that it is formed by a homomeric heptamer that is arranged around a central symmetry axis constituting the permeation pathway (**Figure 1.2a-e**). The channel is $\sim 110\text{\AA}$ long and $\sim 100\text{\AA}$ wide with a flat extracellular domain protruding $\sim 35\text{\AA}$ above the cell membrane and the intracellular domain extending $\sim 35\text{\AA}$ into the cytoplasm. The seven extracellular domains organize to form the most constricted site of the pore $\sim 9\text{\AA}$. As originally determined, the amino (N) and carboxy (C) termini reside on the cytoplasmic side of the channel and each protomer contains four transmembrane domains. Both the extra- and intra-cellular pore entrances are lined with positively charged amino acids, making them favorable for negatively charged cargos such as Cl^- and ATP to enter and leave the pore (Mim et al., 2021). Key residues that have been identified in Panx1 gating are W74 (tryptophan), R75 (arginine) and D81 (aspartic acid). The seven W74 residues form a ring to line the wall of the outer pore, meanwhile each neighbouring R75 forms a cation- π interaction with each W74 and a salt bridge with D81 to provide rigidity to the extracellular entrance (Deng et al., 2020). The W74 residues define the extracellular restriction site and the R75 residues contribute to the positively charged ring (Mou et al., 2020). Prior to the resolution of the structure, electrophysiological experiments identified W74 as a major determinant in the inhibition of the Panx1 blocker carbenoxolone (CBX) (Michalski & Kawate, 2016), and R75 was shown to be critical in inhibition upon high concentrations of extracellular ATP and its analogues (Qiu & Dahl, 2009). Together, these three residues are proposed to govern channel selectivity and permeability based on molecule size and charge.

An interesting observation only resolved by the Ruan et al., 2020 structure, uncovered seven narrow side tunnels in the upper intracellular domain that run perpendicular to the pore like a T-intersection. This network is proposed to allow passage of small anions like Cl^- because each tunnel contains several positively charged and polar residues along its length. These tunnels have been ruled out as ATP passages due to constriction sites that do not permit the size of ATP, and passage of ATP is proposed to only occur via the main pore. Now that the protein structure has been resolved, and the six reported structures appear extremely consistent with each other, they provide a solid foundation and offer a new perspective for understanding molecular mechanisms underlying channel gating.

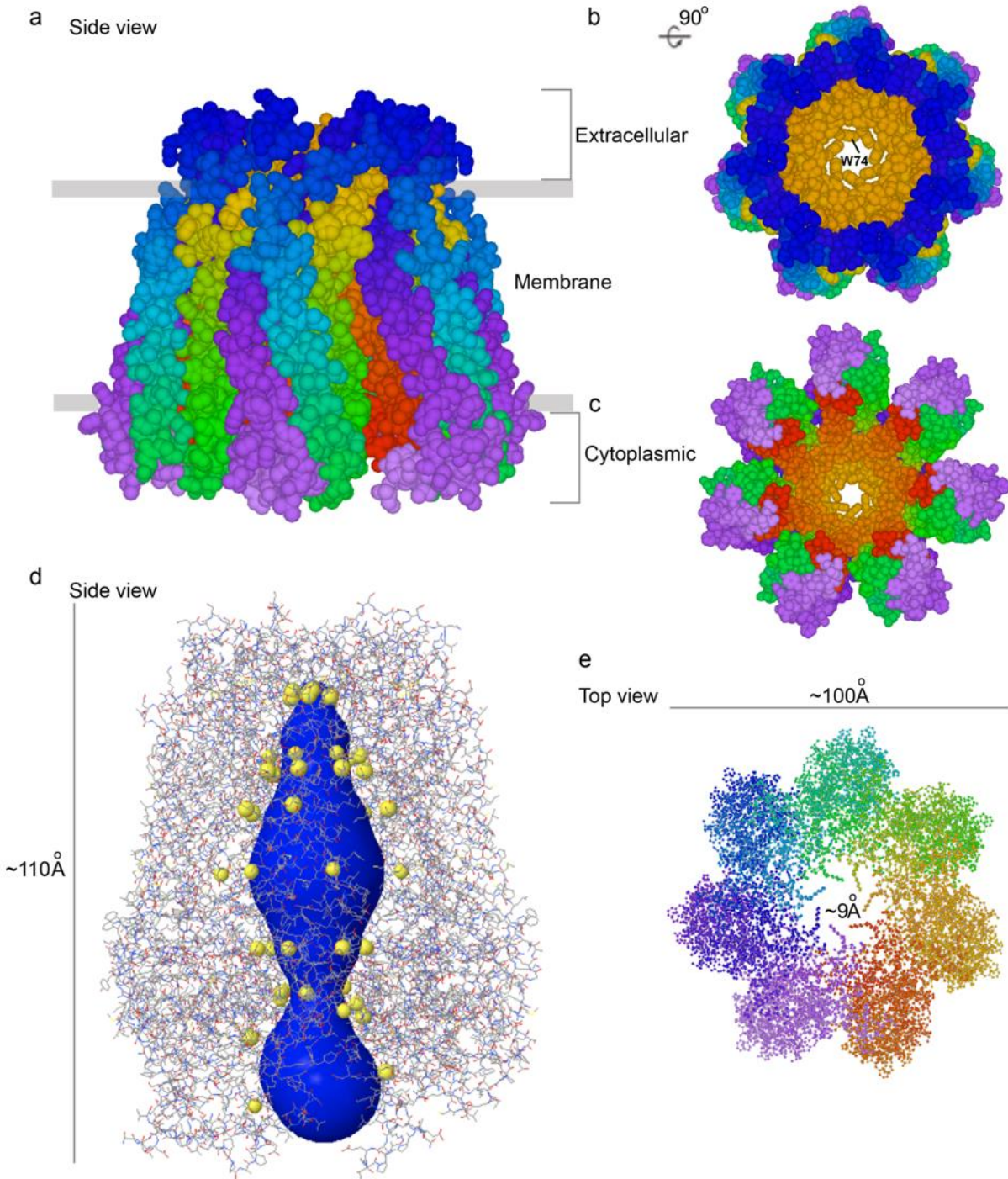


Figure 1.2. Pannexin1 heptameric structure. a) Side view of Panx1 colored based on chains showing portion of the protein that is extracellular, in the membrane, and intracellular or cytoplasmic. Structure is represented in a vanderwall ball spherical form. b) Top view is a rotation of 90 degrees to show the channel from the extracellular side revealing the W74 constriction site. c) Bottom view from the cytoplasmic side showing it has a much larger opening. d) Another side view of the channel represented in ball and stick form with the pore highlighted in order to visualize constriction sites. Pore is lined with hydrophobic amino acids highlighted in yellow. Panx1 is ~110Å long. e) Another top view in ball and stick form to show the heptameric configuration of the ~100Å wide channel and showing the ~9Å constriction site at the extracellular surface. Structure modelled using MOLEonline with the protein databank entry 6v6d for human PANX1.

1.2.2. Gating mechanisms

The study of Panx1 channels remains controversial, however, protocols for both activation and inhibition of channel gating have reached some agreement. Regulatory mechanisms that involve elevated extracellular K^+ , increased intracellular Ca^{2+} , ATP, stretch and mechanical stimulation, voltage, redox regulation, s-nitrosylation, nitric oxide (NO), NMDA stimulation, chemokines, changes in extracellular pH, as well as interactions with purinergic and adenosine receptors or caspases, have been shown to play a role in the process and are summarized in **Figure 1.3** (Bao et al., 2004; Locovei et al., 2006).

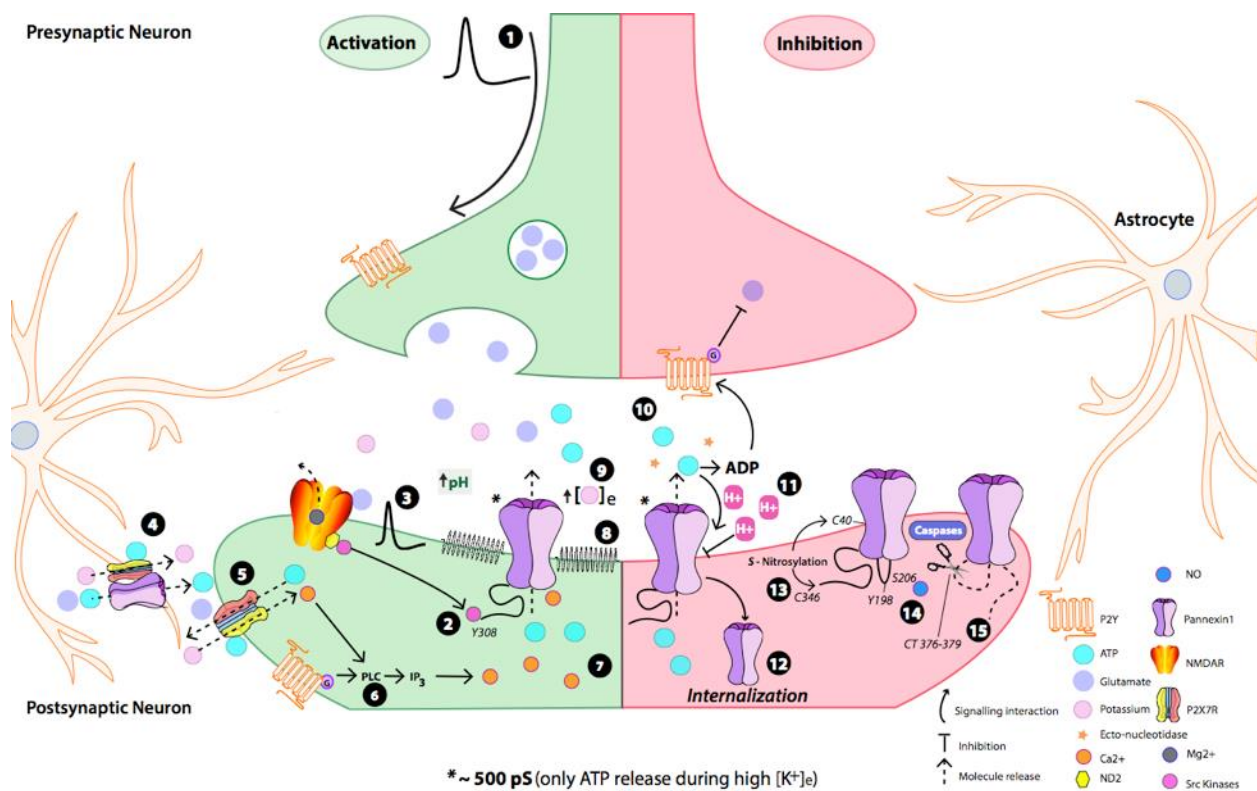


Figure 1.3. Schematic of the complex gating dynamics involved in the inhibition and activation of the pannexin1 channel. Numbers 1–15 refer to modes of Panx1 channel activities. Modes of Panx1 activation are indicated in the green portion of the figure. (1) Presynaptic depolarization leads to vesicular glutamate release, activation of NMDARs and interactions with Src Family Kinases. (2) Src kinases phosphorylate Panx1 at residue Y308 on the CT-tail. (3) Voltage activation of Panx1. (4) Glutamate, Ca^{2+} and ATP released from P2X7 receptors on astrocytes can activate Panx1; P2X7 and Panx1 coupling has been suggested. (5) P2X7-mediated Panx1 activation is identified, intracellular activation is likely via Ca^{2+} . However, exact mechanisms remain to be elucidated and an interaction complex remains to be resolved. (6) ATP activates metabotropic P2Y receptors and ionotropic P2X receptors to evoke a calcium wave or ATP release respectively. Micromolar concentrations of ATP activate Panx1. (7) Extracellular ATP increases and binds to purinergic receptors, increasing inositol 1,4,5-triphosphate (IP_3) and intracellular Ca^{2+} release, opening Panx1 channels. (8) Panx1 is sensitive to mechanical stimulation and stretch. (9) Extracellular K^+ accumulation at concentrations near 100 mM, and experimental modes of K^+ stimulation, can activate Panx1. Modes of Panx1 inhibition are highlighted within

the red portion of the figure. (10) Millimolar concentrations of ATP inhibit Panx1 channels. (11) Metabolic ATP break down to ADP inhibits presynaptic glutamate release and generates protons to decrease pH and inhibit Panx1. Conversely, increased pH levels can activate the channel. (12) Prolonged release and high levels of ATP can stimulate Panx1 internalization to endosomal compartments preventing further excitatory ATP release. (13) S-nitrosylation at C40 and C346 can inhibit Panx1. (14) Phosphorylation of Ser-206 can inhibit Panx1 channel function in the context of NO rich tissues. (15) The CT-tail of Panx1 has been implicated in both the activation and inhibition of Panx1. A 'ball-and-chain' model has been proposed to inhibit Panx1 opening, however, caspase mediated cleavage at residues 376–379 causes sustained, powerful opening of Panx1. In addition, increased number of cleaved CT-tails can lead to increased Panx1 conductance. Figure from Whyte-Fagundes et al., 2018 created by PW-F.

1.2.2.1. Brief description of mechanisms for Panx1 channel activation.

Biophysical properties of Panx1 channels of human, rodent or fish origin demonstrate large-conductance channels with unitary conductance in the range of 300-500pS (Bao et al., 2004; Locovei et al., 2006; Qiu & Dahl, 2009; Wang et al., 2007). Evidence exists regarding channel conformations depending upon modes of stimulation. As such, Potassium ions (K^+) and caspase cleavage of the CT-tail have been shown to promote a high conductance channel (~500pS) permeable to ATP, whereas much lower conductance conformations (~50pS) are present during voltage activation and are impermeable to ATP (Chiu et al., 2017; Wang et al., 2014). Interestingly, although Panx1 is known for the ability to release ATP, the channels activity is also subject to activation by its permeant in micromolar concentrations (Locovei et al., 2006). Further, Panx1 channels show sensitivity to mechanical stimulation in a variety of cell types including neurons and retinal ganglion cells (Xia et al., 2012), which is also thought to promote larger conductance conformations (Wang et al., 2014). This activation property has been proposed as a mode for Panx1 channel participation in a variety of signalling processes in cardiomyocytes and cardiac fibroblasts (Kamkin et al., 2005), as well as in afferent and efferent neurons for pain perception (McBride et al., 2000) to name a few.

Intracellular modes of Panx1 activation can occur via release of calcium (Ca^{2+}) from the endoplasmic reticulum (ER), as a result of increased inositol 1,4,5-triphosphate (IP_3), although a Ca^{2+} binding site has yet to be uncovered. This intracellular increase in Ca^{2+} has also been shown to occur via activated P2X7 receptors (Gulbransen et al., 2012; Kim & Kang, 2011). As previously mentioned, caspases, primarily caspase 3, 7 and 11, have been known to irreversibly activate the channel by binding to amino acids around positions 375-380 located along the CT, which occurs typically during apoptosis (Sandilos et al., 2012). In addition, tyrosine phosphorylation at position

308 has also been linked to channel activation of via NMDA receptor and Src Family Kinase signalling.

1.2.2.2. **Brief description of mechanisms for Panx1 channel inhibition.**

For the Panx1 protein it is not uncommon for activating gating mechanisms to have an opposing role in channel inhibition. For example, once extracellular ATP ends up reaching millimolar concentrations, it can inhibit Panx1 (Qiu & Dahl, 2009). ATP can also degrade into adenosine and release protons, causing local acidification which has also been shown to close Panx1 channels (Kurtenbach et al., 2013). Further, the CT-tail has been proposed to block and inhibit Panx1 via a ‘ball-and-chain’ type mechanism, similar to what occurs in voltage-gated channels (Lee, 1992) and connexins (Anumonwo et al., 2001; Moreno et al., 2002). This mechanism likely occurs via cysteine-mediated cross-linking of the CT-tail between positions 379 to 391 preventing cleavage from occurring and maintaining a basal inhibitory state of the channel (Dourado et al., 2014). Posttranslational modifications are another example of mechanistic properties with dual roles in Panx1 gating, as nitric oxide (NO) regulated S-nitrosylation of cysteines at intracellular positions 40 and 346 have been shown to inhibit Panx1 channels in NO-rich tissues of the nervous system and vasculature (Lohman et al., 2012). NO can also regulate phosphorylation through a PKG dependent pathway of serine at position 206 to mediate inhibition.

Pharmacological interventions of Panx1 function have shown experimental success for channel blocking using; CBX, probenecid (Pb), flufenamic acid, trovoflaxin, spironolactone, brilliant blue food dye, as well as mimetic peptides. Working concentrations of these drugs are model specific and reported concentrations vary, as such, they will not be disclosed here.

1.2.3. **Expression**

Panx1 is almost ubiquitously expressed, found in many organs and in several cell types. Using various methods to detect transcripts and proteins including *in situ* hybridization, northern blotting, qPCR, western blots and immunohistochemistry (IHC), Panx1 has been detected throughout the nervous system across all sensory systems, heart, lung, liver, spleen, male and female reproductive tissues, skeletal muscles and skin (Bruzzone et al., 2003; Penuela et al., 2013). Closer investigations of the CNS revealed expression in both neurons and glia in the cortex, hippocampus, pyramidal cells, amygdala, substantia nigra, thalamus, cerebellum, and spinal cord (Boassa et al., 2007; Dvorianchikova et al., 2006).

In the zebrafish, *Panx1a* and *Panx1b* expression profiles are distinct. *Panx1a* follows the ubiquitous expression patterns characteristic of mammalian Panx1 (Bond et al., 2012; N. Prochnow et al., 2009; Georg Zoidl et al., 2008). Meanwhile, *Panx1b* is primarily detected in the brain and eyes with relatively low expression in the heart, kidneys, spleen, skin and muscles (Bond et al., 2012). Within the major divisions of the adult brain (retina, optic tectum, tegmentum, brain stem, cerebellum, spinal cord, olfactory bulb), both *panx1* transcripts were detected throughout. However, robust expression of *panx1b* transcripts were found in the cerebellum, optic tectum and spinal cord, whereas *panx1a* was relatively lower and less variable in the analyzed tissues (Sarah Kurtenbach et al., 2013).

1.3. Purinergic receptors and signalling

Purinergic signaling refers to the extracellular communication between cells mediated via purine nucleotides and nucleosides, such as ATP and adenosine. ATP serves as a signal for diverse physiological functions; including spreading of Ca²⁺ waves, and propagating ATP release, both of which occur through the activation of purinergic receptors on the initial and neighbouring cells (Burnstock, 2006). The purinergic system is made up of complex machinery involving regulatory proteins for purine release and uptake, like Panx1, as well as purinergic receptors and metabolizing enzymes to remove purines from the extracellular space and contribute to signaling cascades (Burnstock, 2020). Purinergic receptors are divided into two classes based on agonist selectivity, P1 adenosine receptors (A1, A2A, A2B and A3) and P2 nucleotide or ATP receptors. The P2 receptors further divide into subclasses that have specific physiological functions. Of particular importance to Panx1 channel dynamics are the metabotropic G protein-coupled P2Y receptors and the ionotropic ATP-gated P2X7 receptors (Burnstock, 2018) (**Figure 1.4**).

The particularly high expression of different components of the purinergic system within the CNS highlights its importance in (ab)normal brain functions. As such, purinergic signaling is involved in pathways where nucleotides like ATP act as neuro- and glio-transmitters or modulators and can mediate communication between astrocytes and neurons (Coppi et al., 2013; Cotrina et al., 1998). Plenty of research demonstrates the involvement of purinergic signaling in neurotransmission and neuromodulation during physiological behaviours like cognition and sensory system processing (Burnstock, 2006), as well as during CNS disorders like inflammation, stroke or epilepsy (Engel et al., 2016; Miras-Portugal et al., 2017).

The features of the purinergic system that places ATP release via Panx1 alongside ATP activated P2X7 receptors make them interesting candidates to investigate together in the CNS. As such, it is not surprising that some reports of a functional Panx1-P2XR7 complex exists (Iglesias et al., 2008; Kim & Kang, 2011; Locovei et al., 2007; Pelegrin & Surprenant, 2006). However, much controversy remains surrounding this idea (Alberto et al., 2013) and more research continues to investigate the contexts in which coordinated signalling amongst the two proteins occur.

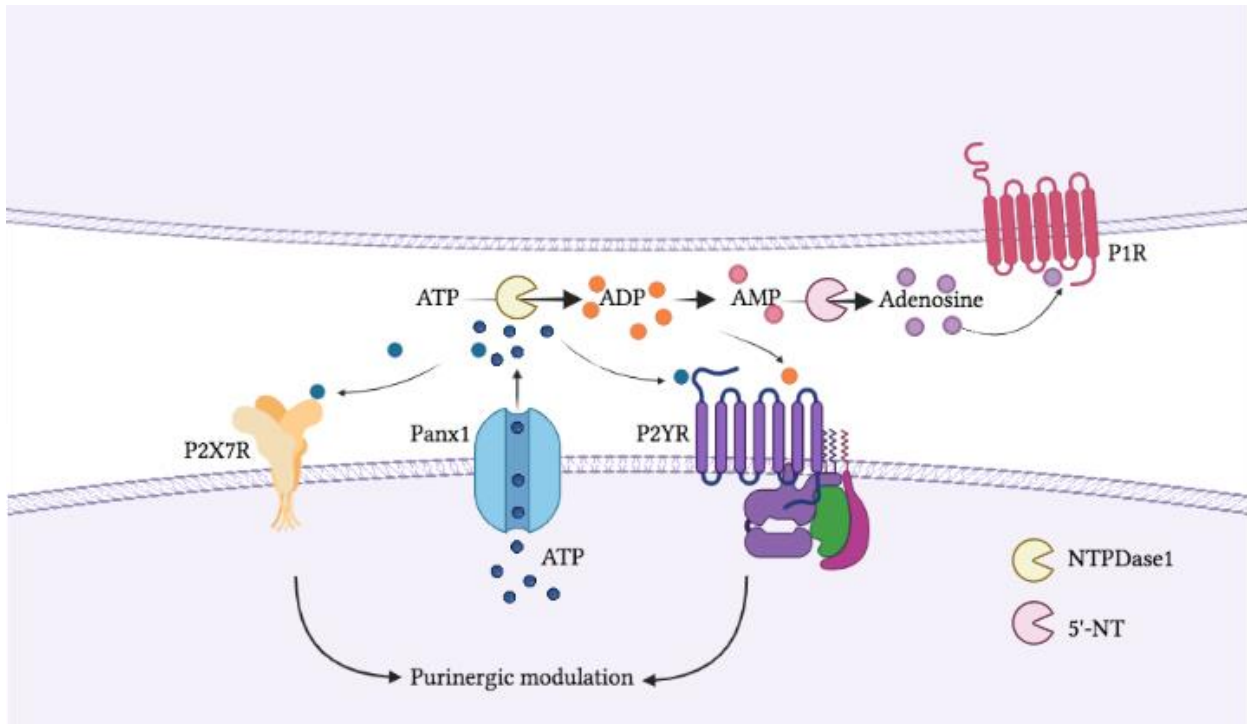


Figure 1.4. Purinergic signaling. ATP release through Panx1 channels initiates a cascade of events involving purinergic receptors. ATP in the extracellular space can stimulate P2X (P2X7R) and/or P2Y (P2YR) receptors. Ectoenzymes catalyze the stepwise hydrolysis of ATP. NTPDase1 facilitates the breakdown of ATP to ADP, which activates P2YRs and 5'NT breaks down AMP to Adenosine which activates P1 receptors. P2 and P1 receptors frequently transduce signals that produce diverse effects and lead to modulation, often via increasing the intracellular Ca^{2+} concentration. Representative ectoenzymes are labelled at the bottom right NTPDase1: Ectonucleoside triphosphate diphosphohydrolase-1, 5'-NT: ecto-5'-nucleotidase. This illustration was created with BioRender by PW-F.

1.4. Pannexin1 in health and disease

Panx1 can permeate molecules up to 1kDa in size such as cations, anions, purine nucleotides and signaling lipids. Overall, Panx1 appears to operate at the crossroads of major signaling pathways, in particular those involving intracellular Ca^{2+} and extracellular ATP, which underscores the potential relevance Panx1 has in synaptic transmission. With its localization and permeation

properties, Panx1 has become a primary candidate for participating in (patho)physiology of the CNS (Yeung et al., 2020).

Until recently, cell-based studies were at the forefront of pannexin research. Lately, the availability of mice with genetic ablation of pannexins opened new avenues for phenotypic exploration of the proteins from a molecular to a systems perspective. The Panx1^{-/-} mouse models permitted the discovery of an auditory role for Panx1, implicated channel functions in vision, and dismissed roles for Panx1 in gustation and primary olfaction (Whyte-Fagundes et al., 2019). Together, highlighting the variability of Panx1 functions across the CNS despite its vast localization in regions primed for important signaling processes (**Figure 1.5 a-d**).

Although we are only at the beginning of understanding the roles of pannexins in health and disease, the field continues to establish pathological roles of Panx1 in epilepsy, stroke, inflammation and pain, to name a few. However, conflicting data do exist regarding putative Panx1 function(s) in sensory systems and pathologies, which will be elaborated in this thesis for olfaction, vision and epilepsy. These conflicts highlight the need for innovating animal models for molecular and behavioural phenotyping in order to study functions of Panxs at a systems level. As a result, this thesis expanded investigations to include *panx1*^{-/-} zebrafish models.

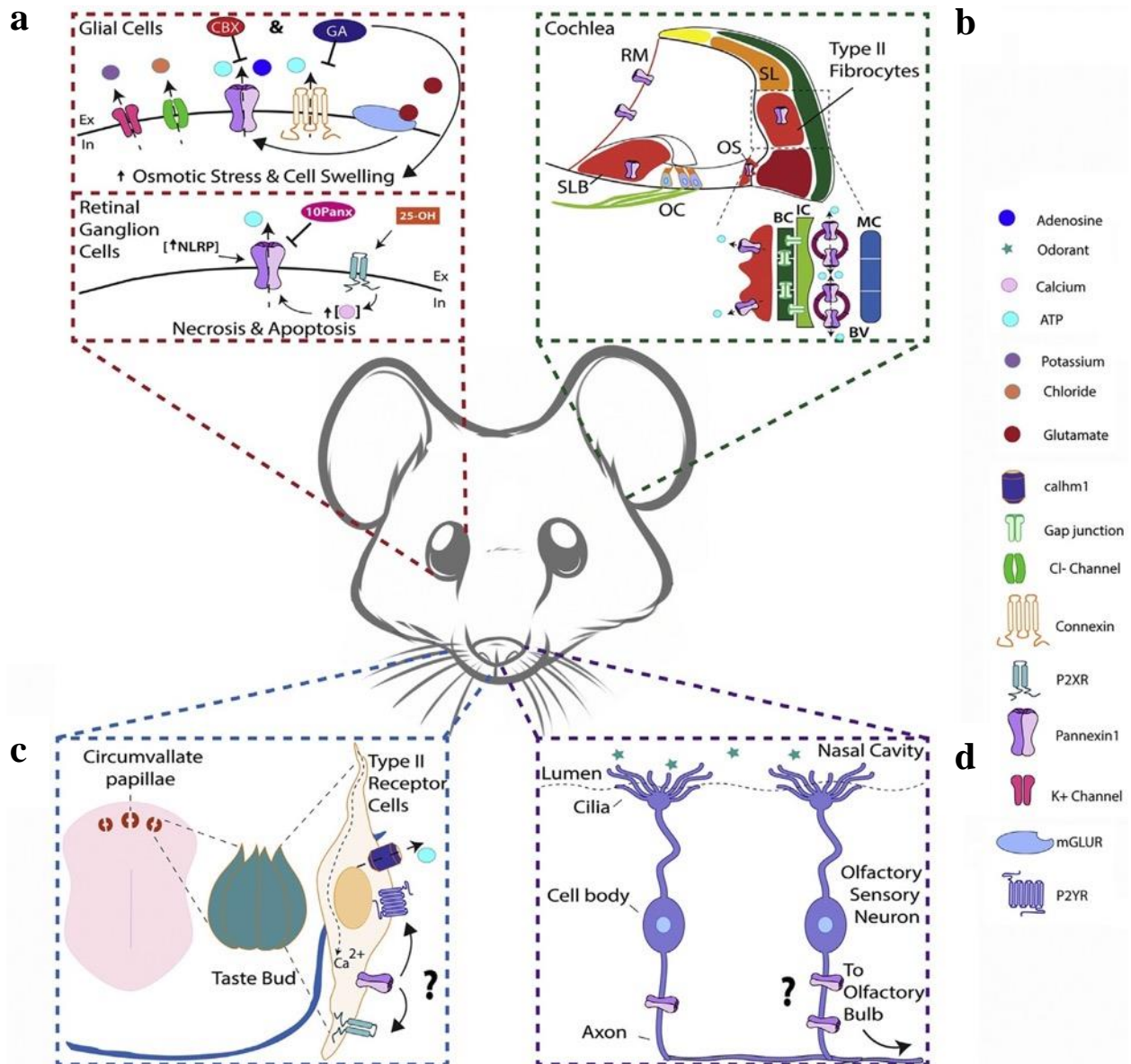


Figure 1.5. Panx1 in rodent sensory systems. a) Vision. Panx1 is expressed in glial cells (Muller and microglia) where it is responsible for ATP release under osmotic stress and cell swelling. Glial cells undergoing osmotic stress opens associated ion channels (K⁺ and Cl⁻). Opening of Panx1 channels, connexin hemichannels, activation of metabotropic glutamate receptors (mGluR) and other ion channels reduce cell swelling and osmotic stress. Carbenoxalone (CBX) and GA (18 α -glycyrrhetic acid) prevent Panx1 and connexin hemichannels from opening and thus preventing ATP release. Panx1 is also found in retinal ganglion cells (RGCs), which release ATP when the inflammasome is activated (NLRPs). ¹⁰Panx has been shown to reduce the inflammasome induced Panx1-mediated ATP release. Hydroxycholesterol (25-OH) has been shown to activate Panx1-dependent P2X7 receptors to elevate intracellular Ca²⁺ and induce ATP release leading to necrosis and apoptosis. b) Auditory. Panx1 expression is found throughout the cochlea, specifically in the SLB, RM, OS, strial BV and Type II fibrocytes of the SL. Panx1 is responsible for ATP release in type II fibrocytes and blood vessels. Lack of Panx1 expression in these regions correlate with impaired hearing in mice. SLB = spiral limbus SL = spiral ligament, OC = organ of corti, RM = Reissners membrane, OS = outer sulcus cells, BC = basal cells, IC = intermediate cells, MC = marginal cells, BV = blood vessel. c) Gustatory. Taste buds in circumvallate papillae encompass three cells types, one of which, type II receptor cells, express Panx1. These cell types are activated in response to bitter, sweet or umami stimuli resulting in a calcium influx, which propagates an action potential and stimulates ATP release. At present, evidence points at CALHM1 as a major

release site for ATP. **Panx1 function has yet to be elucidated, although it is suspected to play a role in taste in conjunction with P2X and P2Y receptors.** d) **Olfaction. In the olfactory epithelium, Panx1 is expressed in axon bundles of olfactory sensory neurons (OSNs), which relay information from the OSNs to the olfactory bulb. Panx1 function(s) in this region remains to be determined. The figure legend to the right lists major components shown in parts A–D. A question mark indicates lack of conclusive information. Figure adapted from Whyte-Fagundes et al., 2019 created by PW-F.**

1.4.1. Olfaction

Evolutionarily speaking, the olfactory system is necessary to detect and discriminate between odours in order to communicate, forage, mate and avoid predators or foul nutrition (Chuah & Zheng, 1992). In order to accomplish this, vertebrates require a highly organized olfactory system, which has developed over time to detect a vast amount of volatile chemicals. In humans, there is only a need for one functional olfactory system known as the main olfactory system (MOS); which contains the main olfactory epithelium (MOE) and the main olfactory bulb (MOB). This is present in lower mammalian vertebrates as well, however, they also developed several subsystems that aid in increasing the complexity of their olfactory systems to allow higher orders of odour discrimination. The olfactory subunits present in mammals, excluding humans, include the Grueneberg ganglion (GG), septal organ (SO), vomeronasal organ, and accessory olfactory bulb (AOB) (**Figure 1.6**) (Storan & Key, 2006).

The VNO is the primary sensory organ in the accessory olfactory system (AOS); located at the base of the nasal septum (Halpern, 1987) containing an apical and basal region that project to different areas of the AOB for further processing. This chemosensory organ contains specialized sensory neurons called vomeronasal sensory neurons (VSNs) that are found in the pseudostratified neuroepithelium and are responsible for pheromone detection. Current research suggests that each region of the VNO is responsible for processing different odorants. However, only fundamental roles of the basal region, which projects to the caudal AOB (Takigami, 2000), have been implicated in mediating instinctive behaviours like aggression, predatory avoidance and sexual attraction (Pérez-Gómez et al., 2014). During olfaction, pheromones are detected by VSNs once they are forced into the lumen of the VNO by a vascular pump triggered by autonomic nervous system stimulation. Mobilization of chemical signals is due to the sympathetic nervous system initiating ATP release (Rummary et al., 2007), which is extremely important in evoking neural contractions of the cavernous tissue on the lateral side of the lumen for further chemical processing (Salazar et al., 2008). The resulting signal transduction in the AOS has been linked to purinergic signaling (Housley et al., 2009), making Panxs candidates for regulating olfactory sensations.

It is important to note that the description of the olfactory system here is specific to mammals, namely rodents. Zebrafish have a single MOS, however, they have adapted accessory olfactory functions as their MOS contains microvillous OSNs that are like those found in the VNO in addition to the ciliated OSNs that are found in MOE (Biechl et al., 2017). Investigations pertaining to only mammalian olfaction are pursued in this thesis.

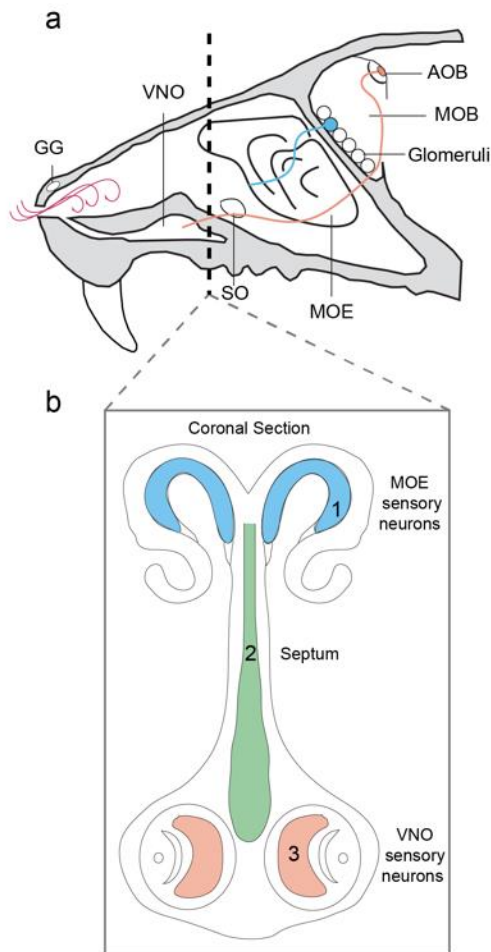


Figure 1.6. Mammalian olfactory system schematic. a) The main olfactory system is made up of the main olfactory epithelium (MOE) where the odorant binding receptors are located and the main olfactory bulb (MOB) where transduction of olfactory sensory neurons occur (blue pathway). The circles indicate the glomeruli where OSNs expressing the same receptor project onto each glomerulus. The accessory olfactory system is made up of the vomeronasal organ (VNO) which detects odors via a pumping mechanism and the accessory olfactory bulb (AOB) where sensory neurons transduce (orange pathway). **b)** A coronal section perspective of the (1) main olfactory system, highlighted in blue is where the sensory neurons are found (2) septum and the (3) accessory olfactory system, highlighted in orange is where the sensory neurons are found. GG: Grueneberg ganglion, SO: Septal organ.

1.4.1.1. Physiological relevance of Panx1 in the olfactory system

Investigations of Panx1 in the olfactory system are lacking, which is surprising in light of the prominent role of olfaction in complex behaviours, and cognitive functions in humans and mammals. One reason may be that olfactory dysfunctions are found to occur with severe disorders like Parkinson's and Alzheimer's disease, Down's syndrome, or even during a stroke and fail to receive prominent attention in light of the greater concern. Regardless, the first report of Panxs in the olfactory system began with investigations of their expression in the brain (Bruzzone et al., 2003). This was later followed up by Zhang et al, who revealed overlapping expression of Panx1 and Panx2 mRNA in the main olfactory system (MOS) and greater Panx2 positive neurons in the olfactory bulb (OB) compared to Panx1 (C. Zhang, 2011). A key finding from this study was the detection of significant Panx1 mRNA expression at the ventral and lateral portions of the turbinates, which include endoturbinates III and IV and some ectoturbinates in the olfactory epithelial layer. Strong Panx1 labeling was also found in cells located in the thickest layer of the epithelium, which spans from the base of the sustentacular cell layer to the basal cell layer where the olfactory neurons lie. In this region, ATP has been shown to play a role in olfactory responsiveness, as well as proliferation and differentiation of olfactory sensory neurons (OSNs) (Jia, C; Doherty, P; Crudgington, S; Hegg, 2009). Based upon this anatomical study, this group proposed a novel role of Panx1 in information processing in the olfactory system. As such, our group followed up this work to implicate a role of Panx1 in olfaction. With the use of a Panx^{-/-} mouse model, Panx1 protein expression was found in the OSN axon bundles rather than in cilia (S. Kurtenbach et al., 2014), which was surprising based upon the access of the ciliary layer to odorant activation. A function of Panx1 in primary olfaction was further ruled out based upon in-depth investigations using electro-olfactogram and ATP release measurements from *ex vivo* preparations of olfactory epithelial tissue. Together, these findings suggest that ATP release through Panx1 channels may play a role in proliferation and differentiation of the OSNs but not in the initial information processing of the olfactory system.

Investigations of the Panxs in the olfactory system are limited to these two studies; which do not consider expression of Panx3, a family member related to Panx1 in size and amino acid composition, and do not take into account accessory olfactory system function (Whyte-Fagundes et al., 2018). This raises the question of whether or not Panx3 channels may function actively

alongside Panx1 during olfaction and indicates a significant knowledge gap in the field of channel membrane proteins and their role in olfaction.

1.4.2. Physiological relevance of Panx1 in the visual system

The visual system constructs mental representations of a vertebrates' surroundings, connecting pathways from the eye through to the visual cortex (**Figure 1.7**). Visual information often dominates locomotion and balance due to the guidance of neuronal mechanisms that mediate and link the visual sensory inputs to the execution of an adaptive locomotor output and also permits the formation of memories based upon visual stimuli. As such, understanding the physiology of the visual system may also aid in understanding neural diseases that affect memory and navigation like Alzheimer's disease and stroke (Ekstrom, 2015).

Efforts to understanding how these neuronal mechanisms function has revealed that synaptic modulation may occur due to Panx1. Using *in situ hybridization* and RT-PCR analysis of tissue from the mouse eye, Panx1 expression was revealed in the ganglion cell layer (GCL), inner nuclear layer (INL), the outer nuclear layer (ONL) and to a lesser extent in the inner plexiform layer (IPL) (Dvorianchikova et al., 2006; Ray et al., 2005). In contrast to adult animals that only showed labeling in the retinal ganglion cells (RGCs), neonatal animals had prominent labeling in amacrine and horizontal cells (HC) in addition to RGCs. Overlapping expression of Panx1 and P2X7-Rs at the tip of HC dendrites suggest that their functions are linked and involve the local release of ATP (Puthussery et al., 2006). This remains to be determined, however, investigations regarding the physiological functions of visual information processing established that Panx1 ablation in mice interferes with the activity of the dark-adapted retina without altering the temporal properties of signal transmission or affecting the cone pathway under light conditions (Bloomfield et al., 1995).

The retina in zebrafish shares many properties with those of higher vertebrates, however, Panx1 expression was more complex as the two *panx1* ohnologs showed distinct localization patterns. *Panx1a* was found in the OPL on HC dendrites, while *Panx1b* was found in the GCL and INL (Sarah Kurtenbach et al., 2013). *Panx1a* has been implicated in inhibiting synaptic transmission at the first retinal synapse due to a hyperpolarization of HCs that decreases channel conductance, a reduction of ATP and causes alkalization in the synaptic cleft (Sarah Kurtenbach

et al., 2013; Vroman et al., 2014). A role of *panx1b* in the visual system remains to be elucidated, highlighting the need for further investigations into the visual system.

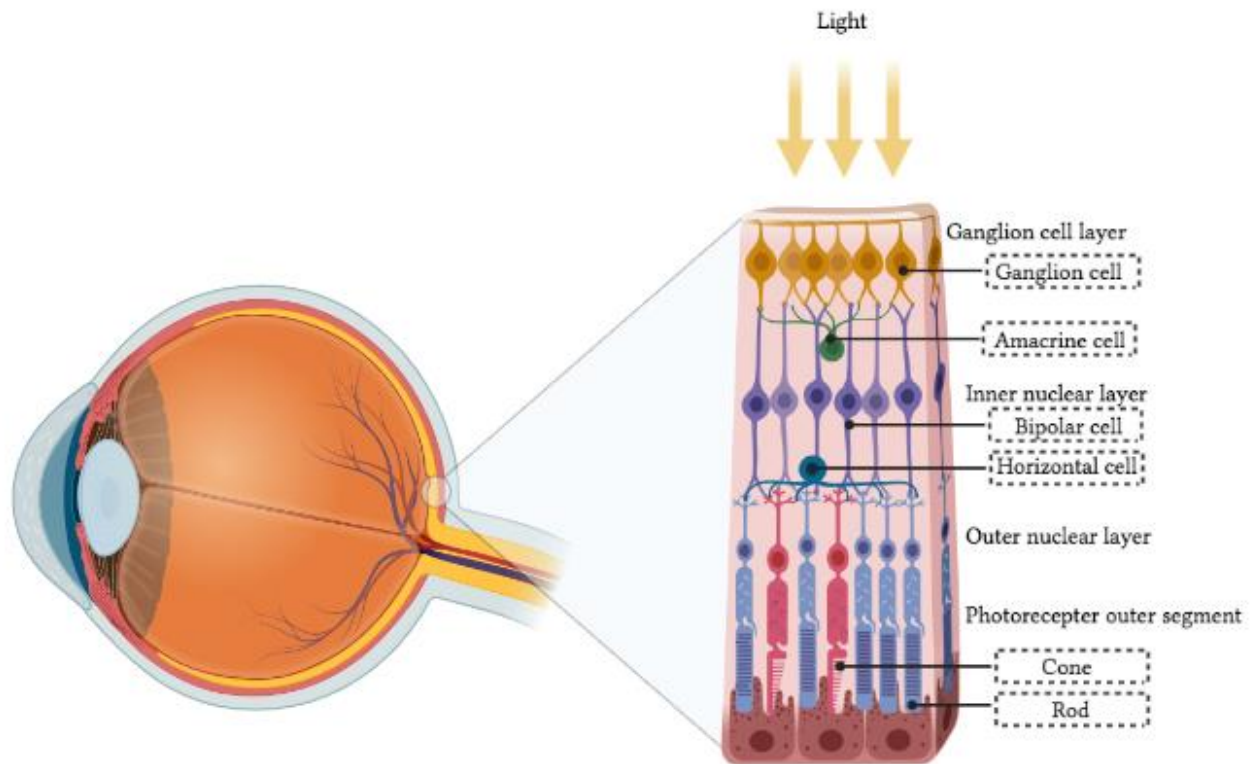


Figure 1.7. Cross section of the eye with an enlarged schematic of the retina. In vertebrates the retina is composed of three layers of nerve cell bodies and two synaptic layers. The outer nuclear layer contains photoreceptor cell bodies. There are two types of photoreceptors, rods and cones. The inner nuclear layer contains cell bodies for horizontal, bipolar and amacrine cells. The ganglion cell layer contains ganglion cell bodies. The first synaptic layer is the outer plexiform layer where connections between rods and cones occur. The second synaptic layer is the inner plexiform layer where bipolar cells connect to ganglion cells. Upon light absorption by photoreceptors the signal is translated into a biochemical signal and then an electrical message. The electrical outputs are then transmitted to the brain via ganglion cell axons that form the optic nerve. This illustration was created with BioRender by PW-F.

1.4.3. Epilepsy

The hallmark of epilepsy is recurrent seizures, which are spontaneous events wherein networks of neurons abnormally fire in synchronized bursts. Seizures can represent an important clinical manifestation of metabolic diseases which interfere with energy breakdown, changing osmolarity, pH, or producing endogenous toxins altering the balance of excitation and inhibition in the nervous system (Rahman, 2015; van Gelder & Sherwin, 2003). Alternative mechanisms underlying causes of epilepsy include altered homeostasis of the major excitatory and inhibitory neurotransmitters, glutamate and GABA; which contribute to the hyperexcitability of neurons in seizure generation.

Evidence from epidemiological, clinical, and molecular studies suggest genetic as well as epigenetic contributions to epileptogenesis, the development of the epileptic state, in addition to focal brain lesions, trauma or tumors. With a variety of causes for brain function impairments underlying epilepsy, it has become one of the leading neurological disorders worldwide. Although many patients do have seizure relief using a single medication, many require combinations of medications, resective surgery, neuromodulation devices, or dietary therapies. Despite having a variety of treatments available on the market, one-third of epileptic patients continue to have uncontrolled seizures. As such, this emphasizes a direct need for discovering alternative therapies and stresses the importance of uncovering novel targets for anti-epileptic drugs (AEDs) like Panx1.

1.4.3.1. **Proposed involvement of Panx1 in epilepsy**

Previous reports have highlighted probable roles of Cxs in epilepsy, arguing how electrical and metabolic coupling through direct cell to cell contacts can contribute to the underlying neuronal synchrony that drives seizure activities (Carlen, 2012; Mylvaganam et al., 2014). Here, evidence that is summarized in **Figure 1.8** linking functions of Panx1 to both the initiation or propagation of seizures as well as their inhibition or termination, will briefly be reported. Further details can be found in Chapters 4 and 5 and is also summarized in **Table 4.2**.

Panx1 expression is raised in animal seizure models and in resected human brain tissue from epileptic patients, lending confidence to its initial implication in the formation of epilepsy (Jiang et al., 2013a; Li et al., 2017; Mylvaganam et al., 2010). After this increased expression was observed, research emerged intending to establish the mechanisms at which Panx1 participates in complex epileptic activities and determine whether they are pro- or anti-convulsant channels. Mechanisms responsible for driving aberrant Panx1 activity in this context have yet to be fully elucidated. However, factors linked to seizure generation via the accumulation of extracellular K^+ , glutamate release leading to hyperexcitability and the activation of NMDARs, and excitatory ATP release, are all proposed mechanisms implicating a role of Panx1 in increasing network excitability (Lopatář et al., 2015; Santiago et al., 2011; Wei et al., 2016). Conversely, some reports suggest that Panx1 can actually limit excitability and increase seizure thresholds by contributing to neuronal inhibition via inhibiting glutamate release as well as promoting extracellular accumulation of adenosine (Kawamura et al., 2010; Mendoza-Fernandez et al., 2000). Together,

Panx1 appears to have a complex dichotomous role in regulating the excitatory/inhibitory balance of neuronal networks that remains to be resolved.

Over the last decade, the wealth of connections between Panx1 and disease continues to grow; with eloquent studies continuing to correlate Panx1 and epilepsy. General agreement on the contribution of Panx1 to seizure activities has yet to be met, as many reports in the field are conflicting, emphasizing the need for new approaches and models for investigation. Enough evidence suggests that Panx1 has important roles for seizure generation, manifestation and/or termination, and in turn encourages the advancement of research in this field.

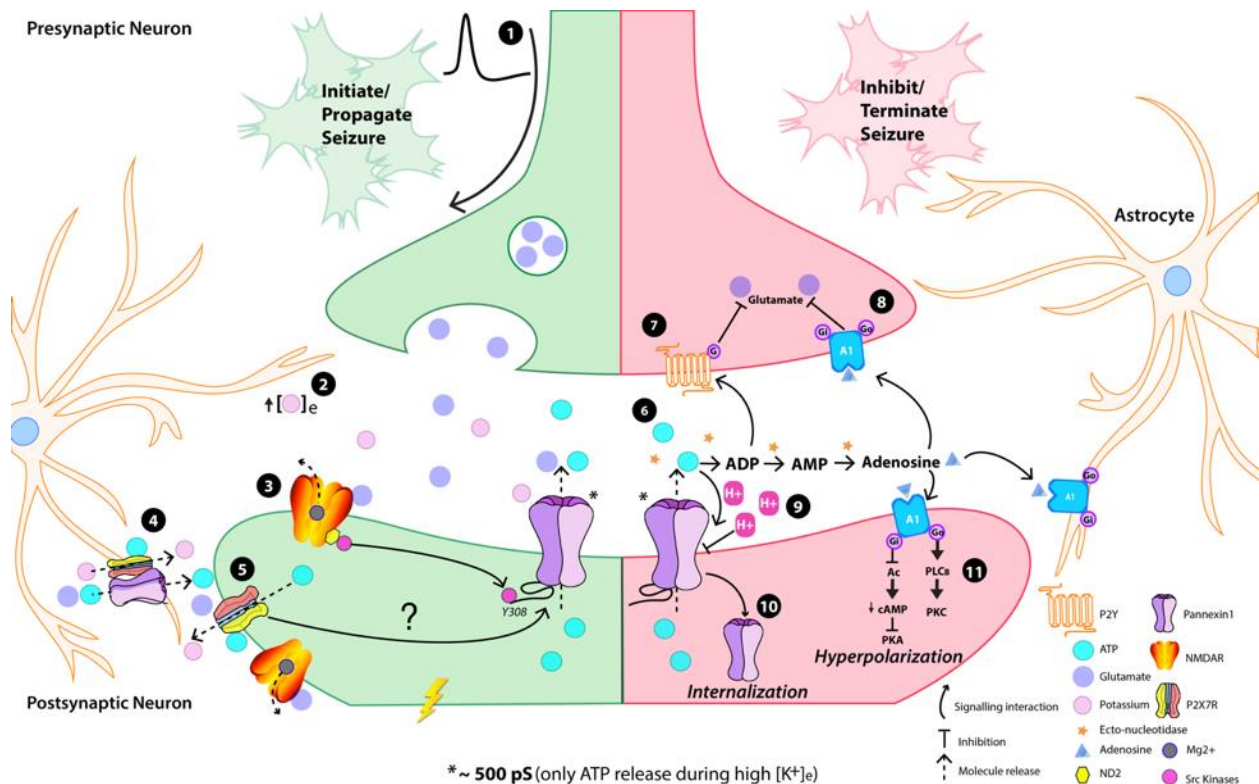


Figure 1.8. Schematic of speculated mechanisms involving Panx1 in epilepsy including initiation and termination of seizure activity. (1) Presynaptic glutamate release upon depolarization activates (2) postsynaptic NMDA receptors, which initiate Src Family Kinase mediated phosphorylation of Panx1. (3) Elevated $[K^+]_e$ promotes the ~500 pS high conductance configuration of Panx1 to allow a surge of ATP release. (4) This released ATP may activate astrocytic P2X purinergic receptors to release glutamate and provide tonic stimulation of surrounding neurons. (5) The reversal potential of Panx1 near 0 mV contributes to neuronal depolarization. (6) ATP, in the presence of ecto-nucleotidases, may break down to ADP, (7) which acts upon G-coupled P2Y receptors to inhibit glutamate release. (8) ATP metabolizes to adenosine and can act on A1 receptors located (8) on the presynaptic neuron to inhibit glutamate release, (9) on astrocytes, (10) and on the postsynaptic neuron to cause hyperpolarization. Figure from Aquilino* & Whyte-Fagundes* et al., 2019 and created by PW-F.

1.5. Hypothesis and research objectives

The overarching purpose of this thesis is to address conflicts in the Panx1 literature related to neurobiological questions touching both physiological and pathological perspectives. Questions regarding the participation of Panx1 in excitability arose when our group previously reported that the loss of Panx1 increased excitability resulting in impaired learning and memory (Prochnow et al., 2012). Around a similar time, the Scemes group reported a suspected role of Panx1 in epilepsy by contributing to prolonged hyperexcitability (Santiago et al., 2011). This conflict was the starting point to investigations regarding altered excitability and Panx1 in olfaction that began in the preceding master thesis (Whyte-Fagudnes, 2015) due to Prochnow et al., utilizing a cookie finding test to establish the impaired learning and memory in Panx1^{-/-} mice. As time progressed, other groups contributed to the epilepsy field and more conflict in that literature grew regarding whether Panx1 was pro- or anti-convulsant. **Here, I hypothesize that Panx1 participates in mediating excitability in both physiological (olfaction, vision) and pathological (epilepsy) contexts.** A multimodal approach towards resolving the gaps in the literature was taken. Specific objectives and hypothesis for each study are outlined below.

1.5.1.1. Determine the involvement of Panx1 in accessory olfaction (Chapter 3)

Our previous investigations of Panx1 in olfaction dismissed a primary functional role of the channel in the main olfactory system despite being localized in olfactory sensory neurons, suggesting that Panx1 is one of several alternative pathways that can release ATP during chemosensation (Kurtenbach et al., 2014). In line with these results, the objective of this study was to expand these olfactory investigations using the same mouse model to include the accessory olfactory system. The purpose of this expanded investigation was to explore if the loss of Panx1 resulted in compensatory upregulation of an alternative channel, namely another Panx member, and if this was not the case then to determine if Panx1 participated only in accessory olfactory systems. Specific hypotheses and corresponding research aims addressed in this chapter include:

- i. Genetic ablation of Panx1 causes changes in the expression of similar channel(s): Explore upregulation of other Panx family members at the mRNA and protein level.
- ii. Due to Panx1 channel properties, localization of Panx1 is found in regions necessary for promoting chemosensation in the vomeronasal organ (VNO): Investigate protein expression of Panx1 and other Panx family members.

- iii. As Panx1 expression levels decrease with age, expression patterns of the protein will alter as well: Examine protein expression of Panx1 and Panx3 in the VNO of both juvenile and adult mice.
- iv. ATP release responsible for sensory system processing is released via Panx1 when the VNO is stimulated: Mechanically stimulate the VNO *ex vivo* to mimic functions *in vivo* and measure ATP release from the organ in WT and Panx1^{-/-} mice.
- v. Upregulated Panx3 can compensate functionally for Panx1: Determine if channel properties of Panx3 are consistent with Panx1 channels. Properties include establishing cell membrane localization and channel function using dye uptake and ATP release assays along with known Panx1 channel stimulants and blockers.

Overall, we hypothesized that Panx3 could compensate for the loss of Panx1 and sustain chemosensory processing in the accessory olfactory system. Data supporting these aims were published in:

Whyte-Fagundes, P., Kurtenbach, S., Zoidl, C., Shestopalov, V., Carlen, P & Zoidl, G. (2018). A potential compensatory role of Panx3 in the VNO of a Panx1 knock out mouse model. *Frontiers in Molecular Neuroscience*. 11(135). 1-16. Doi: 10.3389/fnmol.2018.00135

1.5.1.2. Establish electrophysiological markers of epilepsy linked to Panx1 (Chapter 4)

Previous work by our collaborators established a correlation between induced seizure activity and increased Panx1 expression (Mylvaganam et al., 2010), implicating a role of Panx1 in epilepsy. The Panx1 channel has been implicated in excitability dynamics through its involvement in modifying synaptic plasticity, however, the immediate contribution of Panx1 to seizure-like activity is unclear. Therefore, the objectives of this study were to assess changes in electrophysiological markers of excitability associated with Panx1 in 4-AP induced seizures *in vitro* (presented here) as part of a larger project that also investigated alternative seizure models and included behavioural assessments using the same Panx1^{-/-} mouse model mentioned previously. Specific hypotheses and corresponding research aims addressed in this chapter include:

- i. Targeting Panx1 alters physiological properties of neurons that impact excitability: Utilize whole-cell neuronal patch clamp recordings in WT and Panx1^{-/-} brain slices of juvenile mice to investigate electrical changes in individual cell activity related to panx1. Use Panx1 blocker to pharmacologically corroborate that the results are mediated by the channel.

- ii. Targeting Panx1 alters the excitability of local circuitry and reduces propensity to fire during seizure activity: Record local field potentials (LFPs) from brain slices under 4-AP (100 μ M) application to chemically induce seizures and observe alterations in activity as a result of knocking out Panx1. Assess alterations to oscillatory dynamics by exploring changes to spectral power across frequency bands associated with epilepsy (i.e. theta, gamma and high frequencies).
- iii. Panx1 participates in mediating frequency synchronization: Explore phase amplitude coupling from LFP recordings as it has been suggested as a biomarker for epilepsy.

Overall, we hypothesized that Panx1 targeting (genetically and pharmacologically) would improve seizure outcomes by altering the excitability of the brain and disrupting seizure dynamics. Data supporting these aims have been published in:

Aquilino, M., **Whyte-Fagundes, P.**, Lukewich, M., Zhang, L., Bardakjian, B., Zoidl, G., & Carlen, P. (2020). Pannexin-1 deficiency decreases epileptic activity in mice. *International Journal of Molecular Sciences*. 21(20):7510. Doi: 10.3390/ijms21207510.

1.5.1.3. Uncover functional roles of Panx1 in the retinotectal pathway (Chapter 4)

The Zoidl lab pioneered the discoveries of zebrafish *panx1a* and *panx1b* expression in the retina; uncovering the distinct localization of *panx1a* in horizontal cells (HC) and *panx1b* in ganglion cells (GC) raising the question whether or not their functions were also distinct (Sarah Kurtenbach et al., 2013; N. Prochnow et al., 2009). Investigations in the retina for Panx1 were primarily conducted in mice, however, more recently *Panx1a* has been implicated in negative feedback mechanisms from the HCs to photoreceptors in adult zebrafish similar to murine Panx1 (Cenedese et al., 2017; Vroman et al., 2014). Physiological functions in the retina for *Panx1b* remain to be revealed for zebrafish at the adult or larval stage. Therefore, the objective of this study was to determine whether or not the expression of *panx1* orthologs had an impact on modulating visual inputs within intact retinotectal pathways. Specific hypotheses and corresponding research aims addressed in this chapter include:

- i. Knocking out either *Panx1a* or *Panx1b* will have opposing impacts on processing visual information in the optic tectum: Record LFPs *in vivo* from 7dpf zebrafish with *panx1a*^{-/-}, *panx1b*^{-/-} and both *panx1a*^{-/-}/*panx1b*^{-/-} (DKO) during Light-ON and Light-OFF conditions. Modulation of visual inputs will be measured by, and inferred from, determining changes to brain oscillations upon light stimuli and comparing them to controls (TL). Use of a

Probenecid (100 μ M), a Panx1 blocker, will be used to mimic results from DKO larvae and confirm Panx1 involvement.

Overall, we hypothesized that independent Panx1 targeting will have opposing impacts on processing light stimuli based upon their distinct expression. Some data supporting these aims are currently in preparation for publication, while data regarding *panx1a*^{-/-} zebrafish are published in: Safarian, N., **Whyte-Fagundes, P.**, Zoidl, C., Grigull J., & Zoidl, G. (2020). Visuomotor deficiency of *panx1a* knockout zebrafish is linked to dopaminergic signalling. Scientific Reports. 9538(10). Doi.org/10.1038/s41598-020-66378-y

1.5.1.4. **Resolve conflicts regarding pro- or anti-convulsant actions of Panx1 (Chapter 5)**

The work we completed *in vitro* revealed that knocking out Panx1 reduced 4-AP induced seizure activity, suggesting pro-convulsant properties of the channel, and was able to implicate a role of Panx1 in altering excitability from a single cell to a local network level. However, since this research was completed in an *in vitro* model, networks were disrupted upon sectioning the brain and mechanistic questions still remain regarding the role of Panx1 in epilepsy. Therefore, the objective of this follow up study was to establish a complementary model to investigate Panx1 in seizure activity in order to resolve remaining mechanistic questions and to challenge the leading notion of Panx1 being pro-convulsant. Specific hypotheses and associated research aims addressed in this chapter include:

- i. Targeting *panx1* in zebrafish will improve PTZ induced seizure outcomes: Record LFPs *in vivo* from 7dpf *panx1a*^{-/-}, *panx1b*^{-/-} and DKO zebrafish that are treated with PTZ (15mM) and compare seizure activity (occurrence, duration, spectral power, etcetera) to TLs. Monitor behavioural manifestations of seizure activity in zebrafish larvae as a secondary measure of seizure outcomes. Use a blocker, Probenecid (75 μ M), for *panx1* to corroborate that the results are mediated by the channel. Use an anticonvulsant, Valproic acid (5mM), to compare successful seizure amelioration via probenecid.
- ii. *Panx1a*^{-/-} and *panx1b*^{-/-} larvae have distinct underlying changes to the transcriptome that impact seizure propensity: Assess RNA sequencing data and mine a database for biological gene ontology enrichment to uncover any processes or gene families that may impact each genotype to respond differently to the PTZ treatment. Validate any candidate genes of interest with PCR to determine regulation.

- iii. The role of *Panx1* in seizure activities is mediated by ATP release through the channel: Design an ATP assay for whole zebrafish larvae in order to investigate differences amongst genotypes, ideally find reduced ATP in *panx1* knockouts, and determine the effect of PTZ treatment on ATP release.
- iv. Targeting *p2rx7* will reduce behavioural seizure activity but not as significantly as *panx1* targeting: Monitor locomotor responses of TL and *panx1b*^{-/-} larvae with A-438079 (A-43, 100µM) treatment to target *p2rx7* under PTZ application in order to determine if *p2rx7* targeting will reduce seizure-like activity.
- v. Distinct structural differences between *Panx1a* and *Panx1b* impact ATP release through the channel and in turn seizure activity: Use computational structural modeling in order to investigate differences of *Panx1a* and *Panx1b* structures to the recently resolved human PANX1 structure and establish any consistencies or disparities that may impact ATP release or gating, primarily amino acid residues 74 and 75.

Overall, we hypothesized that *panx1* targeting (genetically and pharmacologically) would reduce seizure propensity and severity by modulating feedback mechanisms regulating ATP release and *p2rx7* activation. Data supporting these aims are submitted and can be found here:

Whyte-Fagundes, P., Taskina, D., Safarian, N., Zoidl, C., Carlen, P., Donaldson, L & Zoidl, G. (2021). Panx1 channels promote both anti- and pro- seizure-like activities in the zebrafish via p2rx7 receptors and ATP signaling. bioRxiv. doi:<https://doi.org/10.1101/2021.06.03.446992>

Chapter 2. **Experimental materials and methods**

“ Science, for me, gives a partial explanation for life. In so far as it goes, it is based on fact, experience and experiment.”

- Rosalind Franklin

2.1. Part I: Materials and methods used to investigate the role of Panx1 in physiology: Olfaction

2.1.1. Panx1^{-/-} mouse generation

The generation and initial characterization of Panx1^{+/+} mice (Panx1^{fl/fl}) with three LoxP consensus sequences integrated into the Panx1 gene flanking exon 3–4, and knock out mice with global loss of Panx1 (Panx1^{-/-}, CMV-Cre/Panx1) was described previously (Grundken et al., 2011; Dvorianchikova et al., 2012; Prochnow et al., 2012; also see chapter 2). Animals were housed with a 12-h light/dark cycle and had free access to food and water, in compliance to the standards and policies of the Canadian Council on Animal Care (CCAC), and as approved by York University’s standing animal care committee (ACC; protocol 2011-09-GZ). Adult male mice (4–8 months of age) were housed individually 1 week before, and during, behavioral testing.

2.1.2. Quantitative real-time PCR (qRT-PCR)

Total RNA was isolated from adult male mice using the RNAeasy Fibrous Tissue Mini Kit (Invitrogen, Canada), and cDNA was synthesized from 1 µg of total RNA with the ReadyScript cDNA Synthesis Kit (Sigma-Aldrich, Canada), according to the manufacturer’s instructions. qPCR was performed using the SsoFast EvaGreen Supermix (Bio-Rad, Canada) using the following oligonucleotide pairs (**Table 2.1**). Experiments were performed in triplicates, using six biological replicates and the CFX Connect™ Real-Time PCR Detection System (Bio-Rad, Canada). All experiments included melt curve analysis verifying the identity of PCR amplicons in each reaction. Raw cycle threshold values (Ct-values) were exported from the CFX Manager™ Software (Bio-Rad, Canada), and the relative gene expression was calculated using the Relative Expression Software tool (REST; Pfaffl et al., 2002). The REST software reported relative expression values.

Table 2.1. Summary of primers for RT-qPCR used in VNO publication.

Gene	Forward (5'-3')	Reverse (5'-3')
mPanx1	CAGGCTGCCTTTGTGGATTC	CGGGCAGGTACAGGAGTATG
mPanx2	GGTACCAAGAAGGCCAAGACT	GGGGTACGGGATTTCCCTTCTC
mPanx3	CTTACAACCGTTCATCCGC	CAGGTACCGCTCTAGCAAGG
P2X7	GACAAACAAGTCACCCGGAT	CGCTCACCAAAGCAAAGCTAAT
P2X5	TGGAAGGGGTTCTGTGTTGTC	AGGGAAGTGTCAATGTCTCTGA
P2Y2	CTGGAACCCCTGGAATAGCACC	CACACCACGCCATAGGACA
Cx43	ACAGCGGTTGAGTCAGCTTG	GAGAGATGGGAAGGACTTGT
TRPC2	CTCAAGGGTATGTTGAAGCAGT	GTTGTTTGGGCTTACCACACT
TRPM5	CCTCGTGCTTTTTGAACTCC	CATAGCCAAAGGTGCTTCTCTC
Calhm1	CTGCTGACCACATTACTAGCG	CTGTGCATGTCTCATCGAAGAG
Calhm2	TCTTCAAGAGCAAGGATGTGATG	TCAGTCCATACAGGTAGTCCG
18s RNA (reference)	TGACTCTTTTCGAGCCCTGTA	TGGAATTACCGCGGCTGCTG
β -Actin (reference)	ATGGAGGGGAATACAGCCC	TTCTTTGCAGCTCCTTCGTT
GAPDH (reference)	TGGATTTGGACGCATTGGTC	TTTGCACTGGTACGTGTTGAT
UBC (reference)	ACCTTTCACCTACCTGCGGATG	GTACCCAGGGGCATCTGC
HSP90 (reference)	TCGTACAGCTGATGATGAAGT	GCGTTTAAACCATCCAACGAAT

2.1.3. *In Situ* hybridization (ISH)

Digoxigenin (dig)-labeled sense and antisense riboprobes were prepared from the full-length mPanx1 (NM_019482) coding sequence sub-cloned into the pcDNA3 plasmid (Thermo Fisher, Canada), as described previously (Ray et al., 2005, 2006). After linearization of the plasmid, sense and antisense riboprobes were transcribed using T7 and SP6 RNA polymerase with a digoxigenin RNA labeling mix (Roche, Germany). The ISH was performed using tissue from the VNOs of postnatal day 7 (P7) mice that were dissected and immediately embedded in tissue freezing medium (Leica, Germany) at -30°C . Cryostat sections ($12\ \mu\text{m}$) were cut immediately and collected on aminoalkylsilane-treated glass slides. The tissue was subsequently fixed in 4% paraformaldehyde in PBS at 4°C for 20 min, washed in PBS and acetylated by a 15-min treatment in 0.1 M triethanolaminhydrochloride solution with 0.25% acetic anhydride on a stirring plate. Individual sections were rinsed in $2\times$ SSC (30 mM NaCl and 3 mM sodium citrate) and pre-hybridized in hybridization buffer (50% formamide, $5\times$ SSC, $5\times$ Denhardt's solution, 2.5 mM EDTA, 50 $\mu\text{g}/\text{ml}$ heparin, 250 $\mu\text{g}/\text{ml}$ tRNA, 500 $\mu\text{g}/\text{ml}$ salmon sperm DNA and 0.1% Tween-20) for 1 h at 55°C . Riboprobes were added to the hybridization buffer (0.25 $\text{ng}/\mu\text{l}$), denatured at 80°C for 2 min and applied to tissue sections. Sections were protected from evaporation with cover slips and incubated over night at 55°C in a water-saturated atmosphere. Post hybridization, slides were gently treated with $2\times$ SSC to remove coverslips. Nonspecific binding was removed by wash steps at 55°C with $0.2\times$ SSC for 1 h and then with $0.1\times$ SSC for 15 min. Sections were subsequently equilibrated for 10 min in PBS containing 0.1% Triton X-100 (PBST), blocked with 10% goat serum in PBST buffer for 1 h and then incubated with 1:1000 alkaline phosphatase (AP) conjugated anti-dig Fab fragment (Roche, Germany) in blocking solution over night at 4°C .

Subsequently, slides were washed in PBST, equilibrated in B3-Buffer (0.1 Tris-HCl, 0.1 M NaCl, 50 mM MgCl₂, 0.1% Tween-20) followed by treatment with NBT/BCIP (Roche, Germany) to visualize the hybridization signals.

2.1.4. Immunohistochemistry (IHC)

Three-week-old and adult mice underwent humane euthanasia, quickly followed by full body perfusion before the separation of the head. The heads were then fixed in 4% PFA at 4°C overnight (ON) and stored until use. After removal of the fur and palate, the VNO was carefully isolated from the bony capsule in physiological Ringers solution (138 mM NaCl, 5 mM KCl, 2 mM CaCl₂, 2 mM MgCl₂, 10 mM HEPES, 10 mM Glucose, pH 7.4) and dehydrated in 30% sucrose at 4°C ON before sectioning. Ten micrometer thick cryosections were prepared using a Leica cryostat. Antigen retrieval was completed with 1% SDS for 5 min, followed by three washes each for 5 min with PBS. Sections were blocked with 5% normal goat serum (NGS), 1% bovine serum albumin (BSA), and 0.1% Triton X100 in PBS for 1 h at room temperature (RT). Primary antibodies (polyclonal anti-Panx1 and anti-Panx3 antibodies were kindly provided by Dr. S. Penuela, Western University, ON, Canada, dilution 1:200; G_{αo} SC- 13532, Santa Cruz, CA, USA dilution 1:100; Panx2, 42–2800, Invitrogen, dilution 1:100; NF200 clone NE14, N5389, Sigma-Aldrich, 1:100) were applied in buffer with 1% BSA in PBS containing 0.1% Triton X-100, and incubated at 4°C ON in a humidified atmosphere. After washing in PBS for 30 min, secondary goat anti-rabbit Alexa Fluor 488 and 568 (Invitrogen, Canada) diluted in PBS (1:1000), and applied for 60 min at RT in the dark. After three 10 min washes with PBS, sections were mounted, stained with Fluoroshield™ with DAPI (Sigma Aldrich, Canada), sealed, and kept at 4°C ON in the dark. Confocal microscopy was performed using ZEISS LSM 700 microscope, and ZEISS ZEN 2010 software was used to control all imaging parameters. Imaging was performed with 40× or 63× oil, both NA1.4, infinity corrected, DIC objectives. All images were taken using identical settings to allow a direct comparison of tissues from Panx1^{+/+} and Panx1^{-/-} mice. LSM images were exported into tiff format and assembled using ImageJ and Photoshop CS6.

2.1.5. Acute *ex vivo* VNO preparation for ATP release assay

The VNO was carefully dissected as described above. Here, the dissection was carefully conducted in Ringer's solution (138 mM NaCl, 5 mM KCl, 2 mM CaCl₂, 2 mM MgCl₂, 10 mM HEPES, 10 mM Glucose, pH 7.4) under an Olympus SZ61 dissecting microscope to ensure minimal

mechanical stimulation or damage to the structure. Isolated VNOs were equilibrated in fresh Ringers solution for 45 min at RT. The Ringers solution was replaced before stimulation and non-stimulation control conditions. Non-stimulated controls remained at rest in Eppendorf tubes for 10-min. Mechanical stimulation was induced by carefully pipetting up and down the Ringers solution around the VNO for a consecutive 10-min period, under visual control ensuring not to capture or disrupt the VNO. After the 10-min incubation time, 50 μ l aliquots of the supernatant were removed, heated for 1 min at 95°C, and stored on ice for detecting ATP concentrations (see section below titled “*In vitro* Luciferase Assay for ATP Determination”). All experiments were repeated five times for ATP measured from the VNO of either genotype.

2.1.6. Behavioural test: Modified resident-intruder assay

Male mice (4–8 months) were housed individually for 1 week before testing. Before the test, the bedding of the resident mice (same age) cages was not changed for three days. Mice were placed into home cages of other male mice for 10 min, which were covered with a glass plate for the duration of the test. Behaviors were recorded on video, and the animals’ interactions were quantified manually by counting and timing the specific behaviors. Biting, tail rattling/flicking, chasing, cornering and tumbling were considered aggressive behaviors, which were quantified using different parameters such as attack and defensive posture frequency and latency. Smell time was also used as a parameter of the investigation. To test for statistical significance student’s *T*-test was used.

2.1.7. Plasmid constructs

Expression vectors contained the full-length open reading frames of mPanx1 (NM_019482, amino acids (aa) 1–426) and mPanx3 (NM_172454, aa 1–392) were cloned into the pEGFP-N1 expression vector (Clontech Laboratories Inc., Mountain View, CA, USA) in two steps. First, the open reading frames were synthesized as gBlocks (Integrated DNA Technologies Inc. (IDT), Coralville, IA, USA) and cloned into the TA cloning vector pJet1.2 (Thermo Fisher Inc., Mississauga, ON, Canada). Then the coding regions were isolated by restriction digest and cloned in-frame into the pEGFP-N1 expression vector. All plasmid constructs used in this study were sequence verified (Eurofins MWG Operon LLC, Huntsville, AL, USA). For plasmid maps see appendix.

2.1.8. Cell culture and transient transfection

Neuroblastoma 2a (Neuro2a) cells ([Olmsted et al., 1970](#)) were cultivated in DMEM with 2 mM glutamine, 1% non-essential amino acids (NEAA), 1% penicillin and streptomycin (PS) and 10% fetal bovine serum (FBS) at 37°C in a humidified atmosphere with 5% CO₂. Approximately 30,000 cells were seeded in each well of 24-well plates or glass-bottom dishes (MatTek Corporation, Ashland, MA, USA) and transfected with 400 ng endotoxin-free plasmid DNA, using the Effectene transfection protocol (Qiagen Inc., Valencia, CA, USA). Cultures were used for western blotting or confocal imaging.

2.1.9. Western blot

Whole cell protein lysates were prepared 48 h after transfection. Twenty micrograms of protein was separated by 10% SDS-PAGE, transferred to 0.2 µm Midi format nitrocellulose membrane and processed using the iBind™ Western System (Bio-Rad Inc., Mississauga, ON, Canada). Primary antibodies were diluted 1:1000 (mouse anti-GFP, Roche; rabbit anti-GFP (FL), Santa Cruz Biotechnologies, TX, USA) and 1:20,000 (mouse anti-β-actin; Sigma-Aldrich Chemie GmbH, Munich, Germany). The secondary antibodies (LI-COR Biosciences, St. Lincoln, NE, USA) were diluted 1:20,000 (donkey anti-rabbit IRDye680LT) or 1:20,000 (goat anti-mouse IRDye800CW). Signals were detected using the Odyssey® CLx Infrared Imaging System (LI-COR Biosciences).

2.1.10. Confocal imaging

Transfected cells were fixed with 4% paraformaldehyde for 20 min at RT, washed with PBS, and mounted with Fluoroshield™ with DAPI (Sigma Aldrich, Canada) for imaging. Samples were visualized using a Zeiss LSM 700 confocal microscope with a Plan-Apochromat 63×/1.4 Oil DIC M27 objective and the ZEN 2010 program to control all hardware parameters. Images were collected by line averaging (4x) at high resolution (2048 x 2048 pixel) using single planes. Images were exported and further processed using ImageJ and finally were combined using Adobe Photoshop CS6 for presentation.

2.1.11. Fluorescent dye uptake assay

Neuro2A cells were grown in 3.5 cm MatTek cell culture dishes and transiently transfected with 400 ng EYFP, EGFP, mPanx1-EYFP or mPanx3-EGFP as described above. After 48 h, cultures were equilibrated for 30 min at 37°C and 5% CO₂ in 1 mL complete DMEM with 2 mM glutamine,

1% NEAA, 1% penicillin and streptomycin (PS) and 10% FBS, but lacking phenol red (for dye uptake workflow refer to **Figure 2.1**). MatTek chambers were placed in a live cell imaging chamber attached to the sample stage using a Zeiss 700 confocal microscope. Cells expressing mPax1 and mPax3 were selected for imaging at 37°C. Then, 1 mL fresh complete DMEM was added to cultures, to reach a final concentration of 10 μ M ethidium bromide (EtBr). Treatment conditions included the application of 50 mM KGlu, 140 mM KGlu, or 3 μ M ATP, as well as Pax1 blockers (3 mM ATP, 500 μ M probenecid, 10 μ M BB FCF). For blocking, cultures incubated for 5 min with blocker alone before application of 140 mM KGlu and EtBr. Images were taken at 1-min intervals, and dye uptake was measured over a period of 20 min. Normalized dye uptake values were calculated by the change in fluorescence of the red channel (EtBr uptake) over 20 min and the protein expression documented by the fluorescence of the green channel (EGFP/EYFP fluorescence). It was possible to normalize dye uptake on a cell to cell basis in this way since there is a linear relationship between protein expression (green channel) and the amount of dye uptake that occurred (see **Figure 2.2** for a sample of this relationship, refer to chapter 4 for the full version of this figure). Statistical analysis for these experiments were completed using the Wilcoxin Mann Whitney *U* test.

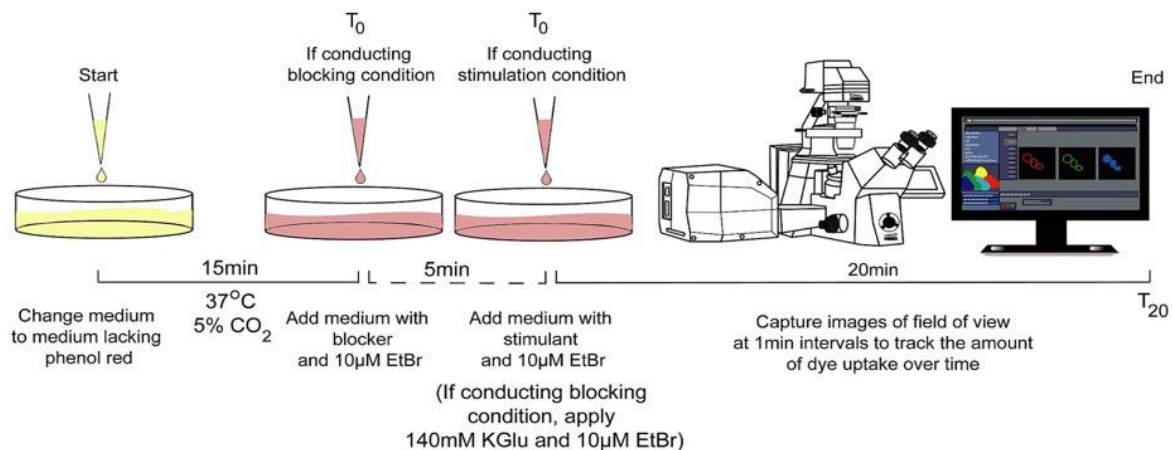


Figure 2.1. Summary of protocol for dye uptake assays. This image represents how the dye uptake assays were conducted. In accordance with the outlined figure, media was changed to media lacking phenol red, and the plate was incubated for 15 min, before transfer to the microscope into a live cell imaging chamber. Next, media with 10 μ M EtBr and a stimulant of choice were applied. For stimulation conditions, this was the start of tracking the amount of dye uptake. For blocking conditions, 5 min after applying 140 mM KGlu, blockers were applied along with EtBr and then dye uptake was tracked. To track dye uptake, images were taken at 1-min intervals for 20 min, and the accumulated fluorescence of EtBr was calculated over time.

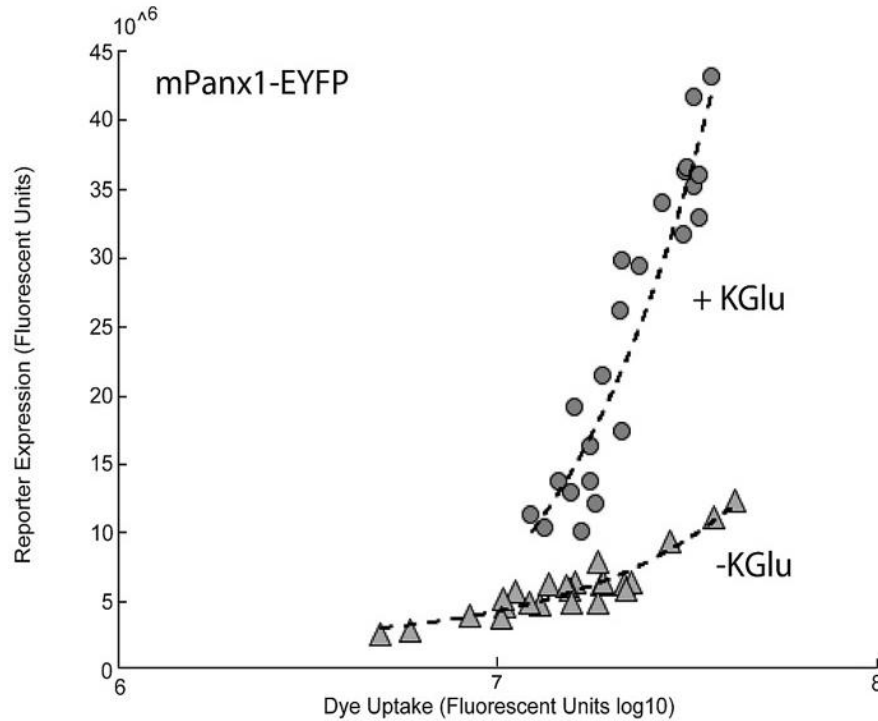


Figure 2.2. Linear correlation analysis of fluorescent reporter expression and uptake of ethidium bromide. Normalizing the amount of dye uptake, the fluorescence of EtBr, to the amount of fluorescent reporter expression (mPanx1-EYFP), reveals a strong and consistent linear relationship under control and stimulated conditions. mPanx1 under DMEM (closed triangles), $R^2 = 0.88$, and mPanx1 with 140 mM KGluc stimulation (closed dots).

2.1.12. *In vitro* luciferase assay for ATP determination

ATP assays were performed in a 96 well format (Greiner Bio-One, Canada) using the Molecular Probes® ATP Determination Kit as described by the manufacturer (Life Technologies, USA). Each well was seeded with 10,000 transiently transfected Neuro2a. Samples were measured using the Synergy H4 hybrid multi-well plate reader (Biotek, USA) as reported previously ([Kurtenbach et al., 2014](#)). ATP concentrations in experimental samples were determined from ATP standard curves (concentrations: 0 μ M, 1 μ M, 5 μ M, 10 μ M and 25 μ M), dissolved in 1x TE buffer, included in each assay. The Gen5 Data Analysis Software (BioTek) was used to set luminescent assay parameters, including automatic gain settings and 5 s integration time per well, and complete data exportation. All *in vitro* ATP assays were repeated three times. See **Figure 2.3** for a representation of luciferase assay methodology *in vitro*. The student's *T*-test was used to test for statistical significance in these assays.

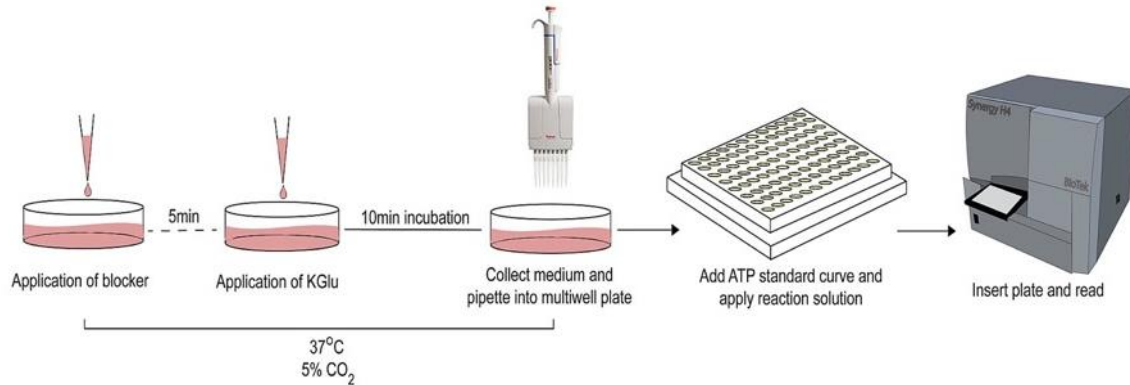


Figure 2.3. Depiction of methodology for ATP detecting luciferase assays. This image is a representation of how the ATP detecting luciferase assays were conducted. Following the figure, cultures were incubated with a blocker for 5 min before application of 140 mM KGlu for 10 min. Otherwise, cultures incubated for 10 min with either low or high concentration of KGlu. Then, the supernatant was collected, and pipette into a 96 well plate along with an ATP standard curve, where reaction solution was applied according to the manufacturer’s protocol and plates were placed into a microplate reader to determine luminescence—indicative of the presence of ATP.

2.1.13. Blocker pharmacology and stimulants

Simulants included 3 μM adenosine triphosphate (ATP, pH-buffered, Sigma-Aldrich), 50 mM and 140 mM potassium gluconate (KGlu, Sigma-Aldrich). Blockers used include; 50 μM carboxolone (CBX, Sigma-Aldrich), 100 nM mefloquine (MFQ, QU024-1, BioBlocks), and 10 μM brilliant blue food dye (BB FCF, Sigma Aldrich). It is important to note that all blocking data were collected after incubation for 5 min before application of 140 mM KGlu and EtBr, and recordings were taken starting immediately after the application of EtBr.

2.1.14. Statistical analysis

Statistical analysis and data presentation were performed using Mathworks Matlab software or Microsoft Excel. Experiments were repeated at least three times. In most experiments, at least three independent replicates were used. All data were analyzed for data distribution and subjected to Mann-Whitney U tests for independent samples or a paired t -test, when appropriate. See figure captions in chapter 4 for further details regarding statistical significance cut offs.

2.2. Part II: Materials and methods used for technical development: a multi-part Panx1 series

2.2.1. *In vitro* field potentials under 4-AP

Mice aged P14–25 days, both wild type and Panx1^{-/-}, were acutely anesthetized with isoflurane (5%) and quickly decapitated. Each brain was dissected and cut into 500 μm thick coronal slices with a Leica vibratome (1200 VT) using an ice-cold oxygenated dissection solution (composition

(in mM)—sucrose (248), KCl (2), MgSO₄ (3), CaCl₂ (1), NaHCO₃ (26), NaH₂PO₄ (1.25), d-glucose (10). These slices were incubated in carbonated artificial cerebrospinal fluid (aCSF, composition (in mM): NaCl (123), KCl (3.5), MgSO₄ (2), CaCl₂ (1.5), NaHCO₃ (25), NaH₂PO₄ (1.2), d-glucose (10) as previously described (L. Wang et al., 2016). These slices were then transferred and pinned to a submerged mesh surface to permit continuous perfusion of carbogenated 35°C aCSF (95% O₂ – 5% CO₂) across the slice at a flow rate of 10 mL/min. All slice electrophysiology recordings were performed with a Multiclamp 700B (Molecular Devices) amplifier and recorded with a Digidata 1322 (Molecular Devices) digitizer.

2.2.2. Whole-cell patch clamp and field recording

Field recording electrodes were filled with ACSF, lowered into the recording fluid and offset prior to entering the tissue. Electrodes were lowered approximately 250 µm into brain slices. Patch pipettes were filled with intracellular solution (135 mM K-Gluconate, 1 mM MgCl₂, 10 mM NaCl, 2 mM NA₂ATP, 0.3 mM NaGTP-Tris, 10 mM NaHEPES, 0.5 mM EGTA, and 0.1 µM CaCl₂; pH 7.2 and the osmolarity at 270 mOsm L⁻¹ (+/- 10 mOsm L⁻¹), lowered into recording solution, offset and then 1mL of pressure was applied and maintained until the pipette reached the surface of the tissue, where 0.6mL of pressure was released. The pipette was carefully lowered through the tissue slice until the cell of interest was located. Once the pipette touched the cell, a very small dimple was seen on the cell membrane, and the remaining positive pressure was released to form a gigaohm seal. When the seal was made, the cell was ‘broken’ through the membrane by light and short suction pulses applied with a syringe to achieve a whole-cell patch configuration.

2.2.3. *In vitro* field potentials under 4-AP: Electrographic classifier

As perturbations into the function of Panx1 were expected to result in changes of the typical SLEs, it was necessary to ensure that electrographic activity of Panx1 deficient animals could be correctly identified as an SLE if one were to occur. As such, multiple classification metrics were used to detect and classify SLEs.

Electrographic SLEs are typically defined by time-series features (Velisek, 2006), such as duration and shape but can also be distinguished from intra-SLE activity by frequency-based features, such as an elevated theta rhythm and high frequency spiking (Douw et al., 2010). As such, three methods were used to identify SLEs from extracellular field potentials. First, a visual

screen of electrographic recordings was completed using time-based features. Recordings were contrasted against classical 4-AP induced SLEs. *In vitro*, SLEs manifest in local field potentials as an initial bursting period, followed by a tonic episode and clonic after discharges, all carried on top of a slow < 1 Hz positive current. SLEs were defined as having a duration of ≥ 5 s and an amplitude of at least twice the baseline signal (Sharmila & Mahalakshmi, 2017). Second, an automated Matlab-based classifier was created and trained on 4-AP-specific ictal events using time and frequency domain features (Chang et al., 2019). Finally, a custom linear classifier was designed to separate and assess high theta events from the *Panx1*^{-/-} animals into seizure and non-seizure states, similar to those previously described for the classification of EEG signals (Ahammad et al., 2014). Note that coding for all classifiers was completed by Mark Aquilino in Dr. Peter Carlens' lab. Features used for developing classifiers based upon the extracellular recordings, include the following: events of variable duration were automatically identified based on theta frequency (4–8 Hz) power greater than twice the average of a one-minute baseline. Once a high-theta event was identified, frequency information was extracted by performing a Morlet complex wavelet transform (using the basis function `cmor6-0.8125` from Matlab R2016a). Following feature extraction, a subsequent analysis in a linear discriminant classification between two states was performed (via Matlab R2016a function “`classify`”). In order to provide a training set for the linear classifier, all high-theta events in control animals exposed to 4-AP were used (including events defined as SLEs) (A. W. L. Chiu et al., 2006).

2.2.4. Analysis of Phase-Amplitude Cross-Frequency Coupling

Local field recordings were processed in 10s windows with a Morlet complex wavelet transform (using the basis function `cmor6-0.8125` from Matlab R2016a) to extract phase and amplitude information of frequencies between 1–500 Hz. The strength of phase-amplitude coupling (PAC) between low-frequency phase information and high-frequency amplitude was measured using the method by Tort et al. (Tort et al., 2010). These strengths were then clustered into groups based on frequency bands.

The frequency bands were delineated as follows: Delta (1–4 Hz), Theta (4–8 Hz), Alpha (8–13 Hz), Beta (13–30 Hz), Gamma (30–80 Hz), High Frequency (HF, 80–120 Hz), Very High Frequency (vHF, 120–500 Hz). For recordings under the 4-AP condition, unless no SLEs were detected, only windows classified as SLEs by both digital classifiers outlined above were selected

for analysis. The median PAC of each 10s window under 4-AP was z-scored relative to windows taken from its baseline and set to a threshold of 6 standard deviations above baseline.

2.2.5. Pharmacology

All chemicals were purchased from Sigma-Aldrich (Mississauga, Canada). Brilliant Blue-FCF (BB), also known as FD&C Blue No. 1 (*in vitro*, 10 μ M in bath perfusate), dosage was selected based on an effective dose-response curve (Whyte-Fagundes et al., 2018) and previous trials with the structural counterpart, BBG (J. Wang et al., 2013b). Probenecid (Pb; 500 μ M, *in vitro* in bath perfusate) (Murana et al., 2017). 4-aminopyridine (4-AP, *in vitro*, 100 μ M in the bath perfusate) was used as a convulsant to induce seizure-like events (SLEs) by blocking voltage gated potassium channels and prolonging action potentials of neurons, facilitating the nonspecific release of neurotransmitters (Gupta, 2014).

2.2.6. Electrophysiological and Statistical Analysis

Analysis of electrophysiological recordings was performed in Matlab R2016a (Mathworks). All statistical testing was performed in Matlab R2016a (Mathworks) and Prism (GraphPad). Values are reported as mean \pm standard error of the mean (SEM, where n = number of trials) unless otherwise stated. A one- or two-way ANOVA was performed, followed by Bonferroni's or Dunnett's post-hoc tests. In testing the significance of changed incidence of SLEs, a Fisher's Exact test was used with a confidence interval (CI) of 95%.

2.3. Part III: Materials and Methods used to investigate the role of Panx1 in pathology: Epilepsy

2.3.1. Fish husbandry and embryo collection

All zebrafish (*Danio Rerio*) of strain Tupfel long fin (TL) were obtained from Dr. Wen's laboratory (Zebrafish Centre for Advanced Drug Discovery, St. Michael's Hospital, Toronto, ON). Fish were maintained in a recirculation system (Aquaneering Inc., San Diego, CA) at 28⁰C on a 14 hours light/10 hours dark cycle. Experiments and procedures with animals were performed at York Universities zebrafish vivarium or a licensed S2 biosafety lab according to the CACC guidelines of the Canadian Council for Animal Care (CCAC) after approval of the protocol by the Animal Care Committee (ACC) (GZ#2014-19 (R3)) and York Biosafety Committee (YUBC) (Permit#04-11). The number of experiments, including zebrafish larvae, was kept to the necessary minimum.

Embryos obtained were reared in Egg water (**Supplementary Table 2.4**) according to standard protocols put in place by the staff in York University vivarium. All *panx1* mutant lines were generated in house, project piloted by Dr. Nickie Safarian, see TALEN design and constructs used for *panx1*^{-/-} lines below.

2.3.2. TALEN design

Potential TALENs target sites were identified using Mojo Hand software (<http://talendesign.org>) (Neff et al., 2013). TALENs targeted exon 4 for both *panx1a* (NM_200916.1) and *panx1b* (NM_001100030.2) (**Figure 2.4a**). The following criteria were used for TALEN design: TALENs target sites were 15-17 bases long with an initial 5' T nucleotide to the TALE domain. The spacer length was restricted to 15-16 base pairs. Target sites with a unique restriction enzyme sequence located in the middle of the spacer sequence were selected to simplify screening for insertion-deletion (indel) mutations. The specificity of selected TALENs target sequences was determined using the BLAST interface built into the Mojo Hand software (see **Figure 2.4b,c** for TALENs specific sequences).

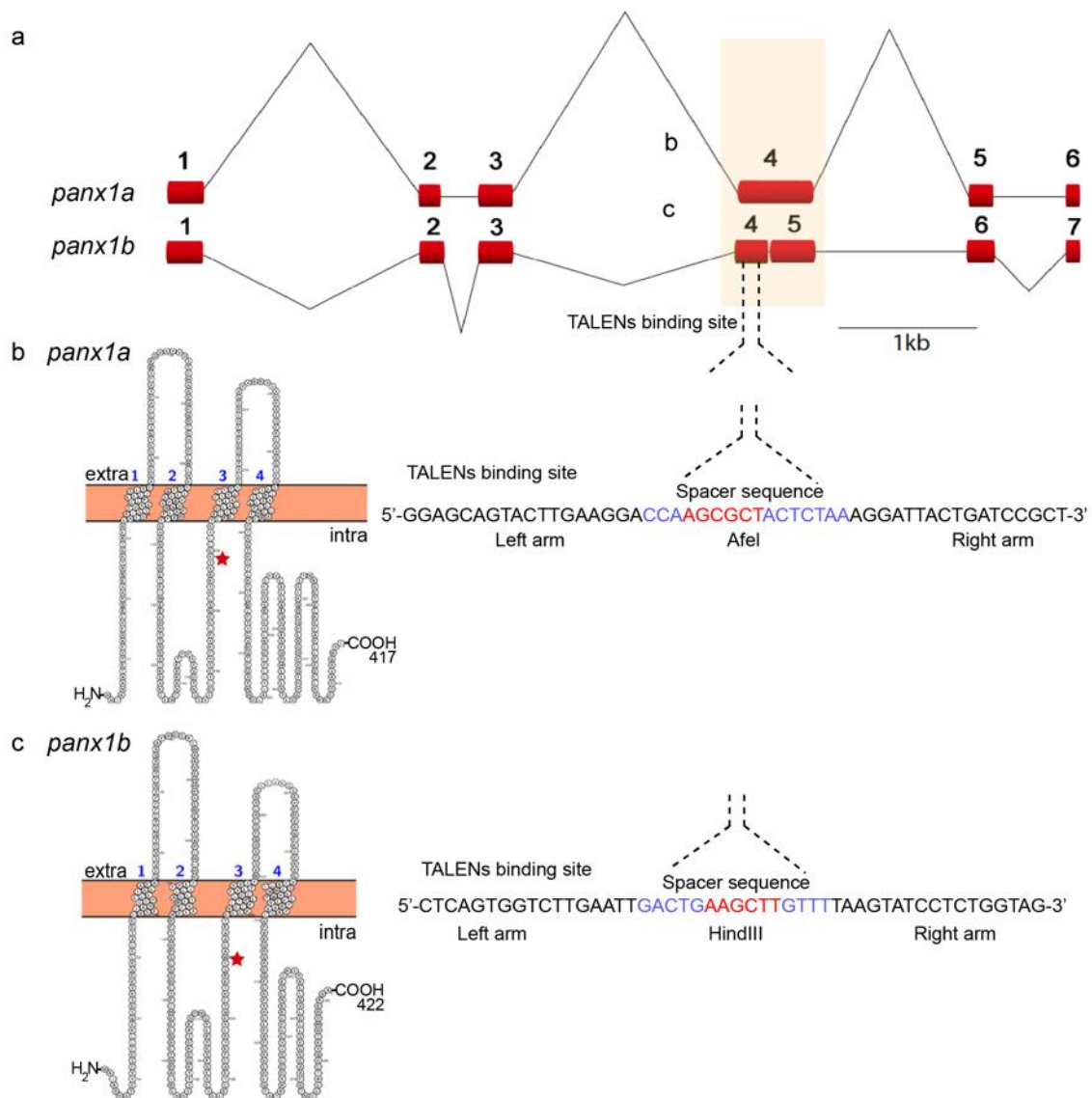


Figure 2.4. TALEN design. a) The zebrafish *panx1a* (top) and *panx1b* (bottom) gene structure with six and seven coding exons, respectively, highlighting that exon 4 was targeted for both *panx1* genes for knockout. b) The predicted sequence features of *panx1a* were visualized with the Protter open-source tool (wlab.ethz.ch/protter) and depicted on the left. A 4 bp deletion in *panx1a* exon 4 resulted in a frameshift causing a premature stop codon at amino acid 195 (site indicated by the red star). The left and right TALENs sequence is shown with the spacer sequence (blue) and Afel restriction site (red) highlighted on the right. c) The predicted sequence features of *panx1b* were visualized with the Protter open-source tool (wlab.ethz.ch/protter) and depicted on the left. An 11 bp deletion in *panx1a* exon 4 resulted in a frameshift causing a premature stop codon at amino acid 196 (site indicated by the red star). The left and right TALENs sequence is shown with the spacer sequence (blue) and HindIII restriction site (red) highlighted on the right.

2.3.3. TALEN constructs

TALEN constructs were synthesized in Dr. Stephen Ekker's lab (Mayo Clinic Cancer Center, Rochester, MN). TALEN assemblies of the repeat-variable di-residues (RVD-containing repeats) were conducted using the Golden Gate approach (Cermak et al., 2011). TALE repeats were cloned in pT3TS-GoldyTALEN expression vectors (Bedell et al., 2012; A. C. Ma et al., 2013; A. C. H. Ma et al., 2016), which were linearized with the SacI restriction endonuclease (ThermoFisher Scientific, Canada) for 15 min at 37°C and used as templates for *in vitro* transcription. Capped cRNAs were synthesized from TALEN pairs mixed 1:1 using the mMMESSAGE mMACHINE T3 Transcription kit (Life Technologies, Canada) and the two TALEN cRNAs were mixed and purified using the Oligotex mRNA Mini Kit (Qiagen Inc., Toronto, Canada). TALEN cRNAs were diluted in DNase/RNase-free water (Life Technologies) to the final concentration of 1 µg/µL and stored at -80 °C before microinjection.

2.3.4. TALEN microinjection and genotyping

One-cell stage zebrafish embryos were microinjected with TALEN cRNAs pair at doses ranging from 30-100 pg/nl. The toxicity of the injected cRNAs was determined at 24 hours post fertilization (1dpf) by calculating the proportion of healthy, dead, and malformed embryos at each dose. The concentration that resulted in more than 50% post-injection survival was selected for further injections. Genomic DNA (gDNA) was extracted from groups of 10 injected embryos at 4dpf to examine the TALEN mutagenesis efficiency. Individual larvae were incubated in 100mM NaOH at 95°C for 15 min. After cooling to room temperature, one-tenth of the 1 M Tris (pH8.0) volume was added to the extracts to neutralize the NaOH (Meeker et al., 2007). Finally, 1 volume TE buffer pH8.0 was added, and gDNAs were stored at -20°C. PCR was used as a screen to detect a small indel mutations followed by AfeI (for *panx1a*) or HindIII (for *panx1b*) restriction enzyme (RE) digests. Indel mutations were confirmed by sequencing (Eurofins Genomics LLC, KY, USA) of gel-purified PCR products cloned into the pJet1.2 cloning vector (Life Technologies).

2.3.5. Generation of *panx1*^{-/-} zebrafish lines

Adult mosaic zebrafish (First generation (F0)) were anesthetized in pH-buffered 0.2 mg/ml ethyl 3-aminobenzoate methanesulfonate solution (MS-222, Sigma-Aldrich). The caudal fin (2 mm of the end) was removed using dissecting scissors (WPI Inc., FL, USA) and placed into 1.5 ml collecting tubes. The fin gDNA was isolated and screened for indel mutations as described above

(Bedell et al., 2012). Adult F0 zebrafish with a mutation in the related locus were out-crossed to wild-type (WT) TL zebrafish and their F1 offspring were analyzed by PCR and *AfeI/HindIII* restriction digestions to verify germline transmission of mutations. Heterozygous (*panx1a*^{+/-}, *panx1b*^{+/-}) F1 mutants were in-crossed to establish homozygous F2 mutants (i.e., *panx1a*^{-/-} and *panx1b*^{-/-}). To produce double knockout (DKO; lacking both *panx1* genes: *panx1a*^{-/-}/*panx1b*^{-/-}) fish, two rounds of inbreeding were performed. First, F3 *panx1a*^{-/-} fish were in-crossed with the *panx1b*^{-/-} mutants. Next, the heterozygous F4 progenies (i.e., *panx1a*^{+/-}/*panx1b*^{+/-}) were in-crossed, and the F5 fish bearing the homozygous mutations in both loci (i.e. *panx1a*^{-/-}/*panx1b*^{-/-}) were selected (by gDNA screening) to produce DKO model.

All experiments described were performed with progenies of >F4 generations. Later generations were routinely tested for the identity of the genotype.

2.3.6. *In vivo* electrophysiology

Zebrafish larvae 7 days post fertilization (dpf) were briefly anesthetized using 0.3mM pancuronium bromide (Panc) (Sigma-Aldrich) for 2-3 min until there was no touch response. Anesthetized larvae were immobilized in freshly prepared 2% low melting temperature agarose with the dorsal aspect of the larvae oriented to the gel surface using an Olympus dissecting microscope. Embedded larvae were placed on the upright stage of an Olympus BX51 fluorescence microscope. 1mL of egg water (E3; pH 7.2-7.4) was applied to the agar topically. Under direct visual guidance a glass microelectrode (1.2mm OD, approximately 1μM tip diameter, 2-7MΩ), backloaded with 2M NaCl, was placed into the right optic tectum. Local field potentials were recorded using a Multiclamp 700B amplifier (Axon Instruments, San Jose, CA, USA), low-pass filtered at 1kHz (-3 dB; eight-pole Bessel), high-pass filtered at 0.1 Hz, digitized 10 kHz using a Digidata 1550A A/D interface and stored on a PC computer running pClamp11 software (all Axon Instruments). Basal activity was recorded for 10 minutes under Light-ON conditions (1000 lux), during which images of the electrode placement were taken for reference. Then, 1mL of E3 containing PTZ, for a final concentration of 15mM, was added topically to the agar and recorded for an hour under Light-ON conditions to monitor fish viability. Seizure activity was normalized to the baseline activity of each individual fish in order to account for biological variance. In experiments testing treatment drugs, zebrafish larvae were exposed to egg water containing 75μM

Pb or 5mM VPA at the start of baseline recordings, 10min prior to the application of PTZ. Refer to **Figure 2.5** for a schematic of *in vivo* electrophysiological workflow.

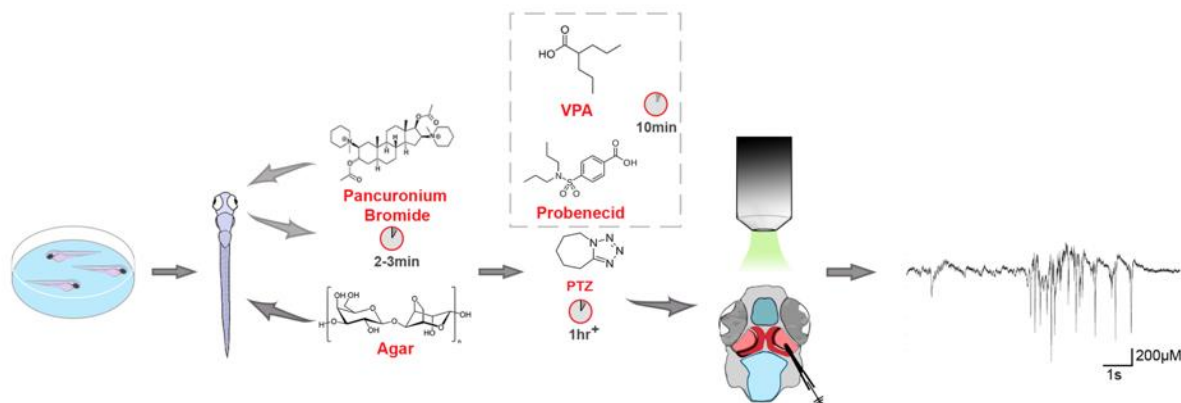


Figure 2.5. *In vitro* electrophysiology schematic. Outline of depicted workflow from left to right: collect individual zebrafish larvae, anaesthetize with pancuronium bromide, remove and apply agar to immobilize, apply egg water containing experimental treatments (i.e. VPA, Pb, PTZ; if VPA or Pb were tested with PTZ they were applied 10min ahead of PTZ application, otherwise they were recorded for an hour without PTZ) topically to larvae, insert recording electrode under visual guidance into the optic tectum (coral). Sample seizure-like (ictal-like) event depicted here (condition: TL larvae with PTZ treatment).

2.3.7. Seizure-like event detection and power spectral density

Ictal-like event identification was determined as high frequency events with large amplitudes (3 times the standard deviation of the baseline activity), polyspikes, and a duration of 3 seconds or greater. Inter-ictal-like events were identified as high-frequency events, with shorter amplitude compared to ictal-like events, but greater than baseline activity (minimum 1.5 times the standard deviation of baseline), and much shorter in duration (1-3 seconds). To account for variability between fish, seizure-like activity for each animal was normalized to its own baseline activity. Event detection was automated using custom developed codes in Matlab R2019b (Colic et al., 2013; Hunyadi et al., 2017; Jacobs et al., 2019; further details in chapter 5) and visually confirmed. Events were quantified for comparison across genotypes and measured for significance using the Mann-Whitney test.

Power spectral density (PSD) estimation was performed by Welch's method for baseline and PTZ recordings. A moving window for fast Fourier transform (FFT) computation was used and all windows were averaged. Changes in delta power were determined using the area under the power spectrum between 1-4Hz, calculated using the trapz function in Matlab R2019b. PSD was

measured for significance using a one-way ANOVA (between genotypes) or an unpaired t-test (between treatments) and presented as the mean \pm SEM.

2.3.8. Behavioural locomotor assays

The ZebraBox behaviour system and the ZebraLab analytical suite was used for automated observation and video tracking locomotor activity of 7dpf zebrafish larvae in clear 96 well plates maintained at 28°C (ViewPoint Life Technology, Lyon, France). Rest and baseline locomotor activity for TL and *panx1*^{-/-} larvae (n = 70 per group) were recorded for 25 and 30min respectively, prior to drug administration of PTZ. PTZ was added to the bathing medium for a final concentration of 15mM and recorded for 1hr. For treatment conditions with Pb (75µM final concentration), VPA (5mM final concentration) and A-438079 (100µM final concentration) (n = 36 per group), drug application occurred 30min prior to PTZ. VPA (Baraban et al., 2005) and A-438079 (Donnelly-Roberts et al., 2019) concentrations were chosen based upon previous reports. Pb concentration was selected based upon literature (Silverman et al., 2008; de Marchi et al., 2019) and behavioural dose-response tests conducted in lab with TL larvae (**Figure 2.6**). Refer to **Figure 2.7** for a schematic of behavioral locomotor assessment workflow.

Tracking videos were recorded at 30 frames per second (fps) with a lightbox that provided visible light at 30% of the final output intensity, considered ambient light. For analysis, the activity score generated by the software was extracted which was indicative of the total pixel change based on the activity of an individual larva (Δ pixel \pm s.e.m.; n = 36 per group). The Areas Under the Curve (AUCs) were determined from activity plots and analyzed by one-way ANOVA followed by a Tukey's multiple comparison test, via an unpaired t-test or a Mann-Whitney test. Videos were blindly monitored in order to score behavioural seizure-like manifestations (further details below). Behavioural data were analysed using repeated-measurements two-way ANOVA with a Bonferroni's multiple comparison.

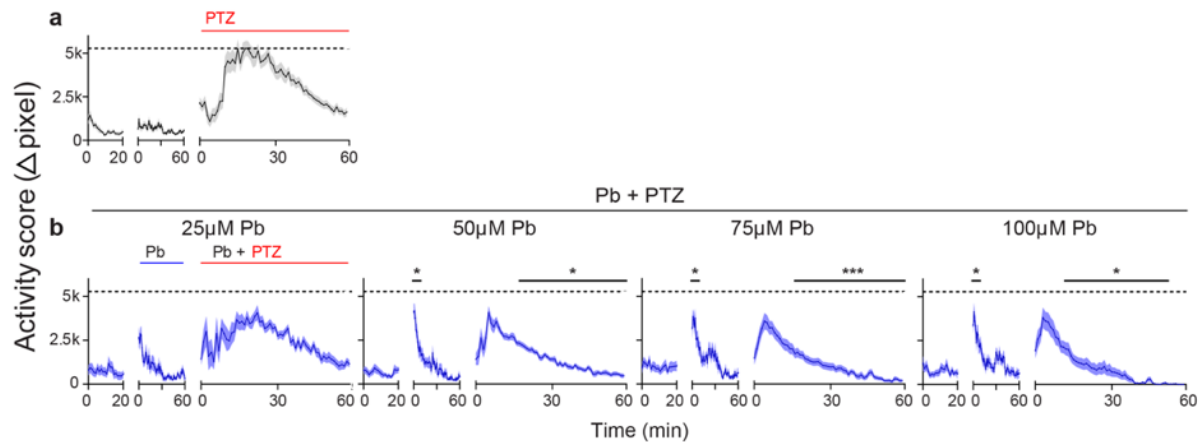


Figure 2.6. Concentration dependent reduction of PTZ-related hyperactivity in TL larvae by Probenecid. a 7dpf TL larvae ($n = 30$) were treated with 15mM PTZ, or b incubated with 25 μ M, 50 μ M, 75 μ M, and 100 μ M Probenecid (Pb; $n = 18$ per concentration) one hour before treatment with PTZ. Pb significantly increased activity (Δ pixel; mean \pm s.e.m.) compared to baseline, and significantly reduced PTZ-induced activity above 50 μ M. Pb applied at 75 μ M reduced PTZ-induced activity, without the evidence of substantial toxicity (activity level 0 within one hour). Dashed lines indicate max average activity for PTZ treated TL. * $p < 0.05$, *** $p < 0.001$.

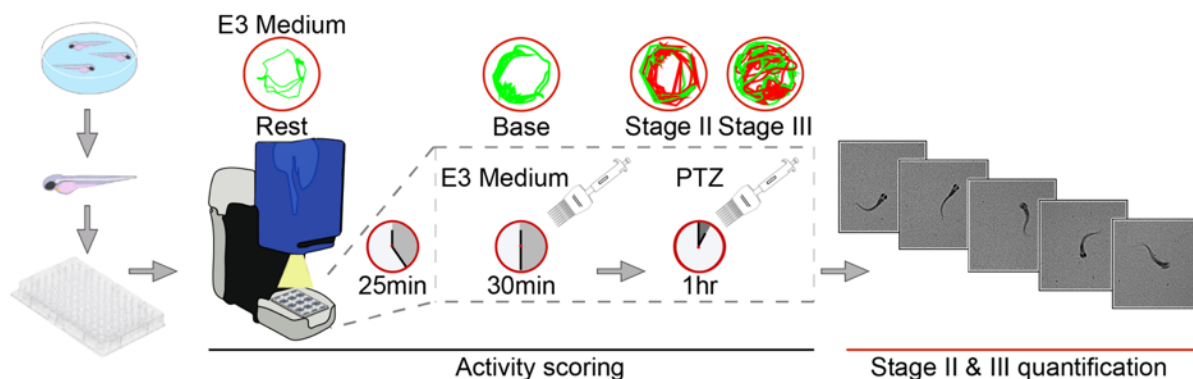


Figure 2.7. Workflow for behavioral locomotor assessments in zebrafish larvae. Outline of behavioral assay workflow from left to right: individual larvae were collected and transferred to a clear 96well plate (1 larvae/well) maintained in the Zebabox at 28°C. Larvae were in the Zebabox at rest in egg water (E3 medium) for 25min to adapt to the environment. E3 medium was added and they were tracked for 30min in 30% light to gather baseline activity, PTZ was then added to induce seizure-like activity (stage II and III activity visible by the tracking plots above). If Pb or VPA were tested they were added after E3 medium and activity was recorded for 30min. During tracking for activity scoring, videos were also recorded in order to allow quantification of stage II and III seizure-like events.

2.3.9. Stage II and III seizure-associated behaviour scoring

Video recordings and tracking data of 7dpf TL and *panx1*^{-/-} larvae ($n=16$ per group) were exported from ZebraLab software and utilized for scoring 3 stages (Stage I – III) of seizure-related behaviour, based upon previously published work (Baraban et al., 2005; Bergham et al., 2007). Stage I is behaviourally presented as an increase in locomotor activity (a.u), activity thresholds

were defined as slow (<2mm), and fast (>20mm) and represented as overall activity over time that was retrieved as an output of from the Zebbox. Since stage I is described as excessive hyperactivity but is ambiguous to score based on lack of quantifiable features, it is represented in the first 10min of all activity plots as the sharp increase in locomotor activity but is not scored separately. Stage II and III were manually and blindly scored for an hour after the application of PTZ. Stage II is presented as “whirlpool-like’ circular swimming around the perimeter of the well and stage III as clonus-like convulsions which were defined by periods of bursting activity followed by immobility and loss of posture. Stage II and III were scored at 2min intervals for a total of one hour after PTZ application. Events were analyzed via repeated-measurements two-way repeated measures ANOVA with a Greenhouse-Geisser correction.

2.3.10. Survival assessment

7dpf TL and *panx1*^{-/-} larvae (n=80 per group, per treatment/condition) were assessed for survival under brightfield microscopy every hour for a total of ten hours and once 24-hours after the application of PTZ. Assessment included examination for circulation/heartbeat, as well as body movement or a touch response, and degradation. Group survival rates were analyzed with the log-rank (Mantel-Cox) test and plotted as Kaplan Meier curves.

2.3.11. Extracellular ATP assay

Larvae were collected (~50 pooled larvae per sample), water was completely removed, and samples were weighed prior to being flash frozen and stored at -80°C. Treated larvae were incubated in a 6cm dish containing 15mM PTZ and/or 75µM Pb for 1hour at 28°C prior to collection. Pooled samples of larvae were homogenized in phosphate-buffered saline (PBS) containing 100µM ARL-67156 (Sigma-Aldrich) and Halt Protease inhibitor (Thermo-Scientific) (1:100), to prevent excessive proteolytic and ATP degradation, for 1min at 30Hz using the TissuelyserLT (Qiagen) set to 4°C. Homogenates were transferred to cold Eppendorf tubes (-20°C) and centrifuged at 12KRPM for 2min. Supernatants were collected and immediately used to measure extracellular ATP performed in 96-well format (Greiner Bio-One) using the Molecular Probes® ATP determination Kit as described by the manufacturer (Life Technologies) (refer to **Figure 2.8** for workflow). Samples were measured in replicates of 6 using the Synergy H4 Hybrid Multi-well Plate Reader (Biotek) as reported previously (Whyte-Fagundes et al., 2018). ATP

concentrations in experimental samples were determined from ATP standard curves (concentrations ranging from 0-1 μ M) included with each assay. To ensure standardized assay performance PBS, PTZ and PTZ +1 μ M ATP control wells were also included. The Gen5 Data Analysis Software (Biotek) was used to complete data exportation and to set luminescent assay parameters; internal temperature set to 28 $^{\circ}$ C, a low intensity shake of the plate for 3s prior to reading, a 5s integration time per well and gain setting at 150. Data was exported and analyzed in Excel and Matlab. Graphpad's estimation plot feature was used to test for statistical significance between and within treatment groups. ATP was presented as a normalized concentration per mg of protein to account for biological variance in larval size as we determined that there was a linear relationship between the weight of pooled larvae and the homogenate protein content (**Figure 2.9**).

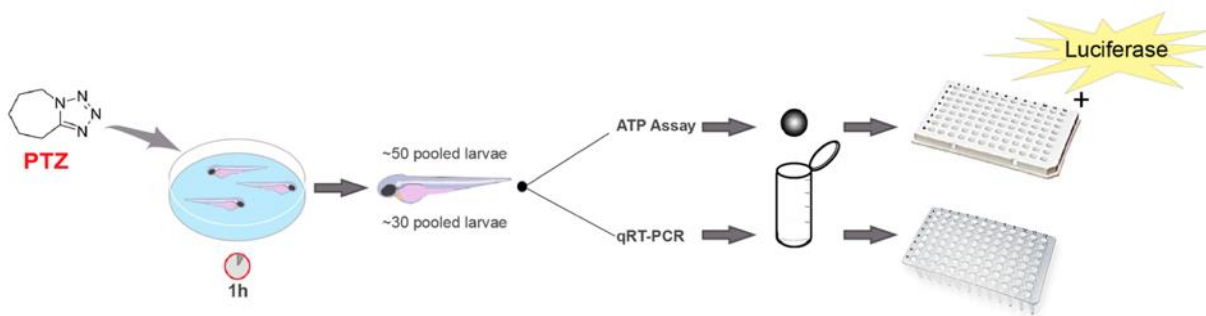


Figure 2.8. Method workflow for molecular assessments in zebrafish larvae. This schematic demonstrates the workflow from left to right for molecular investigations of zebrafish larvae challenged with PTZ: larvae were incubated in egg water with and without 15mM PTZ for 1hr and maintained at 28 $^{\circ}$ C. For treatment conditions with Pb, Pb was added 30min prior to PTZ. Larvae were collected (n = 50 pooled for ATP assays, n = 30 pooled for qRT-PCR) in Eppendorf tubes and all water was removed. Pooled larvae were weighed, and flash frozen prior to homogenization for ATP or PCR analysis. ATP was measured using a luciferase ATP determination kit.

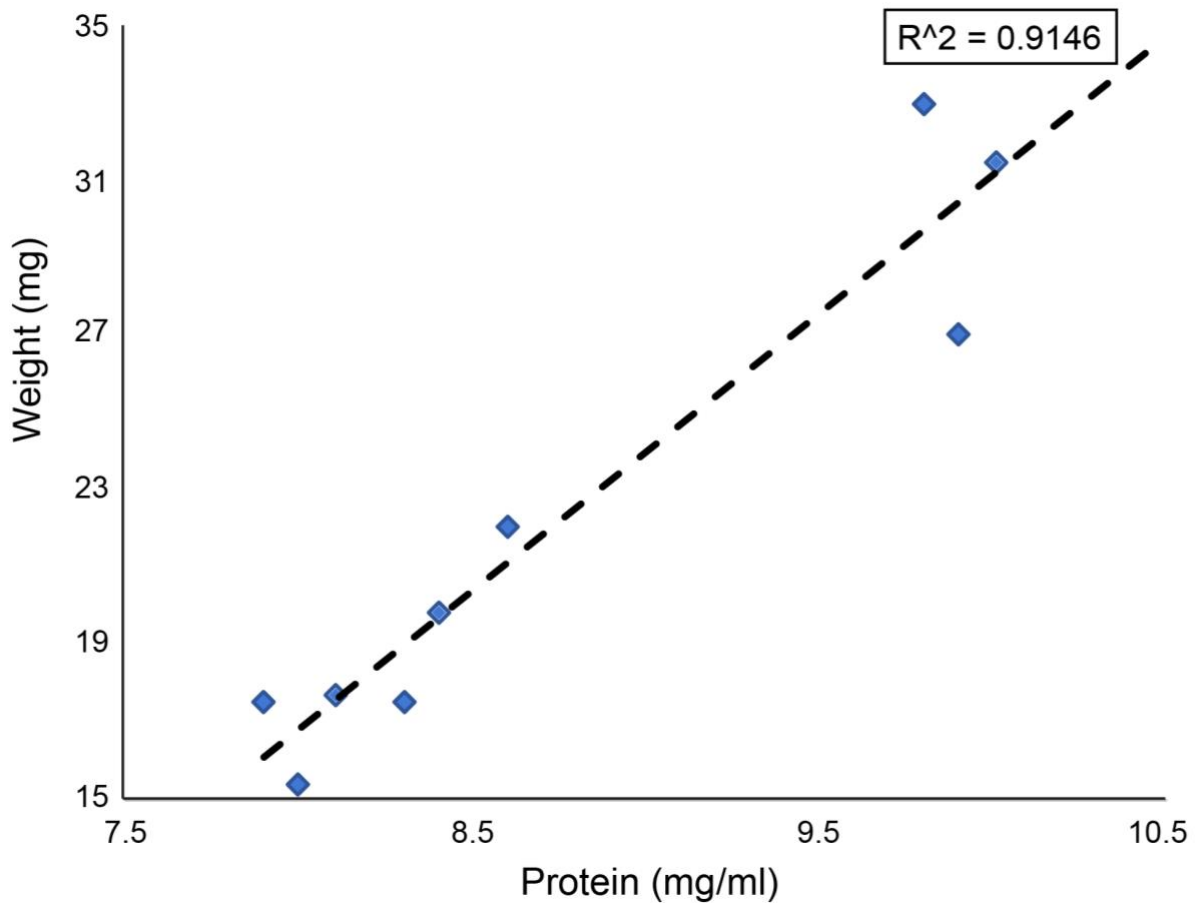


Figure 2.9. Linear correlation of larval weight and protein concentration. Plotting the weight of pooled larvae ($n = 50$ larvae/sample) in mg against the amount of protein in mg/ml that was measured from the supernatant of the homogenate with a spectrophotometer demonstrates a clear linear relationship ($R^2 = 0.9146$). Therefore, ATP concentrations were plotted per protein content in order to account for biological variance of larval weight.

2.3.12. Protein quantification

A NanoDrop Spectrophotometer Protein a280 protocol was used to measure protein content (mg/ml) in $2\mu\text{L}$ of supernatant from homogenized samples. Samples were recorded three times to ensure there was no variability. The final ATP content was expressed with respect to the amount of protein content in each sample of pooled larvae.

2.3.13. RNA-seq Analysis

The RNA library preparation was performed following the NEB NEBNext Ultra II Directional RNA Library Preparation protocol (New England Biolabs Inc., Ipswich, MA, USA). The data derived from the sequencing of three independent pools of ~ 30 age matched larvae (6dpf). RNA libraries were loaded on a Bioanalyzer 2100 DNA High Sensitivity chip (Agilent Technologies)

to check for size, quantified by qPCR using the Kapa Library Quantification Illumina/ABI Prism Kit protocol (KAPA Biosystems, Wilmington, MA, USA). Pooled libraries were paired-end sequenced on a High Throughput Run Mode flow cell with the V4 sequencing chemistry on an Illumina HiSeq 2500 platform (Illumina, Inc., San Diego, CA) following Illumina's recommended protocol to generate paired-end reads of 126-bases in length. The post-sequencing processing to final read counts, normalization, and differential gene expression analysis used multiple software packages, included RSEM version 1.3.3 (<http://deweylab.github.io/RSEM/>) and bowtie2 version bowtie/2.3.4.2 (<http://bowtie-bio.sourceforge.net/index.shtml>) to estimate the expression level of each sample. For each sample, RSEM reports read counts, estimated lengths and FPKM for each transcript and gene. For differential expression analysis estimated read counts for each transcript from RSEM output were compiled. This transcript expression matrix was supplied to DESeq2 (<https://bioconductor.org/packages/release/bioc/html/DESeq2.html>) v.1.22.2 to detect differentially expressed transcripts. Filtering of the low expressed transcripts to increase power was automatically applied via independent filtering on the mean of normalized counts within the DESeq results() function. Note: The transcripts that are filtered out have padj (FDR) value of "NA". The final output of the *DESeq2 results included* TranscriptID, GeneID – Ensembl IDs; GeneVersion, GeneName, GeneBiotype, baseMean - Mean of normalized counts for all samples; log2FoldChange - Log2 fold change; lfcSE - Standard error; stat - Wald statistic; *p*-value - Wald test *p*-value; padj - Benjamini+ Hochberg multiple testing; BH adjusted *p*-values.

2.3.14. Transcriptome analysis

The transcriptomes of all zebrafish lines (*Panx1a*, *Panx1b*, and DKO) were analysed by RNA-seq (NGS-Facility, The Center for Applied Genomics, SickKids, Toronto, ON). Genes that were significantly regulated according to the padjusted value (<0.05) were organized by up (>1) and down (<-1) regulation based on the associated logFC value. Gene ontology (GO) enrichment of biological processes from the FishEnrichR database were established using these two gene lists for each genotype. Relevant biological processes, related to the nervous system and *panx1*, were categorized into broader GO terms for analysis and presentation. Clustergrams were produced for differential expression analysis using curated gene lists and procedures implemented in the Matlab2019b Bioinformatics toolbox using Euclidean distance for hierarchal clustering.

2.3.15. RNA extraction and RT-qPCR on immediate-early genes (IEGs)

Total RNA was extracted from TL and all *panx1*^{-/-} zebrafish larvae (7dpf) using the RNeasy Plus Mini Kit (Qiagen) (n=30 pooled larvae per sample). The iScript Reverse Transcription Supermix (Bio-Rad Laboratories, Mississauga, Canada) was used to reverse transcribe 1µg of total RNA. The cDNA equivalent of ~133ng was analyzed by quantitative Real Time-PCR using the SsoAdvanced SybrGreen PCR mix and a Bio-Rad CFX96 real time PCR system as described by the manufacturer (Bio-Rad). All experiments represent three independent RNA preparations from TL and *panx1*^{-/-} lines, each analyzed in triplicate. Each experiment included a melt curve analysis of PCR amplicons generated in each reaction. Raw cycle threshold values (Ct-values) were exported from the CFX Manager Software (Bio-Rad, Canada). Expression ratios of IEGs for PTZ-treated (1hour) larvae were analyzed against their respective nontreated controls using the Relative Expression Software Tool (REST-2009) software (Pfaffl et al., 2002). The statistical significance was tested by a Pair Wise Fixed Reallocation Randomisation Test[®] and plotted using standard error (SE) estimation. All primers (**Supplementary Table 2.5**) were designed using the Real-Time qPCR Assay design tool and were synthesized by the same provider (Integrated DNA Technologies, Toronto, Canada).

2.3.16. Molecular modelling

Protein sequences were aligned initially with Clustal Omega (Sievers et al., 2018): human PANX1 (Uniprot: Q96RD7), zebrafish Panx1a (Uniprot: Q7ZUN0) and Panx1b (Uniprot: F1QSR7). Using the alignment as a guide, zebrafish Panx1a and Panx1b were then threaded into the cryo-EM structure of human PANX (PDB:6LTO) using SWISS-MODEL (Waterhouse et al., 2018). Using the FixBB module of Rosetta v3.12 (Kuhlman et al., 2003), the side chains of amino acids 74 and 75 were altered and repacked following along the standard rotamer selection parameters of the program. The diameter of the extracellular gate was measured with PoreWalker (Pellegrini-Calace et al., 2009).

2.3.17. Pharmacology

All chemicals were purchased from Sigma-Aldrich (Mississauga, Canada): Pentretetrazol (PTZ; 15mM; cat#P6500), Pancuronium bromide (Panc; 300µM; cat#P1918), Probenecid (Pb; 75mM; cat#P8761), and Valproic Acid (VPA; 5mM; cat# P4543). All concentrations referred to in the results are final.

Seizure-like activity is chemically induced in this model when PTZ acts trans-synaptically by blocking gamma aminobutyric acid (GABA)-A receptors and thereby inhibiting dominant inhibitory networks. Characteristic seizure-like events induced by 15mM PTZ demonstrate an initial action potential burst followed by short paroxysmal action potential bursts, representative of a seizure pattern. It is important to note that PTZ was chosen as a convulsant method in the fish because it induces similar results in mammals physiologically and behaviorally (Baraban et al., 2005; Grone & Baraban, 2015).

2.3.18. **Statistical analysis**

All statistical analyses were performed in Matlab R2019b or in Graph Pad. Results are represented as the mean \pm standard error of the mean (SEM). For each analysis, a minimum of $n \geq 3$ independent experimental replicates were generated. A p-value <0.05 was considered statistically significant. Unless otherwise stated, the Mann-Whitney test (nonparametric) and two-way repeated measures ANOVA (parametric) with the Greenhouse-Geisser correction followed by a Bonferroni's multiple comparison test were used. The number of samples were reached when calculated statistical power was satisfied to ensure biological reproducibility (G*Power analysis confirmed the statistical power and the required sample size of the acquired data (Faul et al., 2007)). For all experiments, sample sizes are indicated in the figure legends.

2.4. **Part IV: General materials and methods used**

2.4.1. **Biosafety**

The research projects completed in this thesis were performed in accordance with federal, provincial and institutional regulations for the containment Level 2 Laboratories located at the Life Science Building (LSB), Department of Biology at York University.

2.4.2. **Organisms**

Handling, manipulation, storage and housing of all recombinant bacterial or eukaryotic cell lines, as well as zebrafish, was performed in licensed S2 laboratories located at the Department of Biology at York University, Toronto, Ontario. Handling, manipulation, storage and housing of mice was performed in licensed S2 laboratories located at both York University and Krembil Discovery Tower, Toronto, Ontario.

2.4.2.1. Bacterial strains

Escherichia coli (*E. coli*) DH5 α (Invitrogen, Burlington, Canada)

Genotype: F Φ 80*lacZ* Δ M15 Δ (*lacZYA-argF*) U169 *recA1 endA1 hsdR17* (*r_K⁻, m_K⁺*)
phoA supE44 thi-1 gyrA96 relA1 λ ⁻

E. coli NEB 5-alpha competent (New England Biolabs, Whitby, Canada)

Genotype: *fhuA2 Δ (argF-lacZ)U169 phoA glnV44 Φ 80 Δ (lacZ)M15 gyrA96 recA1 relA1 endA1 thi-1 hsdR17*

2.4.2.2. Eukaryotic cells

Neuroblastoma 2a cells (Neuro2a or N2a cells) were derived from *Mus musculus*, which were developed by Klebe and Ruddle in 1967 from a strain of A albino mouse spontaneous tumor. Neuro2a cells used in this thesis were generously provided by Dr. David C. Spray (Albert Einstein College of Medicine, NY, USA)

2.4.2.3. Mice

Handling and housing of mice used to complete this thesis was performed in compliance with the guidelines and policies of the Canadian Council on Animal Care (CCAC) and had formal approval by the Animal Care Committee (York University & The University Health Network, Toronto, Canada). Animals were maintained in a vivarium with a 12-hour light/dark cycle and had free access to food and water. For experiments related to the investigation of the olfactory system, only male mice were used. For behavioural testing, adult mice (4-8 months) were housed individually 1 week prior to, and during, testing. For molecular biological techniques, RNA was isolated from adults, and immunohistochemistry was performed on both adults and juveniles (3 weeks). For experiments related to the investigation of epilepsy, there was no preference for sex, and mice ranged from P14-25 days. For all experiments, *Panx1* knockout (*Panx1*^{-/-}) mice were used (generation described in brief below) along with a control wildtype (*Panx1*^{+/+}) line of the same background (C₅₇Bl/6) (Charles River Laboratory). All experiments and procedures were within CACC guidelines.

The generation and initial characterization of *Panx1*^{+/+} mice (*Panx1*fl/fl) with three LoxP consensus sequences integrated into the *Panx1* gene flanking exon 3-4, and knockout mice with global loss of *Panx1* (*Panx1*^{-/-}, CMV-Cre/*Panx1*) was described previously (Grundken et al., 2011; Dvorientchikova et al., 2012; Prochnow et al., 2012) and provided to our lab courtesy of Dr. Valery Shestopalov (University of Miami, FL, USA) from the Bascom Palmer Eye Institute at the

University of Miami. Panx1 expression in tissues is ubiquitous, however, no major abnormalities were noted in the overall health or anatomy of the Panx1^{-/-} mice.

2.4.2.4. Zebrafish

Handling and housing of zebrafish (*Danio rerio*) used to complete this thesis was performed in compliance with the guidelines and policies of the Canadian Council on Animal Care (CCAC) and had formal approval by the Animal Care Committee (York University, Toronto, Canada). Fish were maintained in a recirculation system (Aquaneering Inc., San Diego, CA) at 28°C in the vivarium with a 14-hour light/ 10-hour dark cycle. Embryos were reared in E3 medium (egg water, 5.0 mM NaCl, 0.17 KCl, 0.33 mM CaCl₂, 0.33 mM MgSO₄) at a density of approximately 50 embryos per 10 cm petri dish in a 28°C incubator according to standard procedures (Nüsslein-Volhard 2002). Zebrafish larvae 6 - 7 days post fertilization (dpf) were used for experimentation and were housed in 28°C incubators until use. All experiments and procedures were within CACC guidelines.

2.4.3. Antibodies

Supplementary Table 2.1. Description of the primary (top) and secondary (bottom) antibodies used for completion of western blot and IHC for Panx1 localization experimentation in the olfactory system.

Name	Species of Origin	Source	Dilution
anti-GFP (Poly)	Rabbit	Santa Cruz	1:200
Anti-β-actin	Mouse	Sigma-Aldrich	1:3000
anti-Panx1 (Poly)	Rabbit	Dr. S. Penuela UWO	1:200
anti-Panx3 (Poly)	Rabbit	Dr. S. Penuela UWO	1:200
Panx2 42-2800	Rabbit	Invitrogen	1:200
Gαo SC-13532	Rabbit	Santa Cruz	1:100
NF200 clone NE14	Rabbit	Sigma-Aldrich	1:100
Anti-mouse iRDye (Poly) 800	Goat	Li-Cor	1:2000
Anti-rabbit iRDye (Poly) 680	Donkey	Li-Cor	1:3000
Alexa Fluor 488	Goat	Invitrogen	1:1000
Alexa Fluor 568	Goat	Invitrogen	1:1000

2.4.4. Commercial kits

Supplementary Table 2.2. List of kits utilized for various laboratory applications.

Procedure	Kit Name	Company Name
Immunodetection	iBind™ Western Systems	Life Technologies
iBIND Western Blot	iBind™ Solution Kit	Life Technologies
Polymerase Chain Reaction	Phusion High Fidelity PCR Kit	Thermo Scientific
Purification of PCR and DNA fragments	NucleoSpin® Gel and PCR Cleanup Kit	Clontech
DNA transfection	Effectene Transfection Reagent	QiaGen
ATP determination	Molecular Probes® ATP Determination Kit	Life Technologies

2.4.5. Media and Solutions

Supplementary Table 2.3. Solutions used for cell culture.

Solution	Company of retrieval
10% formalin	Sigma-Aldrich
Trypsin	Sigma-Aldrich
PBS with/without calcium/magnesium	Sigma-Aldrich
Penicillin and Streptomycin	BioShop
Fetal Bovine Serum (FBS)	Gibco
Non-essential Amino Acids (NEA)	Sigma-Aldrich
Dulbeccos' Modified Eagles' Medium (DMEM)	Sigma-Aldrich
Mounting Solution: Fluoroshield with DAPI	Sigma-Aldrich
ProLong™ Gold antifade reagent (no DAPI)	Invitrogen
Effectene®	QiaGen
EC Buffer	QiaGen

Enhancer	QiaGen
Dulbecco's Modified Eagle Medium (DMEM)	Sigma-Aldrich
G418	Sigma-Aldrich

Note: composition of growth media for N2a cells: DMEM (4.5 g/l D-glucose, +L-glutamine, - pyruvate) + 10% FBS, 1% L-glutamine, 1% NEA, 1% penicillin/streptomycin (10,000 U/ml/10mg/ml), 1mM Na-pyruvate, used both with and without phenol red – which had additional +1% L-glutamine supplemented.

Composition of Trypsin: 0.05% trypsin, 0.02% EDTA (1x) in D-PBS (PAA)

Composition of PBS: 130mM NaCl, 2.8 mM KCl, 10mM Na₂HPO₄

Supplementary Table 2.4. Composition of solutions used for biological protocols.

Solution	Composition
6x DNA Loading Buffer	10 mM Tris-HCl (pH 7.6), 0.03% bromophenol blue, 0.03% xylene cyanol FF, 60% glycerol, 60 mM EDTA, (Fermentas)
1x Tris-acetate-EDTA (TAE) Gel Loading Buffer	40mM Tris, 20mM acetic acid, 1mM EDTA
Laemmli Sample Buffer	2% SDS, 10% glycerol, 5% β-mercaptoethanol, 0.1% Orange G, 50 mM Tris-HCl: pH 6.8
Laemmli Running Buffer	192mM glycine, 0.1% SDS, 25 mM Tris-HCl: pH 8.3
Staining Solution	Coomassie PAGE BLUE (BioRad)
Blocking Solution	Odyssey Blocking Buffer (Li-Cor Bioscience)
Phosphate Buffered Saline (PBS)	130mM NaCl, 28mM KCl, 10mM Na ₂ HPO ₄ , 1.8mM KH ₂ PO ₄ , pH 7.4
iBIND™ Solution	1% iBind 100X Additive, 20% iBIND 5X buffer
Standard Reaction Solution	8.9 mL dH ₂ O • 0.5 mL 20X Reaction Buffer (Component E) • 0.1 mL 0.1 M DTT (from step 1.3) • 0.5 mL of 10 mM D-luciferin (from step 1.2, store the

	remaining 0.5 mL at $\leq -20^{\circ}\text{C}$ for up to several weeks) • 2.5 μL of firefly luciferase 5 mg/mL stock solution
Ringers	7.2g/L NaCl, 0.17g/L CaCl_2 , 0.37g/L KCl; Dissolve all reagents in dH ₂ O, adjust to 7.3-7.4 pH. Filter through 0.22 μm filter once everything is dissolved
Henkle 100	An odorant solution provided by a company in Germany, used at 1:10000
Potassium gluconate	Used for panx1 stimulation, purchased from Sigma, used at 25mM
ARL 67156 trisodium salt hydrate	Cocktail to prevent ATP degradation purchased from Sigma, used at 100 μM
Halt™ Protease and Phosphatase Inhibitor Cocktail	Cocktail to prevent protein degradation purchased from Thermo Scientific, used at 1:100
Artificial cerebral spinal fluid (ACSF)	119 mM NaCl; 26.2 mM NaHCO_3 ; 2.5 mM KCl; 1 mM NaH_2PO_4 ; 1.3 mM MgCl_2 ; 10 mM glucose; 2.5-mM CaCl_2
Stock salts for E3 medium (egg water)	40g Instant Ocean Salt; 1L Distilled water
E3 medium for raising zebrafish embryos	Add 1.5 ml of stock salts solution to 1 litre of distilled water to reach to a final concentration of 60 $\mu\text{g/ml}$. Methylene blue (10-5%; Sigma Aldrich) was added as a mold inhibitor.
Agar for embedding	Agar Nobel (purchased from sigma) was added to E3 medium for a final 2% concentration to embed larvae for electrophysiology

2.4.6. Genes and Primers used

Supplementary Table 2.5. Summary of genes and primers.

Gene	Gene-ID	Function	Forward Primer (5' – 3')	Reverse Primer (5' – 3')	Application
<i>panx1a</i>	NM_200916	pannexin	AGCTCTGTGATAGAC CTCACTGAGAGC	GATGTAGCTCA GGAGCTGAAAG ATGC	genotyping

<i>panx1b</i>	NM_001 100030	pannexin	AAGTATAAAGGCGTG CGGCTGG	TGATCTGAGTA CCCACGGAGAC	genoty ping
<i>fosab</i>	NM_2055 69	Proto-oncogene, cell proliferation & differentiation	GTGAACGAAACAAGAT GGCTG	TTTCATCCTCAAG CTGGTCAG	IEG
<i>egr1</i>	NM_1312 48	Early growth response 1, transcription regulatory factor	TCAACATATCCCAGTGC CAAG	TGTGTCTGGATG GGTTTCTG	IEG
<i>egr2a</i>	NM_0013 28404	Early growth response 2a	CTTCTCCTGTGACTTCT GCG	GCTTTCTGTCCTT ATGTCTCTGG	IEG
<i>egr2b</i>	NM_1309 97	Early growth response 2b	GATGCGGAGAGGTCTAT CAAG	AGGAGTAGGATG GCGGAG	IEG
<i>egr4</i>	NM_0011 14453	Early growth response 4	ACAGCACCTCAAAGACT ACAG	ACGACAAGGTAA AAGACTGGAG	IEG
<i>jun</i>	NM_1999 87	Jun proto- oncogene, AP1 transcription factor subunit	CACAAGGCTCTGAAAC ACAAC	TGATGCCAGTTT GAGAAGTCC	IEG
<i>bdnf</i>	NM_0013 08648	Brain derived neurotrophic factor	ACAAGCGGCACTATAA CTCG	ACTATCTGCCCT CTTAATGG	IEG
<i>eif4ebp2</i>	NM_2128 03	Eukaryotic translation	AGTGACGGGCAAGAAC ATC	GTTGTTACGTA GGTTCCTCTTC	IEG

		initiation factor 4e binding protein			
<i>knc3a</i>	NM_0011 95240	Potassium voltage-gated channel subfamily c	CCATGATAGGGCCTGCT TC	AGAGATGTTATT GAGGCTGCG	RT- qPCR
<i>scn4bb</i>	NM_0010 77573	Sodium voltage- gated channel subunit 4,	ACCTATGCCAGCTGTAT TGG	CGCTCACGGTAA ATTTGCAC	RT- qPCR
<i>snap25b</i>	NM_1314 34	Synaptosomal- associated protein, regulates intracellular calcium dynamics	TGAGAATTTGGAGCAG GTCG	TGTTGGAGTCAG CCATGTC	RT- qPCR
<i>sema6ba</i>	NM_0013 66315	Semaphorin 6B, axon guidance	TGATGGAGGGCTGTTTG TG	CGTTTGC GTGTTT GGGATC	RT- qPCR
<i>slc8a1b</i>	NM_0010 39144	Sodium-calcium exchanger, transporter member 1	GGAGGGACCAGTTTATT GAGG	GGCACGAAAGCA AAGAGAAC	RT- qPCR
<i>slc8a2b</i>	NM_0011 23284	Sodium-calcium exchanger, transporter member 2	TCACCAATGACCAGACA ACTC	TGCACTCAACTG ACCTTCTG	RT- qPCR

<i>slco2b1</i>	NM_0010 37678	Sodium-calcium exchanger, transporter member 2	AGATGGATTGGTGCTTG GTG	TTCTCAGTTGATG GCTCCAC	RT- qPCR
<i>caena1da</i>	NM_2034 84	Voltage- dependent l-type calcium channel subunit	GGATGAGAAGGATAAT GCCGAG	GGGTTTGTGTTG CTGAAGATG	RT- qPCR
<i>grin2bb</i>	NM_0011 28337	Glutamate receptor, NMDA subtype, subunit 2B	ATGAGGGACAGGGATA GAGG	AGGTTGGGATGA ATGGGTTC	RT- qPCR
<i>p2rx7</i>	NM_1989 84	P2X Purinoreceptor	GTGTCATTTGTGGACGA GGAC	CACTCAACAGAG TCTTCATGCTG	RT- qPCR
<i>p2ry12</i>	NM_0013 08557	P2Y Purinergic Receptor	TCTTCGGTTTGATCAGC ATCG	TCAGGATTACAT TTGGGAGCG	RT- qPCR
<i>entpd1</i>	NM_0010 03545	CD39, Ectonucleoside Triphosphate Diphosphohydroly ase 1	ACCTGACCAACATGATT CCG	GCTGTTTTAGTA AAGCGACGG	RT- qPCR
<i>nt5e</i>	NM_2009 32	CD73, surface enzyme to breakdown nucleotides	CAAACGGAAATGTGCT GGAG	GTCTGTCCCACCTT GCTGAG	RT- qPCR

<i>adora1b</i>	NM_0011 28584	Adenosine receptor subunit	GGAACAATTTACACAGC CTGC	ACGAGCATGAAA AGCAGAGG	RT- qPCR
<i>tuba1a</i>	AF02925 0	Tubulin, cytoplasmic	GAGCGTCCTACTTACAC CAAC	AGGGAAGTGGAT ACGAGGATAG	Refere nce
<i>actb2 (ref)</i>	NM_1816 01	Actin, cytoskeleton	GCCCCTAGCACAATGAA GATC	GACTCATCGTAC TCCTGCTTG	Refere nce

2.4.7. Software

Table 2.2. Program tools used for thesis and publication completion.

Purpose	Program(s)
Image processing	ImageJ, Adobe Photoshop & Illustrator CS6
Protein sequence alignments	Clustal
Image acquisition and processing	ZEN 2010 (Carl Zeiss Microscopy), HImageLive, & Femtonics
Fluorescence Assay	ZEN 2010
Luminescence Assay	Gen5
Protein Concentration	Nanodrop2000 a280
Electrophysiological Analysis & Visualization	pCLAMP10.5
Electrophysiological Recording & Acquisition	Axon Multiclamp
Coding for EEG analysis	Matlab - Mathworks R2019b
Statistical Analysis	Microsoft Excel 2016, Matlab R2019b
Text processing	Microsoft Word 2016

2.5. References

Ahammad, N., Fathima, T., & Joseph, P. (2014). Detection of Epileptic Seizure Event and Onset Using EEG. *BioMed Research International*, 2014. <https://doi.org/10.1155/2014/450573>

- Baraban SC, Taylor MR, Castro PA, Baier H (2005). Pentylentetrazole induced changes in zebrafish behavior, neural activity and c-fos expression. *Neuroscience*. 131(3):759-68. doi: 10.1016/j.neuroscience.2004.11.031.
- Bedell VM, Wang Y, Campbell JM, Poshusta TL, Starker CG, Krug RG 2nd, Tan W, Penheiter SG, Ma AC, Leung AY, Fahrenkrug SC, Carlson DF, Voytas DF, Clark KJ, Essner JJ, Ekker SC (2012). In vivo genome editing using a high-efficiency TALEN system. *Nature*. 491(7422):114-8. doi: 10.1038/nature11537.
- Berghmans S, Hunt J, Roach A, Goldsmith P (2007). Zebrafish offer the potential for a primary screen to identify a wide variety of potential anticonvulsants. *Epilepsy Res*. 75(1):18-28. doi: 10.1016/j.epilepsyres.2007.03.015.
- Cermak T, Doyle EL, Christian M, Wang L, Zhang Y, Schmidt C, Baller JA, Somia NV, Bogdanove AJ, Voytas DF (2011). Efficient design and assembly of custom TALEN and other TAL effector-based constructs for DNA targeting. *Nucleic Acids Res*. 39(12):e82. doi: 10.1093/nar/gkr218.
- Chang, M., Dufour, S., Carlen, P. L., & Valiante, T. A. (2019). Generation and On-Demand Initiation of Acute Ictal Activity in Rodent and Human Tissue. *Journal of Visualized Experiments*, 143. <https://doi.org/10.3791/57952>
- Chen EY, Tan CM, Kou Y, Duan Q, Wang Z, Meirelles GV, Clark NR, Ma'ayan A (2013). Enrichr: interactive and collaborative HTML5 gene list enrichment analysis tool. *BMC Bioinformatics*. 128(14). doi: 10.1186/1471-2105-14-128.
- Chiu, A. W. L., Jahromi, S. S., Khosravani, H., Carlen, P. L., & Bardakjian, B. L. (2006). The effects of high-frequency oscillations in hippocampal electrical activities on the classification of epileptiform events using artificial neural networks. *Journal of Neural Engineering*, 3(1). <https://doi.org/10.1088/1741-2560/3/1/002>
- Colic S, Wither RG, Zhang L, Eubanks JH, Bardakjian BL (2013). Characterization of seizure-like events recorded in vivo in a mouse model of Rett syndrome. *Neural Netw*. 46:109-15. doi: 10.1016/j.neunet.2013.05.002.
- de Marchi FO, Cruz FF, Menezes FP, Kist LW, Bogo MR, Morrone FB (2019). P2X7R and PANX-1 channel relevance in a zebrafish larvae copper-induced inflammation model. *Comp Biochem Physiol C Toxicol Pharmacol*. 223:62-70. doi: 10.1016/j.cbpc.2019.05.012.
- Donnelly-Roberts, D. L., Namovic, M. T., Han, P. & Jarvis, M. F (2019). Mammalian P2X7 receptor pharmacology: comparison of recombinant mouse, rat and human P2X7 receptors. *Br J Pharmacol* 157, 1203-1214, doi:10.1111/j.1476-5381.2009.00233.x.
- Douw, L., de Groot, M., van Dellen, E., Heimans, J. J., Ronner, H. E., Stam, C. J., & Reijneveld, J. C. (2010). 'Functional Connectivity' Is a Sensitive Predictor of Epilepsy Diagnosis after the First Seizure. *PLoS ONE*, 5(5). <https://doi.org/10.1371/journal.pone.0010839>
- Dvorientchikova, G., Ivanov, D., Barakat, D., Grinberg, A., Wen, R., Slepak, V. Z., et al. (2012). Genetic ablation of Pannexin1 protects retinal neurons from ischemic injury. *PLoS One* 7:e31991. doi: 10.1371/journal.pone.0031991
- Faul F, Erdfelder E, Lang AG, Buchner A (2007). G*Power 3: a flexible statistical power analysis program for the social, behavioral, and biomedical sciences. *Behav Res Methods*. 39(2):175-91. doi: 10.3758/bf03193146.
- Grone BP, Baraban SC (2015). Animal models in epilepsy research: legacies and new directions. *Nat Neurosci*. 18(3):339-43. doi: 10.1038/nn.3934.

- Grundken, C., Hanske, J., Wengel, S., Reuter, W., Abdulazim, A., Shestopalov, V. I., et al. (2011). Unified patch clamp protocol for the characterization of Pannexin 1 channels in isolated cells and acute brain slices. *J. Neurosci. Methods* 199, 15–25. doi: 10.1016/j.jneumeth.2011.04.016
- Gupta, R. C. (2014). Aminopyridine, 4- (4-AP). In *Encyclopedia of Toxicology*. Elsevier. <https://doi.org/10.1016/B978-0-12-386454-3.00096-8>
- Hunyadi B, Siekierska A, Sourbron J, Copmans D, de Witte PAM (2017). Automated analysis of brain activity for seizure detection in zebrafish models of epilepsy. *J Neurosci Methods*. 1;287:13-24. doi: 10.1016/j.jneumeth.2017.05.024.
- Jacobs D, Liu Y.H, Hilton T, Del Campo M, Carlen P L and Bardakjian B L, (2019). Classification of Scalp EEG States Prior to Clinical Seizure Onset, in *IEEE Journal of Translational Engineering in Health and Medicine*, vol. 7, pp. 1-3, doi: 10.1109/JTEHM.2019.2926257.
- Kuhlman B, Dantas G, Ireton GC, Varani G, Stoddard BL, Baker D (2003). Design of a novel globular protein fold with atomic-level accuracy. *Science*. 302(5649):1364-8. doi: 10.1126/science.1089427.
- Kuleshov MV, Jones MR, Rouillard AD, Fernandez NF, Duan Q, Wang Z, Koplev S, Jenkins SL, Jagodnik KM, Lachmann A, McDermott MG, Monteiro CD, Gundersen GW, Ma'ayan A (2016). Enrichr: a comprehensive gene set enrichment analysis web server 2016 update. *Nucleic Acids Research*. doi: 10.1093/nar/gkw377.
- Kurtenbach, S., Whyte-Fagundes, P., Gelis, L., Kurtenbach, S., Brazil, E., Zoidl, C., et al. (2014). Investigation of olfactory function in a Panx1 knock out mouse model. *Front. Cell. Neurosci*. 8:266. doi: 10.3389/fncel.2014.00266
- Ma AC, Lee HB, Clark KJ, Ekker SC (2013). High efficiency In Vivo genome engineering with a simplified 15-RVD GoldyTALEN design. *PLoS One*. 8(5):e65259. doi: 10.1371/journal.pone.0065259.
- Ma AC, Chen Y, Blackburn PR, Ekker SC (2016). TALEN-Mediated Mutagenesis and Genome Editing. *Methods Mol Biol*. 1451:17-30. doi: 10.1007/978-1-4939-3771-4_2.
- Meeker ND, Hutchinson SA, Ho L, Trede NS (2007). Method for isolation of PCR-ready genomic DNA from zebrafish tissues. *Biotechniques*. 43(5):610, 612, 614. doi: 10.2144/000112619.
- Murana, E., Pagani, F., Basilio, B., Sundukova, M., Batti, L., di Angelantonio, S., Cortese, B., Grimaldi, A., Francioso, A., Heppenstall, P., Bregestovski, P., Limatola, C., & Ragozzino, D. (2017). ATP release during cell swelling activates a Ca²⁺-dependent Cl⁻ current by autocrine mechanism in mouse hippocampal microglia. *Scientific Reports*, 7(1). <https://doi.org/10.1038/s41598-017-04452-8>
- Neff KL, Argue DP, Ma AC, Lee HB, Clark KJ, Ekker SC. (2013). Mojo Hand, a TALEN design tool for genome editing applications. *BMC Bioinformatics*. 14:1. doi: 10.1186/1471-2105-14-1.
- Pellegrini-Calace M, Maiwald T, Thornton JM (2009). PoreWalker: A Novel Tool for the Identification and Characterization of Channels in Transmembrane Proteins from Their Three-Dimensional Structure. *PLoS Comput Biol* 5(7): e1000440. doi:10.1371/journal.pcbi.1000440.
- Pfaffl MW, Horgan GW, Dempfle L (2002). Relative expression software tool (REST) for group-wise comparison and statistical analysis of relative expression results in real-time PCR. *Nucleic Acids Res*. 30(9):e36. doi: 10.1093/nar/30.9.e36.

- Prochnow, N., Abdulazim, A., Kurtenbach, S., Wildforster, V., Dvorianchikova, G., Hanske, J., et al. (2012). Pannexin1 stabilizes synaptic plasticity and is needed for learning. *PLoS One* 7:e51767. doi: 10.1371/journal.pone.0051767
- Ray, A., Zoidl, G., Weickert, S., Wahle, P., and Dermietzel, R. (2005). Site-specific and developmental expression of pannexin1 in the mouse nervous system. *Eur. J. Neurosci.* 21, 3277–3290. doi: 10.1111/j.1460-9568.2005.04139.x
- Ray, A., Zoidl, G., Wahle, P., and Dermietzel, R. (2006). Pannexin expression in the cerebellum. *Cerebellum* 5, 189–192. doi: 10.1080/14734220500530082
- Sharmila, A., & Mahalakshmi, P. (2017). Wavelet-based feature extraction for classification of epileptic seizure EEG signal. *Journal of Medical Engineering & Technology*, 41(8). <https://doi.org/10.1080/03091902.2017.1394388>
- Sievers F, Higgins DG (2018). Clustal Omega for making accurate alignments of many protein sequences. *Protein Sci* 27, 135–145. doi: 10.1002/pro.3290.
- Silverman W, Locovei S, Dahl G. Probenecid, a gout remedy, inhibits pannexin 1 channels (2008). *Am J Physiol Cell Physiol.* 295(3):C761-7. doi: 10.1152/ajpcell.00227.2008.
- Tort, A. B. L., Komorowski, R., Eichenbaum, H., & Kopell, N. (2010). Measuring Phase-Amplitude Coupling Between Neuronal Oscillations of Different Frequencies. *Journal of Neurophysiology*, 104(2). <https://doi.org/10.1152/jn.00106.2010>
- Velisek, L. (2006). Models of Chemically-Induced Acute Seizures. In *Models of Seizures and Epilepsy*. Elsevier. <https://doi.org/10.1016/B978-012088554-1/50013-X>
- Vogt, A., Hormuzdi, S. G., & Monyer, H. (2005). Pannexin1 and Pannexin2 expression in the developing and mature rat brain. *Brain Research. Molecular Brain Research*, 141(1), 113–120. <https://doi.org/10.1016/j.molbrainres.2005.08.002>
- Wang, J., Jackson, D. G., & Dahl, G. (2013). The food dye FD&C Blue No. 1 is a selective inhibitor of the ATP release channel Panx1. *Journal of General Physiology*, 141(5). <https://doi.org/10.1085/jgp.201310966>
- Wang, L., Dufour, S., Valiante, T. A., & Carlen, P. L. (2016). Extracellular Potassium and Seizures: Excitation, Inhibition and the Role of Ih. *International Journal of Neural Systems*, 26(08). <https://doi.org/10.1142/S0129065716500441>
- Waterhouse A, Bertoni M, Bienert S, Studer G, Tauriello G, Gumienny R, Heer FT, de Beer TAP, Rempfer C, Bordoli L, Lepore R, Schwede T (2018). SWISS-MODEL: homology modelling of protein structures and complexes. *Nucleic Acids Res.* 46(W1):W296-W303. doi: 10.1093/nar/gky427.
- Whyte-Fagundes, P., Kurtenbach, S., Zoidl, C., Shestopalov, V. I., Carlen, P. L., & Zoidl, G. (2018). A Potential Compensatory Role of Panx3 in the VNO of a Panx1 Knock Out Mouse Model. *Frontiers in Molecular Neuroscience*, 11. <https://doi.org/10.3389/fnmol.2018.00135>

Chapter 3. Loss of *Panx1* does not affect primary and secondary olfaction

“Scientific work must not be considered from the point of view of the direct usefulness of it. It must be done for itself, for the beauty of science, and then there is always the chance that a scientific discovery may become like the radium, a benefit.”

- Marie Curie

This chapter is modified from the following original published article:

Paige Whyte-Fagundes, Stefan Kurtenbach, Christiane Zoidl, Valery I. Shestopalov, Peter L. Carlen and Georg Zoidl. 2018. “A potential compensatory role of *Panx3* in the VNO of a *Panx1* knock out mouse model.” *Frontiers in Molecular Neuroscience* (11).
<https://doi.org/10.3389/fnmol.2018.00135>

Author Contributions

PW-F, SK, CZ performed experiments. VIS, PLC provided animals and materials. PW-F wrote the manuscript. PW-F & SK analyzed the data. All authors took part in editing the manuscript. PW-F & GZ developed the concept and coordinated the research. All authors approved the final manuscript.

Copyright

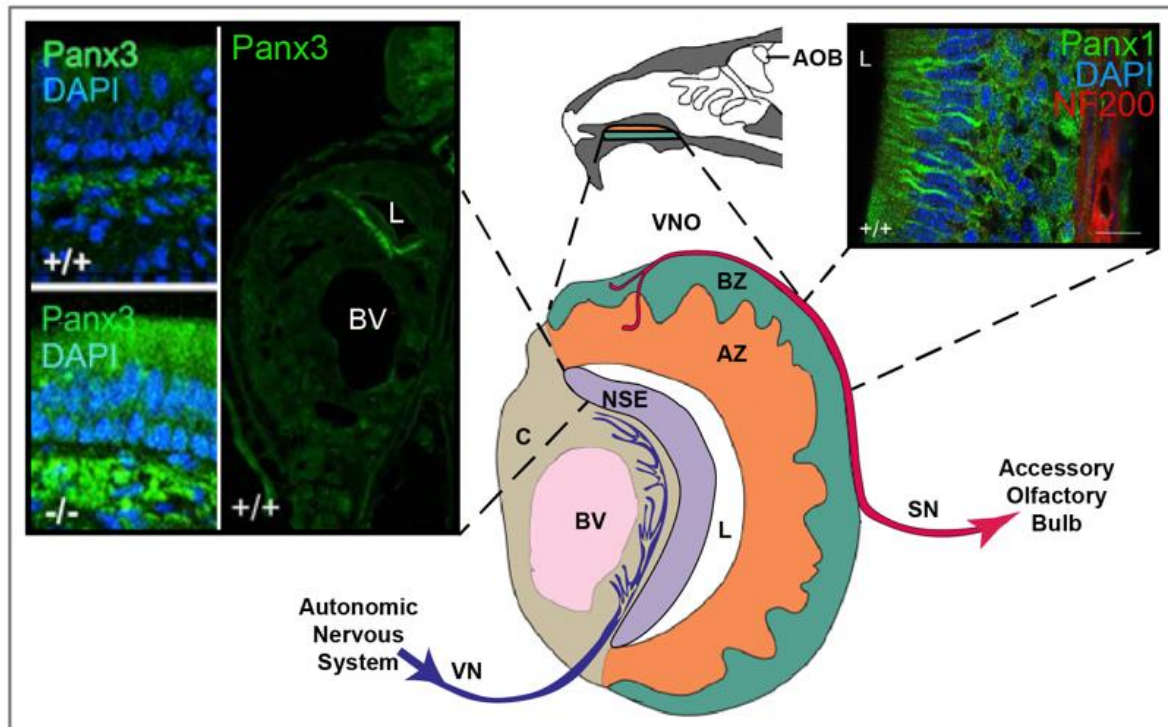
© 2018 Whyte-Fagundes, Kurtenbach, Zoidl, Shestopalov, Carlen and Zoidl. This is an open-access article distributed under the terms of the **Creative Commons Attribution License (CC BY)**. The use, distribution or reproduction in other forums is permitted, provided the original author(s) and the copyright owner are credited and that the original publication in this journal is cited, in accordance with accepted academic practice. No use, distribution or reproduction is permitted which does not comply with these terms.

Correspondence

Georg Zoidl, Phd: gzoidl@yorku.ca

A potential compensatory role of Panx3 in the VNO of a Panx1 knock out mouse model

Graphical Abstract



Authors:

Paige Whyte-Fagundes^{1,2},
Stefan Kurtenbach^{1,3},
Christiane Zoidl¹,
Valery I. Shestopalov³,
Peter L. Carlen^{2,4}
Georg Zoidl^{1,2,5}

Affiliations:

¹Department of Biology, York University, Toronto, ON, Canada
²Krembil Research Institute, University Health Network, Toronto, ON, Canada
³Department of Ophthalmology, Bascom Palmer Institute, University of Miami Miller School of Medicine, Miami, FL, United States
⁴Department of Physiology, University of Toronto, Toronto, ON, Canada
⁵Department of Psychology, York University, Toronto, ON, Canada

In Brief:

Whyte-Fagundes et al., demonstrated that loss of Panx1 does not impact olfaction. Although Panx1 expression patterns demonstrate a pivotal position for signalling dynamics involved in sensory processing, there are inconclusive results to demonstrate the necessity of this protein in chemosensation. This led to the novel discovery that Panx3, another Panx family member, is able to compensate in expression and function for Panx1 in its absence. This suggests that these proteins are coordinated in order to maintain sensory processing, thereby suggesting Panx1 functions synergistically in a complex molecular network.

Highlights:

- Panx1 is localized to regions of the olfactory system that are highly relevant for function
- Olfaction is not impaired in Panx1^{-/-} mice and no deficits in ATP release were found.
- Panx3 appears to upregulate expression in regions where Panx1 is lost in juveniles and adults
- Panx3 has conserved ‘Panx1-like’ functional channel properties, suggestive of compensatory regulation *in vivo*

3.1. Abstract

Pannexins (Panx) are integral membrane proteins, with Panx1 being the best-characterized member of the protein family. Panx1 is implicated in sensory processing, and knockout (KO) animal models have become the primary tool to investigate the role(s) of Panx1 in sensory systems. Extending previous work from our group on primary olfaction, the expression patterns of Panxs in the vomeronasal organ (VNO), an auxiliary olfactory sense organ with a role in reproduction and social behavior, were compared. Using qRT-PCR and Immunohistochemistry (IHC), we confirmed the loss of Panx1, found similar Panx2 expression levels in both models, and a significant upregulation of Panx3 in mice with a global ablation of Panx1. Specifically, Panx3 showed upregulated expression in nerve fibers of the non-sensory epithelial layer in juvenile and adult KO mice and in the sensory layer of adults, which overlaps with Panx1 expression areas in WT populations. Since both social behavior and evoked ATP release in the VNO was not compromised in KO animals, we hypothesized that Panx3 could compensate for the loss of Panx1. This led us to compare Panx1 and Panx3 channels *in vitro*, demonstrating similar dye uptake and ATP release properties. Outcomes of this study strongly suggest that Panx3 may functionally compensate for the loss of Panx1 in the VNO of the olfactory system, ensuring sustained chemosensory processing. This finding extends previous reports on the upregulation of Panx3 in

arterial walls and the skin of Panx1 KO mice, suggesting that roles of Panx1 warrant uncharacterized safeguarding mechanisms involving Panx3.

3.2. Introduction

The pannexin's (Panx) is a three-member (in rodents: Panx1, Panx2 and Panx3) family of integral membrane proteins. This gene family has received considerable attention since their initial discovery (Panchin et al., 2000; Bruzzone et al., 2003), with a particular focus on Panx1. The expression of this gene seems ubiquitous throughout the central nervous system (CNS; Ray et al., 2005, 2006) and multiple sensory systems, making Panx1 channels attractive candidates for sensory perception, which is important for interpreting stimuli in an environmental context (Brignall and Cloutier, 2015). Thus far, Panx1 expression in sensory systems has been found in the auditory (Wang et al., 2009), visual (Ray et al., 2005; Dvorianchikova et al., 2006), gustatory (Huang et al., 2007; Romanov et al., 2007), and main olfactory system (Zhang et al., 2012; Kurtenbach et al., 2014) as well as in pain perception (Zhang et al., 2015, 2017). Given that Panx1 is an adenosine triphosphate (ATP) release channel (Bao et al., 2004), and is present in multiple sensory systems, it is tempting to investigate roles in the modulation of sensory processes.

The introduction of different transgenic mouse lines with distinct Panx1 ablation strategies (Bargiotas et al., 2011; Qu et al., 2011; Dvorianchikova et al., 2012; Hanstein et al., 2013), has initiated ample opportunities to investigate Panx1 functions in a translational manner—from genes through to systems and behavioral outcomes. The availability of one mouse model (Dvorianchikova et al., 2012) allowed us to determine a new localization of Panx1 in olfactory sensory neuron (OSN) axon bundles and further dismiss a primary function of Panx1 in olfaction—based upon behavioral testing, electroolfactogram measurements and analysis of ATP release from the olfactory epithelium (OE). The data suggested that Panx1 is one of several alternative pathways to release ATP in the primary olfactory system during chemosensation, likely playing a secondary role only (Kurtenbach et al., 2014).

Here, we report on the presence of Panxs in the accessory olfactory system (AOS), which is home to the accessory olfactory bulb (AOB) and the vomeronasal organ (VNO)—building on previous findings using the same mouse model. The VNO is the primary sensory organ in the AOS. It is located at the base of the nasal septum (Halpern, 1987) and is a chemosensory organ containing specialized sensory neurons called vomeronasal sensory neurons (VSNs), which are found in the pseudostratified neuroepithelium and send signals to the AOB for processing in the

brain. In mice, the VSNs recognize chemical signals and initiate innate behavioral responses, like aggressive and reproductive behaviors (Pérez-Gómez et al., 2014). Importantly, ATP appears to play a significant role in triggering these behavioral responses. At the physiological level, ATP release in the VNO is responsible for eliciting a concentration-dependent increase in intracellular calcium, as well as initiating inward currents in VSNs. In turn, increased levels of ATP heighten the responsiveness of VSNs to chemical stimuli (Vick and Delay, 2012). At this time, ATP release is thought to be reliant on purinergic receptor activity upon activation of the vasomotor pump. Exact mechanisms of release are poorly understood, however, known properties of connexins (Cxs) and Panxs (Scemes et al., 2007) suggest that they could contribute either in conjunction or competition with ionotropic P2X or metabotropic P2Y receptors to the release of ATP responsible for signal transduction in the AOS (Gayle and Burnstock, 2005; Vick and Delay, 2012).

To address this knowledge gap, we have characterized the impact of genetic ablation of Panx1 in the AOS. Expression and localization studies demonstrated Panx1 expression in the VNO, with surprising up-regulation of Panx3 both in the sensory and non-sensory neuroepithelium, as well as in nerve fibers innervating the VNO of the Panx1 knockout (KO; ^{-/-}) population. Behavioral analysis and a quantitative comparison of steady-state extracellular ATP concentration, via mechanical stimulation in an ex vivo preparation, did not reveal significant differences between the two genotypes. The lack of phenotype and the regulation of Panx3 let us conclude that there are likely compensatory mechanisms at play. To further support this conclusion, we showed that in an established cell culture model Panx3 shares some properties with Panx1 including ATP release, as well as responses to stimulation and pharmacological blocking during dye uptake analysis under physiological conditions. To our knowledge, this research provides the first evidence that Panx3 can compensate, at least in part, for Panx1 function(s) in a sensory organ.

3.3. Results

3.3.1. Pannexin3 mRNA expression is upregulated in the vomeronasal organ of panx1^{-/-} mice

In situ hybridizations with cRNA probes specific for mouse Panx1 (mPanx1; Ray et al., 2005) confirmed expression of mPanx1 in the vomeronasal organ (VNO; **Figure 3.1a**). The antisense cRNA revealed strong staining of the VNO epithelia of 7-day-old mice, indicated by the yellow arrowheads, while the sense RNA probes only generated very faint staining, verifying the probes'

specificity. Next, Panx expression was quantified in total RNA isolated from the VNO, using quantitative Real Time-PCR (qRT-PCR) and primers specific for the mPanx1 (GI:8626133), mPanx2 (GI:163838634) and mPanx3 (GI:86262154) mRNAs. Significant expression of mPanx1 was detected in the VNO of adult wild-type mice (**Figure 3.1b**). Consistent with the gene targeting strategy ablating exons 3 and 4 of the Panx1 gene (Dvoriantchikova et al., 2012), no mPanx1 expression was detected in the VNO of mPanx1^{-/-} animals (relative expression ratio: 0.0019 ± 0.0006-fold, p < 0.0001, n = 6; mean cycle threshold (Ct) ± SD: wild type 30.36 ± 0.87, mPanx1^{-/-} 38.56 ± 1.61). mPanx2 and mPanx3 mRNA expression were determined to address the possibility of compensatory mechanisms that may affect Panx expression. A significant upregulation of the mPanx3 mRNA expression (2.03 ± 0.78-fold, p = 0.007, n = 6; Ct ± SD: wild type 30.47 ± 1.01, mPanx1^{-/-} 29.50 ± 0.39) in the VNO of Panx1^{-/-} mice was measured. In contrast, no change in the expression of mPanx2 was found in the VNO of the Panx1^{-/-} mice (1.08 ± 0.23-fold, p = 0.89, n = 6, Ct ± SD: wild type 30.09 ± 0.21, mPanx1^{-/-} 30.24 ± 0.46).

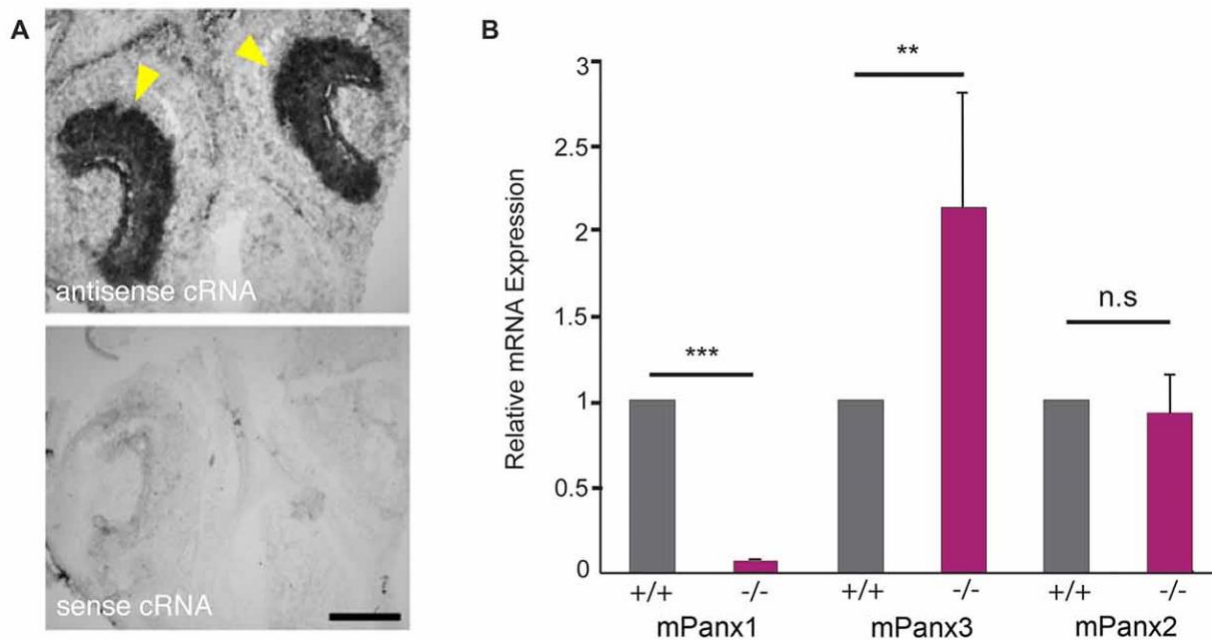


Figure 3.1. Pannexin mRNA expression in the mouse VNO. a) In situ hybridizations (ISHs) from juvenile mice (P7) with mPanx1 riboprobes. Panx1 antisense cRNA delivered strong labeling in the VNO. The strongest staining was detectable in the basal cell layer of the sensory epithelium (SE) indicated by yellow arrowheads. Note the absence of specific staining when the Panx1 sense cRNA was used. VNO = vomeronasal organ. Scale bar = 100 µm. (b) Quantitative real time (RT)-PCR data for Panx expression in the VNO. Panx1^{-/-} mice lacked detectable mPanx1 expression in the VNO (n = 6). Mouse Panx3 mRNA expression showed a significant 2-fold upregulation in the VNO of Panx1^{-/-} mice. No differential mRNA regulation was found for mPanx2. Primers specific for 18S rRNA were used as a reference. Experiments were performed in triplicates; significance is denoted by asterisks: Student's T-test ***p < 0.001, **p < 0.01, Error Bars denote SEM.

3.3.2. Localization of pannexin proteins in the VNO of wild-type and *Panx1*^{-/-} mice

The mouse VNO is part of the AOS, composed of sensory and non-sensory layers as shown in the cartoon in **Figure 3.2a**. In the sensory layer, cell bodies of the sensory neurons, situated in the sensory epithelium (SE), segregate into the apical and basal zones (AZ, BZ) and project to the anterior or posterior portion of the AOB (details not shown) respectively. Cells in the non-sensory layer (NSE) are separated by a nerve fiber tract responsible for the autonomous innervation of local assemblies of the vasculature in cavernous tissue, which respond to increased sympathetic tone with vasoconstriction and in turn regulate the lumen (L) of the VNO.

The localization of Panx proteins in the VNO of juvenile mice was tested by IHC. Abundant mPanx1 protein expression was found in nerve fibers innervating blood vessels in the cavernous part of the VNO, with relatively lower levels of expression in the non-sensory epithelial layers (**Figures 3.2b,c**). Further, the Gαo protein, a protein known to couple neurotransmitter receptors to ion channels in sympathetic neurons (Jeong and Ikeda, 1998), co-localized with mPanx1 immunoreactive nerve fibers (**Figure 3.2d**). The overview in **Figure 3.2e** shows that expression of mPanx1 in the sensory part of the VNO was negligible. Zoomed in views of the complementary areas of the non-sensory part of the VNO using identical immunostaining and imaging conditions, demonstrated an absence of mPanx1 immunoreactivity in *Panx1*^{-/-} mice (**Figures 3.2f,g**; **Supplementary Figure 3.1** shows secondary antibody control).

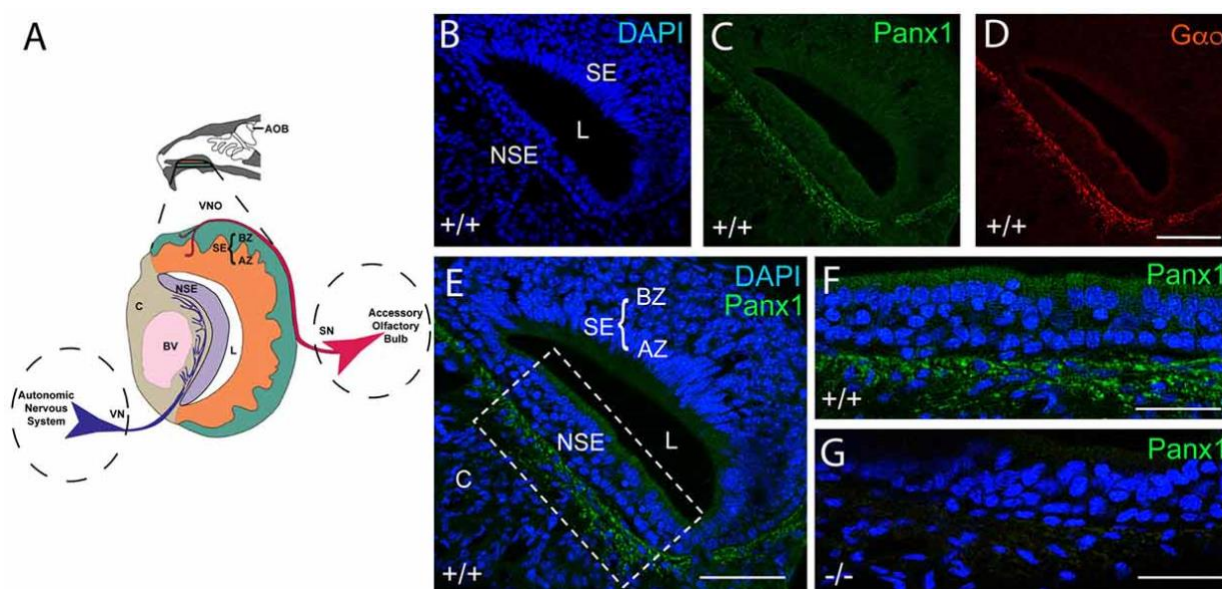


Figure 3.2. Panx1 protein expression in the NSE of the juvenile mouse VNO. a) Overview of the murine VNO adapted from Sánchez-Andrade and Logan (2014) (b–d). The intact wild-type VNO imaged at 40x magnification is shown in (b) depicting DAPI staining of nuclei, the localization of (c) mPanx1 and (d) of the

G-alpha protein Gαo. The region highlighted by the box in the overview in (e) is shown at 63x magnification in (f) highlighting the significant mPanx1 expression in the basal and lower expression in the ciliated epithelium of the NSE. (g) A comparable region in Panx1^{-/-} mice lacked Panx1 expression. Abbreviations: AZ, apical zone; BZ, basal zone; SE, sensory epithelium; L, lumen; NSE, non-sensory epithelium; C, cavernous tissue; BV, a blood vessel. Scale bars: (b–e) = 100 μm, (f,g) = 50 μm.

Interestingly, in juvenile wild-type mice, mPanx3 expression was detectable and confined to regions similar to mPanx1, as well as in cartilage (**Figure 3.3a**). Meanwhile, in Panx1^{-/-} mice, Panx3 immunoreactivity was elevated in the non-sensory part of the VNO in regions of Panx1 protein expression in wild-type controls, but not detectable in the SE (**Figure 3.3b,c**). This result strongly argues for protein upregulation in subpopulations of cells with loss of mPanx1 expression or nearby thereof. In contrast, mPanx2 was equally expressed in wild-type and Panx1^{-/-} populations, demonstrating ubiquitous expression within and beyond the VNO (**Figure 3.3d**), and showing higher levels of expression in connective tissue (CT) compared to mPanx1 and mPanx3. The significant expression of the Panx2 protein in the VNO, despite low mRNA levels, is consistent with a previous report demonstrating that Panx1, 2 and 3 mRNA and protein expression were disconnected in most tissues (Le Vasseur et al., 2014).

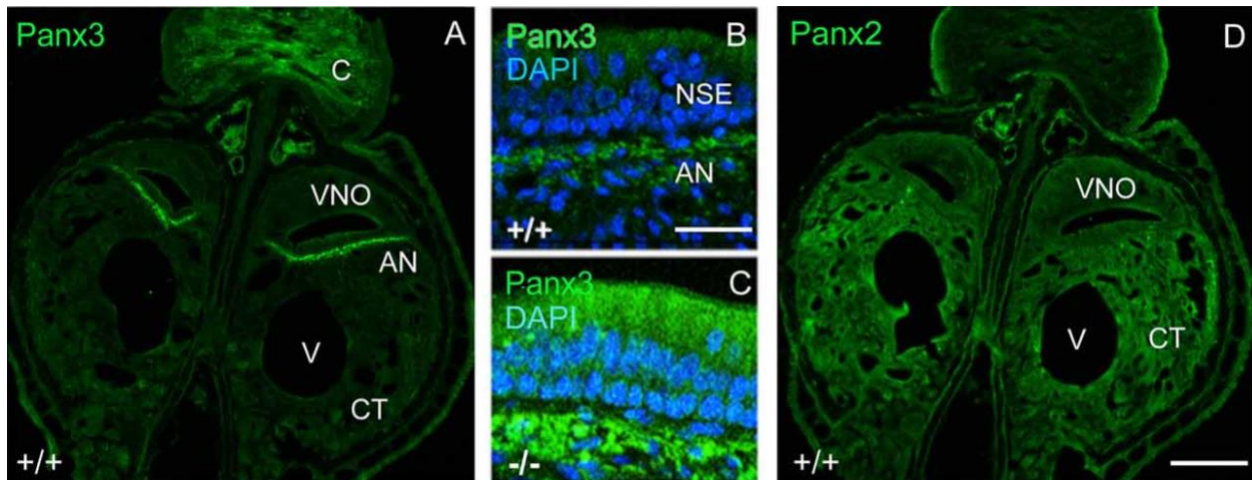


Figure 3.3. Localization of mPanx2 and mPanx3 proteins showing upregulation of mPanx3 in the NSE of juvenile Panx1^{-/-} mice. a) The left panel demonstrates an overview taken at 10x magnification showing the entire VNO and surrounding structures after Panx3 immunostaining. Mouse Panx3 has increased expression where mPanx1 has been demonstrated previously to be found, basal to the NSE, in the autonomous sensory nerve. There is also increased expression in the cartilaginous zone, which is characteristic of mPanx3. (b,c) The two panels in the middle show higher magnifications (63x) of the region indicated by the white box, demonstrating some mPanx3 expression in the cilia of the NSE and cell bodies basal to the NSE in wild-type mice. (c) The panel below shows that there is a clear increase in mPanx3 expression in Panx1^{-/-} in the same regions. (d) Mouse Panx2 is ubiquitously localized in the VNO and the CT. Abbreviations: VNO, vomeronasal organ; V, vasculature; CT, cavernous tissue; C, cartilage; NSE, non-sensory epithelium; AN, autonomous (parasympathetic/sympathetic) nerve; +/+ = WT, -/- = Panx1 knockout (KO). Scale bars 10x overviews = 350 μm, 63x magnifications = 50 μm.

Next, we investigated mPax1 and mPax3 protein localization in the VNO of adult mice. Abundant mPax1 expression was detected in the sensory epithelial (SE) layer, with negligible levels of expression in the non-sensory epithelial (NSE) layer. Meanwhile, no mPax1 protein expression was found in Pax1^{-/-} mice (**Figures 3.4a,b**). At higher magnification, images of the SE of wild-type animals revealed Pax1 localization along the tracts of neurons in the AZ as well as distinct punctate expression in the BZ (**Figure 3.4c**). In the SE of the VNO of wild-type mice, only traces of the mPax3 protein were found, which we dismissed as background staining (**Figures 3.4d,e**). However, similar to juvenile Pax1^{-/-} mice, the mPax3 protein was significantly upregulated in both the SE and NSE (**Figure 3.4f**). The zoomed in views shown in **Figures 3.4g,h** revealed that mPax3 was localized in both layers of the SE, as well as in the NSE, AN and the cavernous tissue. At the highest magnification, mPax3 showed a punctate localization. Together, the tissue distribution of mPax1 protein found in adult and P7 mice tissue partially overlapped with the mPax3 protein expression found in Pax1^{-/-} mice, raising the question of whether mPax3 could functionally compensate for the loss of mPax1.

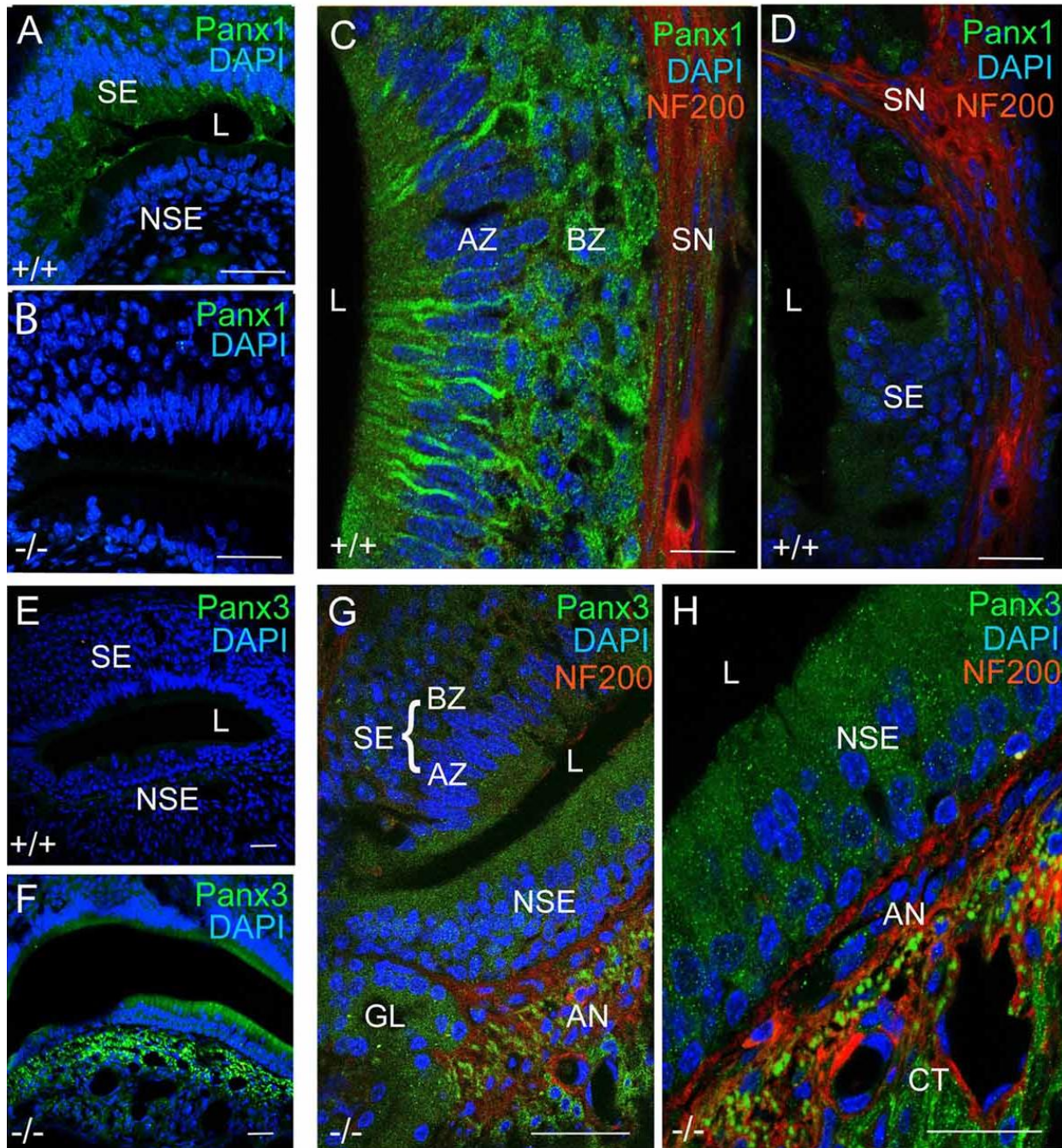


Figure 3.4. Panx1 and Panx3 localization in the VNO of adult mice. a,b) Overviews showing mPanx1 expression (green) and DAPI staining (blue) in the VNO of wild-type and $Panx1^{-/-}$ mice. In the adult $Panx1$, wild-type VNO the mPanx1 protein is detected in the SE layer, with some expression in the NSE layer. The $Panx1^{-/-}$ VNO showed no mPanx1 staining. Scale bars (a,b) = 200 μ m. (c) In the SE layer of wild-type mice, the mPanx1 protein (green) is localized along tracts of sensory neurons in both AZ and BZ, with some immunoreactivity found in NF200 (red) immunoreactive nerve fibers (SN). The mPanx1 protein showed punctate localization in both the apical zone (AZ) and basal zone (BZ). A very low level of mPanx3 immunoreactivity was detectable in the SE layer, which was dismissed as background (d) Scale bars (c,d) = 50 μ m. (e,f) Overviews include DAPI staining of nuclei (blue) and Panx3 expression (green) in wild-type and $Panx1^{-/-}$ mice, showing upregulation of Panx3 expression in the VNO of $Panx1^{-/-}$ mice. Scale bars (e,f) = 100 μ m. At higher magnification (g,h) of VNOs from $Panx1^{-/-}$ mice showed localization of Panx3 in both the SE and NSE layers, and the NF200

immunoreactive nerve fibers, with the highest magnification demonstrating a punctate pattern of localization. Scale bars (g,h) = 100 μ m, 50 μ m. Abbreviations: SE, sensory epithelium; NSE, non-sensory epithelium; AZ, apical zone; BZ, basal Zone; L, lumen; SN, sensory nerve; AN, autonomous (parasympathetic/sympathetic) nerve; GL, gland.

3.3.3. ATP release in the VNO of wild-type and *Panx1*^{-/-} mice

ATP is a known mediator of VSNs, and *Panx1* has been described as a major ATP release channel. Since ATP release can be evoked in the adult VNO by mechanical stimulation (Vick and Delay, 2012), it is possible to quantify extracellular ATP using acute ex vivo preparations of the VNO. Here, basal levels of extracellular ATP were detectable in the VNO of both adult *Panx1*^{+/+} and *Panx1*^{-/-} mice (ATP concentration: *Panx1*^{+/+}, 0.08 ± 0.007 pM, *Panx1*^{-/-}, 0.13 ± 0.1 pM; $p = 0.5$; $n = 5$). Repeated mechanical stimulations reliably elevated ATP release in both *Panx1*^{+/+} and *Panx1*^{-/-} mice VNO preparations (*Panx1*^{+/+}, 1.02 ± 0.5 pM; *Panx1*^{-/-}, 0.95 ± 0.9 pM, $p = 0.9$; $n = 5$; **Figure 3.5**). The increase was significant for both genotypes (*Panx1*^{+/+}, $p = 0.01$; *Panx1*^{-/-}, $p = 0.05$), although the concentration of ATP was indistinguishable for both non-stimulated and stimulated conditions. Since evoked ATP release in the VNO was not compromised in KO animals, differential expression of genes encoding for proteins known for interacting with ATP (purinergic receptors), or channels permeable for ATP (connexin, calcium homeostasis modulator), or opening upon mechanical stimulation (transient receptor potential cation channel) were investigated. Using qPCR, the expression of connexin-43 (Cx43), the transient receptor potential cation channel, subfamily C, gene 2 (TRPC2), the transient receptor potential cation channel, subfamily M, gene 5 (TRPM5), the purinergic receptors P2X7, P2X5 and P2Y2, as well as the calcium homeostasis modulator 1 and 2 (Calhm1, Calhm2) were detectable in the VNO. Non-significant expression changes were found for the purinergic receptors P2X7 (Mean \pm Standard Error; 0.893 ± 0.310 , $p = 0.541$) and P2X5 (1.235 ± 0.354 , $p = 0.250$), as well as TRPC2 (1.351 ± 0.450 , $p = 0.138$). Furthermore, Cx43 (Cx43: 0.397 ± 0.144 , $p = 0.004$), P2Y2 (0.533 ± 0.183 , $p = 0.0001$), TRPM5 (0.506 ± 0.201 , $p = 0.016$), Calhm1 (0.369 ± 0.176 , $p = 0.011$) and Calhm2 (0.477 ± 0.166 , $p = 0.001$) were significantly downregulated. Together, evidence for compensatory upregulation of the most likely alternative sources contributing to ATP release in the VNO was not found. This result suggests that compensatory upregulation of *Panx3*, and ATP release through *Panx3*, could contribute to the similar increase in ATP release upon mechanical stimulation in both genotypes.

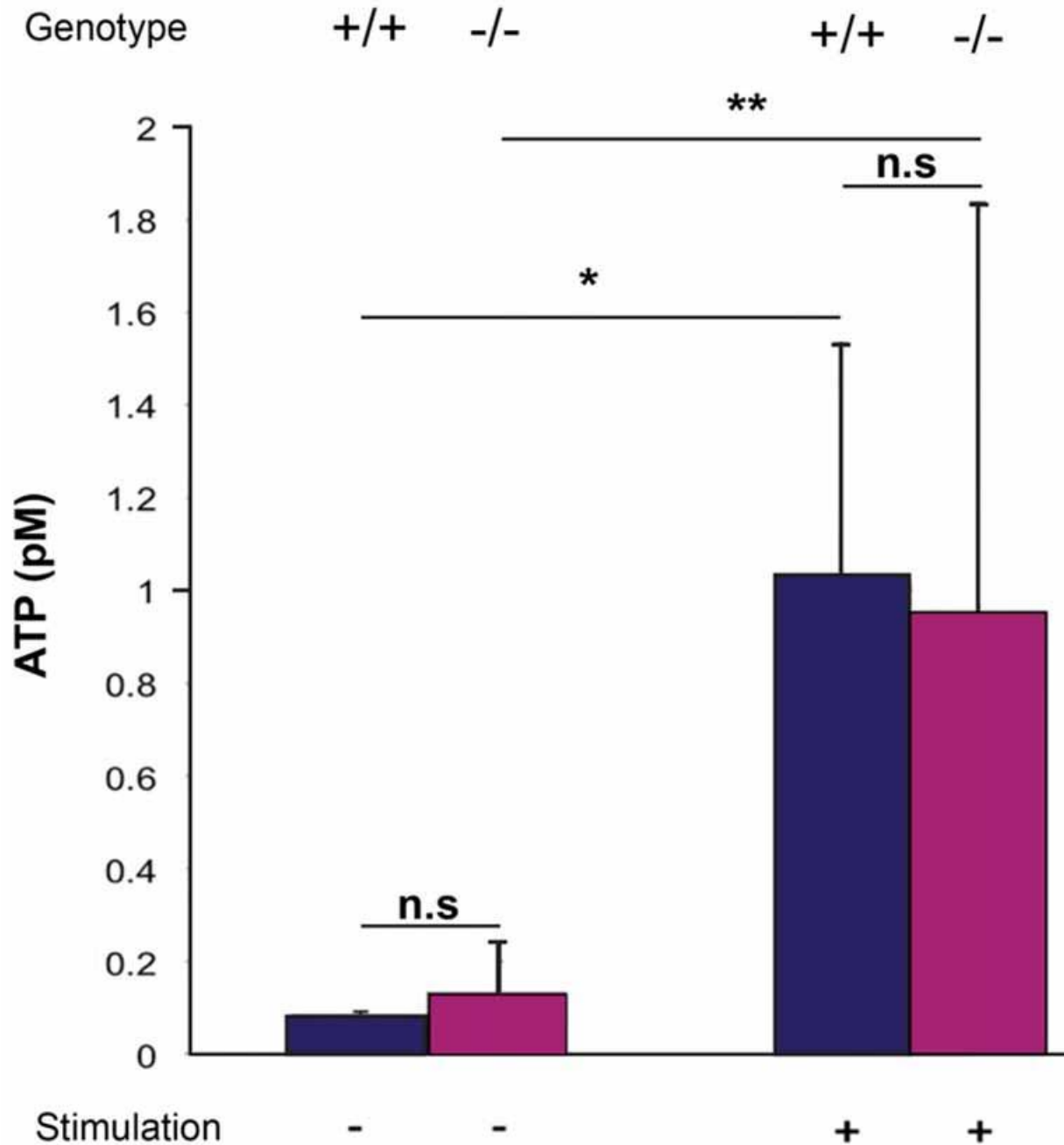


Figure 3.5. Quantification of extracellular ATP after mechanical stimulation of the VNO. ATP release from the VNO of wild-type and knock out animals was determined as outlined in materials and methods using a luminescent ATP detection assays. Without stimulations, very low levels of ATP were detectable, with no differences between the two genotypes. Mechanical stimulation significantly increased ATP release, again, with no difference between wild-type and *Panx1*^{-/-} animals. Error bars indicate standard deviation. **p* < 0.01, ***p* < 0.05.

3.3.4. Aggression and defensive behaviour in wild-type and *Panx1*^{-/-} mice

Since the VNO plays a major role in social interactions, a modified resident-intruder assay was performed to identify discernible behavioral differences between the two populations. Adult male mice were used to test for aggressive and defensive behaviors by the resident, as well as social stress evoked by the intruder. This analysis included quantification of three categories, smell, attack and tail flicks, which are typical behaviors elicited by specific chemosensory ligands present in the sensory epithelial layer of the VNO. **Figure 3.6** shows that adult *Panx1*^{-/-} mice (n = 14) did not show any significant difference in these measures compared to age-matched wild-type *Panx1*^{+/+} mice (n = 15). Interestingly, no significant differences were found in six behavioral responses. A single significant increase in smell time of *Panx1*^{-/-} animals was observed when intruders were placed in their cage. In summary, the behavioral data suggested that lack of *Panx1* function(s) in the VNO were not affecting behavioral outcomes in the knockout mice. Considering that the change in behavior was minor, albeit statistically significant, the result was interpreted as an indication of a compensatory role of *Panx3*.

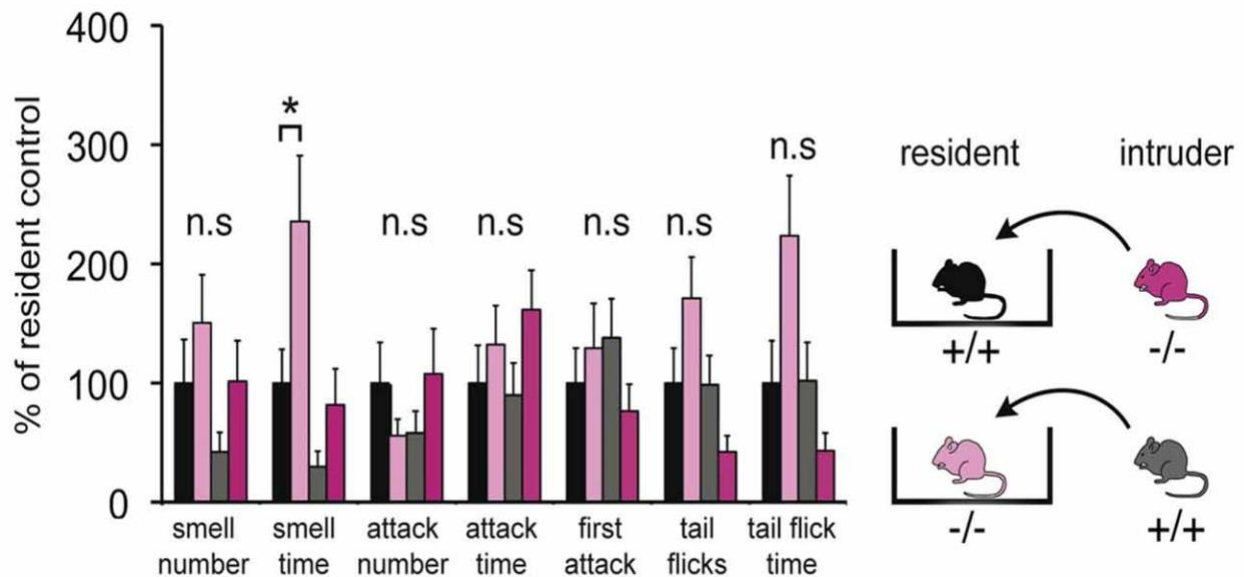


Figure 3.6. Behavioural comparison of *Panx1*^{+/+} and *Panx1*^{-/-} mice. This modified intruder assay with *N* = 14 (*Panx1*^{+/+}) and *N* = 15 (*Panx1*^{-/-}) mice demonstrates that there are no significant differences in three behavioral categories, including aggressive behaviors mediated by the VNO (tail flicks, attacks indicated by biting, chasing, cornering and tumbling), between the two different mouse lines. A significant increase in smell time was found for *Panx1* KO resident mice. The cartoon outlines the strategy used. Error bars indicate SEM. **p* < 0.05.

3.3.5. Expression properties of panx1 and panx3 in neuro2a cells are similar

Testing the hypothesis that mPanx3 could functionally compensate for mPanx1 in Panx1^{-/-} mice, we analyzed both proteins in Neuro2a cells. It is worth noting that Neuro2a cells express Panx1 mRNA, but not Panx2 or Panx3 (**Supplementary Figure 3.2**), however, very low levels of endogenous Panx1 protein expression have not been detected by western blot (data not shown). Transient transfection of mPanx1-EYFP and mPanx3-EGFP increased steady-state mRNAs \approx 95 fold (mPanx1) or \approx 3400 fold (mPanx3) relative to endogenous levels (**Supplementary Figure 3.3**). The western blot analysis after transient overexpression of mPanx1-EYFP and mPanx3-EGFP in Neuro2a cells demonstrated that both proteins were expressed similarly to previous reports (Boassa et al., 2007; Penuela et al., 2007, 2008; **Figure 3.7a**). Also, confocal imaging revealed that both proteins localized in the cell membrane and internal membranes, consistent with the typical distribution of Panx proteins (**Figures 3.7b,c**).

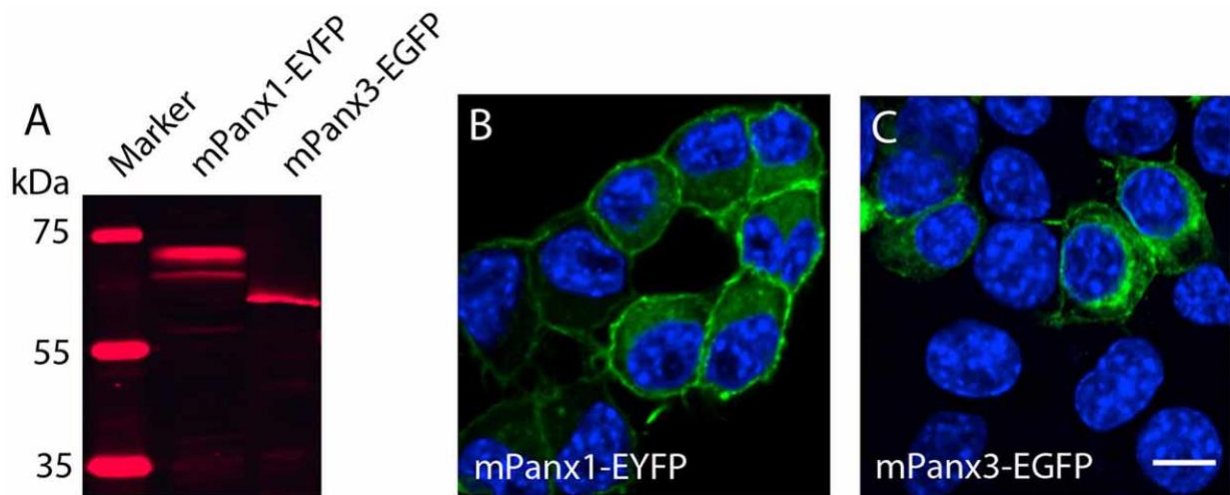


Figure 3.7. Panx1 and Panx3 localization in Neuro2A cells. a) western blot showing Panx1-EYFP and Panx3-EGFP proteins 48h after transient transfection into Neuro2A cells. b,c) Merged images, including DAPI staining of nuclei (blue), and Panx1-EYFP (Left) and Panx3-EGFP (Right) localization (green) in Neuro2A cells. Scale bars = 10 μ m.

3.3.6. Mouse Panx1 and panx3 release ATP *in vitro*

Panx1 channels are well established ATP release channels and the expression and localization of mPanx1 and mPanx3 were similar *in vitro*, therefore, an *in vitro* luciferase assay was used to test whether Panx3 demonstrated similar ATP release channel properties. As shown in **Figure 3.8**, both mPanx1-EYFP and mPanx3-EGFP release detectable amounts of ATP upon stimulation with

50 mM potassium gluconate (ATP concentration in pM: mPax1, 50 mM KGlu: 2.71 ± 0.05 , p value = $5.06e-5$; mPax3: 50 mM KGlu 1.75 ± 0.006 , p value = $7.10e-4$, N = 3 independent experiments) and 140 mM KGlu (mPax1: 140 mM KGlu 3.09 ± 0.19 , p value = $1.78e-4$; mPax3: 140 mM KGlu 1.72 ± 0.05 , p value = $4.55e-5$, N = 3 independent experiments), when normalized to EGFP or EYFP transfected Neuro2a cells with no stimulation, as well as when compared to non-transfected Neuro2A cells under the same conditions (Neuro2A: 50 mM KGlu 1.05 ± 0.07 , N = 3; 140 mM KGlu 0.55 ± 0.3 , N = 3). The specificity of the observed ATP release was tested using the Pax1 blockers carbenoxelone (CBX), mefloquine (MFQ) and blue food dye (BB FCF). All blockers showed reliable reduction of ATP release induced by high potassium when cells expressed mPax1 (CBX 0.26 ± 0.005 , p value = $1.10e-4$, N = 3; MFQ 0.20 ± 0.007 , p value = $1.10e-4$, N = 3; BB FCF 0.31 ± 0.01 , p value = $1.20e-4$, N = 3). Interestingly, all Pax1 blockers caused the same effect on Pax3 expressing cultures (CBX 0.23 ± 0.01 , p value = $8.71e-6$, N = 3; MFQ 0.27 ± 0.01 , p value = $1.05e-5$, N = 3; BB FCF 0.23 ± 0.02 , p value = $1.05e-5$, N = 3). It is important to note that these blockers also reduce the amount of ATP release in non-transfected Neuro2A cells as well (CBX 0.14 ± 0.003 , p value = $3.00e-4$, N = 3; MFQ 0.10 ± 0.002 , p value = $2.06e-4$, N = 3; BB FCF 0.07 ± 0.005 , p value = $1.77e-4$, N = 3), an observation we attribute to endogenously expressed low levels of mPax1. These results established similar channel properties *in vitro*, with respect to ATP release, amongst mPax1 and mPax3 in response to medium and high concentrations of KGlu and inhibitors that act upon mPax1. This provides a strong rationale to continue comparing channel function properties *in vitro* and to investigate the potential functional replacement of Pax1.

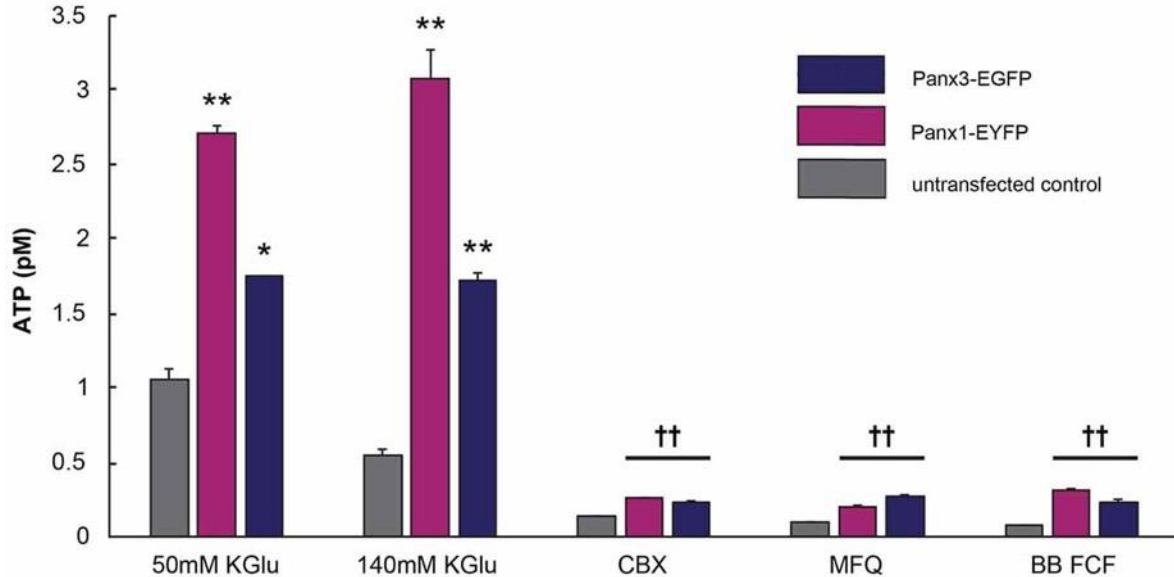


Figure 3.8. Panx3 has ATP releasing properties like Panx1. Luciferase assay depicting the amount of released ATP by Neuro2A cells that were untransfected (gray) or transfected with mPanx1 (Pink) or mPanx3 (Indigo). Using either medium (50 mM) or high (140 mM) concentrations of potassium gluconate (KGlu) stimulates mPanx1 and mPanx3 to release significantly more ATP compared to Neuro2A cells. Traditional Panx1 blockers carbenoxolone (CBX), mefloquine (MFQ) and brilliant blue food dye (BB FCF) also block mPanx3 and Neuro2a cells when stimulated with 140 mM KGlu prior incubation with the blockers. *Indicate significance compared to Neuro2A controls, * $p < 0.001$, ** $p < 0001$. ††Indicates significance compared to 140 mM KGlu stimulation condition. †† $p < 0.001$.

3.3.7. Dye uptake properties of Panx1 and Panx3 in neuro2a cells are similar

ATP release properties of mPanx1 and mPanx3 were comparable in vitro. Hence, a robust ethidium bromide (EtBr) uptake assay (Kurtenbach et al., 2013; Shao et al., 2016) was used to further test channel activities. In this assay (**Figures 3.9a,b**), Neuro2a cells expressing either EYFP or EGFP showed no dye uptake under physiological conditions in complete growth medium (EYFP: $0.026 \pm 6.87e-4$, EGFP: $0.060 \pm 2.30e-3$), as well as after stimulation with 140 mM KGlu (EYFP: $0.078 \pm 8.50e-4$, EGFP: $0.022 \pm 1.20e-3$). In contrast, Neuro2a cells overexpressing mPanx1-EYFP or Panx3-EGFP showed an increasing and linear relationship between the amount of dye uptake and protein expression under both physiological conditions (mPanx1: $R^2 = 0.89$, mPanx3: $R^2 = 0.90$; **Supplementary Figure 3.4a**) and after treatment with 140 mM KGlu (mPanx1: $R^2 = 0.88$, mPanx3: $R^2 = 0.91$; **Supplementary Figure 3.4b**), demonstrating that the dye uptake was correlated with Panx expression. Therefore, dye uptake analysis was conducted after normalizing the amount of dye uptake to the level of protein expression.

Mouse Panx1-EYFP expression caused significantly increased dye uptake under basal conditions (0.9544 ± 0.018 , $n = 198$, $p \text{ value} = 4.46e-10$) when compared to EYFP transfected cells (Figure 9A). In addition, treatment with 50 mM KGlu (1.78 ± 0.012 , $n = 114$, $p \text{ value} =$

2.95e-8), 140 mM KGlu (1.51 ± 0.0042 , $n = 407$, p value = $2.45e-6$), or 3 μ M ATP (3.63 ± 0.061 , $n = 90$, p value = $1.92e-11$) caused a significant increase in dye uptake when compared to mPanx1-EYFP under physiological conditions. In contrast, treatment with 3 mM ATP (0.87 ± 0.0067 , $n = 125$, p value = $1.85e-10$), 500 μ M probenecid (Prob; 0.85 ± 0.013 , $n = 407$, p value = $3.88e-7$) or 10 μ M brilliant blue food dye (BB FCF; $0.99 \pm 6.6e-3$, $n = 407$, p value = $1.59e-6$) prior to stimulation with 140 mM KGlu, a condition previously reported to open Panx1 channels from different species and in difference expression systems showed a significant decrease of dye uptake when compared to treated conditions with 140 mM KGlu alone (**Figure 3.9a**). Together, these results confirmed the effectiveness of two concentrations of KGlu to evoke dye uptake by Neuro2A cells expressing mPanx1. They verified that low and high ATP concentrations increase and reduce dye uptake, respectively, as previously shown in the oocyte expression system (Qiu and Dahl, 2009). Further, they confirm that probenecid (Prob) and brilliant blue food dye (BB FCF) are reliable blockers of mPanx1 in this cell model.

Using the identical experimental conditions, mPanx3-EGFP expressing cells without treatment showed a significant increase in dye uptake when compared to EGFP transfected Neuro2a cells ($0.33 \pm 3.20e-3$, $n = 157$, p -value = $1.21e-8$; **Figure 3.9b**), though it is important to note that this uptake is relatively lower than the average amount of uptake by mPanx1 under the same condition. Similarly, treatment of mPanx3 expressing cells with 50 mM KGlu (1.17 ± 0.013 , $n = 96$, p -value = $1.12e-18$), 140 mM KGlu (1.20 ± 0.0037 , $n = 392$, p -value = $5.12e-40$) or 3 μ M ATP (1.43 ± 0.012 , $n = 102$, p -value = $4.69e-23$) significantly increased dye uptake compared to untreated control cells expressing mPanx3-EGFP. Similar to mPanx1, application of 3 mM ATP inhibited the amount of dye uptake during stimulation with 140 mM KGlu when compared to stimulated controls (0.89 ± 0.010 , $n = 151$, p -value = $1.20e-10$; **Figure 9B**). Further investigation into blocking the mPanx3 channel showed that application of 500 μ M Prob, prior to application of KGlu, efficiently inhibited dye uptake (0.46 ± 0.0077 , $n = 407$, p -value = $2.16e-12$), however, application of 10 μ M BB FCF significantly increased mPanx3 channel activity (2.33 ± 0.022 , $n = 407$, p -value = $1.38e-14$). These results further established mPanx3 channel properties in vitro, in response to stimulants and inhibitors that act upon mPanx1. In summary, this quantitative assessment allowed us to conclude that Panx1 and Panx3 share two significant properties, dye uptake, and ATP release, suggesting that Panx3 can at least in part functionally compensate for Panx1.

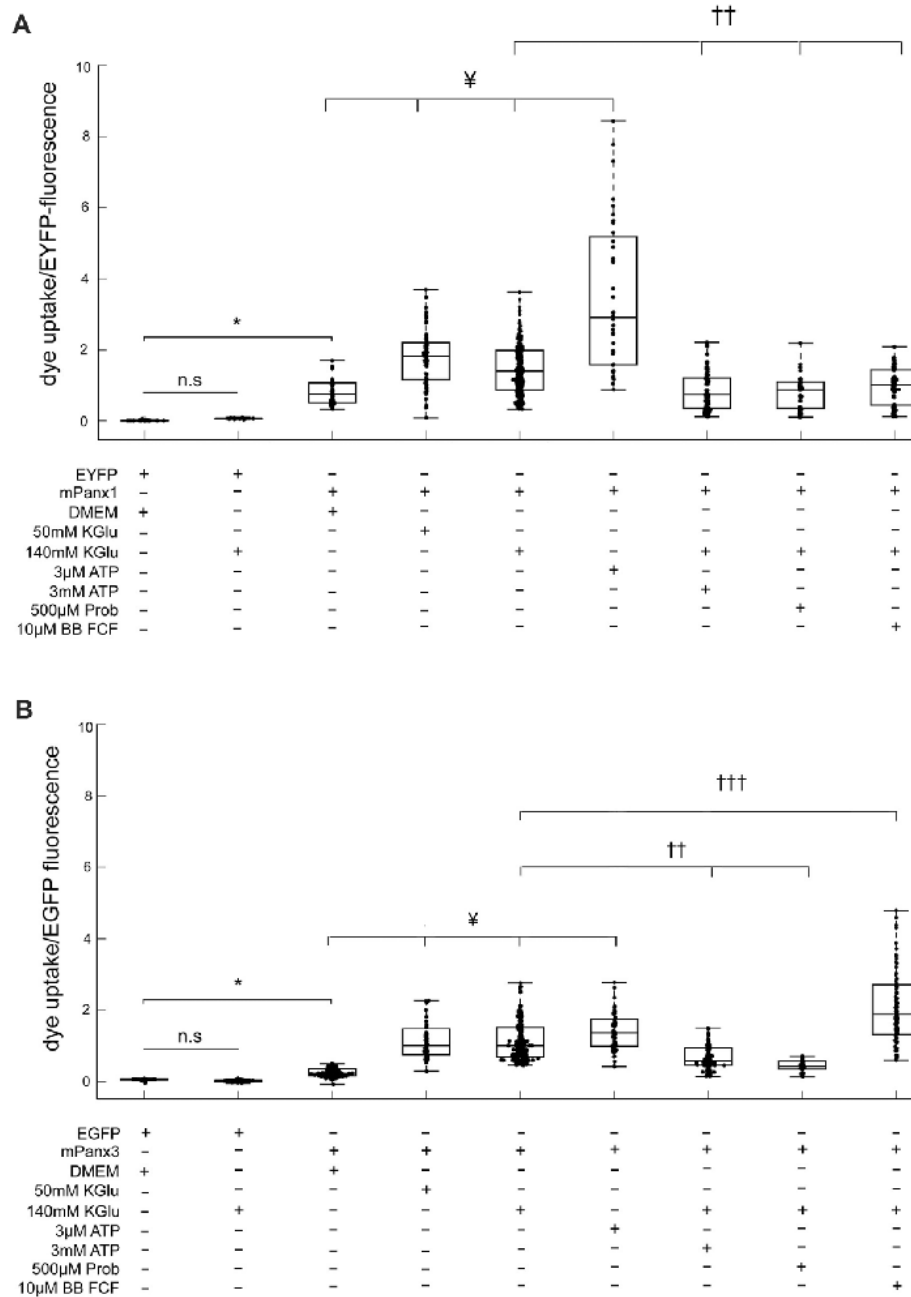


Figure 3.9. Panx1 and Panx3 dye uptake properties. EtBr uptake assay is depicting the amount of dye taken up by Neuro2A cells that were transfected with EYFP, EGFP, mPanx1-EYFP or with mPanx3-EGFP. a) Neuro2A-EYFP cells did not uptake dye, even when trying to stimulate with 140 mM KGlu. However, using either 50mM KGlu, 140 mM KGlu, 3 μM ATP on mPanx1 transfected cultures, significantly stimulated channel opening. 3 mM ATP, 500 μM Prob or 10 μM BB FCF application, after stimulation with 140 mM KGlu for 5 min, block the channel from taking up the dye. b) EtBr uptake assay is depicting the amount of dye taken up by Neuro2A cells that were transfected with EGFP or with mPanx3. Neuro2A-EGFP cells did not uptake dye, even when trying to stimulate with 140 mM KGlu. However, using either 0 mM KGlu, 140 mM KGlu, 3 μM ATP on mPanx3 transfected cultures, significantly stimulated channel opening. 3 mM ATP or 500 μM Prob application, after stimulation with 140 mM KGlu for 5 min, block the channel from taking up the dye. Treatment with 10 μM BB FCF after application of 140 mM KGlu enhanced dye uptake activity significantly compared to treatment with 140 mM KGlu alone. *Indicate significance compared to Neuro2A controls, * $p <$

0.0001. [¥]Indicate significance compared to basal conditions, [¥] $p < 0.0001$. ^{††}Indicates significant decrease compared to 140 mM KGlu stimulation conditions, ^{†††}indicates significant increase compared to 140 mM KGlu stimulation conditions ^{††} $p < 0.0001$ and ^{†††} $p < 0.0001$. KGlu (potassium gluconate), ATP (adenosine triphosphate), Prob (probenecid), BB FCF (Brilliant blue food dye).

3.4. Discussion

This research shows the expression and localization of three Panxs in the VNO of both wild-type and a well-established mouse model with genetic ablation of mPanx1. Both mPanx1 and mPanx3 show differential expression in juvenile and adult mice, with a remarkable upregulation of Panx3 in the VNO—specifically in areas with no Panx1 expression after genetic ablation. Panx2 was ubiquitously distributed in the VNO, but not differentially regulated. The compensatory regulation of Panx3 in Panx1^{-/-} mice raised the question whether Panx3 forms channels, which, at least in part, can compensate for the loss of Panx1. Using another established model, Neuro2A cells expressing mPanx1 or mPanx3, channel function was demonstrated using two independent methods exhibiting that Panx3 could take up dye, release ATP, and respond to Panx1 blockers—providing the first evidence that Panx3 is forming functional channels with properties similar to Panx1.

3.4.1. Pannexins in the mouse VNO

Extending our previous research on Panxs in olfaction—suggesting indirect or even negligible roles of Panx1 in primary olfaction (Kurtenbach et al., 2014), we have shown in this study the expression of mRNA and protein localization of the three Panxs in the VNO. The results are different to our findings in the OE of mice, which express mPanx1, low levels of mPanx2, but no mPanx3 mRNA. Also, the IHC of the OE revealed a significant, but restricted, labeling of the OSN axon bundles that project to the olfactory bulb, but lacked immunoreactivity in the OSNs themselves (Kurtenbach et al., 2014). Further, no compensatory regulation of Panx3 was found in the OE of Panx1^{-/-} mice. To our knowledge, only one other sensory organ, the cochlea, expresses all Panxs in the same tissue (Wang et al., 2009; Zhao, 2016), whereas other parts of the nervous system typically express Panx1 and Panx2, but lack Panx3 (Bruzzone et al., 2003). In fact, our previous studies of other sensory organs, including the eye (Ray et al., 2005; Dvorianchikova et al., 2006), primary olfactory system (Kurtenbach et al., 2014), or lacrimal gland (Basova et al., 2017) showed either lack, or very low levels of Panx3 gene expression.

The localization of mPax1, as well as mPax3 in Pax1^{-/-} mice, is consistent with the requirement for ATP release in the VNO (see “Discussion” section below). The expression and localization of Pax3 in the VNO after loss of Pax1 is remarkable, since Pax3 expression has typically been limited to skin, bone and cartilage (Celetti et al., 2010; Moon et al., 2015; Oh et al., 2015; Caskenette et al., 2016; Ishikawa et al., 2016), skeletal myoblasts (Langlois et al., 2014) or low diameter arteries (Lohman et al., 2012). Multiple studies have highlighted the importance of VNO function in reproductive behaviors in mice. Hence, it makes sense that a compensation system has evolved to maintain its function in extreme circumstances, e.g., loss of an essential protein. Our behavior tests did not reveal major changes of Pax1 KO for behaviors associated with VNO function, showing that Pax3 might be able to compensate for Pax1 loss efficiently. We did find a significant increase in smell time of resident Pax1^{-/-} mice towards intruders. This difference is potentially an interesting observation because investigating and sniffing at intruders may also be influenced by memory deficits (Prochnow et al., 2012). Generally speaking, the availability of Pax3 KO mice (Moon et al., 2015; Abitbol et al., 2016) has allowed for the investigation of the role(s) Pax3 plays in the bone, with results suggestive of Pax3 regulating chondrocyte and osteoprogenitor cell proliferation and differentiation, long bone growth, and skeletal formation and development (Moon et al., 2015; Oh et al., 2015; Abitbol et al., 2016; Caskenette et al., 2016). However, the investigation of the roles of Pax3 functions beyond these tissues have yet to be reported, with this study being the first to implicate a role for Pax3 in a sensory system.

3.4.2. What is the evidence that ATP release plays a critical role in VNO function?

We propose that ATP release is the key physiological role served by Pax1 and Pax3 in the VNO. Gerhard Dahl and his coworkers were the first to demonstrate the role of Pax1 as a major ATP release site (Locovei et al., 2006, 2007). Since then, Pax1 mediated ATP release has been found in many tissues and cell types, substantiating that this mode of regulated ATP release, alongside other non-vesicular ATP release pathways, is important to achieve tissue function(s) (for review see (Dahl and Keane, 2012; Scemes, 2012; Dahl et al., 2013; Penuela et al., 2013; Good et al., 2015). It is important to note that ATP release via Pax1 has not consistently been found (Taruno et al., 2013), which may indicate that some tissues do not rely on Pax1 mediated ATP release to achieve function, or compensatory upregulation was not investigated.

Pheromones are detected by VSNs once they are forced into the lumen of the VNO by a vascular pump triggered by sympathetic stimulation of the Vidian nerve (Eccles and Eccles, 1981), where we see an expression of Panx1 and Panx3 in juveniles. This mobilization of chemical signals is due to the sympathetic nervous system initiating ATP release (Rummery et al., 2007), which is also extremely important in evoking neural contractions of the vascularized erectile tissue on the lateral side of the lumen for further chemical processing. The signal transduction cascade is complex in the VNO, as the neuroepithelium consists of multiple distinct populations of VSNs. However, recent advances have implicated that there are subzone-specific ligands and sensory transduction components that enable VNO subdivisions to control specific olfactory-mediated behaviors (Kumar et al., 1999; Oboti and Peretto, 2014; Pérez-Gómez et al., 2014). For example, research conducted by Leinders-Zufall et al. (2014) has already demonstrated that aggressive behavior toward intruder males requires sensory transduction from basal VSNs. This is a region in adults where we saw the expression of Panx1 and increased Panx3 expression in KOs. We propose that important paracrine signaling functions of ATP for signal transduction are mediated by Panxs. The observed lack of upregulation of alternative channels and receptors is evidence in support of this concept. Together, the significant expression of Panx1 and Panx3 in both the basal and apical regions of the adult sensory layer, implicates the involvement of Panxs in olfaction in the context of adult social behavior, whereas the more restricted expression found in juvenile mice is more likely to serve the biomechanical functions of the developing VNO. Once Panx1 and Panx3 single and double KO mice become more broadly available, it will become possible to address this knowledge gap in longitudinal studies from juvenile to adult stages.

3.4.3. Is Panx3 a channel that can compensate for Panx1?

This study provides evidence that Panx3 is an ATP release channel similar to Panx1, supporting two claims of ATP release via Panx3, suggestive of channel function, in cultured ATDC5 skeletal cells (Iwamoto et al., 2010) and human odontoblast-like cells (Fu et al., 2015). Further, Panx3, like Panx1, takes up dye in a linear relationship with protein expression, albeit at different efficiency, and in response to known Panx1 blockers. Several results are notable. Both ATP release and dye uptake through mPanx1 and mPanx3 were activated by stimulation with a medium (50 mM) and a high (140 mM) concentration of KGlu. The later concentration of 140 mM has been used

repeatedly since the introduction to the field (Bao et al., 2004; Silverman et al., 2009), providing robust activation in our hands.

It is also noteworthy that blockers previously reported acting individually on Panx1 block Panx3 as well. This effect is most likely due to the structural homology of both proteins, which share a 73.25% similarity at the amino acid level, and that Panx1 and Panx3 channels can interact to some, albeit low, extent with no observed change to the channel function when intermixed (Penuela et al., 2009). Interestingly, BB FCF, a selective blocker of Panx1 channels (Wang et al., 2013), reliably blocked ATP release in both mPanx1-EYFP and mPanx3-EGFP expressing Neuro2a cells. However, it selectively affected only mPanx1 mediated dye uptake. At present, the reason for the difference in BB FCF blocking efficiency of mPanx3 during dye uptake vs. measuring ATP release is unclear. Although, we surmise that this model imitates the model in vivo by efficiently blocking mPanx1 channels in vitro and observing the enhanced activity of mPanx3. Despite the fact that the blocker pharmacology of Panx1 channels remains bizarre, as eloquently highlighted by Dahl et al. (2013), the distinct responses to BB FCF could be a starting point for isolating Panx1 and Panx3 channel activities separately. Ultimately, the observation that BB FCF can increase dye uptake provides a unique opportunity to determine the mode of interaction between BB FCF and protein targets by domain swapping experiments using chimeras of mPanx1 and mPanx3.

While we can provide evidence for Panx3 channel activities using two different methods, key biophysical properties accessible only through electrophysiological methods are lacking. However, our results point to the possibility that the biophysical properties of Panx3 channels can be investigated using similar procedures used for Panx1. It is very likely that these properties would be difficult to isolate when the cell culture model used expresses endogenous Panx1 or Panx3, in particular when the robust activity of Panx1 may mask those contributed by Panx3. Therefore, generating genetically engineered cell lines, with ablation of Panx1 and Panx3, for example by using Cas9/CRISPR or Transcription activator-like effector nucleases (TALEN), could help to overcome this knowledge gap. Together, our results point to the possibility that Panx3 channels are more subtle and challenging to study using traditional biomolecular techniques including electrophysiology, which is in line with the lack of data in the literature. On a similar note, more specific Panx blockers need to be found, which will allow distinguishing Panx1 from Panx3 functions in vitro and in vivo.

3.4.4. Compensatory regulations of pannexins: Why and how?

The upregulation of Panx3 observed in this study, has also been found in the vasculature (Lohman et al., 2012) and skin (Penuela et al., 2014) of different knock out mouse models. This suggests that the mobilization of Panx3 expression due to the absence of Panx1, as well as the properties shared between Panx1 and Panx3, is not restricted to a single loss of function phenotype.

Why is Panx3 upregulation required in the absence of Panx1? We hypothesize that the VNO requires tight control of ATP concentrations in a physiological range as a means of supporting prominent roles in triggering innate behavioral responses, like aggressive and reproductive behaviors (Pérez-Gómez et al., 2014). Since these behaviors are critical for the survival as a species, Panx3 upregulation could represent a safeguarding mechanism of unknown complexity that is innate to the cell type affected by the genetic KO and able to compensate for the loss of Panx1 as a major ATP release site—important in paracrine signaling.

The molecular mechanism of the compensatory regulation is open to speculations. Comparative studies of wild-type and KO mice at the level of the transcriptome, epigenome, proteome, or by promoter studies are likely to provide insight into the underlying molecular mechanism. In addition, the availability of Panx1 (Bargiotas et al., 2011; Qu et al., 2011; Dvorianchikova et al., 2012; Hanstein et al., 2013) and Panx3 KO mice (Moon et al., 2015; Abitbol et al., 2016), as either single or double KOs, will be critical in this process. Further, future studies are also likely to aid in clarifying other evidence for compensatory regulation of Panxs, like in the vasculature (Lohman and Isakson, 2014) and skin (Penuela et al., 2014). However, whether these examples of compensatory regulation share a common mechanism, or a cell type or tissue-specific mechanism, needs to be determined.

Additional Information

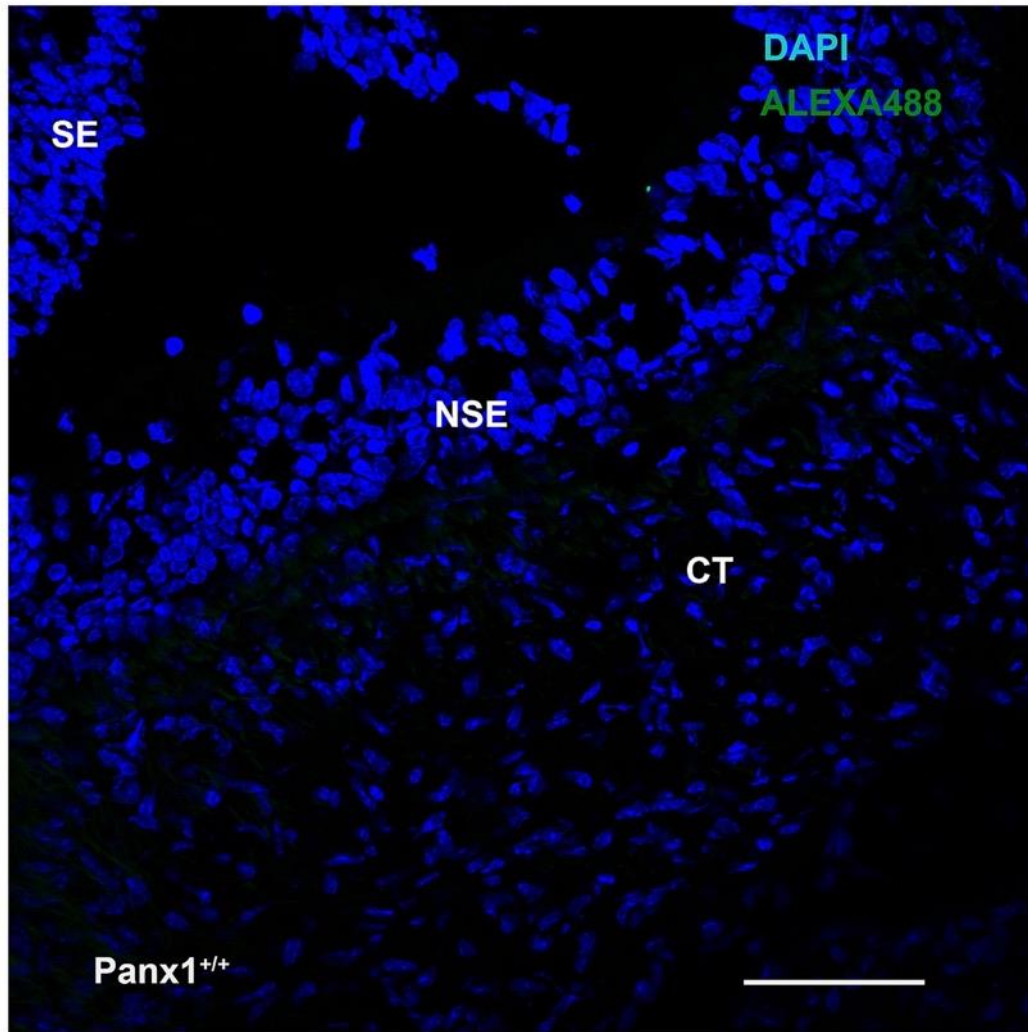
Acknowledgements

We thank Uilki Tufa (University of Toronto, ON, Canada) for kindly providing aid in developing the ImageJ macros used for automated cell selection and the Matlab code used to analyze the dye uptake data. This research was supported by an Natural Sciences and Engineering Research Council (NSERC) discovery grant 418142-2012 (GZ), Canadian Institutes of Health Research (CIHR) grant MOP 119603 (PLC), and National Institutes of Health (NIH) grant EY R01-021517 (VIS).

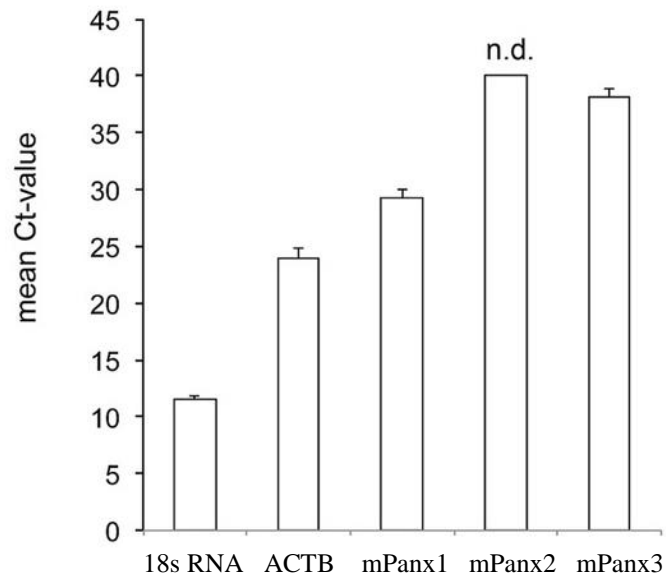
Conflict of Interest Statement

The authors declare that the research was conducted in the absence of any commercial or financial relationships that could be construed as a potential conflict of interest.

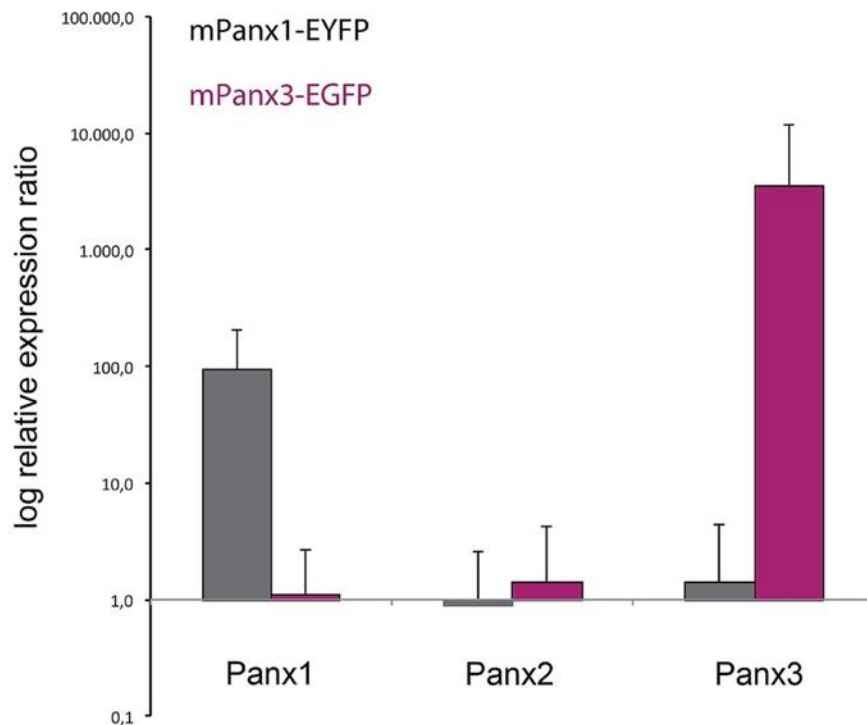
3.5. Supplementary Data – Included in published manuscript



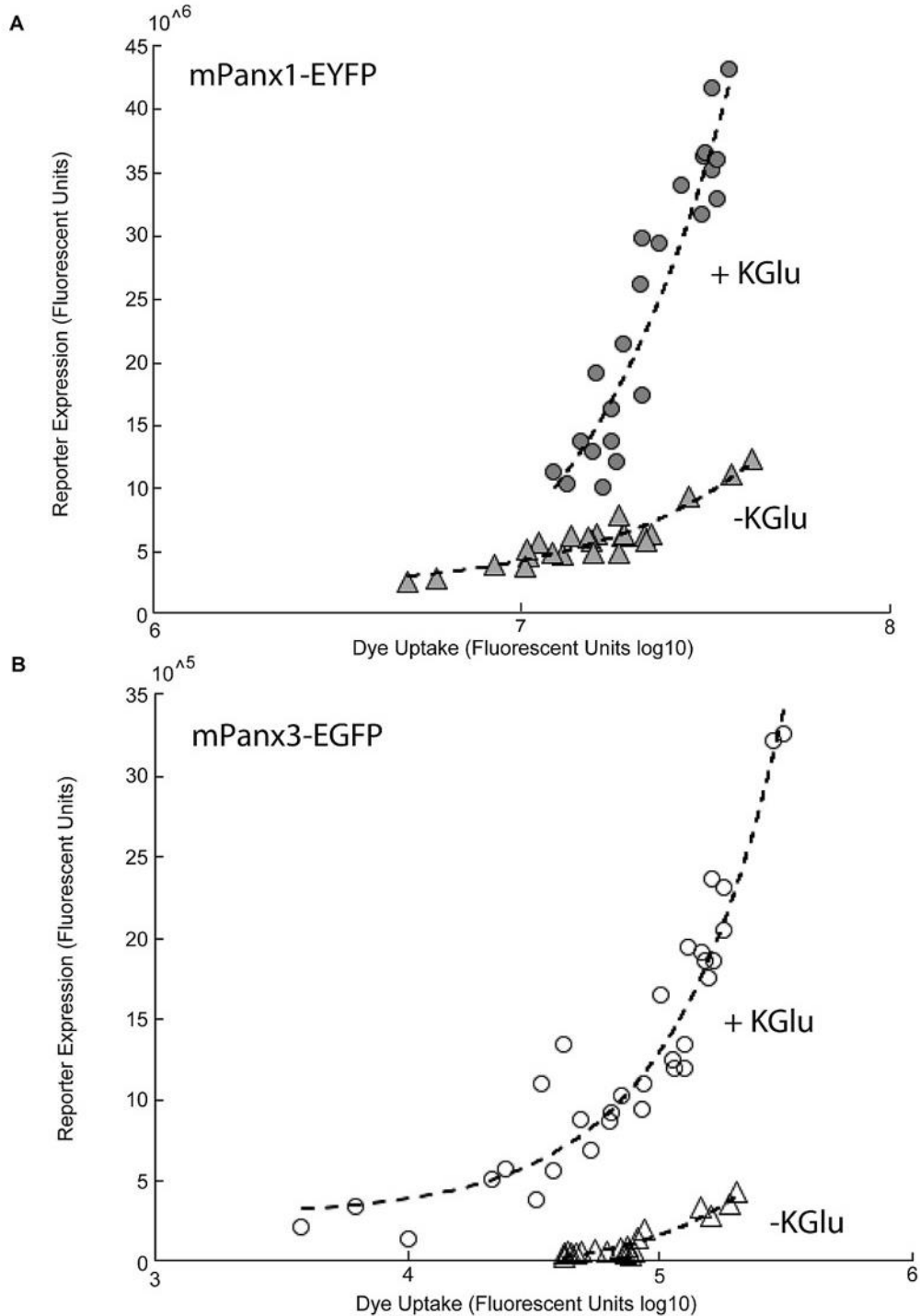
Supplementary Figure 3.1. Secondary antibody control for Immunohistochemistry (IHC). A section of the juvenile VNO was processed for IHC and incubated with secondary goat anti-rabbit Alexa Fluor 488 antibody (Invitrogen, Canada) only. The confocal image showing background signal was captured using the identical settings used in Figure 3.2. Scale bar = 200 μ M.



Supplementary Figure 3.2. Quantitative PCR analysis of total RNA isolated from Neuro2a cells. The average cycle threshold (Ct) values demonstrated the expected high (18 s RNA; Ct < 20) and medium (β -actin/ACTB; Ct 20–30) expression levels for the reference RNAs. Mouse Panx1 and mPanx3 mRNAs were expressed at medium (mPanx1; Ct 20–30) and low levels (mPanx3; Ct > 30). The very low expression of mPanx3 was positively identified through melt curve analysis of the PCR generated amplicon (data not shown). No expression of Panx2 mRNA was detected. Values represent mean \pm SD. Abbreviation: n.d. = not detected.

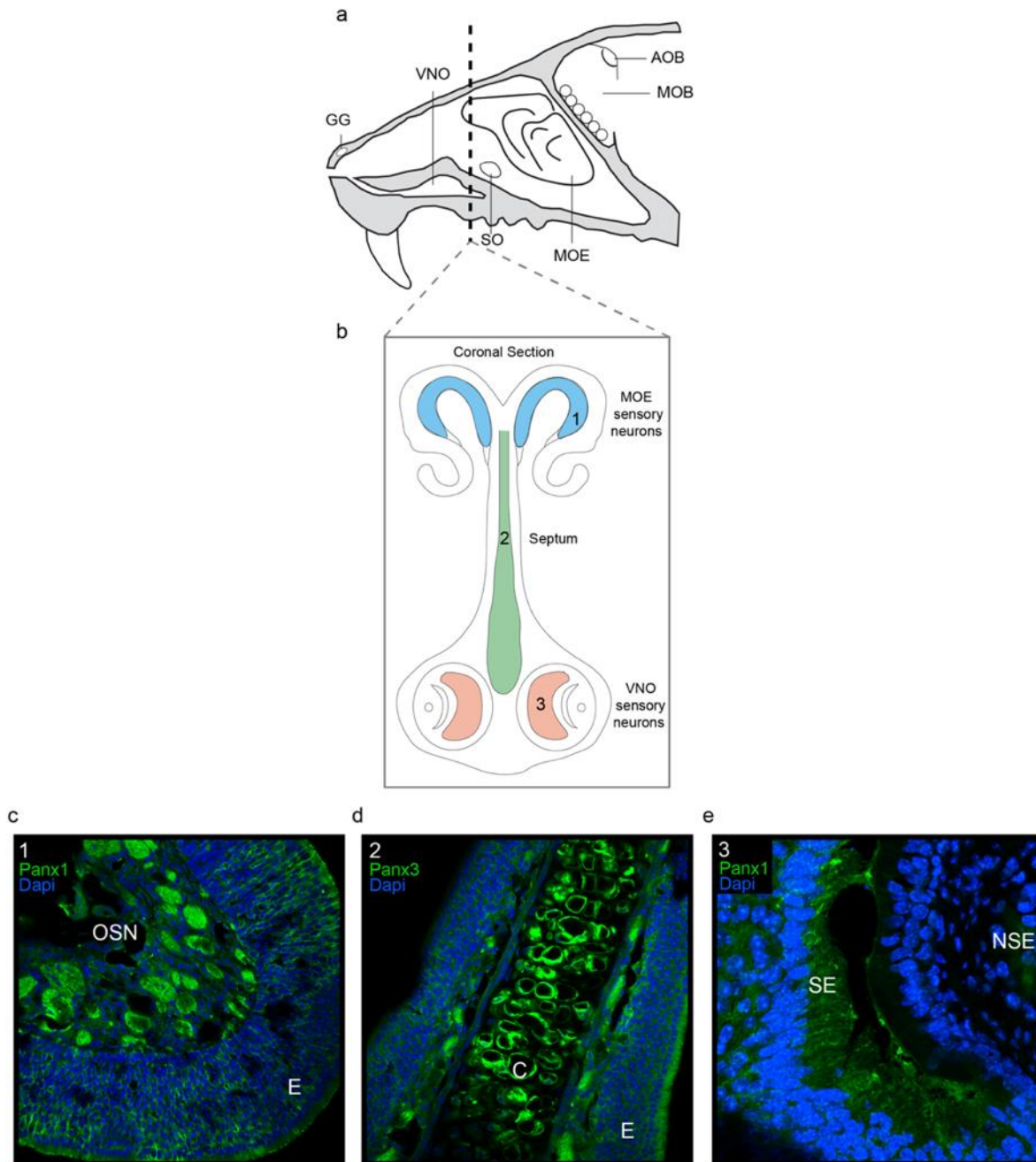


Supplementary Figure 3.3. Expression of pannexin mRNAs in transiently transfected Neuro2a cells. QRT-PCR showed overexpression of mPanx1 and mPanx3 in Neuro2a cells transiently transfected with mPanx1-EYFP or mPanx3-EGFP. All experiments were performed in triplicates. Values represent mean \pm SD.



Supplementary Figure 3.4. Linear correlation analysis of fluorescent reporter expression and uptake of ethidium bromide. Normalizing the amount of dye uptake, the fluorescence of EtBr, to the amount of fluorescent reporter expression (mPanx1-EYFP and mPanx3-EGFP), reveals a strong and consistent linear relationship under control and stimulated conditions. (A) mPanx1 under DMEM (closed dots), $R^2 = 0.88$, and mPanx1 with 140 mM KGlU stimulation (closed triangles), $R^2 = 0.89$. (B) mPanx3 with DMEM (open dots), $R^2 = 0.90$, and mPanx3 with 140 mM KGlU stimulation (open triangles), $R^2 = 0.91$.

3.6. Supplementary Data – Not included in published manuscript



Supplementary Figure 3.5. Panx1 and Panx3 expression in the mouse olfactory system of WT mice. a) Schematic of the mouse olfactory system. **b)** Schematic of coronal section depicting 3 main regions of interest for localization investigation. (1. Main olfactory epithelium 2. Septum 3. Accessory olfactory epithelium). Each region, part of main and accessory olfactory systems, was tested for Panx expression. **c)** Panx1 expression in (green) found in the axon bundles of olfactory sensory neurons (OSN) and some diffuse expression in the epithelial layer (E) of juvenile WT mice. **d)** Panx3 expression in the septum of juvenile WT mice confirming selectivity of the antibody showing expression in chondrocytes which is unique to panx3 and not found for panx1. **e)** Panx1 expression in the adult VNO in the sensory epithelial layer (SE) as a reference for continuous, but altered (note juvenile expression in NSE of VNO for panx1), panx1 expression throughout the development of the mouse olfactory system. IHC images in c-e were incubated with secondary goat anti-rabbit Alexa Fluor 488 antibody (Invitrogen, Canada). Dapi is in blue for nuclei staining. The confocal images were captured at 40x magnification. Scale bar = 100 μ m.

3.7. References

- Abitbol, J. M., Kelly, J. J., Barr, K., Schormans, A. L., Laird, D. W., and Allman, B. L. (2016). Differential effects of pannexins on noise-induced hearing loss. *Biochem. J.* 473, 4665–4680. doi: 10.1042/bcj20160668
- Bao, L., Locovei, S., and Dahl, G. (2004). Pannexin membrane channels are mechanosensitive conduits for ATP. *FEBS Lett.* 572, 65–68. doi: 10.1016/j.febslet.2004.07.009
- Bargiotas, P., Krenz, A., Hormuzdi, S. G., Ridder, D. A., Herb, A., Barakat, W., et al. (2011). Pannexins in ischemia-induced neurodegeneration. *Proc. Natl. Acad. Sci. U S A* 108, 20772–20777. doi: 10.1073/pnas.1018262108
- Basova, L. V., Tang, X., Umasume, T., Gromova, A., Zyrianova, T., Shmushkovich, T., et al. (2017). Manipulation of panx1 activity increases the engraftment of transplanted lacrimal gland epithelial progenitor cells. *Invest. Ophthalmol. Vis. Sci.* 58, 5654–5665. doi: 10.1167/iovs.17-22071
- Boassa, D., Ambrosi, C., Qiu, F., Dahl, G., Gaietta, G., and Sosinsky, G. (2007). Pannexin1 channels contain a glycosylation site that targets the hexamer to the plasma membrane. *J. Biol. Chem.* 282, 31733–31743. doi: 10.1074/jbc.M702422200
- Brignall, A. C., and Cloutier, J. F. (2015). Neural map formation and sensory coding in the vomeronasal system. *Cell. Mol. Life Sci.* 72, 4697–4709. doi: 10.1007/s00018-015-2029-5
- Bruzzone, R., Hormuzdi, S. G., Barbe, M. T., Herb, A., and Monyer, H. (2003). Pannexins, a family of gap junction proteins expressed in brain. *Proc. Natl. Acad. Sci. U S A* 100, 13644–13649. doi: 10.1073/pnas.2233464100
- Caskenette, D., Penuela, S., Lee, V., Barr, K., Beier, F., Laird, D. W., et al. (2016). Global deletion of Panx3 produces multiple phenotypic effects in mouse humeri and femora. *J. Anat.* 228, 746–756. doi: 10.1111/joa.12437
- Celetti, S. J., Cowan, K. N., Penuela, S., Shao, Q., Churko, J., and Laird, D. W. (2010). Implications of pannexin 1 and pannexin 3 for keratinocyte differentiation. *J. Cell Sci.* 123, 1363–1372. doi: 10.1242/jcs.056093
- Dahl, G., and Keane, R. W. (2012). Pannexin: from discovery to bedside in 11±4 years? *Brain Res.* 1487, 150–159. doi: 10.1016/j.brainres.2012.04.058
- Dahl, G., Qiu, F., and Wang, J. (2013). The bizarre pharmacology of the ATP release channel pannexin1. *Neuropharmacology* 75, 583–593. doi: 10.1016/j.neuropharm.2013.02.019
- Dvorianchikova, G., Ivanov, D., Barakat, D., Grinberg, A., Wen, R., Slepak, V. Z., et al. (2012). Genetic ablation of Pannexin1 protects retinal neurons from ischemic injury. *PLoS One* 7:e31991. doi: 10.1371/journal.pone.0031991
- Dvorianchikova, G., Ivanov, D., Panchin, Y., and Shestopalov, V. I. (2006). Expression of pannexin family of proteins in the retina. *FEBS Lett.* 580, 2178–2182. doi: 10.1016/j.febslet.2006.03.026
- Eccles, R., and Eccles, K. S. (1981). Sympathetic innervation of the nasal mucosa of the pig. *Res. Vet. Sci.* 30, 349–352.
- Fu, D., Song, F., Sun, H., Pei, D., Wang, Y., Lei, J., et al. (2015). Expression of Pannexin3 in human odontoblast-like cells and its hemichannel function in mediating ATP release. *Arch. Oral. Biol.* 60, 1510–1516. doi: 10.1016/j.archoralbio.2015.07.005
- Gayle, S., and Burnstock, G. (2005). Immunolocalisation of P2X and P2Y nucleotide receptors in the rat nasal mucosa. *Cell Tissue Res.* 319, 27–36. doi: 10.1007/s00441-004-0979-2

- Good, M. E., Begandt, D., Delalio, L. J., Keller, A. S., Billaud, M., and Isakson, B. E. (2015). Emerging concepts regarding pannexin 1 in the vasculature. *Biochem. Soc. Trans.* 43, 495–501. doi: 10.1042/BST20150045
- Grundken, C., Hanske, J., Wengel, S., Reuter, W., Abdulazim, A., Shestopalov, V. I., et al. (2011). Unified patch clamp protocol for the characterization of Pannexin 1 channels in isolated cells and acute brain slices. *J. Neurosci. Methods* 199, 15–25. doi: 10.1016/j.jneumeth.2011.04.016
- Halpern, M. (1987). The organization and function of the vomeronasal system. *Annu. Rev. Neurosci.* 10, 325–362. doi: 10.1146/annurev.neuro.10.1.325
- Hanstein, R., Negoro, H., Patel, N. K., Charollais, A., Meda, P., Spray, D. C., et al. (2013). Promises and pitfalls of a Pannexin1 transgenic mouse line. *Front. Pharmacol.* 4:61. doi: 10.3389/fphar.2013.00061
- Huang, Y. J., Maruyama, Y., Dvoryanchikov, G., Pereira, E., Chaudhari, N., and Roper, S. D. (2007). The role of pannexin 1 hemichannels in ATP release and cell-cell communication in mouse taste buds. *Proc. Natl. Acad. Sci. U S A* 104, 6436–6441. doi: 10.1073/pnas.0611280104
- Ishikawa, M., Williams, G. L., Ikeuchi, T., Sakai, K., Fukumoto, S., and Yamada, Y. (2016). Pannexin 3 and connexin 43 modulate skeletal development through their distinct functions and expression patterns. *J. Cell Sci.* 129, 1018–1030. doi: 10.1242/jcs.176883
- Iwamoto, T., Nakamura, T., Doyle, A., Ishikawa, M., de Vega, S., Fukumoto, S., et al. (2010). Pannexin 3 regulates intracellular ATP/cAMP levels and promotes chondrocyte differentiation. *J. Biol. Chem.* 285, 18948–18958. doi: 10.1074/jbc.M110.127027
- Jeong, S. W., and Ikeda, S. R. (1998). G protein α subunit $G\alpha_z$ couples neurotransmitter receptors to ion channels in sympathetic neurons. *Neuron* 21, 1201–1212. doi: 10.1016/s0896-6273(00)80636-4
- Kumar, A., Dudley, C. A., and Moss, R. L. (1999). Functional dichotomy within the vomeronasal system: distinct zones of neuronal activity in the accessory olfactory bulb correlate with sex-specific behaviors. *J. Neurosci.* 19:RC32. doi: 10.1523/JNEUROSCI.19-20-j0003.1999
- Kurtenbach, S., Prochnow, N., Kurtenbach, S., Klooster, J., Zoidl, C., Dermietzel, R., et al. (2013). Pannexin1 channel proteins in the zebrafish retina have shared and unique properties. *PLoS One* 8:e77722. doi: 10.1371/journal.pone.0077722
- Kurtenbach, S., Whyte-Fagundes, P., Gelis, L., Kurtenbach, S., Brazil, E., Zoidl, C., et al. (2014). Investigation of olfactory function in a Panx1 knock out mouse model. *Front. Cell. Neurosci.* 8:266. doi: 10.3389/fncel.2014.00266
- Langlois, S., Xiang, X., Young, K., Cowan, B. J., Penuela, S., and Cowan, K. N. (2014). Pannexin 1 and pannexin 3 channels regulate skeletal muscle myoblast proliferation and differentiation. *J. Biol. Chem.* 289, 30717–30731. doi: 10.1074/jbc.M114.572131
- Le Vasseur, M., Lelowski, J., Bechberger, J. F., Sin, W. C., and Naus, C. C. (2014). Pannexin 2 protein expression is not restricted to the CNS. *Front. Cell. Neurosci.* 8:392. doi: 10.3389/fncel.2014.00392
- Leinders-Zufall, T., Ishii, T., Chamero, P., Hendrix, P., Oboti, L., Schmid, A., et al. (2014). A family of nonclassical class I MHC genes contributes to ultrasensitive chemodetection by mouse vomeronasal sensory neurons. *J. Neurosci.* 34, 5121–5133. doi: 10.1523/JNEUROSCI.0186-14.2014

- Locovei, S., Scemes, E., Qiu, F., Spray, D. C., and Dahl, G. (2007). Pannexin1 is part of the pore forming unit of the P2X₇ receptor death complex. *FEBS Lett.* 581, 483–488. doi: 10.1016/j.febslet.2006.12.056
- Locovei, S., Wang, J., and Dahl, G. (2006). Activation of pannexin 1 channels by ATP through P2Y receptors and by cytoplasmic calcium. *FEBS Lett.* 580, 239–244. doi: 10.1016/j.febslet.2005.12.004
- Lohman, A. W., Billaud, M., Straub, A. C., Johnstone, S. R., Best, A. K., Lee, M., et al. (2012). Expression of pannexin isoforms in the systemic murine arterial network. *J. Vasc. Res.* 49, 405–416. doi: 10.1159/000338758
- Lohman, A. W., and Isakson, B. E. (2014). Differentiating connexin hemichannels and pannexin channels in cellular ATP release. *FEBS Lett.* 588, 1379–1388. doi: 10.1016/j.febslet.2014.02.004
- Moon, P. M., Penuela, S., Barr, K., Khan, S., Pin, C. L., Welch, I., et al. (2015). Deletion of Panx3 prevents the development of surgically induced osteoarthritis. *J. Mol. Med. (Berl)* 93, 845–856. doi: 10.1007/s00109-015-1311-1
- Oboti, L., and Peretto, P. (2014). How neurogenesis finds its place in a hardwired sensory system. *Front. Neurosci.* 8:102. doi: 10.3389/fnins.2014.00102
- Oh, S. K., Shin, J. O., Baek, J. I., Lee, J., Bae, J. W., Ankamerddy, H., et al. (2015). Pannexin 3 is required for normal progression of skeletal development in vertebrates. *FASEB J.* 29, 4473–4484. doi: 10.1096/fj.15-273722
- Olmsted, J. B., Carlson, K., Klebe, R., Ruddle, F., and Rosenbaum, J. (1970). Isolation of microtubule protein from cultured mouse neuroblastoma cells. *Proc. Natl. Acad. Sci. U S A* 65, 129–136. doi: 10.1073/pnas.65.1.129
- Panchin, Y., Kelmanson, I., Matz, M., Lukyanov, K., Usman, N., and Lukyanov, S. (2000). A ubiquitous family of putative gap junction molecules. *Curr. Biol.* 10, R473–R474. doi: 10.1016/s0960-9822(00)00576-5
- Penuela, S., Bhalla, R., Gong, X. Q., Cowan, K. N., Celetti, S. J., Cowan, B. J., et al. (2007). Pannexin 1 and pannexin 3 are glycoproteins that exhibit many distinct characteristics from the connexin family of gap junction proteins. *J. Cell Sci.* 120, 3772–3783. doi: 10.1242/jcs.009514
- Penuela, S., Bhalla, R., Nag, K., and Laird, D. W. (2009). Glycosylation regulates pannexin intermixing and cellular localization. *Mol. Biol. Cell* 20, 4313–4323. doi: 10.1091/mbc.E09-01-0067
- Penuela, S., Celetti, S. J., Bhalla, R., Shao, Q., and Laird, D. W. (2008). Diverse subcellular distribution profiles of pannexin 1 and pannexin 3. *Cell Commun. Adhes.* 15, 133–142. doi: 10.1080/15419060802014115
- Penuela, S., Gehi, R., and Laird, D. W. (2013). The biochemistry and function of pannexin channels. *Biochim. Biophys. Acta* 1828, 15–22. doi: 10.1016/j.bbamem.2012.01.017
- Penuela, S., Kelly, J. J., Churko, J. M., Barr, K. J., Berger, A. C., and Laird, D. W. (2014). Panx1 regulates cellular properties of keratinocytes and dermal fibroblasts in skin development and wound healing. *J. Invest. Dermatol.* 134, 2026–2035. doi: 10.1038/jid.2014.86
- Pérez-Gómez, A., Stein, B., Leinders-Zufall, T., and Chamero, P. (2014). Signaling mechanisms and behavioral function of the mouse basal vomeronasal neuroepithelium. *Front. Neuroanat.* 8:135. doi: 10.3389/fnana.2014.00135

- Pfaffl, M. W., Horgan, G. W., and Dempfle, L. (2002). Relative expression software tool (REST) for group-wise comparison and statistical analysis of relative expression results in real-time PCR. *Nucleic Acids Res.* 30:e36. doi: 10.1093/nar/30.9.e36
- Prochnow, N., Abdulazim, A., Kurtenbach, S., Wildforster, V., Dvorientchikova, G., Hanske, J., et al. (2012). Pannexin1 stabilizes synaptic plasticity and is needed for learning. *PLoS One* 7:e51767. doi: 10.1371/journal.pone.0051767
- Prochnow, N., Hoffmann, S., Dermietzel, R., and Zoidl, G. (2009). Replacement of a single cysteine in the fourth transmembrane region of zebrafish pannexin 1 alters hemichannel gating behavior. *Exp. Brain Res.* 199, 255–264. doi: 10.1007/s00221-009-1957-4
- Qiu, F., and Dahl, G. (2009). A permeant regulating its permeation pore: inhibition of pannexin 1 channels by ATP. *Am. J. Physiol. Cell Physiol.* 296, C250–C255. doi: 10.1152/ajpcell.00433.2008
- Qu, Y., Misaghi, S., Newton, K., Gilmour, L. L., Louie, S., Cupp, J. E., et al. (2011). Pannexin-1 is required for ATP release during apoptosis but not for inflammasome activation. *J. Immunol.* 186, 6553–6561. doi: 10.4049/jimmunol.1100478
- Ray, A., Zoidl, G., Wahle, P., and Dermietzel, R. (2006). Pannexin expression in the cerebellum. *Cerebellum* 5, 189–192. doi: 10.1080/14734220500530082
- Ray, A., Zoidl, G., Weickert, S., Wahle, P., and Dermietzel, R. (2005). Site-specific and developmental expression of pannexin1 in the mouse nervous system. *Eur. J. Neurosci.* 21, 3277–3290. doi: 10.1111/j.1460-9568.2005.04139.x
- Romanov, R. A., Rogachevskaja, O. A., Bystrova, M. F., Jiang, P., Margolskee, R. F., and Kolesnikov, S. S. (2007). Afferent neurotransmission mediated by hemichannels in mammalian taste cells. *EMBO J.* 26, 657–667. doi: 10.1038/sj.emboj.7601526
- Rummery, N. M., Brock, J. A., Pakdeechote, P., Ralevic, V., and Dunn, W. R. (2007). ATP is the predominant sympathetic neurotransmitter in rat mesenteric arteries at high pressure. *J. Physiol.* 582, 745–754. doi: 10.1113/jphysiol.2007.134825
- Sánchez-Andrade, G., and Logan, D. W. (2014). Deconstructing pheromone-mediated behavior one layer at a time. *BMC Biol.* 12:33. doi: 10.1186/1741-7007-12-33
- Scemes, E. (2012). Nature of plasmalemmal functional “hemichannels”. *Biochim. Biophys. Acta* 1818, 1880–1883. doi: 10.1016/j.bbamem.2011.06.005
- Scemes, E., Suadicani, S. O., Dahl, G., and Spray, D. C. (2007). Connexin and pannexin mediated cell-cell communication. *Neuron Glia Biol.* 3, 199–208. doi: 10.1017/S1740925X08000069
- Shao, Q., Lindstrom, K., Shi, R., Kelly, J., Schroeder, A., Juusola, J., et al. (2016). A germline variant in the PANX1 gene has reduced channel function and is associated with multisystem dysfunction. *J. Biol. Chem.* 291, 12432–12443. doi: 10.1074/jbc.M116.717934
- Silverman, W. R., de Rivero Vaccari, J. P., Locovei, S., Qiu, F., Carlsson, S. K., Scemes, E., et al. (2009). The pannexin 1 channel activates the inflammasome in neurons and astrocytes. *J. Biol. Chem.* 284, 18143–18151. doi: 10.1074/jbc.M109.004804
- Taruno, A., Matsumoto, I., Ma, Z., Marambaud, P., and Foskett, J. K. (2013). How do taste cells lacking synapses mediate neurotransmission? CALHM1, a voltage-gated ATP channel. *Bioessays* 35, 1111–1118. doi: 10.1002/bies.201300077
- Vick, J. S., and Delay, R. J. (2012). ATP excites mouse vomeronasal sensory neurons through activation of P2X receptors. *Neuroscience* 220, 341–350. doi: 10.1016/j.neuroscience.2012.06.004

- Wang, J., Jackson, D. G., and Dahl, G. (2013). The food dye FD&C Blue No. 1 is a selective inhibitor of the ATP release channel Panx1. *J. Gen. Physiol.* 141, 649–656. doi: 10.1085/jgp.201310966
- Wang, X. H., Streeter, M., Liu, Y. P., and Zhao, H. B. (2009). Identification and characterization of pannexin expression in the mammalian cochlea. *J. Comp. Neurol.* 512, 336–346. doi: 10.1002/cne.21898
- Zhang, H., Chen, Y., and Zhang, C. (2012). Patterns of heterogeneous expression of pannexin 1 and pannexin 2 transcripts in the olfactory epithelium and olfactory bulb. *J. Mol. Histol.* 43, 651–660. doi: 10.1007/s10735-012-9443-x
- Zhang, Y., Laumet, G., Chen, S. R., Hittelman, W. N., and Pan, H. L. (2015). Pannexin-1 up-regulation in the dorsal root ganglion contributes to neuropathic pain development. *J. Biol. Chem.* 290, 14647–14655. doi: 10.1074/jbc.M115.650218
- Zhang, C., Medzihradzky, K. F., Sánchez, E. E., Basbaum, A. I., and Julius, D. (2017). Lys49 myotoxin from the Brazilian lancehead pit viper elicits pain through regulated ATP release. *Proc. Natl. Acad. Sci. U S A* 114, E2524–E2532. doi: 10.1073/pnas.1615484114
- Zhao, H. B. (2016). Expression and function of pannexins in the inner ear and hearing. *BMC Cell Biol.* 17:16. doi: 10.1186/s12860-016-0095-7

Chapter 4. **Panx1** is implicated in seizure activity and visual processing

“ The most damaging phrase in the language is: It’s always been done that way.”

- Grace Hopper

Aspects from **Part I** of this chapter were done in collaboration with Dr. Peter Carlens’ group at Krembil research institute, Toronto Western Hospital, as part of an independent training opportunity in electrophysiology. The work completed at Krembil, contributes to a broader, yet impactful, investigation of mammalian Panx1 in a variety of seizure models with the primary objective of assessing changes in behavioural and electrophysiological markers of excitability associated with the channel during seizures. As such, only contributions completed by me in collaboration with the Carlen lab are presented here; modified from the following original published research article:

Mark Aquilino, **Paige Whyte-Fagundes**, Mark Lukewich, Liang Zhang, Berj Bardakjian, Georg Zoidl, & Peter Carlen. 2020. “Pannexin-1 deficiency decreases epileptic activity in mice.” *International Journal of Molecular Sciences*. 21(20):7510. Doi: 10.3390/ijms21207510.

The skills developed in Dr. Carlens’ lab were essential for spearheading a cutting-edge project in Dr. Zoidls’ lab at York University where we sought out to record brain activity from zebrafish larvae *in vivo*. **Part II** of this chapter depicts this self-directed process, where continued investigations of Panx1 in seizure activity were pursued. During this process, expertise was developed in this technique in order to collaborate with a fellow colleague, Dr. Nickie Safarian, to explore the role *panx1a* has in visuomotor control. Only contributions completed by me in this investigation are presented here; modified from the following original published research article. It is important to note that independent investigation of the visual system was expanded to include other *panx1* ohnologs in order to determine physiological ramifications of knocking out *panx1* in the zebrafish. This data is presented here, currently part of unpublished data.

Safarian, N., **Whyte-Fagundes, P.**, Zoidl, C., Grigull J., & Zoidl, G. (2020). Visuomotor deficiency of *panx1a* knockout zebrafish is linked to dopaminergic signalling. *Scientific Reports*. 9538(10). Doi.org/10.1038/s41598-020-66378-y

Dr. Carlens’ lab is primarily made up of members that are part of the biomedical engineering program at the University of Toronto. The opportunity to work alongside these individuals created an environment where I was exposed to exploring new avenues of handling large datasets from the perspective of engineers. As such, with the guidance of Uilki Tufa, a PhD candidate in the labs of Dr. Carlen and Dr. Bardakjian, a tremendous effort was dedicated to gaining knowledge in coding in order to automate data analysis and execute higher level signal processing of electrophysiological data. This technical research and development is presented alongside specific objectives in **Part III** of this chapter.

4.1. Part I: Electrophysiological markers of epilepsy associated with Pannexin1

4.1.1. Introduction

Epilepsy is widely regarded as a disease of distorted neuronal network excitability, where seizures occur upon spontaneous shifts in synaptic transmission causing an imbalanced excitatory state (Buchin et al., 2018). A hypothetical framework exists regarding the imbalance between excitation and inhibition that places Panx1 at the centre of these dynamics. This is due to the combination between channel function, expression and gating. Functionally, Panx1 is known to mediate the release of ATP, which modulates neurotransmitter receptors and voltage gated ion channels (Khakh et al., 2003), as well as release of the excitatory neurotransmitter glutamate (Herrera-Calderon et al., 2018; Zoidl et al., 2007). It is expressed in regions that become hyper-excitable in experimental models of epilepsy (Pernelle et al., 2018), and is found in excitatory synapses of hippocampal and cortical pyramidal neurons lateral to the postsynaptic density also in close proximity to astrocytes (Zoidl et al., 2007). This localization pattern exposes the channel to dynamic molecular, structural, ionic and electrical changes in actively communicating neurons that can influence Panx1 gating. In particular, elevated levels of extracellular potassium is characteristic to driving seizure activities and is known to open the channel (Raimondo et al., 2015). The combination of these features is considered critical for linking Panx1 channel function with neuronal excitability and seizure generation, although this remains to be resolved.

Electrophysiology has been the most reliable diagnostic tool for epilepsy since the early twentieth century, being able to answer questions regarding the identification of seizure onset zones, defining resection areas for surgery candidates and the pathology of epilepsy in general (Bertram, 2014). As such, this remains to be the best research tool to investigate underlying causes of the neurological disorder. Here, we used both intracellular and extracellular recording techniques *in vitro* in order to determine whether Panx1 contributes to the hyperexcitable dynamics in epilepsy from both a single cell and a network level, respectively. Using a global Panx1 knockout (Panx1^{-/-}) mouse model with 4-Aminopyridine (4-AP) to induce seizure activities that mimic those found in EEGs from patients (Fueta & Avoli, 1992), it provided an opportunity to assess changes in electrophysiological markers of epilepsy associated with Panx1.

4.1.2. Results

4.1.2.1. Single cell recordings reveal that targeting Panx1 results in a hyperpolarized membrane potential

There is evidence surrounding the implication of Panx1 in modulating neuronal excitability (Scemes & Velíšková, 2019; Shestopalov & Slepak, 2014) and in turn either augmenting or terminating seizures (Aquilino & Whyte-Fagundes et al., 2019). However, there is no direct evidence of Panx1 modulating excitability at a single cell level. Therefore, prior to establishing a role of Panx1 in 4-AP induced seizures, whole-cell neuronal patch clamp was employed to investigate electrical changes in individual cell activity in order to characterize distinct cell properties related to panx1 (**Figure 4.1a**). Capturing cell current dynamics from cortical area II/III of wild type (WT) brain slices confirmed that the neuronal resting membrane potential (RMP) was around -70mV and revealed that for Panx1^{-/-} slices the -74.8mV RMP was significantly different to controls (**Figure 4.1b**), suggesting that the removal of Panx1 hyperpolarizes the cell ($p = 0.04$). To confirm this was a Panx1 mediated phenomenon and rule out any effects of genetic modifications, brilliant blue FCF (BB) was used as an established pharmacological Panx1 blocker (J. Wang et al., 2013a). WT cells exposed to BB also appeared significantly hyperpolarized with a RMP of -76mV ($p = 0.04$), indicating that Panx1 may be directly involved in regulating cellular excitability. These results imply a fundamental role of Panx1 in maintaining homeostatic membrane potentials which may contribute to altered seizure propensities in Panx1^{-/-} mice.

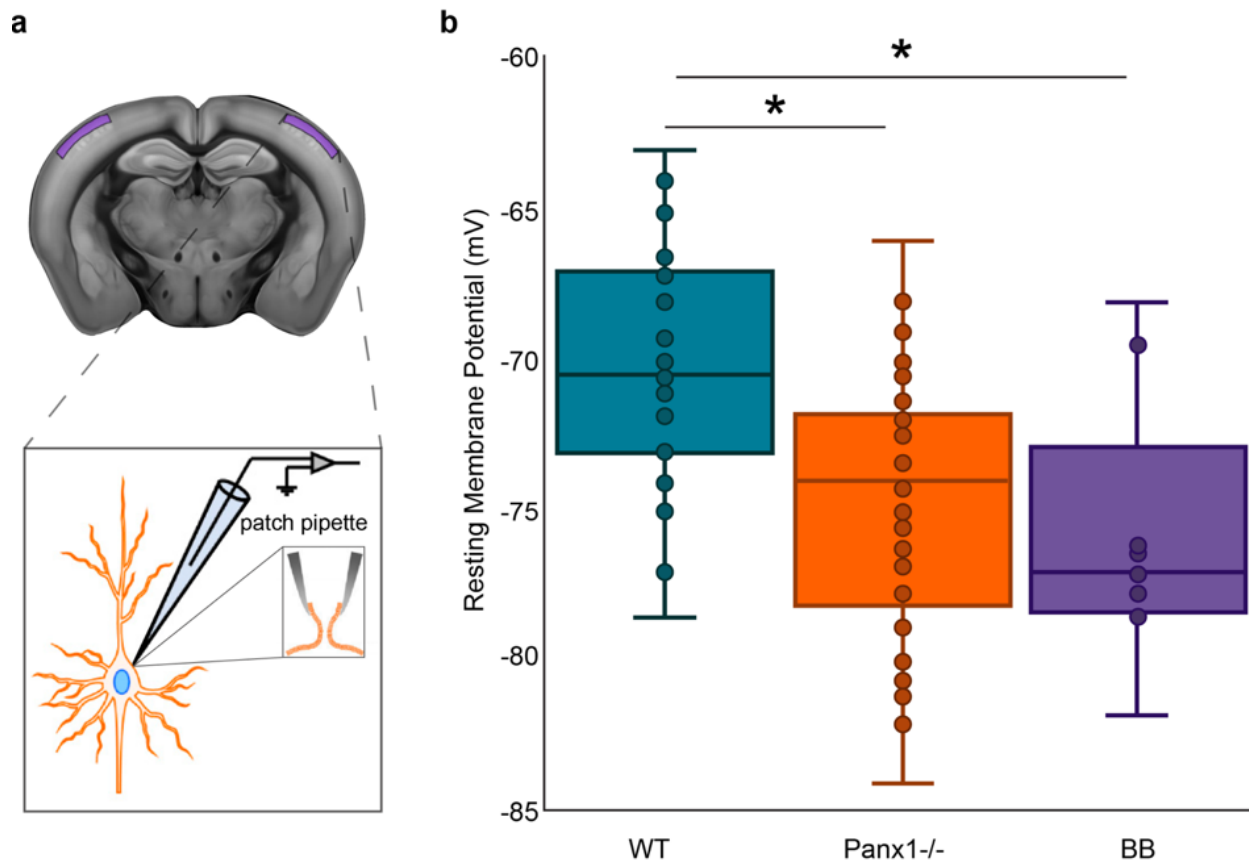


Figure 4.1. The resting membrane potential of Panx1^{-/-} cells is hyperpolarized. **a** *in vitro* whole cell patch clamp recordings were taken from neurons in cortical layers II/III. Corresponding recording sites from brain slices are highlighted in purple and single cells were recorded intracellularly as shown in the depiction below. **b** Average resting membrane potentials (RMP) were documented once cells were patched for WT (N = 26) and Panx1^{-/-} (N = 54) mice as well as WT mice treated with Brilliant Blue FCF a Panx1 blocker (N = 9; BB). The RMP was significantly hyperpolarized when Panx1 was targeted both genetically and pharmacologically. Average RMP is around -70mV for WT cells which is considered normal, for Panx1^{-/-} it was around -75mV and for BB it was -76mV. * = p<0.05.

4.1.2.2. Recordings of LFPs from cortical slices exposed to 4-AP reveal anti-convulsant properties of Panx1

The hyperpolarized neuronal membrane potentials of Panx1^{-/-} mice suggested that firing properties of the cells are altered in a way that may affect seizure generation. Therefore, to investigate altered electrophysiological activities as a result of knocking out Panx1 at a local circuitry level, local field potentials (LFPs) in neocortical slices were examined *in vitro*. Recording electrodes were lowered into slices and placed in layer II/III in order to record chemically induced, self-sustained population responses to the convulsant 4-AP (100μM). In slices from WT animals, 4-AP reliably produced SLEs (**Figure 4.2a**), whereas Panx1 inhibition, either via pharmacology or genetic

targeting, resulted in extremely rare epileptiform responses (see **Table 4.1**). In transgenic Panx1 knockout (KO) mice, traces from cortical slices exposed to 4-AP showed small population spikes (0.75 ± 0.02 s in duration) and only 2 of the 12 slices tested revealed any evidence of seizure-like events (SLE) (**Figure 4.2b**). Events in the KO population presented more frequently as bursts and can be seen contrasted to a typical SLE found in WTs in **Figure 4.2c**.

When comparing only the slices that produced SLEs, there was no significant differences in the duration of events (WT: 0.45 ± 0.06 min, KO: 0.44 ± 0.04 min, $p = 0.861$, t-test) or in the inter-SLE interval (Wild type (WT): 2.29 ± 0.20 min, KO: 2.19 ± 0.31 min, $p = 0.794$, t-test) between WT and KO groups (**Figure 4.2d**). This suggested that Panx1 inhibition may have a more anti-epileptogenic role; as it appears to be involved in suppressing the mechanisms triggering seizures as opposed to decreasing the severity of the seizures themselves.

Additional experiments were performed to distinguish the direct contribution of Panx1 function to SLEs from either developmental or compensatory effects that may have arisen due to creating the transgenic Panx1 KO mouse line. Therefore, Brilliant-Blue-FCF (BB) and Probenecid (Pb), common Panx1 blockers, were applied to cortical slices 10min prior to the application of 4-AP to ensure efficient Panx1 blockade. Extracellular field recordings from WT mouse slices treated with BB often contained small synchronous spiking events (1.63 ± 0.13 s in duration), similar to what was observed in the KO traces. Further, SLEs were rarely exhibited as only one instance of the events occurred following pretreatment with $10\mu\text{M}$ BB across 10 independent experiments (**Figure 4.2e**). Similarly, the WT slices pretreated with $500\mu\text{M}$ Pb also only showed one instance of SLEs occurring across 13 experiments, however, these slices exhibited no noteworthy spontaneous activity (**Figure 4.2f**).

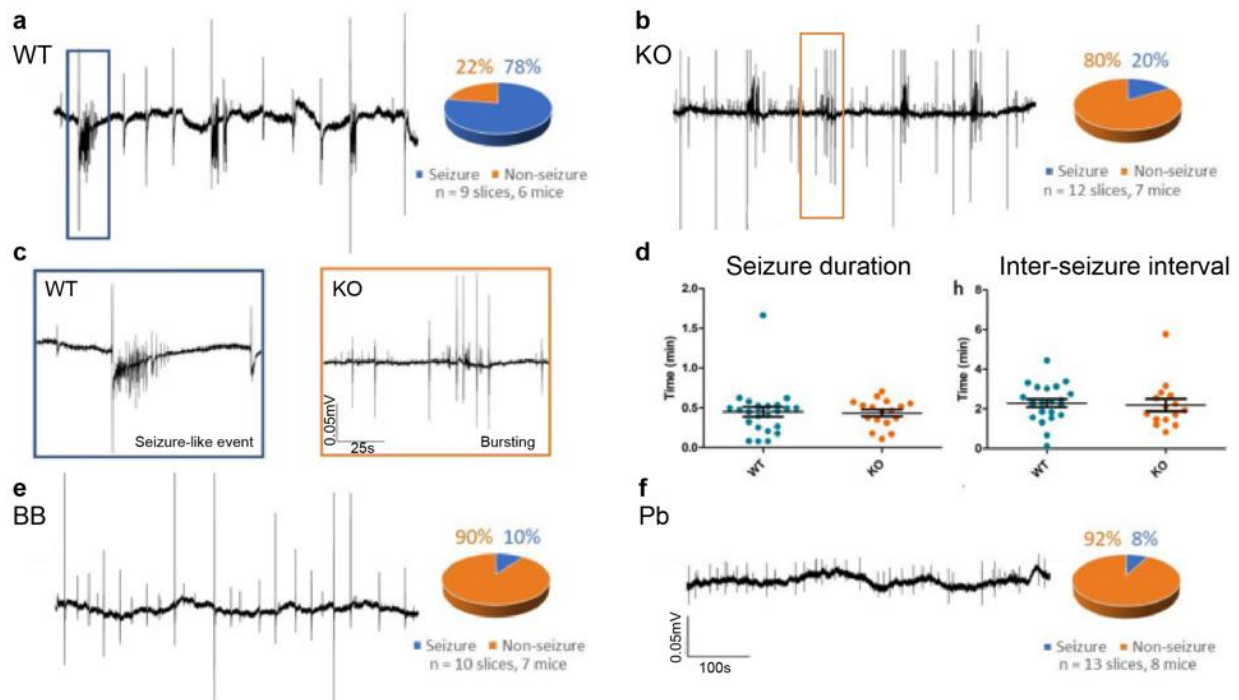


Figure 4.2. Seizure-like events *in vitro* in WT, KO, BB (Brilliant Blue-FCF-treated) and Pb (probenecid-treated) groups. Sample recordings of local field potentials from a WT and b KO groups, along with pie charts summarizing seizure incidence with 4-AP. c higher magnification of SLE in WT (left, blue) and typical bursting seen in KO (right, orange), indicative of the most common responses to 4-AP for each group. d Comparison of seizure duration and inter-seizure interval of SLEs in both WT and KO slices. Despite a reduced incidence, once initiated, KO SLEs remained similar to WT SLEs. Sample recordings of local field potentials from WT slices pretreated with e BB or f Pb, along with pie charts summarizing seizure incidence with 4-AP. Recordings from WT mice often had one or more seizure-like events (78%), whereas KO, BB and PB mice often had only small synchronous bursting events (20%, 10% and 8% respectively). Scale bars for a,b,e,f: 0.05mV by 100s; c: 0.05mV by 25s. Figure adapted from Aquilino et al., 2020.

Table 4.1. Incidence of seizure-like events (SLEs) *in vitro* following perfusion of cortical slices with 100 μ M 4-AP. 12 slices from 7 KO mice had fewer 4-AP-induced SLEs than in the 9 slices from 6 of their WT counterparts ($p = 0.0051$, Chi-squared). Mice treated with Brilliant Blue-FCF (7 mice, 10 slices) or probenecid (8 mice, 13 slices) before 4-AP exposure also had fewer instances of at least one SLE as compared to untreated slices of WT mice (BB $p = 0.0028$; PB $p = 0.0008$, Chi-squared).

Type	Total number	SLE-positive	SLE-negative	Percentage	$\tilde{\chi}^2 p$
WT	9	7	2	78	-
KO	12	2	10	20	0.0051
BB	10	1	9	10	0.0028
Pb	13	1	12	8	0.0008
ALL	-	-	-	-	<0.0001

4.1.2.3. Cross-Frequency coupling *in vitro* is absent in Panx1 KOs

Extracellular recordings also enable the collection of data regarding oscillatory dynamics. Therefore, to determine if there were any alterations in excitability for Panx1 KO mice *in vitro* that may explain reduced seizure activities, changes in a wide range of frequency bands compared to controls were assessed. As 4-AP induced a broadband increase in spectral power, the change of power across each frequency band was normalized to the overall increase in spectral power (**Figure 4.3a**). This revealed a diminished effect of 4-AP on gamma (30-80Hz), high frequency (HF; 80-120Hz) and very high frequency bands (vHF; 120-500Hz) in the KO, each of which are frequencies associated epileptic signaling (Ren et al., 2015; Zijlmans et al., 2012). There were no changes found for KOs in the delta (1-4Hz), theta (4-8Hz), alpha (8-13Hz) or beta (13-30Hz) bands compared to controls.

In addition to quantifying differences in the raw frequency power, the role of Panx1 in mediating frequency synchronization was also explored via phase amplitude coupling (PAC). PAC has been suggested to be a biomarker for epilepsy, as reports have shown a positive increase in coupling strength and seizure occurrence (Samiee et al., 2018). Therefore, PAC strengths were computed for WT (n=9) and KO (n=12) slices exposed to 4-AP to determine if intact Panx1 signaling was required for synchronization underlying SLEs. Sample traces are shown for WT (**Figure 4.3b**) and KO (**Figure 4.3c**) groups with baseline (blue) and 4-AP-induced activities (orange) highlighted. WT slices demonstrated strong PAC during SLEs, which was void in baseline recordings (**Figure 4.3d**). There was only very minor evidence of coupling in KOs, which was indistinguishable between baseline and 4-AP induced activities (**Figure 4.3e**). PAC was also not evident in WT samples treated with Panx1 blockers, BB and Pb (see Appendix B: **Figure 6.1**)

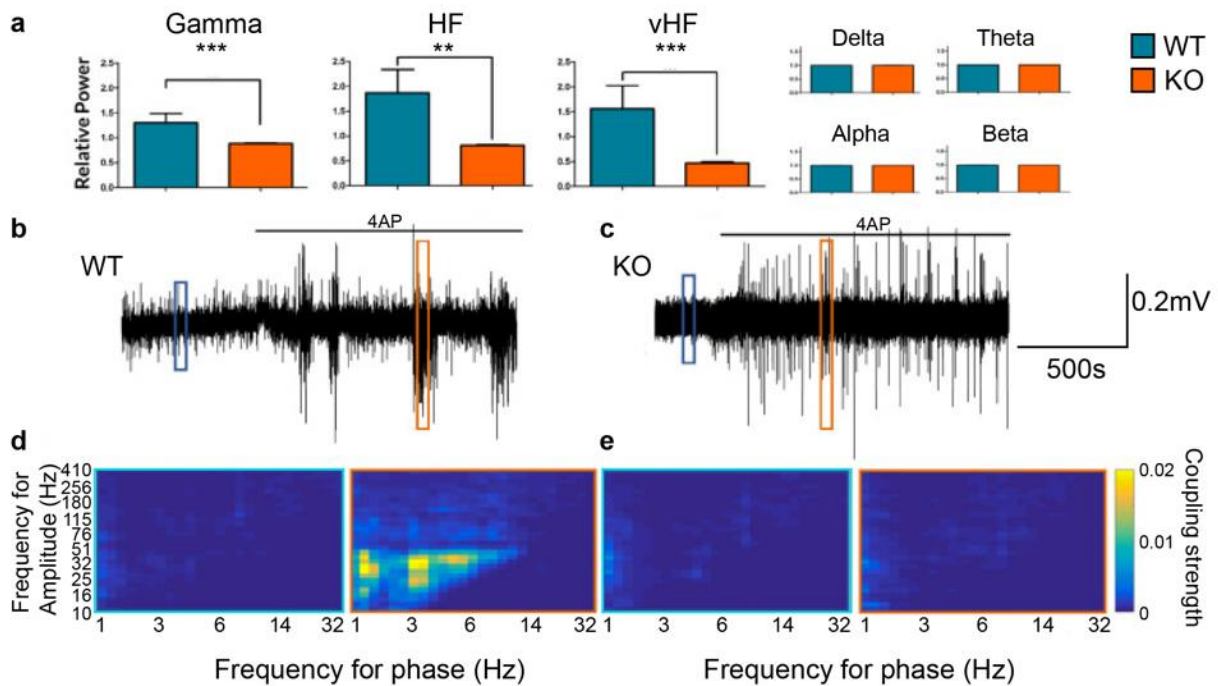


Figure 4.3. Frequency-based analysis of the extracellular recordings of WT and Panx1 KO mice. **a** The relative increase for various frequency bands in neocortical field potentials after bath application of 4-AP. As 4-AP induces broadband increased spectral power, the relative increase in power of each band is normalized to the overall increase in spectral power. While changes in Delta through Beta bands were not significant, the increase in spectral power in Gamma ($p = 0.0009$), HF ($p = 0.0011$) and vHF ($p = 0.0008$) bands were significantly lower in Panx1 deficient animals following 4-AP. **b,c** Traces of WT and KO extracellular recordings under 4-AP. **d,e** Phase-amplitude coupling comodulograms of 10-s windows during baseline (blue) and 4-AP (orange) conditions, as highlighted in subfigures **b** and **c** respectively, highlighting periods of enhanced PAC in the WT 4-AP response which are absent in the KO. Coupling strength indicated to the right of comodulograms. ** $p < 0.01$, *** $p < 0.001$. Figure adapted from Aquilino et al., 2020.

4.1.3. Conclusion

A pro-epileptic effect of the Panx1 channel was demonstrated using the 4-AP model for epilepsy *in vitro*, as reduced epileptiform activity was observed when genetically or pharmacologically targeting Panx1. Due to Panx1^{-/-} having the most robust impact on SLE incidence, without drastically altering duration or inter-SLE intervals, it is possible that Panx1 may play a role in epileptogenesis (Fu et al., 2009). However, taking into consideration the hyperpolarized neuronal RMPs, reduced gamma and high frequency powers and the lack of PAC in Panx1^{-/-} tissue these results suggest that Panx1 may modulate network excitability in order to mediate seizure activities. Overall this research corroborates previous reports positively correlating Panx1 and seizure activity (Jiang et al., 2013b; Mylvaganam et al., 2010). However, despite these findings, mechanistic explanations for Panx1 involvement in seizures are still lacking. Therefore, ongoing

efforts for a comprehensive and interdisciplinary investigation are required which can possibly place Panx1 mediated ATP release at the center of SLE generation. For this reason, the zebrafish is proposed as a model to support this research objective as molecular investigations are robust, and it is possible to keep neuronal circuitry intact in order to maintain network integrity necessary for understanding epileptic dynamics.

4.2. Part II: Pannexin1 investigations in seizure generation and visual processing using electrophysiology in zebrafish

Zebrafish have emerged as a valuable vertebrate animal model for neuroscience research, as their gross brain architecture is conserved and they have a rich repertoire of behaviors (Basnet et al., 2019). The larval zebrafish are of particular convenience due to their optical transparency, small size, and high fecundity, with the added benefit of all major subdivisions of the adult zebrafish brain being present. The optic tectum (superior colliculus in mammals) in particular, is the largest midbrain structure in the zebrafish and has been well documented as the major visual processing center. It begins to take on a layered ‘cortical’ organization at 5 days post fertilization (dpf) and is an attractive region for investigations of axon guidance, synaptic specification, layer formation and topographic mapping (Scott & Baier, 2009). The three major layers are segmented into superficial, intermediate and deep regions (Suzuki et al., 2019) and are rich in cell diversity. The four main cell types present in the optic tectum are the superficial neurons, radial glial, periventricular (the most abundant) and shallow periventricular neurons (Scott & Baier, 2009). Most importantly, cell types necessary for maintaining the balance of excitatory and inhibitory networks, like excitatory glutamatergic neurons and inhibitory GABAergic interneurons and astrocytes, are also present in the zebrafish larval brain (Panula et al., 2010). However, first and foremost for translational applications, descriptions of gross brain anatomy and modulatory neurotransmitters, including their expression patterns, binding and signaling properties, resembles those of mammals (Panula et al., 2010).

4.2.1. Introduction to epilepsy in zebrafish larvae

Gaining an understanding of the complex mechanisms underlying epileptogenesis and seizure generation requires the use of appropriate animal models. Although valuable, only limited information can be acquired from human studies, as candidate pharmacological and non-

pharmacological interventions must be extensively tested for efficacy and safety prior to clinical use (Wahab, 2010). However, there is no single animal model of epilepsy that fully represents this disease given the range of conditions that fall under the umbrella of ‘epilepsy’ – each with distinct acquired or genetic origins and diverse behavioural manifestations, electrographic signatures, pharmacological profiles and histopathologies (Grone & Baraban, 2015). In line with this, the investigations related to the role of Panx1 in epilepsy appear to be extremely dependent upon the chosen model and experimental method with conflicting results and mechanistic involvement of the channel protein yet to be formally resolved (see **Table 4.2** for a detailed summary of all main conclusions in the Panx1 field related to epilepsy and/or seizures). As a result, the importance of animal models of epilepsy is constantly growing as the field of research continues to grow. This provided an opportunity to expand the field of epilepsy research pertaining to Panx1 involvement to include a zebrafish seizure model not as redundant but rather as complimentary to our previous work presented in mice in order to resolve remaining conflicts in the field.

Zebrafish are an attractive *in vivo* model for higher throughput investigations of epilepsy. They provide the advantage of recording seizure activity from intact neurocircuitry in transparent larvae. With the close homology of zebrafish to the human genome, it is an appropriate model for investigating the pathophysiology of human epilepsies from both a genetic and chemical perspective to model different aspects and subtypes of epilepsy (Hortopan et al., 2010). Primarily, by utilizing zebrafish, there is the additional benefit of having two *panx1* orthologues (*panx1a* and *panx1b*) due to whole genome duplication during evolution (Bond et al., 2012). This provides a unique opportunity to investigate the converging and diverging roles of these genes in the context of epilepsy with the potential to resolve conflicting results in the field. As a result, this portion of the thesis introduces and expands on the initial development of this model but results pertaining to this investigation are detailed in chapter 5.

Table 4.2. Summary of experimental seizure models and main conclusions from the Panx1 literature.

Seizure model	Experimental model	Major conclusions from paper	Pro- or anti-convulsant	Citation
Low Mg²⁺	mouse hippocampal slices	Panx1 opening is triggered by NMDAR stimulation	pro	(Thompson et al., 2008)

		and can contribute to seizure activity		
Co2+ treatment	<i>in vitro</i> whole mouse hippocampi	Induced seizure activity increased Panx1 expression	pro	(Mylvaganam et al., 2010)
Reduced glucose	rat hippocampal slices	Adenosine from ATP release via Panx1 (suggested with use of pharmacology and increased ATPi in electrode) induces an autocrine regulation of CA3 pyramidal neuron excitability	anti	(Kawamura et al., 2010)
Pilocarpine	mouse (WT & P2x7-/- & panx1 block or mRNA knockdown)	P2X7R - Panx1 complex decreases seizure susceptibility via negative modulation of M1 receptors	anti	(Kim & Kang, 2011)
Kainic acid	mouse slices (WT & Panx1-/-)	Panx1 opens by elevated K ⁺ following KA-induced SE and block (MFQ) or deletion of Panx1 reduces the ATP that is released and improves the behavioral manifestation of seizures	pro	(Santiago et al., 2011)
Resected tissue from TLE patients	human tissue	Panx channels are important in the formation of epilepsy due to increased expression found in TLE tissue	'pro'	(Jiang et al., 2013a)

DHPG induced burst firing	mouse hippocampal slices (CA1)	Activation of mGlu5 leads to bursting triggered by the release of ATP via Panx1 channels in area CA3 and the subsequent activation of P2Y1	'pro'	(Lopatář et al., 2015)
Resected cortical tissue from RE patients	human tissue (children)	Increased Panx1 expression found in RE tissue - possibly contribute to intercellular coupling and cellular hyperexcitability	'pro'	(Cepeda et al., 2015)
Resected cortical tissue from FCD patients	human tissue (children)	Expression of panx1 found in neurons and astrocytes, increasing expression found with increased seizure frequency (colocalized mostly with glu positive neurons)	'pro'	(Li et al., 2017)
Proepileptic ACSF with increased K⁺ ion and decreased Mg²⁺ ion concentrations	human neocortical tissue	Panx1 channel activation promoted seizure generation and maintenance through ATP signaling via purinergic 2 receptors	pro	(Dossi et al., 2018)
Kainic acid	mouse (WT & Panx1 ^{-/-})	“	pro	”
Kainic acid	mouse (WT & Panx1 ^{-/-} from neurons & astrocytes)	Cell type specific Panx1 expression has opposing effect for KA seizures; increased seizures when	pro in neurons and anti in astrocytes	(Aquilino et al., 2020; Scemes et al., 2019)

		panx1 ^{-/-} in astrocytes due to low levels of extracellular adenosine		
PTZ	mouse (WT & Panx1 ^{-/-} & block with Pb & BB)	sex differences but overall stage 6 seizures significantly reduced in panx1 KO or blockade (reduced seizure severity in KOs)	pro	(Aquilino et al., 2020)
Electrical kindling	mouse (WT & Panx1 ^{-/-})	reduced propensity to generate ADs in Panx1 KO animals	pro	"
4-AP	mouse hippocampal slices (WT & Panx1 ^{-/-} & block with Pb & BB)	panx1 KO or blockade significantly reduces seizure like events	pro	"
Mg²⁺ free ACSF	mouse hippocampal slices (WT&Panx1 ^{-/-} (global, neuron & astrocyte))	Panx1 in both cell types (not separate) are necessary to sustain epileptiform discharges in this model	'pro'	(Obot et al., 2021)
Kainic acid	mouse hippocampal slices (WT&Panx1 ^{-/-} (global, neuron & astrocyte))	Global deletion of panx1 doesn't alter, neuronal loss increases and astrocyte loss decreases occurrence of events	pro and anti	"
Kainic acid	mouse (WT & Panx1 ^{-/-} from neurons & astrocytes)	neuronal loss of panx1 = delay in seizure onset, astrocyte loss = quicker seizure onset, global loss = no change	pro and anti	"

Note: if pro is in ' ', this indicates that this is an inferred conclusion of this activity and is not explicitly stated by the authors.

4.2.1.1. Electrode placement impacts LFP recordings *in vivo*

The zebrafish larval brain at 7dpf contains on the order of 100 000 neurons, about one millionth of a human brain, yet it still maintains broad anatomical regions down to specific circuits and cell classes (Burrows et al., 2020). As mentioned prior, the larval brain has retained cellular diversity that permits the induction of seizure-like events (SLEs) with PTZ. However, in order to capture these events accurately, access to appropriate brain and cellular architecture is extremely fundamental. Here, recording electrode placement during 15mM PTZ application was systematically investigated in order to reliably induce and visualize typical SLEs in zebrafish larvae (Figure 4.4). The forebrain, specifically the dorsolateral pallium, was the first location assessed (Figure 4.4a), as this brain region in the zebrafish is analogous to the mammalian hippocampus (Cheng et al., 2014) and displays high spontaneous neural activity in adult zebrafish (Vargas et al., 2012). However, upon numerous trials, only single large deflections were induced by PTZ and there was no evidence of SLEs. The optic tectum (OT) was targeted next (Figure 4.4b-g), as the mammalian equivalent is the superior colliculus and the key processing center for sensory information rich in cell diversity (Suzuki et al., 2019). Recordings from larvae embedded on the right lateral side with the electrode inserted dorsally into the OT revealed only infrequent, miniature spikes (Figure 4.4b). Alternative attempts at targeting the OT with right lateral side embedding (Figure 4.4c) yielded recordings from the tegmentum, the structure ventral to the OT that receives inputs from the habenula, which had brain activity comparable to baseline recordings. Larvae were then embedded dorsally, and recordings were taken from the right side of the OT (Figure 4.4d-g). Electrodes placed in the deep tectal layer (d) or too close to the eye (e) also did not yield SLEs, highlighting the technical challenges associated with recording brain activity *in vivo* from deep structures. Recording from the superficial tectal layer was the most optimal region for capturing SLEs (Figure 4.4f,g). However, the angle of the implanted electrode appeared to also play a factor in the appearance of the events as an electrode placed at approximately 45 degrees to the larval body generated the most typical SLE based upon the duration and amplitude of events (Figure 4.4g). Consistent with what is shown in the recordings gathered from these various electrode placements, we believe it is possible that visualizing SLEs is more dramatic in the superficial OT as whole-brain imaging experiments have reported stronger correlation of spontaneous activity between mid and hindbrain regions compared to regions within the forebrain (Dunn et al., 2016). This connectivity is suggestive of a larger synchronous network that is likely to generate SLEs large enough to detect from a single electrode and may reveal how Panx1 may play a role in network dynamics.

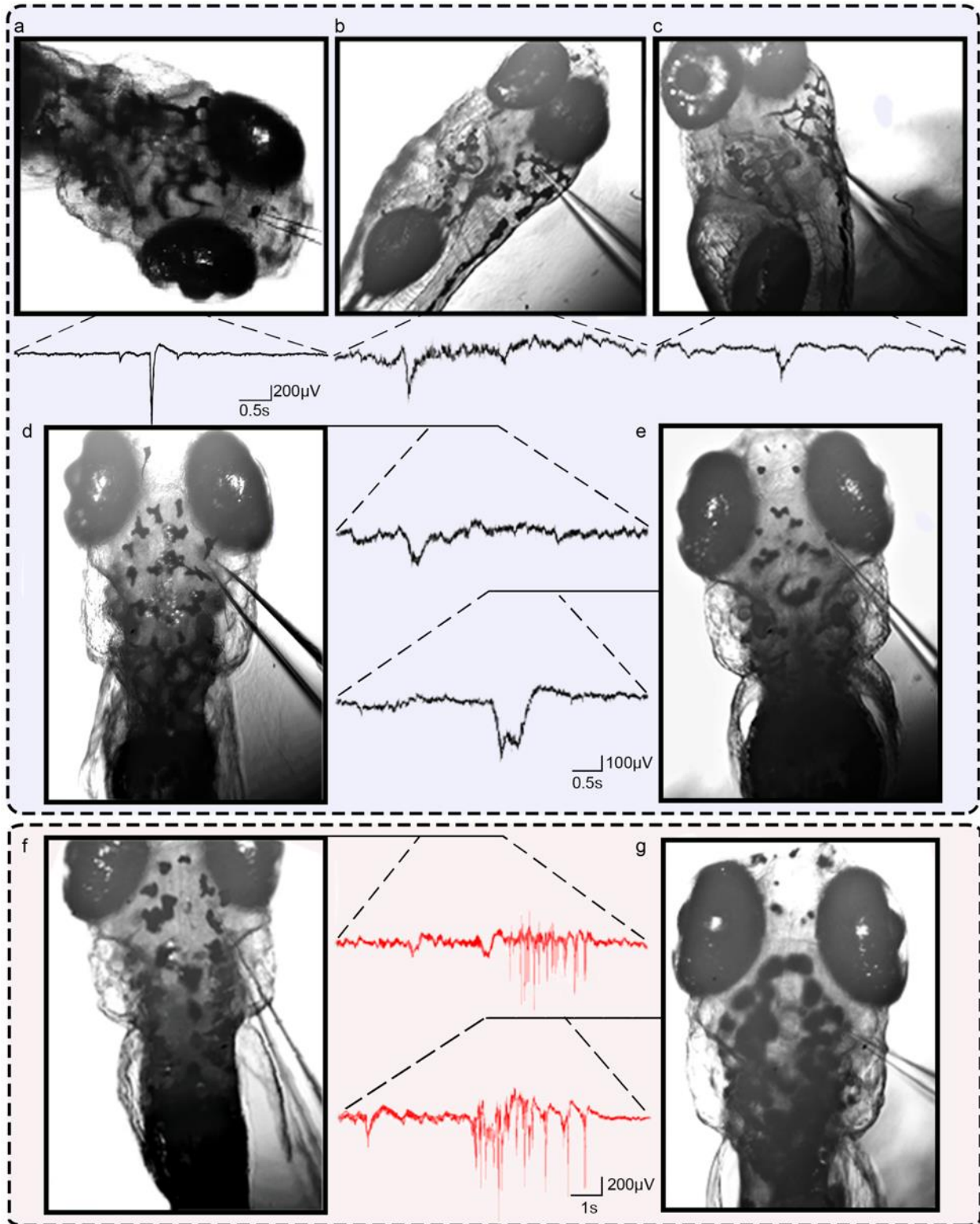


Figure 4.4. Images of electrode placement and corresponding sample recordings from 7dpf zebrafish larvae . PTZ was applied topically to zebrafish larvae for a 15mM final concentration. All recordings depicted are taken around 30min after PTZ application. a Larvae embedded in agar dorsally. Recording taken from the forebrain. Only single large deflections were induced by PTZ, no evidence of seizure-like events (SLE). b Larvae embedded on the right lateral side. Recording taken from midbrain region. PTZ did not induce SLEs

and only miniature spikes very infrequently. c Zebrafish embedded on the right lateral side in a slightly different orientation. Recording taken too deep from the midbrain region. PTZ did not induce any SLEs, spikes were not considered unlike baseline activity. d Larvae embedded dorsally. Recording taken from the right optic tectum, placement is very deep, too close to midline and eye. PTZ did not induce any SLEs, largest spikes seen were not considered unlike baseline activity. e Larvae embedded dorsally. Recording taken from the right optic tectum, placement is too close to the eye. PTZ did not induce any SLEs, largest spikes seen were not considered unlike baseline activity. f Larvae embedded dorsally. Recording taken from the right optic tectum, electrode implanted at ~15 degree angle to the larval body. PTZ induced some SLEs, but spikes were not as large, and events were not as long. g Larvae embedded dorsally. Recording taken from the right optic tectum, electrode implanted at ~45 degree angle to the larval body. PTZ induced SLEs. Scale bars are top: 200 μ V by 0.5s; middle: 100 μ V by 0.5s; bottom: 200 μ V by 1s.

4.2.2. The role of *Panx1* in visually processing light stimuli

Photosensitive seizures, or seizures induced by visual sensitivity or stimuli, have been observed in numerous types of human epilepsies (Guerrini & Genton, 2004). Accordingly, light stimuli has been utilized as a tool to induce and investigate seizures in various animal models including zebrafish (Samarut et al., 2018). This raised the question whether or not the presence or absence of light provoked chemically induced seizures with PTZ differently. We determined that seizure propensity across TL or *Panx1*^{-/-} fish was unaffected by light stimuli. However, the impact of light stimuli on the physiology of *Panx1*^{-/-} larvae remained to be determined.

As mentioned previously, zebrafish have two *panx1* genes, *panx1a* and *panx1b*. Although the two genes have been separated for more than 200 million years, principal channel functions appear to be comparable to mammalian Panx1 (Sarah Kurtenbach et al., 2013). Previous investigations from our group using Panx1 knockout mice provided evidence for physiological functions of Panx1 in sensory processing (S. Kurtenbach et al., 2014). Using the same mouse model, other groups observed physiological alterations to retinal function (Dvorianchikova et al., 2018; Kranz et al., 2013). However, with respect to the visual system in zebrafish, the localization of the two Panx1 proteins were found in distinct layers of the zebrafish retina, highlighting a potential for diverging functional roles *in vivo* that remain to be solved. *Panx1a* was discovered in the outer plexiform layer (OPL) in a band-like pattern that represented horizontal cells (N. Prochnow et al., 2009), and *panx1b* exhibited prominent expression in the inner nuclear layer (INL) and ganglion cell layer (GCL) (Sarah Kurtenbach et al., 2013). As Panx1 operates within major signaling pathways, in particular those involving intracellular calcium and extracellular ATP, this suggests that the *panx1* genes may have varied impact on visually guided synaptic transmission based upon their location in the retina. Here, we recorded brain activity from the retinotectal pathway of *panx1*^{-/-} larvae during varied light conditions to elucidate the physiological implications of *panx1* in vision.

4.2.3. Results

4.2.3.1. Recordings of LFPs reveal *Panx1* dependent alterations in visual system processing

To understand whether the distinct retinal localization of two *panx1* copies translates into differential influences on visual information processing, *in vivo* recordings of local field potentials (LFP) were performed in the optic tectum during varied light stimuli. Recordings were taken for 10min when the light was on, followed by another 10min with the light turned off. For analysis purposes, spectral power was analyzed in the last 4min of each recording to allow time for recordings to stabilize. TL larvae showed higher power in low frequencies during Light-ON stimulus, which shifts to an increase in gamma frequency power when the light is turned off. These frequency bands appear as peaks in the power spectrum. The transitions are quantified as a ratio of normalized power between recordings completed in the light and the dark for low and gamma frequencies, with a normalized power ratio of 1 indicating the lost ability to transition between the frequency bands upon changes in light (**Figure 4.5a**). TL (grey) exhibited transitions in low and gamma frequencies that were significantly greater and lower than 1, respectively. For *panx1a*^{-/-} (purple) and DKO (green) larvae, this ability to shift frequency bands was completely lost and was significantly altered compared to controls. However, the loss of *panx1b* did not appear to impair frequency transitions as their quantified ratio of normalized power was not significantly different to TLs. **Figure 4.5** displays samples of power spectra under light and dark conditions for *panx1b*^{-/-} larvae (**b**) which clearly depict the changes in peak frequencies and for DKO larvae (**c**) that show a distinct overlap in the spectra.

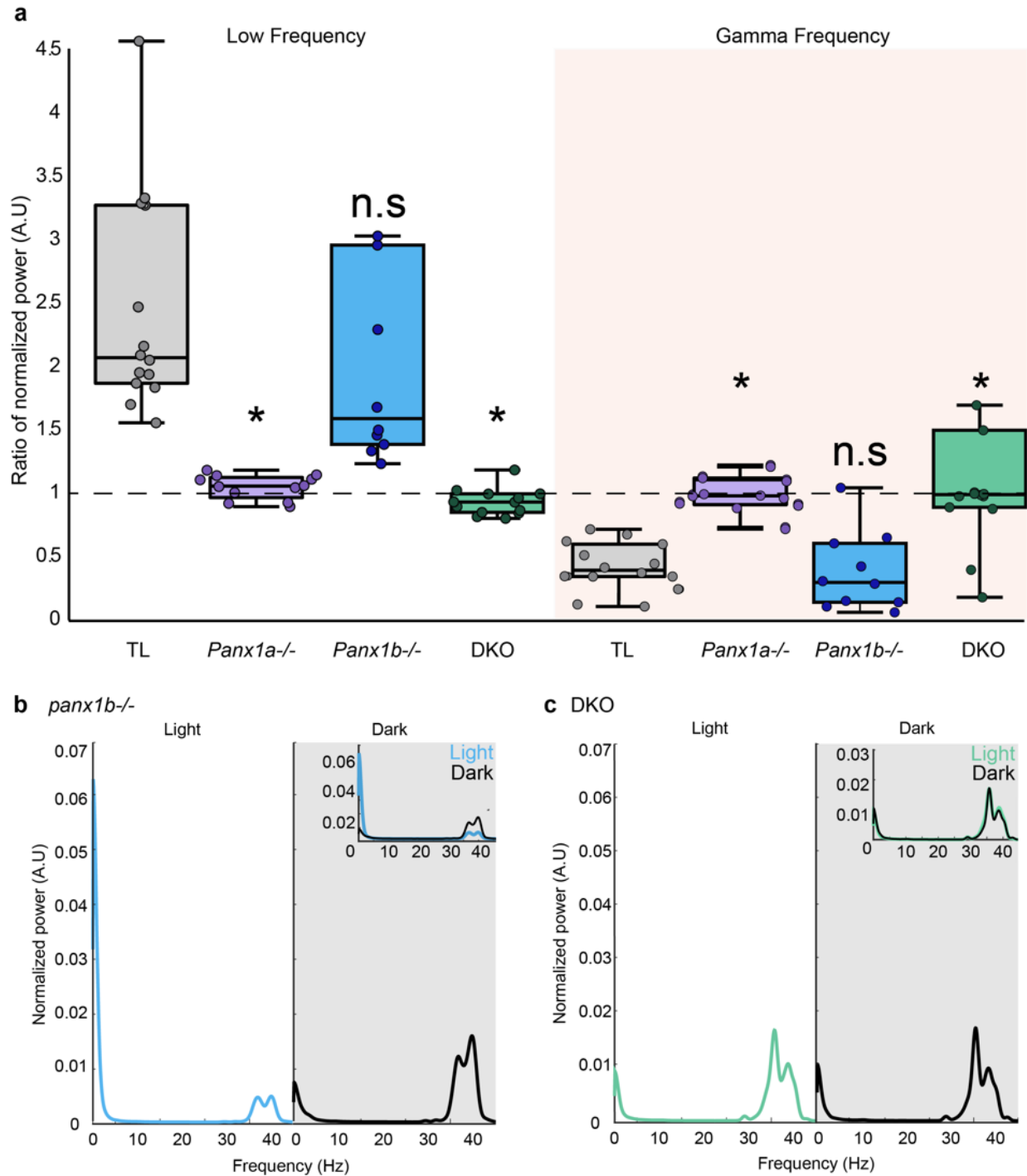


Figure 4.5. *Panx1b* does not modulate local field potentials in the optic tectum upon light stimulation. **a** Quantification of changes in normalized power ratios for low (Left) and gamma (Right, peach) frequencies in response to light conditions. The transition in frequency power is not significantly different between *panx1b*^{-/-} (n=10; blue) and TL larvae (n=15; grey), showing peak power in low frequencies with light stimuli and a peak in gamma frequencies in the dark. *Panx1a*^{-/-} (n=12; purple) and DKO (n=12; green) resulted in a significant loss in the regulation of the transition of frequencies compared to TL controls. **b** Examples of power spectra from *in vivo* recordings of *panx1b*^{-/-} larvae during Light-ON (left) and Light-OFF (right, grey) conditions showing the same frequency responses as TL. Normalized power for Light-ON conditions are primarily low

frequencies (<10Hz) and for Light-OFF conditions, the frequencies are primarily in the low gamma range (30-40Hz). Inset overlaid power spectra shows the change in power according to light (blue) and dark (black) stimuli. c Examples of power spectra from *in vivo* recordings of DKO larvae during Light-ON (left) and Light-OFF (right, grey) conditions. The shift in frequency power with changing light stimuli is lost in DKO larvae as they have equivalent peak frequencies in low and gamma ranges for both Light-ON and Light-OFF conditions. See inset graph for overlaid power spectra showing unchanged frequency power in light (green) and dark stimuli (black). Significance: n.s not significant, * pvalue<0.001.

4.2.3.2. Loss of *Panx1a* modifies transitions in brain wave frequencies in response to light

Knocking out both zebrafish panxs (DKO) resulted in the loss of regulated frequency transitions in the optic tectum between light and dark stimuli. However, the loss of *panx1b* did not alter tectal network responses to these same changes. Therefore, alterations in the retinotectal circuitry of *panx1a*^{-/-} larvae were tested in order to determine if regulated frequency transitions to light stimuli were dependent upon *Panx1a* signaling (**Figure 4.6a**). In wild-type larvae, as mentioned previously, the peak in normalized power shifted from low frequencies (less than 10 Hz) to gamma frequencies (35–40 Hz) when the light was turned off, and larvae were exposed to darkness for 10 minutes (**Figure 4.6b, top**). This response was abolished in *panx1a*^{-/-} larvae (**Figure 4.6b, bottom**), much like what was seen in DKO larvae, where shifting from dark to light conditions gave identical results in peak frequency power. Additionally, targeting Panx1 with 100μM probenecid, a common Panx1 blocker, also significantly reduced the changes in normalized power for both the low and gamma frequency ranges compared to control TL larvae (**Figure 4.6c**).

To elucidate a mechanism by which *Panx1a* is regulating these responses, given that *panx1a*^{-/-} larvae showed impairments to dark stimuli, TL larvae were treated with 50μM apomorphine. Apomorphine is a D1R/D2R agonist and facilitated testing dopamine receptor involvement in the ability of the brain to transition between frequencies in response to altering light stimuli. Interestingly, apomorphine treatment created a significant change to transitions between low and gamma frequencies with varying light stimulus when compared to controls, mimicking responses seen in *panx1a*^{-/-} (**Figure 4.6c**). Together, these results deliver a novel association between targeting *Panx1a*, either with pharmacology or by gene-editing, along with dopaminergic signaling, to modulate properties of the retinotectal pathway.

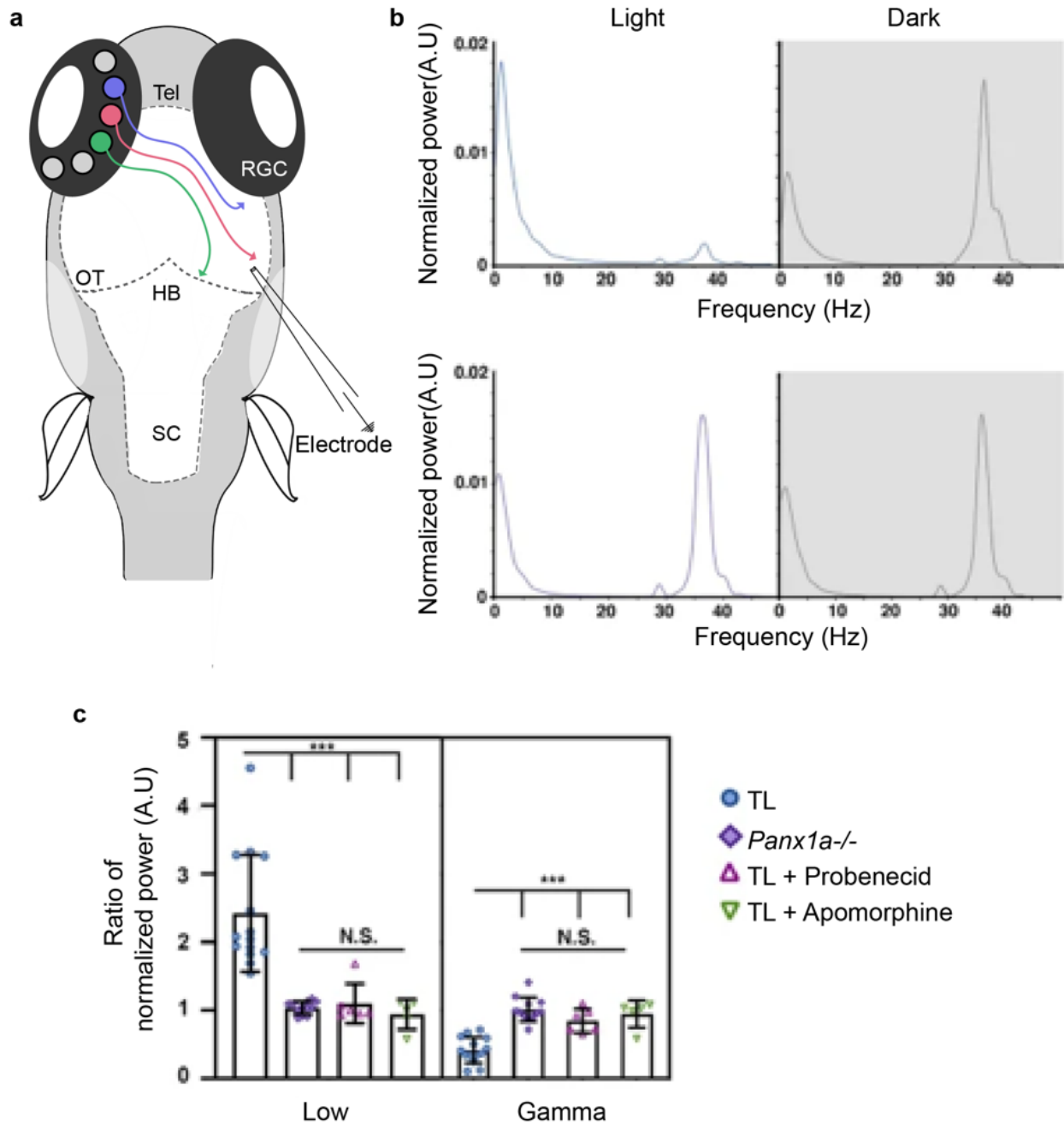


Figure 4.6. Panx1a modulates local field potentials in the optic tectum upon light stimulation. **a** Outline of the recording setup showing the typical placement of electrodes in the optic tectum (OT) in a region where axons from retinal ganglion cells (RGC) terminate. **b** Examples of power spectra from *in vivo* recordings of TL controls (top) and *panx1a*^{-/-} (bottom) during Light-ON (left) and Light-OFF (right) conditions. For TLs, normalized power for Light-ON conditions show primarily low frequencies (< 10Hz) but for Light-OFF conditions they are primarily gamma frequencies (30-45Hz). This shift in frequency power with changing light stimuli is lost in *panx1a*^{-/-} as they have equal peak frequency power in both Light-ON and Light-OFF conditions. **c** Quantification of changes in normalized power ratios for low (Left) and gamma (Right) frequencies in response to light conditions. Knocking out *panx1a* (n=12) and blocking *panx1a* with Probenecid (n=6), or Apomorphine treatment targeting D1/D2 receptors (n=5), results in a significant loss in the regulation of the transition of frequencies compared to TL controls (n=15). Significance: n.s not significant, *** pvalue<0.001. Figure adapted from Safarian et al., 2020.

4.2.4. Conclusion

LFPs display distinct patterns of dominant frequencies as a function of the presence or absence of either pharmacology, capable of altering neuronal firing in the brain, or visual inputs. Therefore, these experiments were conducted with PTZ to induce seizure-like events based upon altering brain excitability, as well as with and without light stimuli in order to capture retinotectal responses. Various frequencies of rhythmic activities have been observed in the brain across many species (Buzsáki, 2006). Here, although not necessarily associated with rhythmicity, we demonstrate that zebrafish larvae are able to exhibit seizure-like events; which are characterized in LFPs as bursts of high frequencies and are typically associated with pathologies like epilepsy (Hortopan et al., 2010).

In humans, characteristics of physiological brain waves are quite well defined, with low frequencies (delta (0.5-4Hz), theta (4-8Hz), alpha (8-12Hz)) associated with sleep, relaxation and passive attention, and gamma frequencies (35Hz⁺) associated with concentration (Schomer & Lopes da Silva, 2017). However, to date there is no clear understanding of what these frequencies are associated with in fish. Thus far, our results indicate that changes in lighting conditions may reveal an interaction between ongoing and induced oscillatory activity in the zebrafish larva brain, with a primary focus on the ability of retinotectal circuitry to shift between frequencies in response to changes in the environment. At this time, we determined that knocking out *panx1b* does not impact this frequency regulation, as their responses to light and dark were indistinguishable from TL controls. However, we cannot rule out the possibility that impairments may be found when using a different stimulus paradigm.

Although the outcomes found in DKO and *panx1a*^{-/-} larvae are very intriguing, it is difficult to determine the consequences of the inability to transition between brain rhythms in response to varying light conditions from LFPs alone. Evolutionarily speaking, it is possible that this impairment in frequency transitions may affect prey or predator detection or reaction in these fish lines (Avitan et al., 2017) . However, alternative behavioural investigations would be required to determine these scenarios for certain. From a developmental perspective, one cannot rule out the possibility that vision may be impacted with the loss of *panx1a* and in turn alter the retinotectal circuitry from birth; possibly having only a minor long standing influence on whole-system functions. Thus far, we utilized pharmacological interventions to gain insight into understanding a possible involvement of *Panx1a* in molecular pathways associated with neural signaling and

rhythmic activities. Given the localization of *panx1a* in the retina and the fact that *panx1a*^{-/-} larvae lost frequency transitions in the dark, we suspected that dopamine receptors may be involved as levels of dopamine release in the retina tune vision for specific light conditions (Roy & Field, 2019). As such, D1 and D2 receptors were targeted in TL larvae by apomorphine to block activation by the neuromodulator dopamine. In doing so, the *panx1a*^{-/-} phenotype was reproduced; suggesting that *Panx1a* affects the role of the optic tectum in modulating sensory information processing received from the retina and that dopaminergic signaling also plays a role in how the network responds to changes in light stimuli. This conclusion is consistent with the known roles of dopamine and Panx1 in horizontal cells (HC). In darkness, dopamine increases the conductance of the glutamatergic synapse between cones and HC through a D1R-mediated mechanism leading to depolarization of HCs (Knapp & Dowling, 1987). Further, when horizontal cells are depolarized in the dark, Panx1 channels are maximally active and release ATP into the synaptic cleft, participating in sending inhibitory feedback to cones (Cenedese et al., 2017; Vroman et al., 2014). Together, these actions may elucidate an underlying mechanism of *Panx1a* along with dopamine in modulating rhythmic activities in the optic tectum during integration of visually acquired information.

4.3. Part III: Utilizing automated data analysis tools to address gaps in Panx1 research

4.3.1. Automated cell detection for dye uptake analysis Data

A traditional way of determining Panx1 channel function in the field has been to use various versions of *in vitro* dye uptake assays to investigate how much dye is taken up by cells based upon the stimulation or inhibition of Panx1 (S. Locovei et al., 2006). Although this method has been utilized for many years, a few pitfalls associated with this technique required addressing. To start, quantification of dye uptake was conventionally performed manually, where cells or regions of interest (ROI) would be selected by hand and fluorescent units calculated to determine the amount of dye that was taken up (Huang et al., 2007). This method introduces many biases into analysis, from regulating cell selection across researchers and experiments, to defining strict features of healthy or apoptotic cells, to selecting ROIs based upon dye uptake properties independent of Panx1, to name a few. Alternatively, dye uptake can be quantified using a multiplate reader, which takes the visual and manual biases out of the equation. However, this mode of quantification is unable to take into account the amount of expression of the Panx1 protein across the cell population

and cannot distinguish between cells with high fluorescent readouts unrelated to Panx1 channel function. Further, no evidence in the literature was found correlating the amount of Panx1 expression in individual cells, which can vary based upon transfection efficiency and cell type, to the amount of dye that cells took up. In order to address the question regarding whether or not Panx1 expression levels impact dye uptake, a method for automating cell detection was established and was designed in a way to improve the shortcomings associated with the traditional dye uptake technique. The advantages of automating cell detection allowed for higher throughput results at the same time as it removed all manual biases; these details are outlined below.

Normalized dye uptake values were calculated by the change in fluorescence of the red channel (EtBr uptake) over 20 min to the protein expression documented by the fluorescence of the green channel (EGFP/EYFP fluorescence). All experiments were repeated at least three times. An automated cell selection and analysis of fluorescence protocol was created using a collection of plugins built into the ImageJ software. At the start, separated channels were background subtracted. A morphological segmentation tool from the MorphoLibJ plugin library was applied to confocal segment images based on the watershed algorithm, creating new images based on watershed lines. This algorithm is classically used to segment overlapping or touching objects, like a group of cells, and is ideal for detecting the outline shapes of healthy cells which are typically round. These images were inverted to analyze particles, and the resulting regions of interest (see **Figure 4.7** as an example of selected and analyzed cells) were filtered using the HiLo algorithm to exclude saturated regions in images. Next, integrated density values were measured from the regions of interest within the green and red channels. As there is a linear relationship between protein expression (green channel) and the amount of dye uptake (red channel; see **Supplementary Figure 3.4**), it was possible to normalize dye uptake by calculating the ratio of dye uptake (in 20 min) and the amount of protein fluorescence on a cell-to-cell basis. This is the first proof of a linear relationship between Panx1 expression and dye uptake.

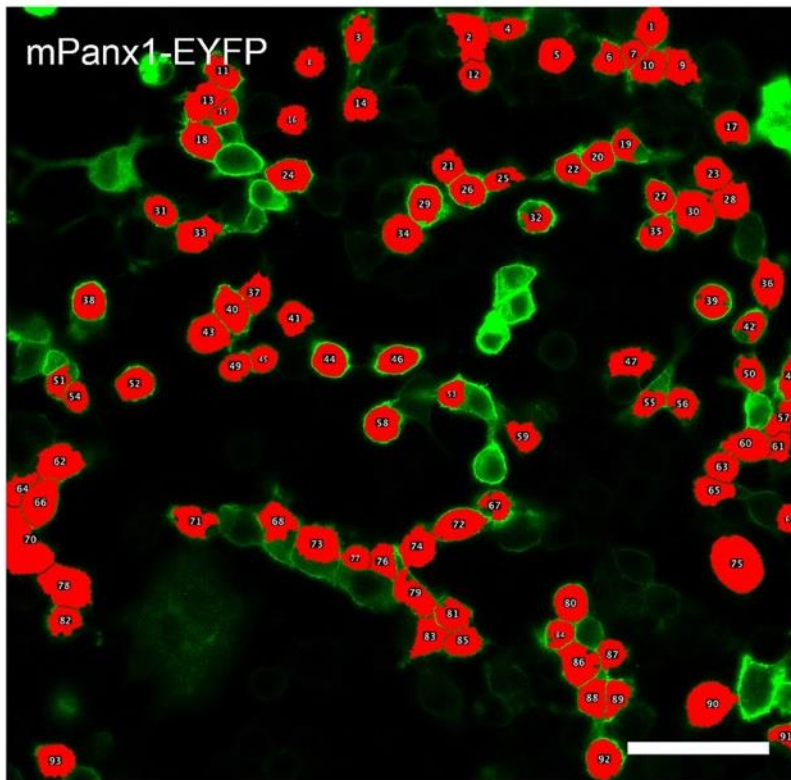


Figure 4.7. Panx1 and Panx3 dye uptake properties. Automated cell selection overlay. The image shown represents an example for mPanx1-EGFP transfected Neuro2A cells (green) captured during a dye uptake assay. Superimposed in red and numbered are the regions of interest captured by the automated cell selection routine developed using ImageJ plugins, which were used for calculation of integrated density values.

4.3.2. Spectral EEG analysis

Obtaining a large data set of brain recordings from zebrafish larvae, or EEG data, raised questions regarding how to begin analyzing neural time series data. There is a wealth of information within EEG data beyond visual inspection, as it has high temporal resolution that can capture neurocognitive processes, as well as being a direct measure of neural activity and biophysical phenomena at the level of populations of neurons (Cohen, 2014). Therefore, the objective arose to determine how to uncover and extract underlying differences in the neural circuits of *panx1*^{-/-} fish and controls as this had yet to be done in the field. This initiated exploration into time-frequency-based analysis, which is outlined in brief below, and required programing skill development in order to accomplish this signal processing.

EEG data is multidimensional, including information from at least five dimensions: time, space, frequency, power (strength of frequency-band-specific activity) and phase (the timing of the activity). Since these recordings from the zebrafish larvae are taken with a single electrode,

minimal information is available regarding the space dimension. Therefore, this data exploration took time, frequency and power dimensions primarily into account. An advantage of this is that the time-frequency-based analysis can be interpreted in terms of neural oscillations, which at present are the most promising bridge linking findings from multiple disciplines within neuroscience and across multiple species (Buzsáki, 2006). There is caution to be taken when interpreting these oscillations, especially when working with a relatively new animal model for EEG, as literature is still limited on linking time-frequency dynamics to specific cognitive processes. Nonetheless, the field is rapidly growing, and this provides ample opportunities for exploratory data analysis. As such, the approach for exploring spectral analysis used to find alterations in *panx1*^{-/-} larvae retinotectal pathways in response to changes in light stimuli are outlined in **Figure 4.8**.

EEG data contains rhythmic activity, reflective of neural oscillations, that can be seen even in raw data (**Figure 4.8a**). From this data, information regarding frequency and power components can be analyzed in the time domain. Frequency is the reciprocal of time. It refers to the speed of the oscillation, or the number of cycles per second, and is represented with the units hertz (Hz). Power refers to the amount of energy or strength in a frequency band and is the squared amplitude of the oscillation. Theta (4-8Hz) and delta (1-4Hz) frequency bands extracted from the sample raw EEG from a TL zebrafish larvae are depicted, with the combination of these low frequencies shown on the raw EEG for reference of how they contribute to the overall signal (**Figure 4.8a**). In order to determine the frequency power of a continuous signal, in brief, the signal is broken down into multiple sine waves over time with different oscillatory cycles and the amplitudes of these waves correspond to specific frequencies (**Figure 4.8b**). What this spectral analysis reveals are the frequency bands that dominate EEG signals, based upon the oscillations that are extracted with the highest power, and may in turn indicate characteristic rhythms associated with cognitive processes linked with environmental stimuli.

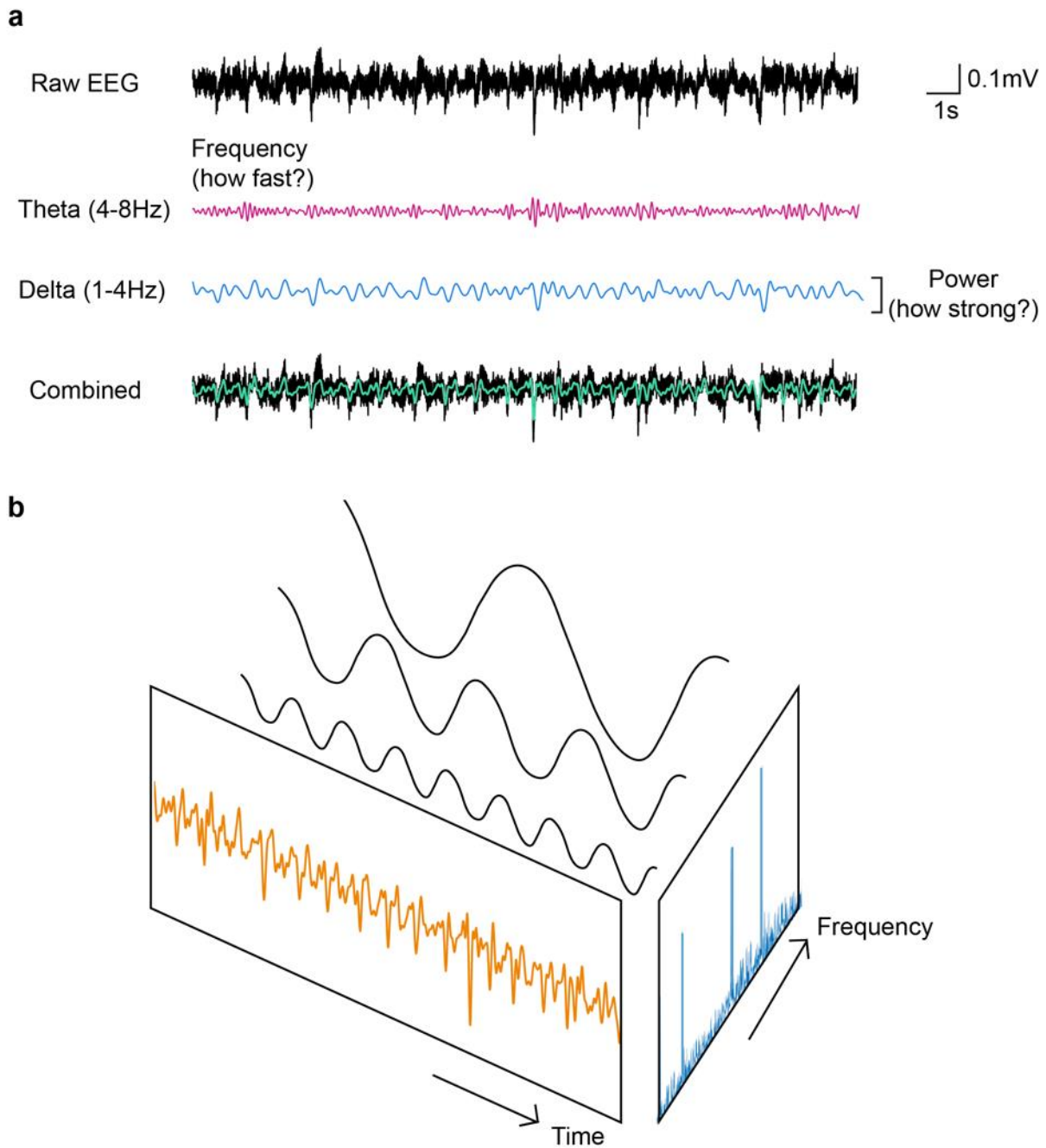


Figure 4.8. Spectral EEG analysis. a Raw EEG from zebrafish larvae (top). Theta frequency extracted from raw EEG signal above (pink). Delta frequency extracted from raw EEG signal above (blue). Power indicated by the amplitude. Combined theta and delta frequencies shown on EEG signal. b Depiction of determining power from the time and frequency domains of a signal.

4.3.3. Automated seizure-like event detection

Invasive local field potentials (LFPs) and non-invasive electroencephalograms (EEGs) serve as the gold standard for diagnosing epilepsy (Paul, 2018). Traditionally, seizure detection from LFPs

and EEGs have relied mostly upon visual inspection completed manually. However, this can be time consuming and prone to subjectivity, bringing to light the importance of automating the detection of seizures. In humans, automated seizure detection algorithms do have an extensive literature dating back to the '80s (Gotman, 1982). In spite of this, as animal models continue to advance the field of epilepsy research there is a requirement for automated detection algorithms to follow. In a zebrafish model with higher throughput, and in particular for the investigations conducted here with 4 different genetic zebrafish lines, manual detection can end up being a bottleneck. Additionally, as this is to the best of my knowledge the first time seizure-like events (SLEs) were explored in a *panx1*^{-/-} zebrafish model it remained unclear whether or not events would be present and if they would appear like controls, highlighting a possibility of manual classification error. Therefore, a signal processing approach towards automating seizure detection in zebrafish *in vivo* was required to expedite analysis and remove any experimental biases in our model.

Electrical patterns generated during an epileptic seizure in humans, rodents and zebrafish can be described by very similar dynamic models and can share some fundamental characteristics, however, they are observed at very different spatiotemporal scales and dissimilarities exist depending upon whether they are LFP or EEG signals (Paul, 2018). As a result, current seizure detection algorithms cannot be directly applied to the *in vivo* zebrafish model as they are based mostly upon mouse or human data with the exception of two groups; one that designed an algorithm for seizure detection in zebrafish EEG (Hong et al., 2016) and another that took a machine learning (ML) approach towards optimal feature mapping and classification (Hunyadi et al., 2017). Features of the events taken from surface electrodes appeared quite different to those recorded *in vivo*, as such there are no overlaps with this algorithm. However, some base features were adapted from reports in mice (Colic et al., 2013; Jacobs et al., 2019) and validated with the ML classifier in zebrafish and together, were instrumental in designing the seizure detection algorithm described here (**Figure 4.9**).

Seizure detection was established using only TL recordings before being tested on *panx1*^{-/-} lines, in order to set an unbiased standard for event detection in the instance that seizure-like events (SLEs) occurred and appeared differently in our genotypes (**Figure 4.9**). Further details regarding SLEs in the zebrafish lines are discussed in chapter 5, however, features of events across genotypes did not differ from TL controls and are outlined here. First, data was down sampled by

a factor of 10 in order to ease signal processing. Any excess noise at 60Hz, including the harmonic frequencies (120Hz, 180Hz...540Hz), were removed if needed. Artifacts were also removed at the start in order to help reduce any false positive hits from larger deflections and assist in avoiding possible electromyographic (EMG) or movement artefacts. The finite impulse response (FIR) band pass filter was used (H. Qiu et al., 2010) to isolate the theta frequency (**Figure 4.9a**; orange) which is shown to be associated with SLEs (Jacobs et al., 2019). Other low frequency bands were explored in the fish, however, theta was the most accurate at capturing events. The Hilbert transform was then used to create an envelope of the filtered signal (**Figure 4.9a**; blue), which peaks at the presence of strong 4-8Hz power, reflecting the occurrence of a discharge event. Envelope thresholds for event detection were determined from baseline recordings, set to 3 times the standard deviation of the average baseline activity. Exploration of LFPs from TLs revealed another type of electrographic event that appeared to be similar to interictal events, pathological activity that occurs between seizures, in mammals (de Curtis et al., 2012) and were 1.5 times the standard deviation of the average baseline activity and shorter compared to SLEs. Event durations were determined by finding the left and right inflection points of the detected events from the Hilbert transform. Based upon literature for the visual classification of SLEs in zebrafish (Baraban et al., 2005), SLEs are around 3 seconds in duration, therefore, any inflections from the Hilbert transform that occur within 3 seconds of each other and had a maximum gap duration of around 0.5 seconds were classified as the same event. Time-frequency analyses were then performed using the continuous wavelet transform (CWT) found in the Matlab digital signal processing toolbox, which provides a complete representation of a signal by letting the translation and scale parameters of the wavelets vary continuously (Faust et al., 2015). This analysis was completed using the mother Morlet wavelet (A. W. L. Chiu et al., 2006), which is a commonly used basis function for LFP analysis as they are well suited for localizing frequency information in time (Cohen, 2014). The analysis was performed on frequencies ranging from 0.5 to 400Hz with 1Hz step size in order to capture enough information regarding all low and high frequencies associated with the SLEs. Performance of automated seizure detection was validated by eye to ensure events were captured accurately (**Figure 4.9b**). With the development of this automated seizure detection approach for LFPs from zebrafish larvae we generated quick and consistent seizure classification across genotypes. This rendered analysis more objective and demonstrated the wide applicability of this

algorithm across many mutant zebrafish models, posing as an opportunity for facilitating future epilepsy research.

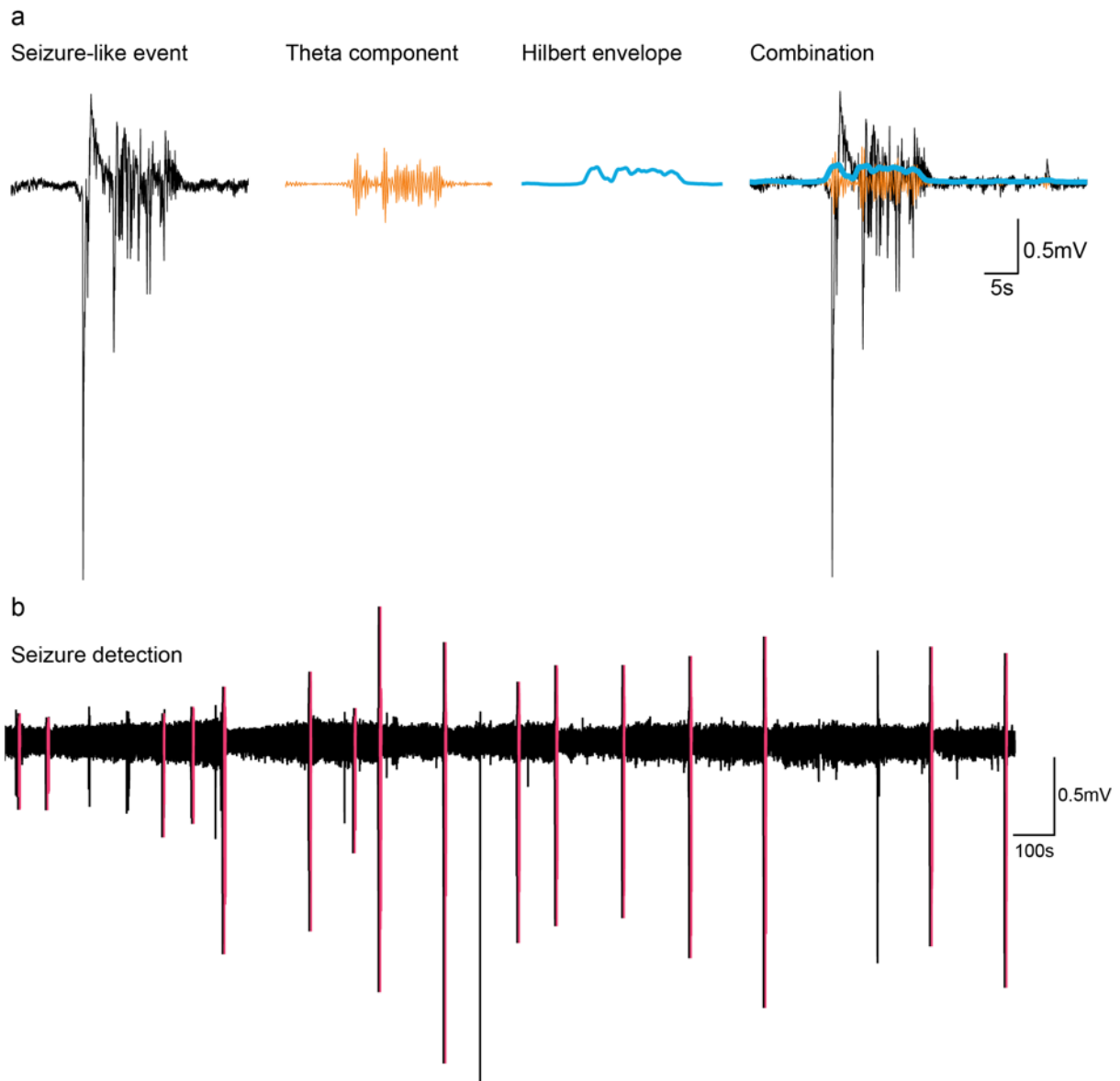


Figure 4.9. Automated seizure detection overview. a Sample seizure-like event (SLE) taken from a TL recording demonstrating the process of event detection. FIR filter isolates the theta frequency (4-8Hz; orange) from the signal and the Hilbert transform applies an envelope (blue) to the isolated theta component. Envelope thresholds of 3 times the standard deviation of baseline activity were used to distinguish SLEs. The theta frequency with the Hilbert envelope is shown overlaid together on the signal to visualize how these features can detect events compared to the rest of the LFP. Single events are calculated from the inflections of the Hilbert transform which are set to have a maximum gap duration between each inflection of 0.5 seconds and minimum full event duration of 3 seconds in order for it to be considered as an event. **b** A full trace is shown here with detected events highlighted in red. A few larger deflections are visible and are not highlighted since these deflections did not meet the classification criteria of the algorithm based upon time and frequency components. These events were also confirmed as non-SLEs visually.

4.4. References

- Ahammad, N., Fathima, T., & Joseph, P. (2014). Detection of Epileptic Seizure Event and Onset Using EEG. *BioMed Research International*, 2014. <https://doi.org/10.1155/2014/450573>
- Alberto, A. V. P., Faria, R. X., Couto, C. G. C., Ferreira, L. G. B., Souza, C. A. M., Teixeira, P. C. N., Fróes, M. M., & Alves, L. A. (2013). Is pannexin the pore associated with the P2X7 receptor? *Naunyn-Schmiedeberg's Archives of Pharmacology*, 386(9). <https://doi.org/10.1007/s00210-013-0868-x>
- Alvarado-Rojas, C., Valderrama, M., Fouad-Ahmed, A., Feldwisch-Drentrup, H., Ihle, M., Teixeira, C. A., Sales, F., Schulze-Bonhage, A., Adam, C., Dourado, A., Charpier, S., Navarro, V., & le Van Quyen, M. (2015). Slow modulations of high-frequency activity (40–140 Hz) discriminate preictal changes in human focal epilepsy. *Scientific Reports*, 4(1). <https://doi.org/10.1038/srep04545>
- Anumonwo, J. M. B., Taffet, S. M., Gu, H., Chanson, M., Moreno, A. P., & Delmar, M. (2001). The Carboxyl Terminal Domain Regulates the Unitary Conductance and Voltage Dependence of Connexin40 Gap Junction Channels. *Circulation Research*, 88(7). <https://doi.org/10.1161/hh0701.088833>
- Aquilino, M. S., Whyte-fagundes, P., Lukewich, M. K., Zhang, L., Bardakjian, B. L., Zoidl, G. R., & Carlen, P. L. (2020). Pannexin-1 deficiency decreases epileptic activity in mice. *International Journal of Molecular Sciences*, 21(20). <https://doi.org/10.3390/ijms21207510>
- Aquilino, M. S., Whyte-Fagundes, P., Zoidl, G., & Carlen, P. L. (2017). Pannexin-1 channels in epilepsy. *Neuroscience Letters*. <https://doi.org/10.1016/j.neulet.2017.09.004>
- Ardiles, A. O., Flores-Muñoz, C., Toro-Ayala, G., Cárdenas, A. M., Palacios, A. G., Muñoz, P., Fuenzalida, M., Sáez, J. C., & Martínez, A. D. (2014). Pannexin 1 regulates bidirectional hippocampal synaptic plasticity in adult mice. *Frontiers in Cellular Neuroscience*, 8. <https://doi.org/10.3389/fncel.2014.00326>
- Avitan, L., Pujic, Z., Mölter, J., van de Poll, M., Sun, B., Teng, H., Amor, R., Scott, E. K., & Goodhill, G. J. (2017). Spontaneous Activity in the Zebrafish Tectum Reorganizes over Development and Is Influenced by Visual Experience. *Current Biology*, 27(16). <https://doi.org/10.1016/j.cub.2017.06.056>
- Bao, L., Locovei, S., & Dahl, G. (2004). Pannexin membrane channels are mechanosensitive conduits for ATP. *FEBS Letters*, 572(1–3), 65–68. <https://doi.org/10.1016/j.febslet.2004.07.009>
- Baraban, S. C., Taylor, M. R., Castro, P. A., & Baier, H. (2005). Pentylentetrazole induced changes in zebrafish behavior, neural activity and c-fos expression. *Neuroscience*, 131(3). <https://doi.org/10.1016/j.neuroscience.2004.11.031>
- Baranova, A., Ivanov, D., Petrash, N., Pestova, A., Skoblov, M., Kelmanson, I., Shagin, D., Nazarenko, S., Geraymovych, E., Litvin, O., Tiunova, A., Born, T. L., Usman, N., Staroverov, D., Lukyanov, S., & Panchin, Y. (2004). The mammalian pannexin family is homologous to the invertebrate innexin gap junction proteins. *Genomics*, 83(4), 706–716. <https://doi.org/10.1016/j.ygeno.2003.09.025>
- Basnet, R., Zizioli, D., Taweedet, S., Finazzi, D., & Memo, M. (2019). Zebrafish Larvae as a Behavioral Model in Neuropharmacology. *Biomedicines*, 7(1). <https://doi.org/10.3390/biomedicines7010023>
- Bedell, V. M., Wang, Y., Campbell, J. M., Poshusta, T. L., Starker, C. G., Krug, R. G., Tan, W., Penheiter, S. G., Ma, A. C., Leung, A. Y. H., Fahrenkrug, S. C., Carlson, D. F., Voytas, D.

- F., Clark, K. J., Essner, J. J., & Ekker, S. C. (2012). In vivo genome editing using a high-efficiency TALEN system. *Nature*. <https://doi.org/10.1038/nature11537>
- Bertram, E. (2014). Electrophysiology in epilepsy surgery: Roles and limitations. *Annals of Indian Academy of Neurology*, *17*(5). <https://doi.org/10.4103/0972-2327.128649>
- Biechl, D., Tietje, K., Ryu, S., Grothe, B., Gerlach, G., & Wullmann, M. F. (2017). Identification of accessory olfactory system and medial amygdala in the zebrafish. *Scientific Reports*, *7*(1). <https://doi.org/10.1038/srep44295>
- Bloomfield, S. A., Xin, D., & Persky, S. E. (1995). A comparison of receptive field and tracer coupling size of horizontal cells in the rabbit retina. *Visual Neuroscience*, *12*(5). <https://doi.org/10.1017/S0952523800009524>
- Boassa, D., Ambrosi, C., Qiu, F., Dahl, G., Gaietta, G., & Sosinsky, G. (2007). Pannexin1 channels contain a glycosylation site that targets the hexamer to the plasma membrane. *The Journal of Biological Chemistry*, *282*(43), 31733–31743. <https://doi.org/10.1074/jbc.M702422200>
- Boassa, D., Qiu, F., Dahl, G., & Sosinsky, G. (2008). Trafficking dynamics of glycosylated pannexin 1 proteins. *Cell Communication & Adhesion*, *15*(1), 119–132. <https://doi.org/10.1080/15419060802013885>
- Bond, S. R., Wang, N., Leybaert, L., & Naus, C. C. (2012). Pannexin 1 Ohnologs in the Teleost Lineage. *The Journal of Membrane Biology*, *245*(8). <https://doi.org/10.1007/s00232-012-9497-4>
- Bruzzone, R., Hormuzdi, S. G., Barbe, M. T., Herb, A., & Monyer, H. (2003). Pannexins, a family of gap junction proteins expressed in brain. *Proceedings of the National Academy of Sciences of the United States of America*, *100*(23), 13644–13649. <https://doi.org/10.1073/pnas.2233464100>
- Buchin, A., Kerr, C. C., Huberfeld, G., Miles, R., & Gutkin, B. (2018). Adaptation and Inhibition Control Pathological Synchronization in a Model of Focal Epileptic Seizure. *Eneuro*, *5*(5). <https://doi.org/10.1523/ENEURO.0019-18.2018>
- Burnstock, G. (2006). Historical review: ATP as a neurotransmitter. *Trends in Pharmacological Sciences*, *27*(3). <https://doi.org/10.1016/j.tips.2006.01.005>
- Burnstock, G. (2018). Purine and purinergic receptors. *Brain and Neuroscience Advances*, *2*. <https://doi.org/10.1177/2398212818817494>
- Burnstock, G. (2020). *Introduction to Purinergic Signalling in the Brain*. https://doi.org/10.1007/978-3-030-30651-9_1
- Burrows, D. R. W., Samarut, É., Liu, J., Baraban, S. C., Richardson, M. P., Meyer, M. P., & Rosch, R. E. (2020). Imaging epilepsy in larval zebrafish. *European Journal of Paediatric Neurology*, *24*. <https://doi.org/10.1016/j.ejpn.2020.01.006>
- Buzsáki, G. (2006). *Rhythms of the Brain*. Oxford University Press. <https://doi.org/10.1093/acprof:oso/9780195301069.001.0001>
- Buzsáki, G., & Wang, X.-J. (2012). Mechanisms of Gamma Oscillations. *Annual Review of Neuroscience*, *35*(1). <https://doi.org/10.1146/annurev-neuro-062111-150444>
- Carlen, P. L. (2012). Curious and contradictory roles of glial connexins and pannexins in epilepsy. *Brain Research*, *1487*, 54–60. <https://doi.org/10.1016/j.brainres.2012.06.059>
- Celetti, S. J., Cowan, K. N., Penuela, S., Shao, Q., Churko, J., & Laird, D. W. (2010). Implications of pannexin 1 and pannexin 3 for keratinocyte differentiation. *Journal of Cell Science*, *123*(8). <https://doi.org/10.1242/jcs.056093>

- Cenedese, V., de Graaff, W., Csikós, T., Poovayya, M., Zoidl, G., & Kamermans, M. (2017). Pannexin 1 Is Critically Involved in Feedback from Horizontal Cells to Cones. *Frontiers in Molecular Neuroscience*, *10*. <https://doi.org/10.3389/fnmol.2017.00403>
- Cepeda, C., Chang, J. W., Owens, G. C., Huynh, M. N., Chen, J. Y., Tran, C., Vinters, H. v., Levine, M. S., & Mathern, G. W. (2015). In Rasmussen Encephalitis, Hemichannels Associated with Microglial Activation are linked to Cortical Pyramidal Neuron Coupling: A Possible Mechanism for Cellular Hyperexcitability. *CNS Neuroscience & Therapeutics*, *21*(2). <https://doi.org/10.1111/cns.12352>
- Cermak, T., Doyle, E. L., Christian, M., Wang, L., Zhang, Y., Schmidt, C., Baller, J. A., Somia, N. V., Bogdanove, A. J., & Voytas, D. F. (2011). Efficient design and assembly of custom TALEN and other TAL effector-based constructs for DNA targeting. *Nucleic Acids Research*. <https://doi.org/10.1093/nar/gkr218>
- Chang, M., Dufour, S., Carlen, P. L., & Valiante, T. A. (2019). Generation and On-Demand Initiation of Acute Ictal Activity in Rodent and Human Tissue. *Journal of Visualized Experiments*, *143*. <https://doi.org/10.3791/57952>
- Cheng, R.-K., Jesuthasan, S. J., & Penney, T. B. (2014). Zebrafish forebrain and temporal conditioning. *Philosophical Transactions of the Royal Society B: Biological Sciences*, *369*(1637). <https://doi.org/10.1098/rstb.2012.0462>
- Chiu, A. W. L., Jahromi, S. S., Khosravani, H., Carlen, P. L., & Bardakjian, B. L. (2006). The effects of high-frequency oscillations in hippocampal electrical activities on the classification of epileptiform events using artificial neural networks. *Journal of Neural Engineering*, *3*(1). <https://doi.org/10.1088/1741-2560/3/1/002>
- Chiu, Y.-H., Jin, X., Medina, C. B., Leonhardt, S. A., Kiessling, V., Bennett, B. C., Shu, S., Tamm, L. K., Yeager, M., Ravichandran, K. S., & Bayliss, D. A. (2017). A quantized mechanism for activation of pannexin channels. *Nature Communications*, *8*(1). <https://doi.org/10.1038/ncomms14324>
- Chuah, M. I., & Zheng, D. R. (1992). The human primary olfactory pathway: fine structural and cytochemical aspects during development and in adults. *Microscopy Research and Technique*, *23*(1), 76–85. <https://doi.org/10.1002/jemt.1070230107>
- Cohen, M. (2014). *Analyzing Neural Time Series Data: Theory and Practice* (Vol. 1). The MIT Press.
- Colic, S., Wither, R. G., Zhang, L., Eubanks, J. H., & Bardakjian, B. L. (2013). Characterization of seizure-like events recorded in vivo in a mouse model of Rett syndrome. *Neural Networks*, *46*. <https://doi.org/10.1016/j.neunet.2013.05.002>
- Coppi, E., Cellai, L., Maraula, G., Pugliese, A. M., & Pedata, F. (2013). Adenosine A2A receptors inhibit delayed rectifier potassium currents and cell differentiation in primary purified oligodendrocyte cultures. *Neuropharmacology*, *73*. <https://doi.org/10.1016/j.neuropharm.2013.05.035>
- Cotrina, M. L., Lin, J. H.-C., & Nedergaard, M. (1998). Cytoskeletal Assembly and ATP Release Regulate Astrocytic Calcium Signaling. *The Journal of Neuroscience*, *18*(21). <https://doi.org/10.1523/JNEUROSCI.18-21-08794.1998>
- Dahl, G. (2015). ATP release through pannexon channels. *Philosophical Transactions of the Royal Society B: Biological Sciences*, *370*(1672), 20140191. <https://doi.org/10.1098/rstb.2014.0191>
- Davis, L. K., Gamazon, E. R., Kistner-Griffin, E., Badner, J. A., Liu, C., Cook, E. H., Sutcliffe, J. S., & Cox, N. J. (2012). Loci nominally associated with autism from genome-wide analysis show enrichment of brain expression quantitative trait loci but not lymphoblastoid cell line

- expression quantitative trait loci. *Molecular Autism*, 3(1). <https://doi.org/10.1186/2040-2392-3-3>
- de Curtis, M., Jefferys, J., & Avoli, M. (2012). Interictal Epileptiform Discharges in Partial Epilepsy: Complex Neurobiological Mechanisms Based on Experimental and Clinical Evidence. In J. Noebels, M. Avoli, M. Rogawski, R. Olsen, & A. Delgado-Escueta (Eds.), *Jasper's Basic Mechanisms of the Epilepsies [Internet]. 4th edition. Bethesda (MD): National Center for Biotechnology Information (US). Oxford University Press.*
- Deng, Z., He, Z., Maksaev, G., Bitter, R. M., Rau, M., Fitzpatrick, J. A. J., & Yuan, P. (2020). Cryo-EM structures of the ATP release channel pannexin 1. *Nature Structural & Molecular Biology*, 27(4). <https://doi.org/10.1038/s41594-020-0401-0>
- Dossi, E., Blauwblomme, T., Moulard, J., Chever, O., Vasile, F., Guinard, E., le Bert, M., Couillin, I., Pallud, J., Capelle, L., Huberfeld, G., & Rouach, N. (2018). Pannexin-1 channels contribute to seizure generation in human epileptic brain tissue and in a mouse model of epilepsy. *Science Translational Medicine*, 10(443). <https://doi.org/10.1126/scitranslmed.aar3796>
- Dourado, M., Wong, E., & Hackos, D. H. (2014). Pannexin-1 Is Blocked by Its C-Terminus through a Delocalized Non-Specific Interaction Surface. *PLoS ONE*, 9(6). <https://doi.org/10.1371/journal.pone.0099596>
- Douw, L., de Groot, M., van Dellen, E., Heimans, J. J., Ronner, H. E., Stam, C. J., & Reijneveld, J. C. (2010). 'Functional Connectivity' Is a Sensitive Predictor of Epilepsy Diagnosis after the First Seizure. *PLoS ONE*, 5(5). <https://doi.org/10.1371/journal.pone.0010839>
- Dufresne, J., & Cyr, D. G. (2014). Regulation of the Pannexin-1 Promoter in the Rat Epididymis 1. *Biology of Reproduction*, 91(6). <https://doi.org/10.1095/biolreprod.114.122168>
- Dunn, T. W., Mu, Y., Narayan, S., Randlett, O., Naumann, E. A., Yang, C.-T., Schier, A. F., Freeman, J., Engert, F., & Ahrens, M. B. (2016). Brain-wide mapping of neural activity controlling zebrafish exploratory locomotion. *ELife*, 5. <https://doi.org/10.7554/eLife.12741>
- Dvorianchikova, G., Ivanov, D., Pestova, A., & Shestopalov, V. (2006). Molecular characterization of pannexins in the lens. *Molecular Vision*, 12, 1417–1426. <http://www.ncbi.nlm.nih.gov/pubmed/17149368>
- Dvorianchikova, G., Pronin, A., Kurtenbach, S., Toychiev, A., Chou, T.-H., Yee, C. W., Prindeville, B., Tayou, J., Porciatti, V., Sagdullaev, B. T., Slepak, V. Z., & Shestopalov, V. I. (2018). Pannexin 1 sustains the electrophysiological responsiveness of retinal ganglion cells. *Scientific Reports*, 8(1). <https://doi.org/10.1038/s41598-018-23894-2>
- Ekstrom, A. D. (2015). Why vision is important to how we navigate. *Hippocampus*, 25(6). <https://doi.org/10.1002/hipo.22449>
- Engel, T., Alves, M., Sheedy, C., & Henshall, D. C. (2016). ATPergic signalling during seizures and epilepsy. *Neuropharmacology*, 104. <https://doi.org/10.1016/j.neuropharm.2015.11.001>
- Faust, O., Acharya, U. R., Adeli, H., & Adeli, A. (2015). Wavelet-based EEG processing for computer-aided seizure detection and epilepsy diagnosis. *Seizure*, 26. <https://doi.org/10.1016/j.seizure.2015.01.012>
- Fu, M., Xie, Z., & Zuo, H. (2009). TRPV1: A potential target for antiepileptogenesis. *Medical Hypotheses*, 73(1). <https://doi.org/10.1016/j.mehy.2009.01.005>
- Fueta, Y., & Avoli, M. (1992). Effects of antiepileptic drugs on 4-aminopyridine-induced epileptiform activity in young and adult rat hippocampus. *Epilepsy Research*, 12.
- Gotman, J. (1982). Automatic recognition of epileptic seizures in the EEG. *Electroencephalography and Clinical Neurophysiology*, 54(5). [https://doi.org/10.1016/0013-4694\(82\)90038-4](https://doi.org/10.1016/0013-4694(82)90038-4)

- Grigorovsky, V., Jacobs, D., Breton, V. L., Tufa, U., Lucasius, C., del Campo, J. M., Chinvarun, Y., Carlen, P. L., Wennberg, R., & Bardakjian, B. L. (2020). Delta-gamma phase-amplitude coupling as a biomarker of postictal generalized EEG suppression. *Brain Communications*, 2(2). <https://doi.org/10.1093/braincomms/fcaa182>
- Grone, B. P., & Baraban, S. C. (2015). Animal models in epilepsy research: legacies and new directions. *Nature Neuroscience*, 18(3). <https://doi.org/10.1038/nn.3934>
- Guerrini, R., & Genton, P. (2004). Epileptic Syndromes and Visually Induced Seizures. *Epilepsia*, 45(s1). <https://doi.org/10.1111/j.0013-9580.2004.451011.x>
- Guirgis, M., Chinvarun, Y., Carlen, P. L., & Bardakjian, B. L. (2013, July). The role of delta-modulated high frequency oscillations in seizure state classification. *2013 35th Annual International Conference of the IEEE Engineering in Medicine and Biology Society (EMBC)*. <https://doi.org/10.1109/EMBC.2013.6611067>
- Gulbransen, B. D., Bashashati, M., Hirota, S. A., Gui, X., Roberts, J. A., MacDonald, J. A., Muruve, D. A., McKay, D. M., Beck, P. L., Mawe, G. M., Thompson, R. J., & Sharkey, K. A. (2012). Activation of neuronal P2X7 receptor–pannexin-1 mediates death of enteric neurons during colitis. *Nature Medicine*, 18(4). <https://doi.org/10.1038/nm.2679>
- Gupta, R. C. (2014). Aminopyridine, 4- (4-AP). In *Encyclopedia of Toxicology*. Elsevier. <https://doi.org/10.1016/B978-0-12-386454-3.00096-8>
- Halpern, M. (1987). The Organization and Function of the Vomeronasal System. *Annual Review of Neuroscience*, 10(1). <https://doi.org/10.1146/annurev.ne.10.030187.001545>
- Herrera-Calderon, O., Santiváñez-Acosta, R., Pari-Olarte, B., Enciso-Roca, E., Campos Montes, V. M., & Luis Arroyo Acevedo, J. (2018). Anticonvulsant effect of ethanolic extract of *Cyperus articulatus* L. leaves on pentylenetetrazol induced seizure in mice. *Journal of Traditional and Complementary Medicine*, 8(1). <https://doi.org/10.1016/j.jtcme.2017.03.001>
- Hong, S., Lee, P., Baraban, S. C., & Lee, L. P. (2016). A Novel Long-term, Multi-Channel and Non-invasive Electrophysiology Platform for Zebrafish. *Scientific Reports*, 6(1). <https://doi.org/10.1038/srep28248>
- Hortopan, G. A., Dinday, M. T., & Baraban, S. C. (2010). Zebrafish as a model for studying genetic aspects of epilepsy. *Disease Models & Mechanisms*, 3(3–4). <https://doi.org/10.1242/dmm.002139>
- Housley, G. D., Bringmann, A., & Reichenbach, A. (2009). Purinergic signaling in special senses. *Trends in Neurosciences*, 32(3). <https://doi.org/10.1016/j.tins.2009.01.001>
- Huang, Y.-J., Maruyama, Y., Dvoryanchikov, G., Pereira, E., Chaudhari, N., & Roper, S. D. (2007). The role of pannexin 1 hemichannels in ATP release and cell-cell communication in mouse taste buds. *Proceedings of the National Academy of Sciences*, 104(15). <https://doi.org/10.1073/pnas.0611280104>
- Hunyadi, B., Siekierska, A., Sourbron, J., Copmans, D., & de Witte, P. A. M. (2017). Automated analysis of brain activity for seizure detection in zebrafish models of epilepsy. *Journal of Neuroscience Methods*, 287. <https://doi.org/10.1016/j.jneumeth.2017.05.024>
- Iglesias, R., Locovei, S., Roque, A., Alberto, A. P., Dahl, G., Spray, D. C., & Scemes, E. (2008). P2X7 receptor-Pannexin1 complex: pharmacology and signaling. *American Journal of Physiology. Cell Physiology*, 295(3), C752-60. <https://doi.org/10.1152/ajpcell.00228.2008>
- Ishikawa, M., Iwamoto, T., Nakamura, T., Doyle, A., Fukumoto, S., & Yamada, Y. (2011). Pannexin 3 functions as an ER Ca²⁺ channel, hemichannel, and gap junction to promote osteoblast differentiation. *Journal of Cell Biology*, 193(7). <https://doi.org/10.1083/jcb.201101050>

- Ishikawa, M., Williams, G. L., Ikeuchi, T., Sakai, K., Fukumoto, S., & Yamada, Y. (2016). Pannexin 3 and connexin 43 modulate skeletal development via distinct functions and expression patterns. *Journal of Cell Science*. <https://doi.org/10.1242/jcs.176883>
- Jacobs, D., Liu, Y. H., Hilton, T., del Campo, M., Carlen, P. L., & Bardakjian, B. L. (2019). Classification of Scalp EEG States Prior to Clinical Seizure Onset. *IEEE Journal of Translational Engineering in Health and Medicine*, 7. <https://doi.org/10.1109/JTEHM.2019.2926257>
- Jia, C; Doherty, P; Crudgington, S; Hegg, C. (2009). Activation of purinergic receptors induces proliferation and neuronal differentiation in swiss webster mouse olfactory epithelium. *Neuroscience*, 163, 102–128. http://journals2.scholarsportal.info/pdf/03064522/v163i0001/120_aopripiswmoe.xml
- Jiang, T., Long, H., Ma, Y., Long, L., Li, Y., Li, F., Zhou, P., Yuan, C., & Xiao, B. (2013a). Altered expression of pannexin proteins in patients with temporal lobe epilepsy. *Molecular Medicine Reports*. <https://doi.org/10.3892/mmr.2013.1739>
- Jiang, T., Long, H., Ma, Y., Long, L., Li, Y., Li, F., Zhou, P., Yuan, C., & Xiao, B. (2013b). Altered expression of pannexin proteins in patients with temporal lobe epilepsy. *Molecular Medicine Reports*. <https://doi.org/10.3892/mmr.2013.1739>
- Kamkin, A., Kiseleva, I., Lozinsky, I., & Scholz, H. (2005). Electrical interaction of mechanosensitive fibroblasts and myocytes in the heart. *Basic Research in Cardiology*, 100(4). <https://doi.org/10.1007/s00395-005-0529-4>
- Kawamura, M., Ruskin, D. N., & Masino, S. A. (2010). Metabolic Autocrine Regulation of Neurons Involves Cooperation among Pannexin Hemichannels, Adenosine Receptors, and KATP Channels. *Journal of Neuroscience*, 30(11). <https://doi.org/10.1523/JNEUROSCI.0055-10.2010>
- Khakh, B. S., Gittermann, D., Cockayne, D. A., & Jones, A. (2003). ATP Modulation of Excitatory Synapses onto Interneurons. *The Journal of Neuroscience*, 23(19). <https://doi.org/10.1523/JNEUROSCI.23-19-07426.2003>
- Kim, J.-E., & Kang, T.-C. (2011). The P2X7 receptor–pannexin-1 complex decreases muscarinic acetylcholine receptor–mediated seizure susceptibility in mice. *Journal of Clinical Investigation*, 121(5). <https://doi.org/10.1172/JCI44818>
- Knapp, A. G., & Dowling, J. E. (1987). Dopamine enhances excitatory amino acid-gated conductances in cultured retinal horizontal cells. *Nature*, 325(6103). <https://doi.org/10.1038/325437a0>
- Kranz, K., Dorgau, B., Pottek, M., Herrling, R., Schultz, K., Bolte, P., Monyer, H., Penuela, S., Laird, D. W., Dedek, K., Weiler, R., & Janssen-Bienhold, U. (2013). Expression of Pannexin1 in the outer plexiform layer of the mouse retina and physiological impact of its knockout. *Journal of Comparative Neurology*, 521(5). <https://doi.org/10.1002/cne.23223>
- Kurtenbach, S., Whyte-Fagundes, P., Gelis, L., Kurtenbach, S., Brazil, É., Zoidl, C., Hatt, H., Shestopalov, V. I., & Zoidl, G. (2014). Investigation of olfactory function in a Panx1 knock out mouse model. *Frontiers in Cellular Neuroscience*, 8. <https://doi.org/10.3389/fncel.2014.00266>
- Kurtenbach, Sarah, Prochnow, N., Kurtenbach, S., Klooster, J., Zoidl, C., Dermietzel, R., Kamermans, M., & Zoidl, G. (2013). Pannexin1 Channel Proteins in the Zebrafish Retina Have Shared and Unique Properties. *PLoS ONE*, 8(10). <https://doi.org/10.1371/journal.pone.0077722>

- Lee, C.-Y. (1992). On the activation-inactivation coupling in *Shaker* potassium channels. *FEBS Letters*, 306(2–3). [https://doi.org/10.1016/0014-5793\(92\)80976-N](https://doi.org/10.1016/0014-5793(92)80976-N)
- Li, S., Zang, Z., He, J., Chen, X., Yu, S., Pei, Y., Hou, Z., An, N., Yang, H., Zhang, C., & Liu, S. (2017). Expression of pannexin 1 and 2 in cortical lesions from intractable epilepsy patients with focal cortical dysplasia. *Oncotarget*, 8(4). <https://doi.org/10.18632/oncotarget.14317>
- Locovei, S., Bao, L., & Dahl, G. (2006). Pannexin 1 in erythrocytes: Function without a gap. *Proceedings of the National Academy of Sciences*, 103(20). <https://doi.org/10.1073/pnas.0601037103>
- Locovei, Silviu, Scemes, E., Qiu, F., Spray, D. C., & Dahl, G. (2007). Pannexin1 is part of the pore forming unit of the P2X7 receptor death complex. *FEBS Letters*, 581(3), 483–488. <https://doi.org/10.1016/j.febslet.2006.12.056>
- Locovei, Silviu, Wang, J., & Dahl, G. (2006). Activation of pannexin 1 channels by ATP through P2Y receptors and by cytoplasmic calcium. *FEBS Letters*, 580(1), 239–244. <https://doi.org/10.1016/j.febslet.2005.12.004>
- Lohman, A. W., Weaver, J. L., Billaud, M., Sandilos, J. K., Griffiths, R., Straub, A. C., Penuela, S., Leitinger, N., Laird, D. W., Bayliss, D. A., & Isakson, B. E. (2012). S-Nitrosylation Inhibits Pannexin 1 Channel Function. *Journal of Biological Chemistry*, 287(47). <https://doi.org/10.1074/jbc.M112.397976>
- Lopatař, J., Dale, N., & Frenguelli, B. G. (2015). Pannexin-1-mediated ATP release from area CA3 drives mGlu5-dependent neuronal oscillations. *Neuropharmacology*, 93. <https://doi.org/10.1016/j.neuropharm.2015.01.014>
- Ma, A. C. H., Chen, Y., Blackburn, P. R., & Ekker, S. C. (2016). TALEN-Mediated mutagenesis and genome editing. In *Methods in Molecular Biology*. https://doi.org/10.1007/978-1-4939-3771-4_2
- Ma, A. C., Lee, H. B., Clark, K. J., & Ekker, S. C. (2013). High Efficiency In Vivo Genome Engineering with a Simplified 15-RVD GoldyTALEN Design. *PLoS ONE*. <https://doi.org/10.1371/journal.pone.0065259>
- McBride, T. A., Stockert, B. W., Gorin, F. A., & Carlsen, R. C. (2000). Stretch-activated ion channels contribute to membrane depolarization after eccentric contractions. *Journal of Applied Physiology*, 88(1). <https://doi.org/10.1152/jappl.2000.88.1.91>
- Mendoza-Fernandez, V., Andrew, R. D., & Barajas-López, C. (2000). ATP inhibits glutamate synaptic release by acting at P2Y receptors in pyramidal neurons of hippocampal slices. *The Journal of Pharmacology and Experimental Therapeutics*, 293, 172–179.
- Michalski, K., & Kawate, T. (2016). Carbenoxolone inhibits Pannexin1 channels through interactions in the first extracellular loop. *Journal of General Physiology*, 147(2). <https://doi.org/10.1085/jgp.201511505>
- Michalski, K., Syrjanen, J. L., Henze, E., Kumpf, J., Furukawa, H., & Kawate, T. (2020). The Cryo-EM structure of pannexin 1 reveals unique motifs for ion selection and inhibition. *ELife*, 9. <https://doi.org/10.7554/eLife.54670>
- Mim, C., Perkins, G., & Dahl, G. (2021). Structure versus function: Are new conformations of pannexin 1 yet to be resolved? *Journal of General Physiology*, 153(5). <https://doi.org/10.1085/jgp.202012754>
- Miras-Portugal, M. T., Sebastián-Serrano, Á., de Diego García, L., & Díaz-Hernández, M. (2017). Neuronal P2X7 Receptor: Involvement in Neuronal Physiology and Pathology. *The Journal of Neuroscience*, 37(30). <https://doi.org/10.1523/JNEUROSCI.3104-16.2017>

- Moreno, A. P., Chanson, M., Anumonwo, J., Scerri, I., Gu, H., Taffet, S. M., & Delmar, M. (2002). Role of the Carboxyl Terminal of Connexin43 in Transjunctional Fast Voltage Gating. *Circulation Research*, 90(4). <https://doi.org/10.1161/hh0402.105667>
- Mou, L., Ke, M., Song, M., Shan, Y., Xiao, Q., Liu, Q., Li, J., Sun, K., Pu, L., Guo, L., Geng, J., Wu, J., & Deng, D. (2020). Structural basis for gating mechanism of Pannexin 1 channel. *Cell Research*, 30(5). <https://doi.org/10.1038/s41422-020-0313-x>
- Murana, E., Pagani, F., Basilico, B., Sundukova, M., Batti, L., di Angelantonio, S., Cortese, B., Grimaldi, A., Francioso, A., Heppenstall, P., Bregestovski, P., Limatola, C., & Ragozzino, D. (2017). ATP release during cell swelling activates a Ca²⁺-dependent Cl⁻ current by autocrine mechanism in mouse hippocampal microglia. *Scientific Reports*, 7(1). <https://doi.org/10.1038/s41598-017-04452-8>
- Mylvaganam, S., Ramani, M., Krawczyk, M., & Carlen, P. L. (2014). Roles of gap junctions, connexins, and pannexins in epilepsy. *Frontiers in Physiology*, 5(172), 1–12. <https://doi.org/10.3389/fphys.2014.00172>
- Mylvaganam, S., Zhang, L., Wu, C., Zhang, Z. J., Samoilova, M., Eubanks, J., Carlen, P. L., & Poulter, M. O. (2010). Hippocampal seizures alter the expression of the pannexin and connexin transcriptome. *Journal of Neurochemistry*, 112(1). <https://doi.org/10.1111/j.1471-4159.2009.06431.x>
- Obot, P., Velíšek, L., Velišková, J., & Scemes, E. (2021). The contribution of astrocyte and neuronal Panx1 to seizures is model and brain region dependent. *BioRxiv for Biology*.
- Panchina, Y., Kelmanson, I., Matz, M., Lukyanov, K., Usman, N., & Lukyanov, S. (2000). A ubiquitous family of putative gap junction molecules [2]. *Current Biology*, 10(13), 473–474. [https://doi.org/10.1016/S0960-9822\(00\)00576-5](https://doi.org/10.1016/S0960-9822(00)00576-5)
- Panula, P., Chen, Y.-C., Priyadarshini, M., Kudo, H., Semenova, S., Sundvik, M., & Sallinen, V. (2010). The comparative neuroanatomy and neurochemistry of zebrafish CNS systems of relevance to human neuropsychiatric diseases. *Neurobiology of Disease*, 40(1). <https://doi.org/10.1016/j.nbd.2010.05.010>
- Paul, Y. (2018). Various epileptic seizure detection techniques using biomedical signals: a review. *Brain Informatics*, 5(2). <https://doi.org/10.1186/s40708-018-0084-z>
- Pelegri, P., & Surprenant, A. (2006). Pannexin-1 mediates large pore formation and interleukin-1beta release by the ATP-gated P2X7 receptor. *The EMBO Journal*, 25(21), 5071–5082. <https://doi.org/10.1038/sj.emboj.7601378>
- Penuela, S., Bhalla, R., Gong, X.-Q., Cowan, K. N., Celetti, S. J., Cowan, B. J., Bai, D., Shao, Q., & Laird, D. W. (2007). Pannexin 1 and pannexin 3 are glycoproteins that exhibit many distinct characteristics from the connexin family of gap junction proteins. *Journal of Cell Science*, 120(Pt 21), 3772–3783. <https://doi.org/10.1242/jcs.009514>
- Penuela, S., Gehi, R., & Laird, D. W. (2013). The biochemistry and function of pannexin channels. *Biochimica et Biophysica Acta (BBA) - Biomembranes*, 1828(1), 15–22. <https://doi.org/10.1016/j.bbamem.2012.01.017>
- Penuela, S., Gyenis, L., Ablack, A., Churko, J. M., Berger, A. C., Litchfield, D. W., Lewis, J. D., & Laird, D. W. (2012). Loss of Pannexin 1 Attenuates Melanoma Progression by Reversion to a Melanocytic Phenotype. *Journal of Biological Chemistry*, 287(34). <https://doi.org/10.1074/jbc.M112.377176>
- Pérez-Gómez, A., Stein, B., Leinders-Zufall, T., & Chamero, P. (2014). Signaling mechanisms and behavioral function of the mouse basal vomeronasal neuroepithelium. *Frontiers in Neuroanatomy*, 8, 135. <https://doi.org/10.3389/fnana.2014.00135>

- Pernelle, G., Nicola, W., & Clopath, C. (2018). Gap junction plasticity as a mechanism to regulate network-wide oscillations. *PLOS Computational Biology*, *14*(3). <https://doi.org/10.1371/journal.pcbi.1006025>
- Prochnow, N., Hoffmann, S., Vroman, R., Klooster, J., Bunse, S., Kamermans, M., Dermietzel, R., & Zoidl, G. (2009). Pannexin1 in the outer retina of the zebrafish, *Danio rerio*. *Neuroscience*, *162*(4). <https://doi.org/10.1016/j.neuroscience.2009.04.064>
- Prochnow, Nora, Abdulazim, A., Kurtenbach, S., Wildförster, V., Dvorianchikova, G., Hanske, J., Petrasch-Parwez, E., Shestopalov, V. I., Dermietzel, R., Manahan-Vaughan, D., & Zoidl, G. (2012). Pannexin1 Stabilizes Synaptic Plasticity and Is Needed for Learning. *PLoS ONE*, *7*(12). <https://doi.org/10.1371/journal.pone.0051767>
- Puthussery, T., Yee, P., Vingrys, A. J., & Fletcher, E. L. (2006). Evidence for the involvement of purinergic P2X₇ receptors in outer retinal processing. *European Journal of Neuroscience*, *24*(1). <https://doi.org/10.1111/j.1460-9568.2006.04895.x>
- Qiu, F., & Dahl, G. (2009). A permeant regulating its permeation pore: inhibition of pannexin 1 channels by ATP. *American Journal of Physiology-Cell Physiology*, *296*(2). <https://doi.org/10.1152/ajpcell.00433.2008>
- Qiu, H., Guo, Z., & Zhang, X. (2010, October). The Design of FIR Band-Pass Filter with Improved Distributed Algorithm Based on FPGA. *2010 International Conference on Multimedia Technology*. <https://doi.org/10.1109/ICMULT.2010.5631230>
- Qu, R., Dong, L., Zhang, J., Yu, X., Wang, L., & Zhu, S. (2020). Cryo-EM structure of human heptameric Pannexin 1 channel. *Cell Research*, *30*(5). <https://doi.org/10.1038/s41422-020-0298-5>
- Rahman, S. (2015). Pathophysiology of mitochondrial disease causing epilepsy and status epilepticus. *Epilepsy & Behavior*, *49*. <https://doi.org/10.1016/j.yebeh.2015.05.003>
- Raimondo, J. v., Burman, R. J., Katz, A. A., & Akerman, C. J. (2015). Ion dynamics during seizures. *Frontiers in Cellular Neuroscience*, *9*. <https://doi.org/10.3389/fncel.2015.00419>
- Ray, A., Zoidl, G., Weickert, S., Wahle, P., & Dermietzel, R. (2005). Site-specific and developmental expression of pannexin1 in the mouse nervous system. *European Journal of Neuroscience*, *21*(12). <https://doi.org/10.1111/j.1460-9568.2005.04139.x>
- Ren, L., Kucewicz, M. T., Cimbalnik, J., Matsumoto, J. Y., Brinkmann, B. H., Hu, W., Marsh, W. R., Meyer, F. B., Stead, S. M., & Worrell, G. A. (2015). Gamma oscillations precede interictal epileptiform spikes in the seizure onset zone. *Neurology*, *84*(6). <https://doi.org/10.1212/WNL.0000000000001234>
- Roy, S., & Field, G. D. (2019). Dopaminergic modulation of retinal processing from starlight to sunlight. *Journal of Pharmacological Sciences*, *140*(1). <https://doi.org/10.1016/j.jphs.2019.03.006>
- Ruan, Z., Orozco, I. J., Du, J., & Lü, W. (2020). Structures of human pannexin 1 reveal ion pathways and mechanism of gating. *Nature*, *584*(7822). <https://doi.org/10.1038/s41586-020-2357-y>
- Rummery, N. M., Brock, J. A., Pakdeechote, P., Ralevic, V., & Dunn, W. R. (2007). ATP is the predominant sympathetic neurotransmitter in rat mesenteric arteries at high pressure. *The Journal of Physiology*, *582*(2). <https://doi.org/10.1113/jphysiol.2007.134825>
- Salazar, I., Sánchez-Quinteiro, P., Alemañ, N., & Prieto, D. (2008). Anatomical, immunohistochemical and physiological characteristics of the vomeronasal vessels in cows and their possible role in vomeronasal reception. *Journal of Anatomy*, *212*(5). <https://doi.org/10.1111/j.1469-7580.2008.00889.x>

- Samarut, É., Swaminathan, A., Riché, R., Liao, M., Hassan-Abdi, R., Renault, S., Allard, M., Dufour, L., Cossette, P., Soussi-Yanicostas, N., & Drapeau, P. (2018). γ -Aminobutyric acid receptor alpha 1 subunit loss of function causes genetic generalized epilepsy by impairing inhibitory network neurodevelopment. *Epilepsia*, *59*(11). <https://doi.org/10.1111/epi.14576>
- Samiee, S., Lévesque, M., Avoli, M., & Baillet, S. (2018). Phase-amplitude coupling and epileptogenesis in an animal model of mesial temporal lobe epilepsy. *Neurobiology of Disease*, *114*. <https://doi.org/10.1016/j.nbd.2018.02.008>
- Sandilos, J. K., Chiu, Y.-H., Chekeni, F. B., Armstrong, A. J., Walk, S. F., Ravichandran, K. S., & Bayliss, D. A. (2012). Pannexin 1, an ATP Release Channel, Is Activated by Caspase Cleavage of Its Pore-associated C-terminal Autoinhibitory Region. *Journal of Biological Chemistry*, *287*(14). <https://doi.org/10.1074/jbc.M111.323378>
- Santiago, M. F., Veliskova, J., Patel, N. K., Lutz, S. E., Caille, D., Charollais, A., Meda, P., & Scemes, E. (2011). Targeting Pannexin1 Improves Seizure Outcome. *PLoS ONE*, *6*(9). <https://doi.org/10.1371/journal.pone.0025178>
- Scemes, E., Velíšek, L., & Velíšková, J. (2019). Astrocyte and Neuronal Pannexin1 Contribute Distinctly to Seizures. *ASN Neuro*, *11*. <https://doi.org/10.1177/1759091419833502>
- Scemes, E., & Velíšková, J. (2019). Exciting and not so exciting roles of pannexins. *Neuroscience Letters*, *695*. <https://doi.org/10.1016/j.neulet.2017.03.010>
- Schomer, D. L., & Lopes da Silva, F. H. (2017). *Niedermeyer's Electroencephalography* (D. L. Schomer & F. H. Lopes da Silva, Eds.; Vol. 1). Oxford University Press. <https://doi.org/10.1093/med/9780190228484.001.0001>
- Scott, E. K., & Baier, H. (2009). The cellular architecture of the larval zebrafish tectum, as revealed by Gal4 enhancer trap lines. *Frontiers in Neural Circuits*, *3*. <https://doi.org/10.3389/neuro.04.013.2009>
- Sharmila, A., & Mahalakshmi, P. (2017). Wavelet-based feature extraction for classification of epileptic seizure EEG signal. *Journal of Medical Engineering & Technology*, *41*(8). <https://doi.org/10.1080/03091902.2017.1394388>
- Shestopalov, V. I., & Slepak, V. Z. (2014). Molecular pathways of pannexin1-mediated neurotoxicity. *Frontiers in Physiology*, *5*. <https://doi.org/10.3389/fphys.2014.00023>
- Sosinsky, G. E., Boassa, D., Dermietzel, R., Duffy, H. S., Laird, D. W., MacVicar, B., Naus, C. C., Penuela, S., Scemes, E., Spray, D. C., Thompson, R. J., Zhao, H. B., & Dahl, G. (2011). Pannexin channels are not gap junction hemichannels. *Channels (Austin, Tex.)*, *5*(3), 193–197. <https://doi.org/10.4161/chan.5.3.15765>
- Storan, M. J., & Key, B. (2006). Septal organ of Grüneberg is part of the olfactory system. *The Journal of Comparative Neurology*, *494*(5), 834–844. <https://doi.org/10.1002/cne.20858>
- Suzuki, D. G., Pérez-Fernández, J., Wibble, T., Kardamakis, A. A., & Grillner, S. (2019). The role of the optic tectum for visually evoked orienting and evasive movements. *Proceedings of the National Academy of Sciences*, *116*(30). <https://doi.org/10.1073/pnas.1907962116>
- Swayne, L. A., Sorbara, C. D., & Bennett, S. A. L. (2010). Pannexin 2 Is Expressed by Postnatal Hippocampal Neural Progenitors and Modulates Neuronal Commitment. *Journal of Biological Chemistry*, *285*(32). <https://doi.org/10.1074/jbc.M110.130054>
- Takigami, S. (2000). Projection Pattern of Vomeronasal Neurons to the Accessory Olfactory Bulb in Goats. *Chemical Senses*, *25*(4). <https://doi.org/10.1093/chemse/25.4.387>
- Thompson, R. J., Jackson, M. F., Olah, M. E., Rungta, R. L., Hines, D. J., Beazely, M. A., MacDonald, J. F., & MacVicar, B. A. (2008). Activation of Pannexin-1 Hemichannels

- Augments Aberrant Bursting in the Hippocampus. *Science*, 322(5907). <https://doi.org/10.1126/science.1165209>
- Tort, A. B. L., Komorowski, R., Eichenbaum, H., & Kopell, N. (2010). Measuring Phase-Amplitude Coupling Between Neuronal Oscillations of Different Frequencies. *Journal of Neurophysiology*, 104(2). <https://doi.org/10.1152/jn.00106.2010>
- van Gelder, N. M., & Sherwin, A. L. (2003). Metabolic Parameters of Epilepsy: Adjuncts to Established Antiepileptic Drug Therapy. *Neurochemical Research*, 28(2). <https://doi.org/10.1023/A:1022433421761>
- Vargas, R., Porsteinsson, H., & Karlsson, K. Æ. (2012). Spontaneous neural activity of the anterodorsal lobe and entopeduncular nucleus in adult zebrafish: A putative homologue of hippocampal sharp waves. *Behavioural Brain Research*, 229(1). <https://doi.org/10.1016/j.bbr.2011.12.025>
- Velisek, L. (2006). Models of Chemically-Induced Acute Seizures. In *Models of Seizures and Epilepsy*. Elsevier. <https://doi.org/10.1016/B978-012088554-1/50013-X>
- Vogt, B. A., Vogt, L., Farber, N. B., & Bush, G. (2005). Architecture and neurocytology of monkey cingulate gyrus. *The Journal of Comparative Neurology*, 485(3). <https://doi.org/10.1002/cne.20512>
- Vroman, R., Klaassen, L. J., Howlett, M. H. C., Cenedese, V., Klooster, J., Sjoerdsma, T., & Kamermans, M. (2014). Extracellular ATP Hydrolysis Inhibits Synaptic Transmission by Increasing pH Buffering in the Synaptic Cleft. *PLoS Biology*, 12(5). <https://doi.org/10.1371/journal.pbio.1001864>
- Wahab, A. (2010). Difficulties in Treatment and Management of Epilepsy and Challenges in New Drug Development. *Pharmaceuticals*, 3(7). <https://doi.org/10.3390/ph3072090>
- Wang, J., Ambrosi, C., Qiu, F., Jackson, D. G., Sosinsky, G., & Dahl, G. (2014). The membrane protein Pannexin1 forms two open-channel conformations depending on the mode of activation. *Science Signaling*, 7(335), ra69. <https://doi.org/10.1126/scisignal.2005431>
- Wang, J., Jackson, D. G., & Dahl, G. (2013a). The food dye FD&C Blue No. 1 is a selective inhibitor of the ATP release channel Panx1. *The Journal of General Physiology*, 141(5), 649–656. <https://doi.org/10.1085/jgp.201310966>
- Wang, J., Jackson, D. G., & Dahl, G. (2013b). The food dye FD&C Blue No. 1 is a selective inhibitor of the ATP release channel Panx1. *Journal of General Physiology*, 141(5). <https://doi.org/10.1085/jgp.201310966>
- Wang, J., Ma, M., Locovei, S., Keane, R. W., & Dahl, G. (2007). Modulation of membrane channel currents by gap junction protein mimetic peptides: size matters. *American Journal of Physiology. Cell Physiology*, 293(3), C1112-9. <https://doi.org/10.1152/ajpcell.00097.2007>
- Wang, L., Dufour, S., Valiante, T. A., & Carlen, P. L. (2016). Extracellular Potassium and Seizures: Excitation, Inhibition and the Role of Ih. *International Journal of Neural Systems*, 26(08). <https://doi.org/10.1142/S0129065716500441>
- Wei, L., Sheng, H., Chen, L., Hao, B., Shi, X., & Chen, Y. (2016). Effect of pannexin-1 on the release of glutamate and cytokines in astrocytes. *Journal of Clinical Neuroscience*, 23. <https://doi.org/10.1016/j.jocn.2015.05.043>
- Whyte-Fagundes, P., Kurtenbach, S., Zoidl, C., Shestopalov, V. I., Carlen, P. L., & Zoidl, G. (2018). A Potential Compensatory Role of Panx3 in the VNO of a Panx1 Knock Out Mouse Model. *Frontiers in Molecular Neuroscience*, 11. <https://doi.org/10.3389/fnmol.2018.00135>
- Whyte-Fagundes, P., Siu, R., Brown, C., & Zoidl, G. (2019). Pannexins in vision, hearing, olfaction and taste. *Neuroscience Letters*, 695. <https://doi.org/10.1016/j.neulet.2017.05.010>

- Wicki-Stordeur, L. E., & Swayne, L. (2013). Panx1 regulates neural stem and progenitor cell behaviours associated with cytoskeletal dynamics and interacts with multiple cytoskeletal elements. *Cell Communication and Signaling*, *11*(1). <https://doi.org/10.1186/1478-811X-11-62>
- Xia, J., Lim, J. C., Lu, W., Beckel, J. M., Macarak, E. J., Laties, A. M., & Mitchell, C. H. (2012). Neurons respond directly to mechanical deformation with pannexin-mediated ATP release and autostimulation of P2X₇ receptors. *The Journal of Physiology*, *590*(10). <https://doi.org/10.1113/jphysiol.2012.227983>
- Yeung, A. K., Patil, C. S., & Jackson, M. F. (2020). Pannexin-1 in the CNS: Emerging concepts in health and disease. *Journal of Neurochemistry*, *154*(5). <https://doi.org/10.1111/jnc.15004>
- Zappalà, A., Li Volti, G., Serapide, M. F., Pellitteri, R., Falchi, M., la Delia, F., Cicirata, V., & Cicirata, F. (2007). Expression of pannexin2 protein in healthy and ischemized brain of adult rats. *Neuroscience*, *148*(3). <https://doi.org/10.1016/j.neuroscience.2007.06.028>
- Zhang, C. (2011). Expression of connexin 57 in the olfactory epithelium and olfactory bulb. *Neuroscience Research*, *71*(3), 226–234. <https://doi.org/10.1016/j.neures.2011.07.1832>
- Zhang, Y., Laumet, G., Chen, S.-R., Hittelman, W. N., & Pan, H.-L. (2015). Pannexin-1 Up-regulation in the Dorsal Root Ganglion Contributes to Neuropathic Pain Development. *Journal of Biological Chemistry*, *290*(23). <https://doi.org/10.1074/jbc.M115.650218>
- Zijlmans, M., Jiruska, P., Zelmann, R., Leijten, F. S. S., Jefferys, J. G. R., & Gotman, J. (2012). High-frequency oscillations as a new biomarker in epilepsy. *Annals of Neurology*, *71*(2). <https://doi.org/10.1002/ana.22548>
- Zoidl, G., Petrasch-Parwez, E., Ray, a., Meier, C., Bunse, S., Habbes, H. W., Dahl, G., & Dermietzel, R. (2007). Localization of the pannexin1 protein at postsynaptic sites in the cerebral cortex and hippocampus. *Neuroscience*, *146*(1), 9–16. <https://doi.org/10.1016/j.neuroscience.2007.01.061>
- Zoidl, Georg, Kremer, M., Zoidl, C., Bunse, S., & Dermietzel, R. (2008). Molecular Diversity of Connexin and Pannexin Genes in the Retina of the Zebrafish *Danio rerio*. *Cell Communication & Adhesion*, *15*(1–2). <https://doi.org/10.1080/15419060802014081>

Chapter 5. Loss of *Panx1* in zebrafish reveal novel seizure outcomes

“If you know you are on the right track, if you have this inner knowledge, then nobody can turn you off...no matter what they say.”

- Barbara McClintock

This chapter is modified from the following original research article:

Paige Whyte-Fagundes, Daria Taskina, Nickie Safarian, Christiane Zoidl, Peter L. Carlen, Logan W. Donaldson, and Georg R. Zoidl. 2021. “Panx1 channels promote both anti- and pro-seizure-like activities in the zebrafish via p2rx7 receptors and ATP signaling. *bioRxiv*; doi:<https://doi.org/10.1101/2021.06.03.446992>

Author Contributions

Conceptualization, PW-F, GRZ; analysis, PW-F, DT, LCD.; investigation, PW-F, DT, NS, CZ; writing—original draft preparation, PW-F, DT, LCD; writing—review and editing, all authors; visualization, PW-F, DT, LCD; supervision, PLC, GRZ; project administration, GRZ; funding acquisition, GRZ. All authors have read and agreed to the published version of the manuscript.

Copyright

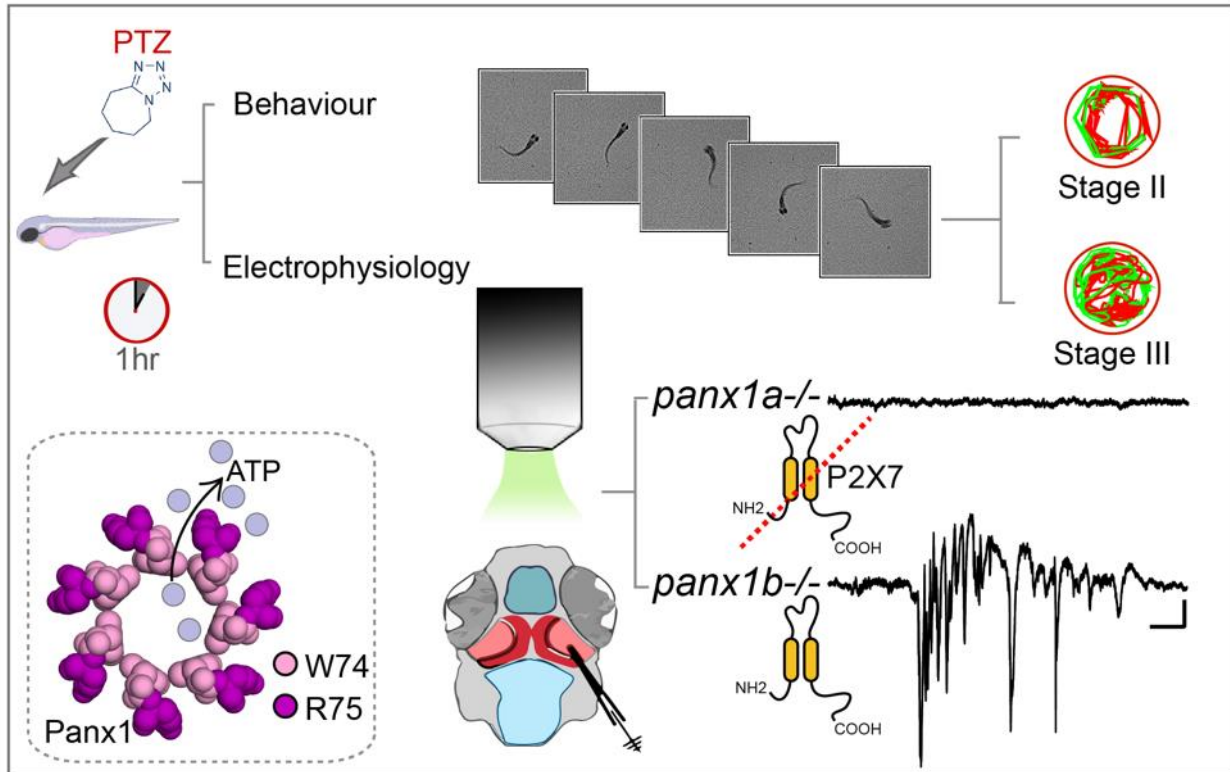
© 2021 Whyte-Fagundes, Taskina, Safarian, Zoidl, Carlen, Donaldson and Zoidl. This is a preprint and not certified by peer review, therefore, the authors are the copyright holders. All rights reserved, no reuse allowed without permission.

Correspondence

Paige Whyte-Fagundes: whytefp@yorku.ca; Georg Zoidl, Phd: gzoidl@yorku.ca

Panx1 channels promote both anti- and pro-seizure-like activities in the zebrafish via p2rx7 receptors and ATP signaling

Graphical Abstract



Authors:

Paige Whyte-Fagundes^{1,2,4},
Daria Taskina^{1,2},
Nickie Safarian^{1,2},
Christiane Zoidl¹,
Peter L. Carlen^{3,4},
Logan W. Donaldson¹,
Georg R. Zoidl^{1,2,4}.

Affiliations:

- ¹ Department of Biology, York University, Toronto, ON, Canada
- ² Center of Vision Research, York University, Toronto, ON, Canada
- ³ Department of Medicine, Physiology, and BME, University of Toronto, Toronto, ON, Canada
- ⁴ Krembil Research Institute, University Health Network, Toronto, ON, Canada

In Brief:

Whyte-Fagundes et al., challenged the leading concept that Panx1 is proconvulsant. Using zebrafish, that have a genome duplication of the *panx1* gene, they revealed that this notion becomes more complicated in teleosts; with *Panx1a* and *Panx1b* presenting a pro- and anti-convulsant phenotype respectively. This discovery elucidated a probable mechanism of *panx1* involvement in seizure dynamics via *p2rx7* receptors and ATP signaling that appears consistent with human PANX1 and offers opportunities for specific drug targeted anticonvulsant therapies in the future.

Highlights:

- *Panx1a* is pro-convulsant, as zebrafish with *Panx1b*^{-/-} exhibit PTZ-induced electrographic and behavioural seizure-like activities.
- *Panx1b* is non-convulsant and has impaired ATP release properties compared to mammalian Panx1 or *Panx1a*.
- Knocking out *panx1a* downregulates the expression of P2rx7, which targeting also improved behavioural PTZ induced seizure outcomes.
- Structural modeling of Panx1 revealed the W74-R75 gate is likely critical in seizure dynamics

5.1. Abstract

The molecular mechanisms of excitation-inhibition imbalances promoting seizure generation in epilepsy patients are not fully understood. Experimental evidence suggests that Pannexin1 (*Panx1*), an ATP release channel, modulates excitability of the brain. In this report, we have performed behavioral and molecular phenotyping experiments on zebrafish larvae bearing genetic or pharmacological knockouts of *panx1a* or *panx1b* channels, each highly homologous to human PANX1. When *Panx1a* function is lost or both channels are under pharmacological blockage, treatment with pentylenetetrazol to induce seizures causes reduced ictal-like events and seizure-like locomotion. These observations were extended by transcriptome profiling, where a spectrum of distinct metabolic and cell signaling states correlates with the loss of *panx1a*. The pro- and anticonvulsant activities of both *panx1* channels affects ATP release and involves the purinergic receptor *p2rx7*. By presenting *panx1* zebrafish models with dual roles in seizures, our work enables the study of mechanisms that would not otherwise be resolved.

5.2. Introduction

A widely accepted view in epilepsy research is that neuronal hyperexcitability during epileptic seizures is caused by an imbalance of excitatory and inhibitory activities. This view places the imbalance of neuronal transmitters glutamate and GABA release first, but evidence is accumulating for altered ATP- and adenosine-mediated signaling between neurons and glial cells contributing to heightened states of excitability and epileptic seizures¹. ATP release and signaling can be both excitatory and inhibitory, but adenosine strongly inhibits electrical activity. Five groups of ATP-release channels with expression in the nervous system are known: pannexin-1 (Panx1)², connexin (Cx) hemichannels³, calcium homeostasis modulator 1 (CALHM1)⁴, volume-regulated anion channels (VRACs, also known as volume-sensitive outwardly rectifying (VSOR) anion channels)⁵, and maxi-anion channels (MACs)⁶. Panx1 is recognized as a pro-convulsant channel after behavioral and electrophysiological markers of excitability are ameliorated in distinct models of epilepsy once Panx1 is inhibited pharmacologically or by global deletion in mice⁷⁻¹⁰. Other evidence for pro-convulsant actions of Panx1 derived from increased expression of human and rodent Panx1 found in epileptic tissue^{8,11-13}. However, the simplistic view of inhibiting mammalian Panx1 and causing anti-convulsant effects is challenged. The targeted deletion of mouse Panx1 in astrocytes potentiates, while the absence of Panx1 in neurons attenuates seizure manifestation¹⁴. Furthermore, the contribution of Panx1 to seizures is also brain region dependent¹⁵, raising questions about the underlying molecular and cellular mechanisms.

Zebrafish have two *panx1* orthologues, *panx1a* and *panx1b*, with distinct expression localizations and biophysical properties¹⁶⁻¹⁸. Like mammalian Panx1¹⁹⁻²¹, the zebrafish *panx1a* is broadly expressed in all tissues tested^{16,17}, whereas the expression of *panx1b* is highest in the nervous system¹⁷. We had suggested that both pannexins fulfill different functions *in vivo* based on differences in the unitary conductance of Panx1a (~380pS) and Panx1b (480-500pS) channels, the complexity of subconductance stages, and the cumulative open and closed times¹⁷. Here, we interrogated Panx1 channels genetically and pharmacologically, and induced seizure-like activities in the zebrafish using pentylentetrazole (PTZ)²² to suppress inhibitory networks by blocking gamma aminobutyric acid (GABA)-A receptors. The zebrafish responses to PTZ were physiologically and behaviorally comparable to mammals^{22,23}.

Gene-edited zebrafish lacking *panx1a* or *panx1b*^{24,25} revealed opposite seizure-like phenotypes and PTZ-related morbidity. Targeted ablation of *panx1b* potentiates, while the absence

of *panx1a* attenuates seizure manifestations according to recordings of *in vivo* local field potentials (ivLFP) and locomotor behavior. A deletion of both fish *panx1* genes, in a double knockout fish (DKO), causes a moderate phenotype with reduced seizures. In line with these observations are significant changes to extracellular ATP levels and biological processes demonstrating that the propensity of developing seizure like activities is correlated with altered regulation of energy metabolism, cell death, and the cellular transportome. The acute pharmacological blocking of both Panx1 channels using Probenecid (Pb) abolished PTZ-induced seizures. The molecular, electrophysiological, and behavioral changes are overlapping, but not identical to genetic interference. Likewise, pharmacological blocking of the Panx1 interaction partner P2rx7²⁶ reduces seizure-like activities like Pb treatment. Finally, structural modeling and comparing the pores of the two Panx1 orthologues and the human PANX1 channel supports our experimental data implicating the Panx1a protein as a driver of pro-convulsant activities.

In summary, our analysis of genetic and pharmacological models in the zebrafish establishes Panx1a channels as the pro-convulsant Panx1 channel. The different propensities of Panx1a and Panx1b channels in developing seizure-like activities can take us a step closer to understanding seizure mechanisms and can prompt initiatives for drug discovery by targeting shared properties of zebrafish and human PANX1.

5.3. Results

5.3.1. Panx1 genotypes determine evoked seizure-like events

Seven days post fertilization (7dpf) larvae were anesthetized, and agar embedded before an electrode was placed into the optic tectum (OT). Seizure-like events (SLE) were recorded after topical application of 15mM PTZ, as described²⁷ (**Figure 5.1a**). Characteristic SLEs induced by PTZ demonstrate an initial action potential burst followed by short paroxysmal bursts, representative of a seizure pattern, which was absent at baseline (**Figure 5.1b**). The number of *panx1a*^{-/-} larvae exhibiting SLEs was reduced by 88% compared to PTZ treated Tubingen Longfin (TL) controls; only one *panx1a*^{-/-} larva responded to PTZ treatment (n = 8). All *panx1b*^{-/-} larvae exhibited SLEs (n = 9). 33% of the DKO larvae seized (*panx1a*^{-/-}: *panx1b*^{-/-}; DKO; n = 12), which was significantly reduced compared to controls (n = 7) and indistinguishable from *panx1a*^{-/-} larvae (p=0.2) (**Figure 5.1c**).

The average number of SLEs per hour was similar for DKO and *panx1a*^{-/-} larvae ($p = 0.58$), with less than one event on average (DKO: 0.58 ± 0.29 ; *panx1a*^{-/-}: 0.38 ± 0.38 events/hour.). Even though all *panx1b*^{-/-} fish had SLEs, the average number of events per hour were significantly less compared to controls (*panx1b*^{-/-}: 36.78 ± 2.67 ; TL: 49.86 ± 3.86 events/hour) (**Figure 5.1d**). The duration of events in all genotypes were comparable to TL controls (TL: $5.5s \pm 0.4s$; DKO: $4.1s \pm 0.2s$, $p = 0.07$; *panx1a*^{-/-}: $4.2s$, $p = n/a$; *panx1b*^{-/-}: $4.8s \pm 0.4s$, $p = 0.09$) (**Figure 5.1e**).

The latency until the first SLE showed differences amongst genotypes. TL larvae exhibited the shortest latent period (12.9 ± 1.3 min). *Panx1b*^{-/-} fish presented a delay until the first SLE, with events starting at 21 ± 1.2 min. DKO (51.1 ± 4.5 min) and *panx1a*^{-/-} responded last to PTZ treatment (47.3 min) (**Figure 5.1f**).

The fractional percentage of seizing time within the first hour revealed additional genotype specific differences. SLEs in *panx1b*^{-/-} larvae were reduced compared to TL controls (*panx1b*^{-/-}: $4.8\% \pm 0.3\%$; TL: $7.6\% \pm 0.8\%$). However, both DKO and *panx1a*^{-/-} fish displayed minimal seizing time ($<0.1\%$). (**Figure 5.1g**).

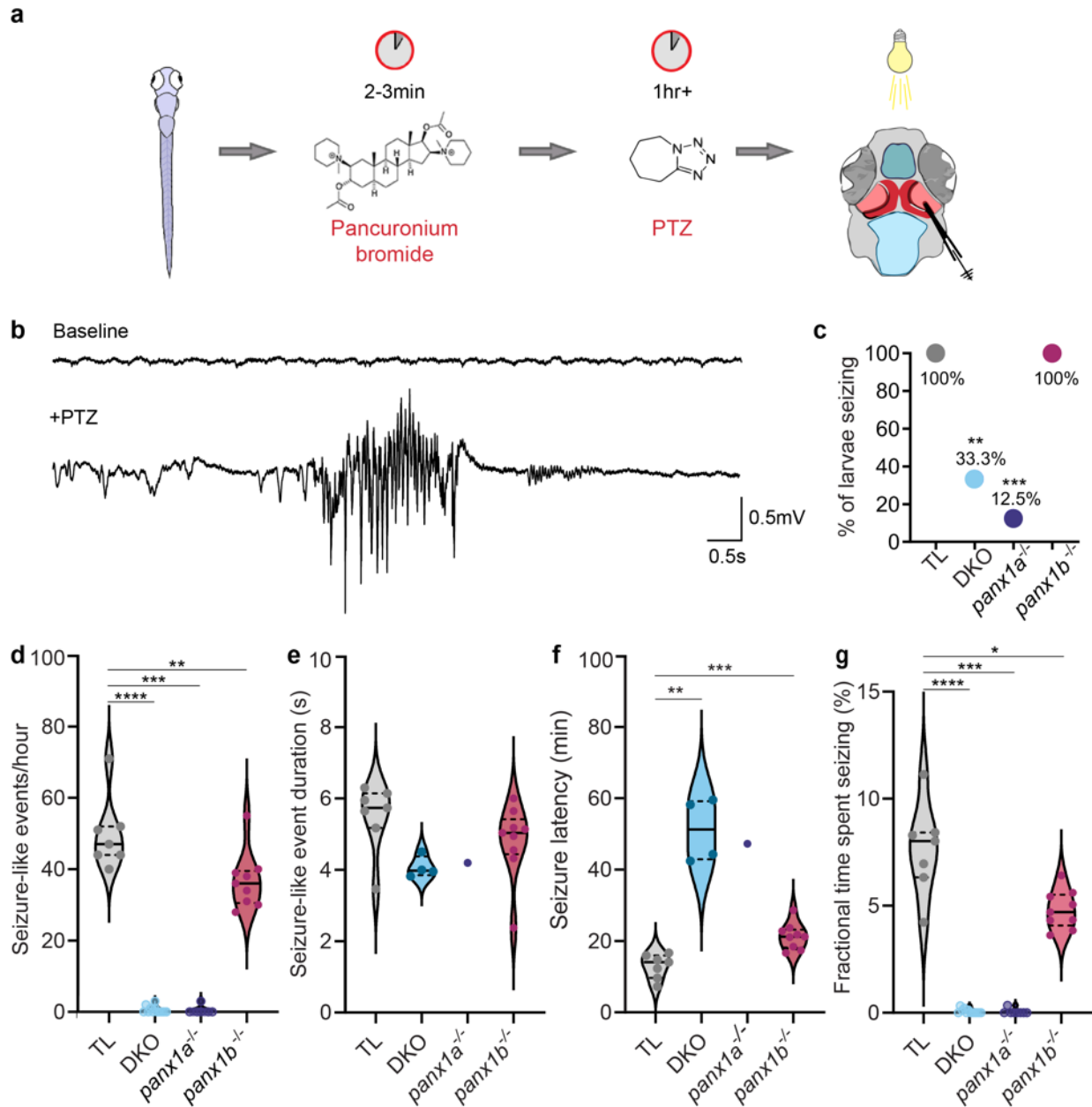


Figure 5.1. *Panx1* knock out larvae showed distinct seizure-like activities *in vivo*. **a** Workflow for recording *in vivo* local field potentials (ivLFP) from the right optic tectum of 7dpf anesthetized larva after 15mM PTZ treatment. **b** Representative recording of baseline activity (top) from TL larvae and a seizure-like event (SLE) sample induced with the addition of PTZ. **c** All TL and *panx1b*^{-/-} larvae had SLEs (TL (grey) n = 7/7; DKO (light blue) n = 4/12; *panx1a*^{-/-} (deep blue) n = 1/8; *panx1b*^{-/-} (magenta) n = 9/9). **d** Quantification of SLEs in the first hour of ivLFP recording revealed that all *panx1* knockout (KO) larvae had a significant reduction in SLEs compared to PTZ treated TL controls, presented as an average number of SLEs/hour \pm s.e.m. **e** The average duration of SLEs (in seconds \pm s.e.m.) for each genotype were not significantly different compared to TLs. Statistical tests were not significant for *panx1a*^{-/-} due to lack of statistical power. **f** All *panx1* knockout larvae had a significant delay in the average onset time (minutes \pm s.e.m.) of the first seizure-like event compared to PTZ treated TL controls. **g** All *panx1* KO larvae spent significantly less time seizing compared to PTZ treated TL controls. Average fractional time spent seizing is presented in percent \pm s.e.m. Scale bars 0.5mV by 0.5s. *p < 0.05, **p < 0.01, ***p < 0.001, ****p < 0.0001.

5.3.2. Loss of *Panx1* caused local network differences in the optic tectum of PTZ treated larvae

The time-frequency domain was examined by visual inspection of ivLFPs combined with an in-house algorithm to automate SLE detection^{28,29}. Representative one-hour traces of electrographic recordings for TL controls, DKO, *panx1a*^{-/-}, and *panx1b*^{-/-} after PTZ application are shown in **Figure 5.2a-d**. The exposure to PTZ elicited discharges characterized by large amplitudes and poly-spiking activities of at least 3 seconds in duration. TL controls and *panx1b*^{-/-} larvae showed typical SLEs (red dotted lines zoom into these regions). Highlighted events near the end of the representative traces for DKO and *panx1a*^{-/-} larvae demonstrated the lack of seizure-like electrographic signatures (blue dotted lines zoom into these regions). LFPs revealed changes in spectral power in the time and frequency domains; visible in expanded views of the ivLFPs and corresponding spectrograms. TL controls (**5.2a**) and *panx1b*^{-/-} (**5.2d**) demonstrated a robust increase in low-frequency power and increased power in high frequencies above 60Hz. The spectrograms for DKO (**5.2b**) and *panx1a*^{-/-} (**5.2c**) were scaled to match TL (**5.2a**) and *panx1b*^{-/-} (**5.2b**) data and revealed frequency power like baseline activity (**Supplementary Figure 5.1**).

Power spectral density was measured to identify tectal network differences. Baseline activities were similar across genotypes ($p = 0.42$ for each comparison). Changes were seen in delta power (highlighted in yellow) after PTZ treatment and quantified by measuring the difference in the area under the power spectrum from 1 – 4Hz (inset bar graphs) (**Figure 5.2 e-h**). PTZ treatment significantly increased delta power for TL (**5.2e**), DKO (**5.2f**), and *panx1b*^{-/-} larvae (**5.2h**). In contrast, delta power for *panx1a*^{-/-} remained at base level (**5.2g**; dark blue bar). Delta power of *panx1a*^{-/-} larvae during PTZ treatment was significantly decreased compared to PTZ treated TL controls (**5.2g**; grey star, $p = 0.0015$). *Panx1b*^{-/-} ($p = 0.99$) and DKO larvae ($p = 0.25$) showed similar delta power during PTZ treatment compared to TL (TL = 0.08 (grey bar), *panx1b*^{-/-} = 0.06 (magenta bar), DKO = 0.05 (light blue bar)).

We concluded that the electrical discharges for both TL controls and *panx1b*^{-/-} larvae were similar in waveform to those previously reported in zebrafish^{22,27}. However, they occurred less frequently in *panx1b*^{-/-} fish and were absent in *panx1a*^{-/-} larvae.

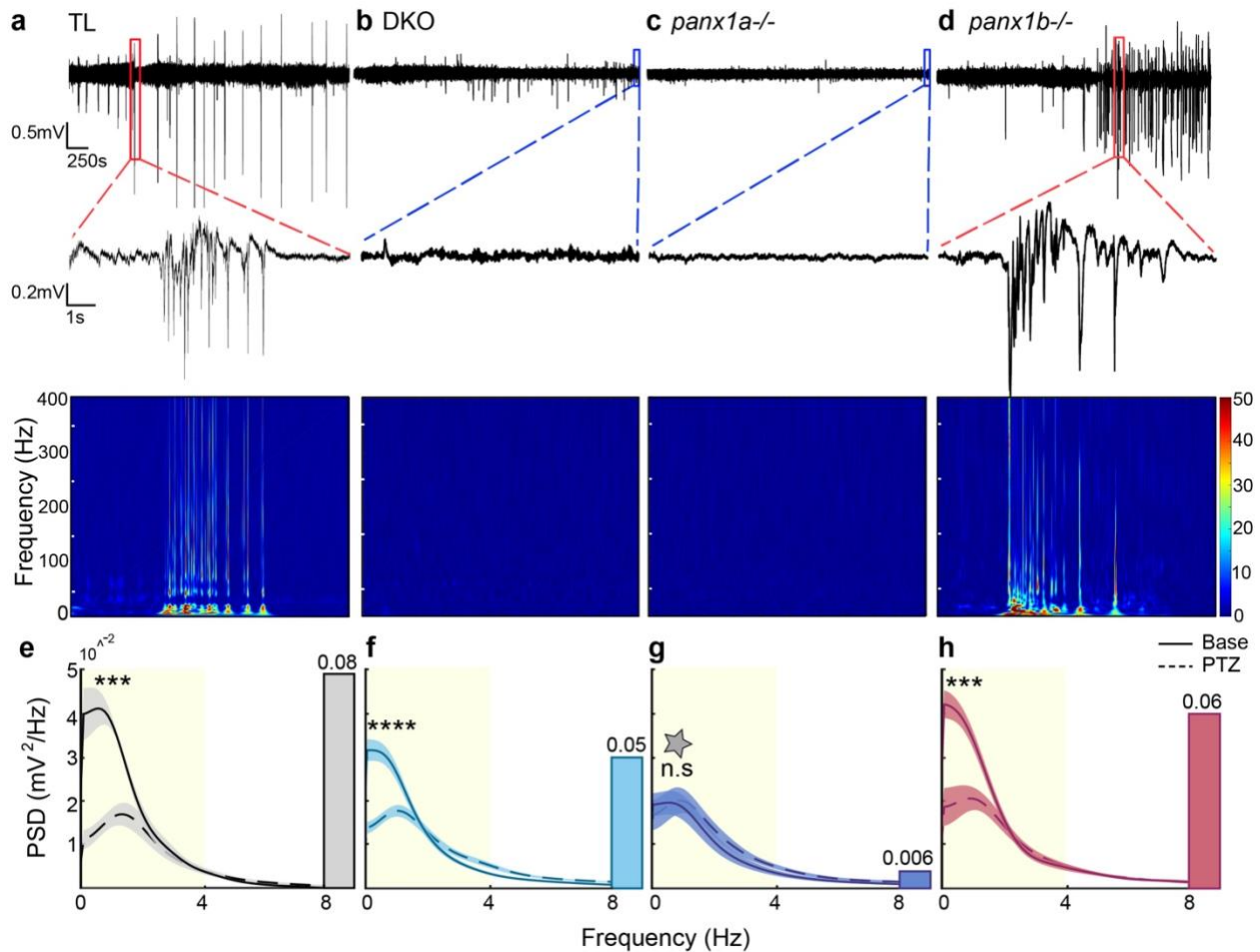


Figure 5.2. Spectral Analysis of LFPs revealed differences in larvae. Representative one-hour long LFP traces with PTZ treatment: a TL b DKO, c *panx1a*^{-/-} and d *panx1b*^{-/-}. TL and *panx1b*^{-/-} traces showed typical seizure-like events. Single events were highlighted by red dotted lines and magnified. Blue dotted lines highlight lack of seizure-like activity in DKO and *panx1a*^{-/-} larvae. Spectrograms below the traces showed increases in low and high frequency power during seizure-like events for TL and *panx1b*^{-/-}. e – h Power spectral density (PSD, mV²/Hz) measured across frequencies revealed no significant differences in baseline (dotted lines) frequencies for all genotypes ($p = 0.42$; e: TL, grey; f: DKO, light blue; g: *panx1a*^{-/-}, dark blue; h: *panx1b*^{-/-}, magenta). The power was significantly increased in the delta band (1-4 Hz) after PTZ treatment (solid line) for all genotypes except *panx1a*^{-/-}. The PSD was plotted as an average across traces with the shaded regions indicating \pm s.e.m. Changes in delta power were quantified from the areas under the curves (AUC) of the power spectrum (in yellow). The changes in AUCs are represented as a bar graphs inserted to the right of the power spectra. TL showed the greatest change in delta, followed by *panx1b*^{-/-}, and DKO. *Panx1a*^{-/-} exhibited insignificant changes and maintained delta power throughout recordings. Scale bars: top = 0.5mV by 250s and bottom = 0.2mV by 1s. * $p < 0.001$, **** $p < 0.0001$, grey star - $p = 0.0015$ compared to TL with PTZ.**

5.3.3. DKO and *panx1a*^{-/-} larvae have reduced interictal-like activity in the optic tectum

Interictal-like epileptiform discharges (ILED) were investigated for genotype-dependent changes in occurrence and waveform. In ivLFP data, ILEDs were defined as events that were shorter than 3 seconds and had amplitudes greater than 1.5 times the baseline activity³⁰. **Figure 5.3a** depicts

typical interictal-like events, with TL (grey line) and *panx1b*^{-/-} (magenta line) appearing most similar. The quantification of ILEDs during a one-hour PTZ application period showed that DKO (119 ± 7.2 events/hour) and *panx1a*^{-/-} (121.4 ± 12.9 events/hour) larvae exhibited interictal-like events. However, their ILEDs occurred significantly less when compared to TL (167.3 ± 9.3 events/hour) and *panx1b*^{-/-} larvae (174.1 ± 11.5 events/hour); both TL and *panx1b*^{-/-} were similar (**Figure 5.3b**).

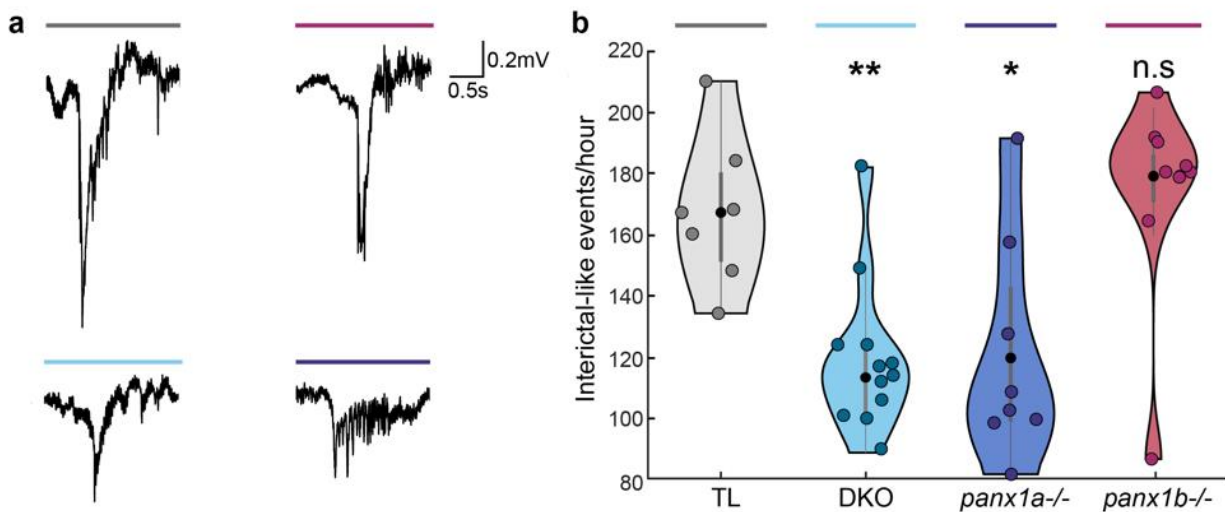


Figure 5.3. Interictal-like activity was decreased in the optic tectum of DKO and *panx1a*^{-/-} larvae. **a** Electrophysiological recordings of PTZ treatment showed interictal-like epileptiform discharges (ILED) in all genotypes; representative ILEDs top: TL (grey line) and *panx1b*^{-/-} (magenta line) shows most similarities and bottom: DKO (light blue line) and *panx1a*^{-/-} (deep blue line). **b** Quantification of ILEDs for the first hour of recording for all genotypes revealed that DKO and *panx1a*^{-/-} had significantly fewer ILEDs. No significant difference was found in the amount of ILEDs for *panx1b*^{-/-} larvae compared to TL. Data presented as an average number of events per hour ± s.e.m. Scale bar: 0.2mV by 0.5s. **p* < 0.05, ***p* < 0.01.

5.3.4. Targeting Panx1 improves PTZ-induced seizure locomotion and molecular responses

Locomotion tracking was used to quantify genotype-specific seizure-related behaviors in response to 15mM PTZ treatment (**Figure 5.4a**). Activity scores (Δ pixel) for locomotor activity were plotted for: rest, baseline, and post-PTZ treatment (**Figure 5.4b**). At the start, addition of fresh E3 medium caused a transient minor activity increase for all larvae (*n* = 36 per genotype), which stabilized at baseline within 30min. PTZ treatment increased locomotor activity significantly in all genotypes. TL larvae showed a continuous activity increase in the first 10 minutes, a peak around 15 to 30min and a gradual decline within the hour. TL and DKO activity curves were statistically similar. The *panx1a*^{-/-} activity curve was significantly reduced compared to TL controls after the

transient peak observed 20min post-PTZ treatment. The *panx1b*^{-/-} larvae exhibited a sharp spike in activity between 10 to 20min, with a steeper decline compared to TL.

PTZ-induced hyperactivity was quantified from the area under the curve (AUC) shown in Figure 4b (**Figure 5.4c**). The baseline AUC was significantly larger in *panx1b*^{-/-} larvae relative to TL in the last 15 minutes of stabilized baseline activity. The AUC post-PTZ treatment, taken over 60min, was greater in *panx1b*^{-/-} and reduced in *panx1a*^{-/-} relative to TL. When the mean baseline activity was extracted from the post-PTZ treatment AUC, only *panx1a*^{-/-} activity was significantly reduced when compared to TL.

Consecutive stages of seizure-like behavior were analyzed next. Stage II, a rapid 'whirlpool-like' circular movement, and stage III, uncontrollable clonus-like twitching of the body followed by a prolonged loss of posture, were scored manually via video recordings of the fish. Stage II and III events were quantified in 2-minute intervals for one hour of PTZ treatment (n = 18 per genotype; **Figure 5.4d**). Stage II onset occurred within a few minutes of treatment and lasted for 30min. TL and *panx1b*^{-/-} entered Stage II first and peaked at ≈10 minutes post-treatment. Stage II activities for DKO and *panx1a*^{-/-} occurred uniformly through-out the first 30min. The onset and total count of stage II locomotion did not significantly differ between genotypes. Stage III convulsive behavior started after 10min of PTZ treatment for all genotypes. Peak stage III activity was observed within 20 to 40min followed by a gradual decline. Stage III events in DKO and *panx1a*^{-/-} were significantly reduced compared to TL controls. The total count of stage III events did not differ between *panx1b*^{-/-} (74.9 ± 5 count/hour) and TL (63.2 ± 5 count/hour; **Figure 5.4e left**). However, the peak activity latency, calculated at the time point with the highest average of stage III activity, was significantly delayed for *panx1b*^{-/-} (34min) compared to TL (26min; **Figure 5.4e middle**). Furthermore, time points at which 50% or more larvae entered stage III, indicated a delayed onset and termination of the stage III in *panx1b*^{-/-} (**Figure 5.4e right**).

Differential expression of Immediate Early Genes (IEGs) was tested after the behavioral assays' experimental endpoint was reached. The IEGs were selected based on previously reported robust activation in a zebrafish PTZ model ²², in the human epileptic neocortex ³¹, and rodent models ^{32,33}. **Figure 5.4f** shows a 100-fold increase in the expression of *fosab* and *egr4* (in red) in PTZ treated TL, which was twice as high compared to the fold change observed in DKO and *panx1b*^{-/-}. DKO and *panx1b*^{-/-} larvae showed a modest upregulation for *fosab*, *egr1*, *egr2b*, *egr4*,

bdnf. In *panx1a*^{-/-} larvae, upregulation of *fosab*, *egr2a*, *egr4*, *bdnf* was moderate, but *egr1*, *egr2b*, and *jun* showed a strong differential upregulation (**Supplementary Table 5.1**).

Kaplan-Meier plots show the larvae survival, which was determined by monitoring blood circulation and heartbeat post-PTZ treatment for ten consecutive hours and again at 24 hours (n = 80 per genotype; **Figure 5.4g**). Although the *panx1a*^{-/-} group displayed a decline between 5 to 10 hours, they had the highest survival rate of 30% at 24 hours. The *panx1b*^{-/-} group's survival rate was stable for the first 10 hours and declined to 13% after 24 hours. The low DKO and TL's survival rate at 24 hours was statistically similar.

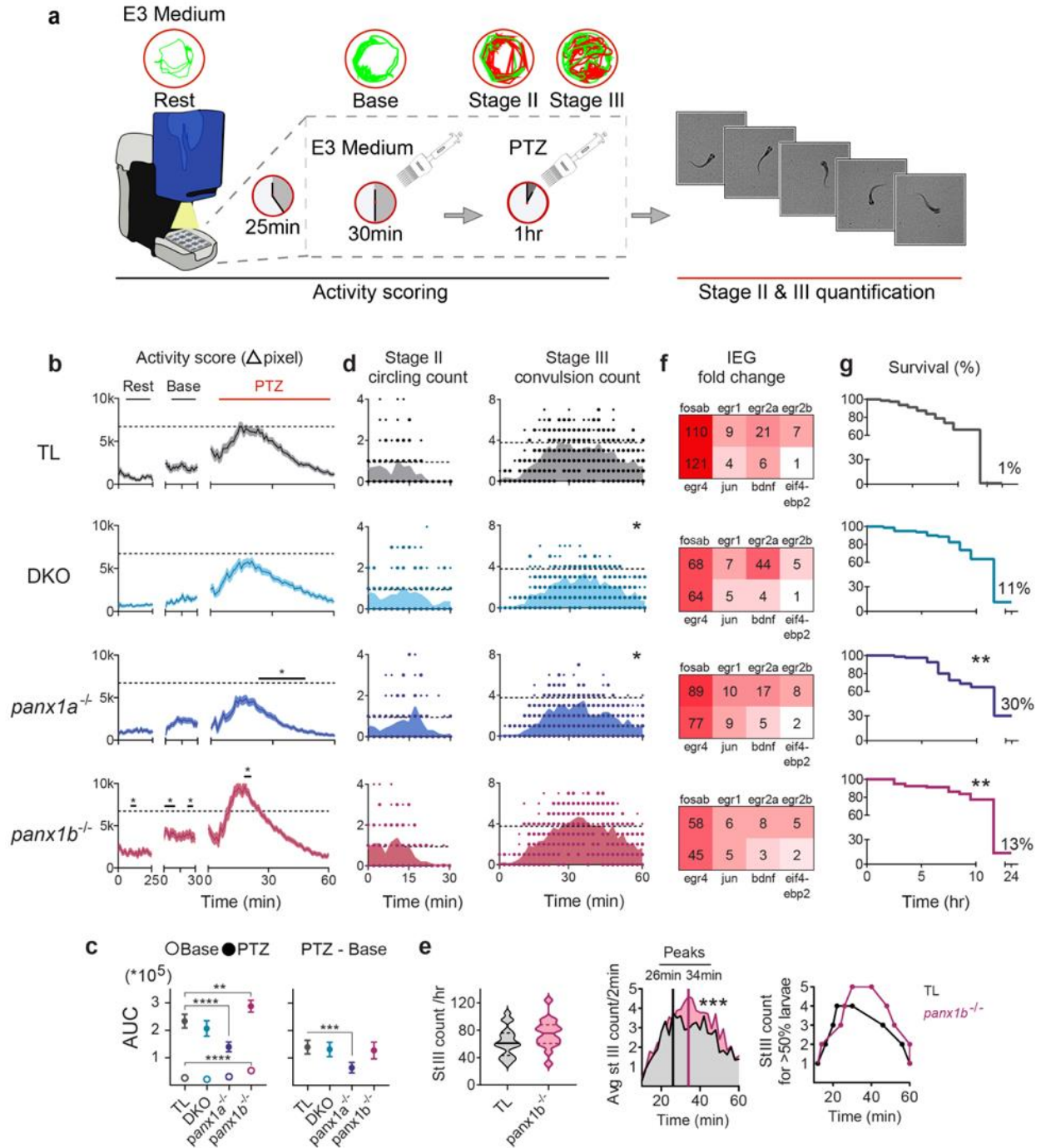


Figure 5.4. Behavioural and molecular outcomes of genetically targeting *panx1*. **a** Methodological workflow of behavioral assays in TL and *panx1* knockout larvae. **b** Larvae's ($n = 36$) baseline and 15mM PTZ-induced activity (Δ pixel \pm s.e.m.) were scored. *Panx1b*^{-/-} baseline activity was higher than TL. PTZ induced hyperactivity peaked at 15-30 minutes for TL (grey, top), was reduced in DKO (blue, second), significantly reduced in *panx1a*^{-/-} (blue, third) for the last 40 minutes, and significantly increased in *panx1b*^{-/-} larvae (red, bottom) around 20min compared to TL. Dashed lines indicate TL's max average activity score. **c** Left: AUC derived from the activity plots in **b** significantly differed between TL and *panx1b*^{-/-} baselines (open points). AUC derived from one-hour post-PTZ treatment was significantly reduced for *panx1a*^{-/-} and increased for *panx1b*^{-/-} (filled points). Right: Change in PTZ treatment from average baseline activity was significantly reduced in *panx1a*^{-/-} compared to TL. **d** Stage

II count (rapid circling) did not differ among groups (n = 18; count/2min). Stage III (convulsion) was significantly reduced in DKO and *panx1a*^{-/-} compared to TL. Dashed lines represent max average stage II and stage III counts for TL. e Left: Total stage III count between TL and *panx1b*^{-/-} did not significantly differ. Middle: Time course of average stage III counts significantly differed between the two groups, peaking at 26min post-PTZ treatment for TL and 34min for *panx1b*^{-/-}. Right: Time course where >50% of the larvae reached 1-5 stage III counts revealed a delayed peak onset for *panx1b*^{-/-}. f IEG upregulation after one-hour PTZ treatment, represented as fold-change for PTZ treated larvae against non-treated controls. *Panx1* knockout larvae had reduced upregulation of the IEGs compared to TL, with DKO and *panx1b*^{-/-} showing the greatest reduction. g Survival rate of larvae (n = 80) post PTZ treatment was significantly higher for *panx1a*^{-/-} followed by *panx1b*^{-/-}, and survival rate of DKOs did not differ from TL. Survival at 24 hours: TL: 1.25%, DKO: 11%, *panx1a*^{-/-}: 30%, *panx1b*^{-/-}: 13%. *p < 0.05, **p < 0.01, ***p < 0.001, ****p < 0.0001.

5.3.5. Acute pharmacological blocking of *Panx1* suppresses seizure-like activities

Pharmacological blocking with Probenecid (Pb), a well-established Panx1 channel blocker³⁴, was used to determine acute changes to electrophysiological discharges, behavioral and molecular outcomes in the presence of PTZ. Valproic acid (VPA), a common anti-convulsant, was applied as a control for the suppression of SLEs³⁵. Electrodes were placed in the right optic tectum. All TL larvae were treated with Pb (75μM) or VPA (5mM) for 10min prior to PTZ application (**Figure 5.5a**). For the duration of PTZ treatment, ivLFPs were monitored and confirmed SLE suppression in all Pb (n = 7) and VPA (n = 7) treated larvae (**Figure 5.5b**). Sample recordings from larvae treated with PTZ and Pb (**Figure 5.5c**) or VPA (**Figure 5.5d**) showed no SLEs. Traces from timepoints near the experimental endpoint were depicted at higher resolution to show the larger deflections that occurred. The spectral analysis of these deflections revealed that no increase in high frequency power was associated with this type of activity. To confirm that Pb was not suppressing SLEs due to toxicity, ivLFPs were recorded from larvae exposed to Pb or VPA without PTZ and compared to larvae with no drug treatments. Electrographic activity was comparable amongst these groups (**Figure 5.5e**, **Supplementary Figure 5.2**).

Locomotor activity was monitored for TL larvae treated with either 75μM Pb (n = 36) or 5mM VPA (n = 60) and compared to untreated controls (**Figure 5.5f**). Pb application alone induced a brief, but sharp, increase in larvae activity that returned to baseline within 30min (**Figure 5.5f middle**). VPA treatment caused reduced activity, which decreased below baseline after 10min (**Figure 5.5f bottom**). After a 30min baseline recording, all larvae were treated with PTZ for 60min. Pb treated larvae had an early onset of spiking activity within the first 10min after PTZ treatment, ahead of larvae treated with PTZ only. Pb treated PTZ-induced activity subsided within 30min and returned to baseline, significantly faster than PTZ only treated larvae. VPA treatment significantly reduced PTZ-induced activity, with a similar timeline and curve profile to the PTZ-only group. AUC analysis on activity plots in **Figure 5.5f** showed that baseline AUC did not

significantly differ between no treatment and Pb treated larvae in the last 15min of stabilized activity (**Figure 5.5g**). Post-PTZ treatment AUC, with or without extracted baseline activity, was larger in the PTZ-only treated group compared to the Pb-PTZ treated group. The analysis of seizure-related Stages II and III of Pb treated larvae (n = 18) every 2min for a duration of 60min (**Figure 5.5h**) showed that Stage II activity was significantly reduced compared to PTZ-only treated larvae, with most of the activity occurring in the first 10min. Stage III activity of Pb treated larvae displayed an immediate onset compared to the PTZ-only group and was significantly reduced after 20min of PTZ treatment. The differential expression of IEGs after Pb treatment was consistent with the changes observed in gene-edited larvae; IEG expression was reduced after Pb treatment when compared to the PTZ only treated group (**Figure 5.5i**). Pb treated TL larvae exhibited IEG expression like DKO, where all IEGs exhibited less upregulation, except for *egr2a*. *Fosab*'s upregulation was reduced by 2-fold and *jun* had no significant upregulation with Pb treatment (**Supplementary Table 5.2**).

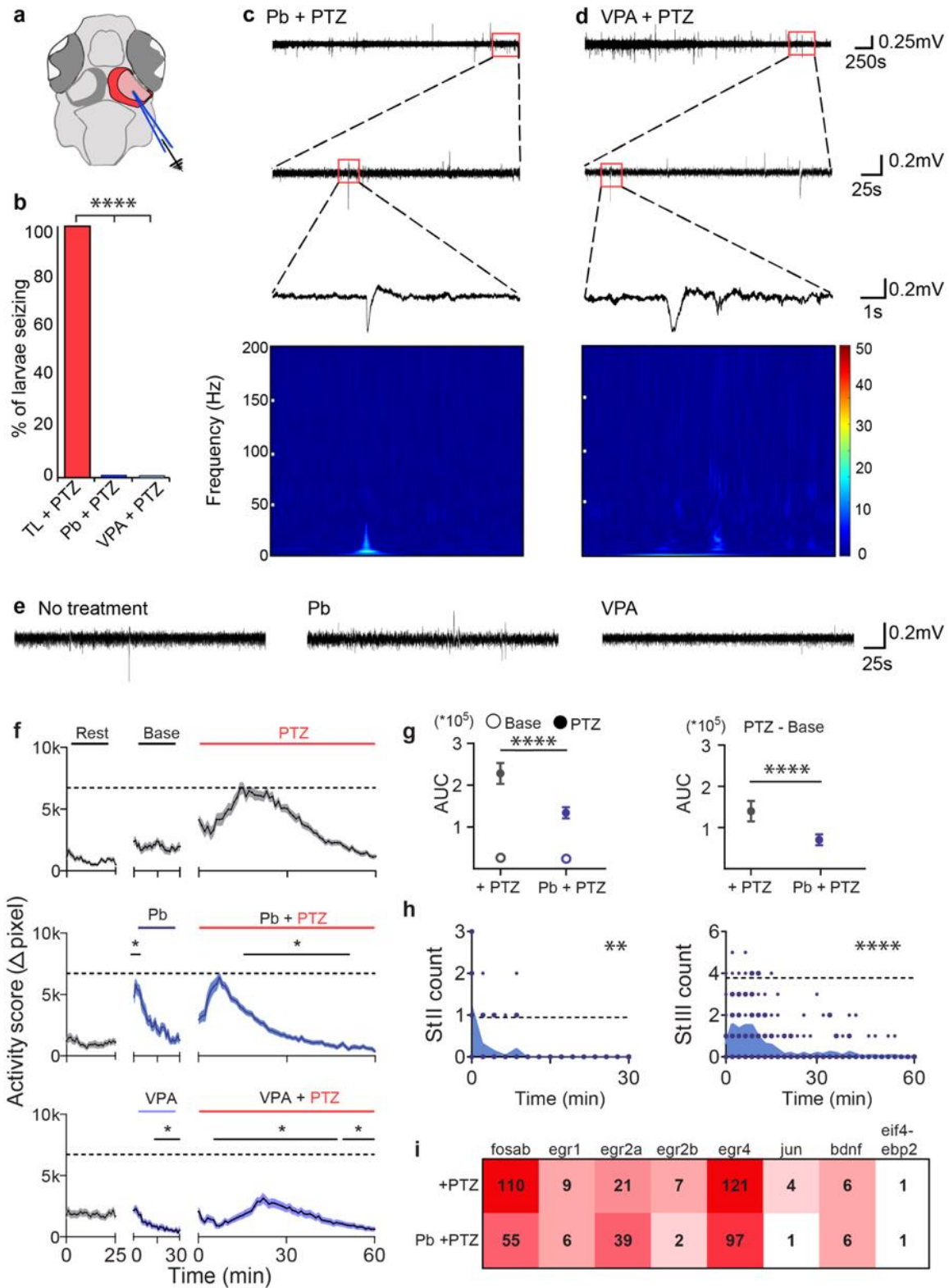


Figure 5.5. Acute blocking of Panx1 with Pb is effective for preventing seizure-like activity. **a** Schematic highlighting the region that LFPs were recorded from. **b** Larvae treated with 75 μ M Pb ($n = 7$) or 5mM VPA ($n = 7$) have no PTZ inducible SLEs compared to 100% of TL larvae ($n = 7$). Representative traces of larvae treated with **c** Pb and **d** VPA treated with PTZ for 60min. Expanded views into the last 5min

of traces showed lack of SLEs. Spectrograms corresponding to small spikes in traces above demonstrate no increase in high frequency power associated with these events. e LFPs of the last 5min of 60min traces revealed no drug induced changes to baseline activity. Left: larvae with no treatment; middle: Pb treatment only; Right: VPA treatment only. f Baseline activity (Δ pixel \pm s.e.m.; n = 36) increased with Pb treatment for the first 5min. PTZ-induced hyperactivity subsided significantly within 15min, sooner than the PTZ only group. VPA treatment (n = 60) decreased baseline and PTZ-induced activity, with a hyperactivity curve like the PTZ only group. Dashed lines indicate max average activity for PTZ only group. g AUCs for baseline activity and Pb treatment did not differ (left, open points). Pb treatment significantly reduced the effect of PTZ without (left, filled points) and with (right) extracted baseline activity. h Stage II and III counts (n = 18; count/2min) were significantly reduced with Pb treatment, majority occurring in the first 10min of treatment. Dashed lines represent max average Stage II and Stage III counts for PTZ-only group. i IEG upregulation was reduced in Pb treated TL larvae except for *egr2a*. Scale bars: Top = 0.25mV by 250s, middle = 0.2mV by 25s, bottom = 0.2mV by 1s, e = 0.2mV by 25s. *p < 0.05, **p < 0.01, ***p < 0.001, ****p < 0.0001.

5.3.6. Seizure phenotypes are linked to transcriptome changes

RNA-seq data representing the transcriptomes of untreated 6dpf larvae^{24,36} were analyzed next. Venn diagrams highlighted considerable differences in the number and regulation of genes when the FishEnrichR database^{37,38} was data-mined for biological processes enriched in the nervous system (**Supplementary Figure 5.3**). The GO biological process categories selected for further analysis represented broad themes based on known (signal transduction, cell death, transport) or anticipated (metabolism, cellular respiration) roles of *Panx1* channels (**Figure 5.6a**, **Supplementary Table 5.3**).

All genotypes shared enrichment of the significant categories, *transport* (GO:0006810) and *signal transduction* (GO:0007165). The lack of enrichment of *cellular respiration* (GO:0045333) in *panx1b*^{-/-} larvae suggested that mitochondrial energy metabolism processes and response to reactive oxygen species were less controlled after losing *panx1b*. Further, *panx1b*^{-/-} larvae stood out for lacking enrichment of *cell death-associated processes* (GO:0008219). The opposite enrichment of the same categories in *panx1a*^{-/-} larvae repeated the pattern of electrographic and behavioral activities. DKO larvae displayed a mixed phenotype, lacking a downregulated metabolism (GO:0008152).

Cluster analysis was performed to link coordinated expression changes with *Panx1* genotypes (**Figure 5.6b**). Genes for cluster analysis were manually curated based on assumptions made from the enriched biological processes (**Supplementary Table 5.4**). Genotype-specific transport and metabolic properties corroborated the pattern of shared and distinct roles of zebrafish *panx1* ohnologs. *Panx1a*^{-/-} and *panx1b*^{-/-} larvae had the opposite coordination of gene expression changes in subcategories of metabolism; mitochondrial ATP production and oxidative phosphorylation processes. However, the coordinated expression was strengthened for genes

encoding proteins that release or degrade ATP in *panx1a*^{-/-} and *panx1b*^{-/-} larvae. Interestingly, transport genes showed similar enhanced coordination in both genotypes consistent with roles of both channel proteins in cell signaling. However, coordinated expression of the solute carrier (SLC) group of membrane transport proteins involved in signal transduction pathways showed more significant variation between genotypes consistent with the GO ontology enrichment analysis; overall, DKO larvae had a less coordinated expression in these categories.

A direct comparison of *panx1a*^{-/-} and *panx1b*^{-/-} larvae corroborated the significant downregulation of *panx1a* and *p2rx7* expression as a major difference between the two genotypes (**Figure 5.6c**). Interestingly, the *slc2a1a* was downregulated in *panx1a*^{-/-} larvae. In Mammalia this glucose transporter is in the blood-brain barrier. Pathogenic SLC2A1 variants are associated with epilepsy³⁹. In *panx1b*^{-/-} larvae, SLC proteins with molecular functions in Na⁺/Ca²⁺ transmembrane transport (*slc8a1b*), or as pyrimidine nucleotide transmembrane transporters (*slc25a36a*) were upregulated, while regulation of sodium dependent amino acid transporters (*slc1a5*), mitochondrial ADP/ATP antiporters (*slc25a4*), or transport across the inner membrane of mitochondria (*slc25a40*), was reduced. Although the exact function of the upregulated *slc3a2b* in the zebrafish is unknown, in humans, heterodimers of SLC3A2 with the large neutral amino acid transporter (LAT1) function as sodium-independent, high-affinity transporters that mediate uptake of large neutral amino acids such as phenylalanine, tyrosine, L-DOPA, leucine, histidine, methionine, and tryptophan. Although the analysis presented only a snapshot of relevant molecular signatures, we concluded that the differences in prominent biological processes primed each genotype differently for the treatment with PTZ.

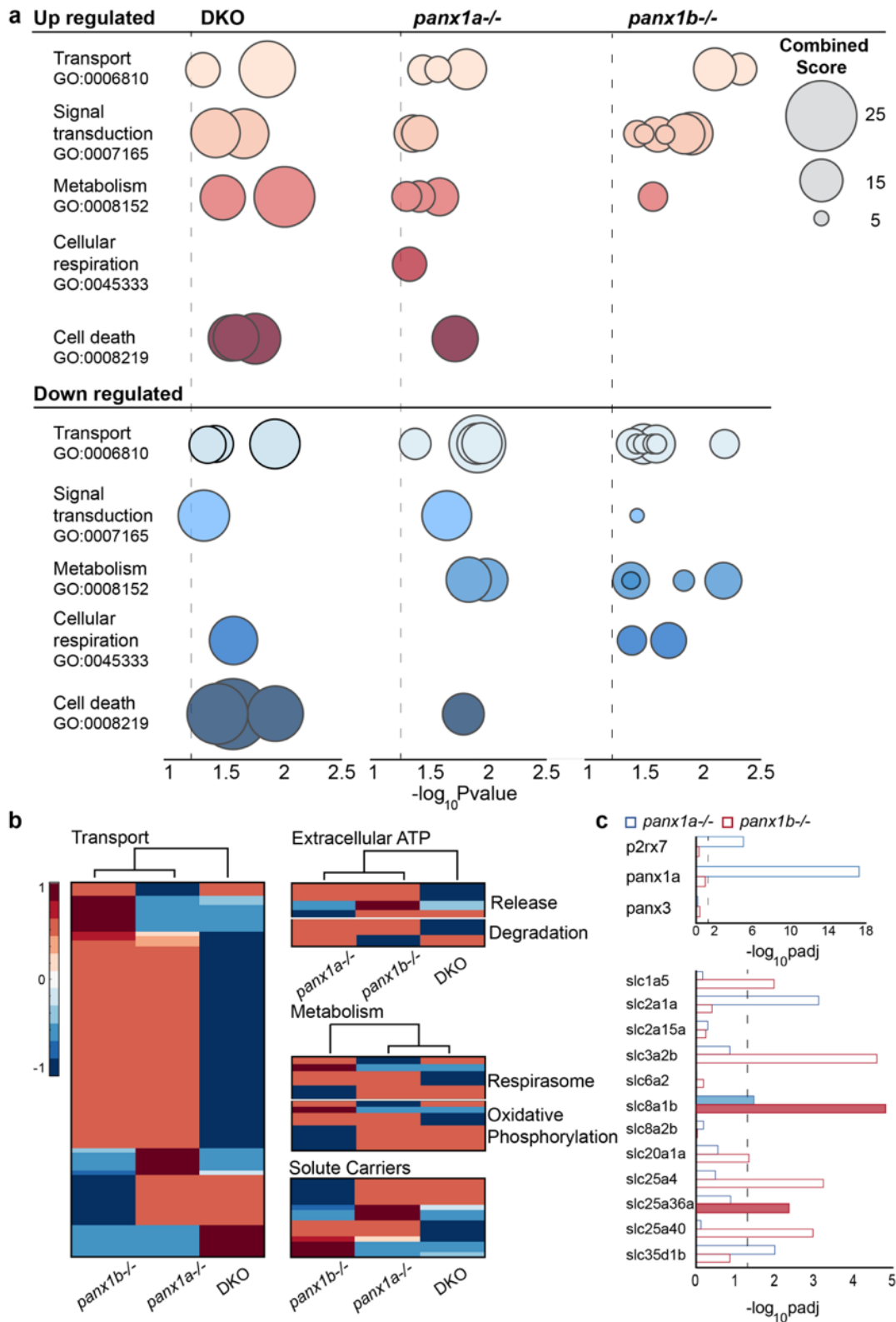


Figure 5.6. Loss of *Panx1a* affects biological processes related to metabolism and transport. a Gene ontology enrichment of biological processes for differentially regulated genes from RNA-seq data of DKO (left), *panx1a*^{-/-} (middle) and *panx1b*^{-/-} (right) found using the FishEnrichR database. Biological processes were grouped into

5 categories; transport (GO:0006810), signal transduction (GO:0007165), metabolism (GO:0008152), cellular respiration (GO:0045333) and cell death (GO:0008219). Data is presented as $-\log p$ -value based upon the fisher exact test and dot size represents the combined score for genes associated with that pathway. Dotted grey lines indicate p -value = 0.05. b Candidate genes were selected and RNA-seq data was mined for differential regulation in *panx1* fish lines. Clustergrams compare *panx1* knockout larvae for correlation amongst chosen genes for (1) transport, (2) extracellular ATP (release & degradation), (3) metabolism (respirasome & oxidative phosphorylation) and (4) solute carriers. Scale shows correlation: red is positive, and blue is negative. Hierarchical cluster branches are shown above each clustergram and labelled below. c Expression (logpadj) of genes part of the ATP release (top) and solute carrier (bottom) clustergrams for *panx1a*^{-/-} (blue) and *panx1b*^{-/-} (top). Filled bars indicate upregulated genes, empty bars are downregulated. p -value = 0.05 indicated with dotted line.

5.3.7. Evidence for an ATP-dependent mechanism contributing to seizure-like activity

Changes to ATP release and differential expression of biomarkers in response to PTZ conditions were quantified as shown in **Figure 5.7a**. Extracellular ATP concentrations [ATP]_{ex} were normalized to TL controls (grey bars) with and without PTZ treatment (baseline). Baseline [ATP]_{ex} (blue bars) was significantly reduced for *panx1a*^{-/-} and Pb-treated TL larvae (**Figure 5.7b**). PTZ treatment (red bars) did not change [ATP]_{ex} for *panx1a*^{-/-} and Pb-treated TL larvae, which was consistent with reduced seizure-like activities. In DKO and *panx1b*^{-/-} larvae, [ATP]_{ex} was significantly elevated overall compared to TL controls and was substantially altered by PTZ treatment. Our results suggested that the propensity of developing SLEs was correlated with regulation of energy metabolism and the availability of extracellular ATP.

Reduced SLEs in gene edited DKOs and pharmacological blocked TL were not simply correlated with low [ATP]_{ex}. This unexpected difference was corroborated by the differential expression of selected biomarkers for signal transduction and transport (**Figure 5.7c**, **Supplementary Table 5.5**). Pb treated TL larvae showed an upregulation of voltage sensitive potassium channels required for rapid repolarization of fast-firing brain neurons (*kcnc3a*), Ca²⁺/Na⁺ antiporters (*slc8a1b* & *slc8a2b*) and NMDA receptors involved in excitatory postsynaptic potentials (*grin2bb*). DKOs had a significant downregulation of *slc8a2b*, which is an important Ca²⁺/Na⁺ antiporter found in axons and at the post synapse that plays a large role in Ca²⁺ and Na⁺ signaling and cell communication. Furthermore, PTZ treatment did not highlight a significant impact on the expression of genes associated with extracellular ATP processing, signal transduction or transport. The regulation of *entpd1*, which encodes for the rate-limiting ATP/ADP-hydrolyzing ectoenzyme CD39 appeared notable, but the expression of *p2rx7*, *p2ry12*, *nt5e*, or *adora1b* were similar in DKOs and Pb-treated TL. The results advocate for an important role of *panx1a* in ATP metabolism and signaling causing genotype-specific outcomes of seizure dynamics and allude to alternative mechanisms for acute versus chronic *panx1* targeting.

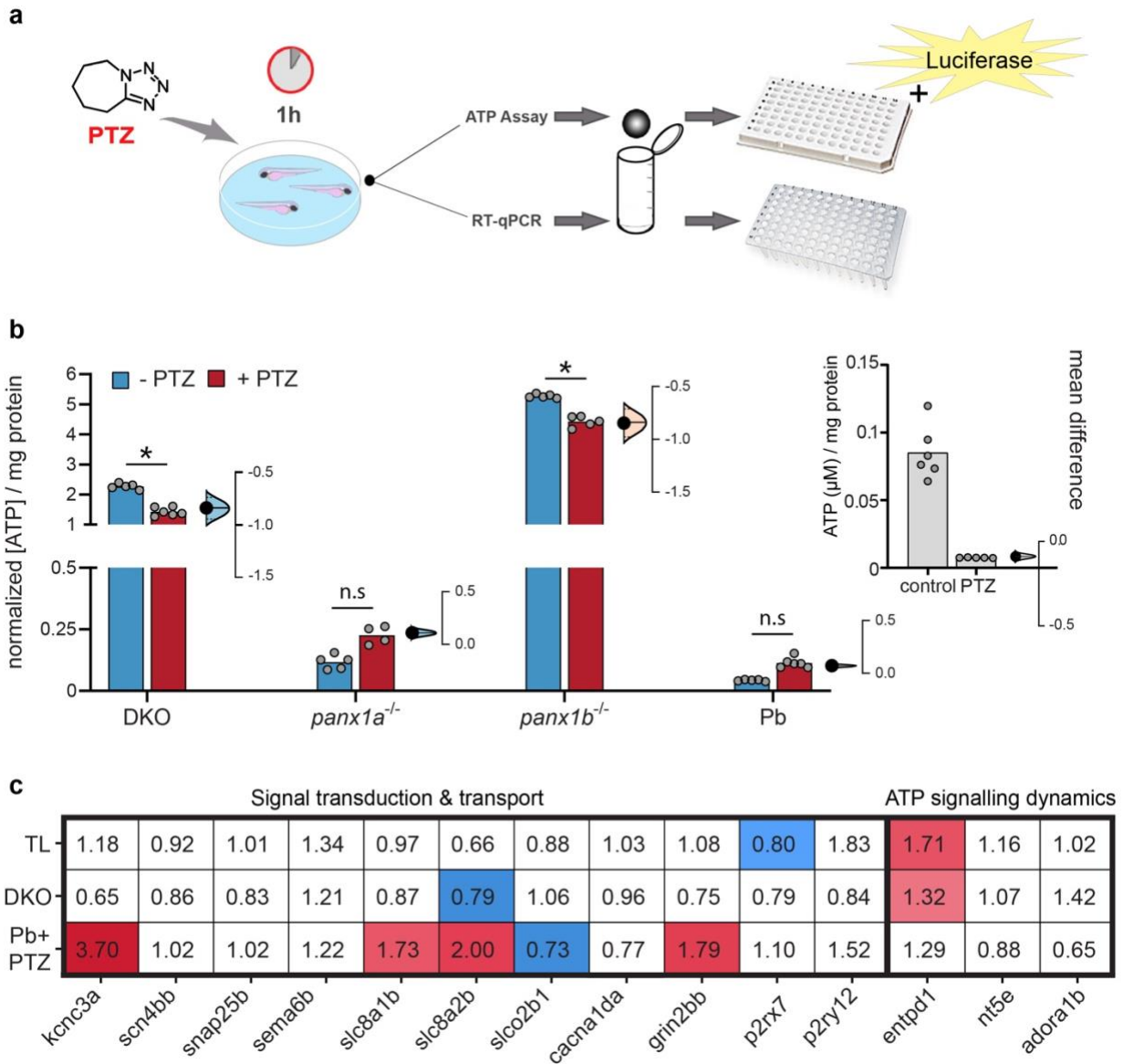


Figure 5.7. Extracellular ATP is associated with propensity for seizure-like activity. **a** Workflow diagram outlining the 1hr PTZ incubation for treated larvae. Larvae were collected for either RT-qPCR (n=30 larvae/sample) or ATP assays (n=50 larvae/sample), followed by homogenization prior to samples being plated in 96well format for measurement. Note for ATP detection, luciferase was used. **b** Estimation plots of extracellular ATP concentrations (μM) with respect to larval protein content (mg/ml) and normalized to the respective TL control. $[\text{ATP}]_{\text{ex}}$ for TL controls are shown on the right (b), showing a significant decrease in ATP with PTZ treatment. Baseline ATP values are depicted by the blue bars, PTZ treatment is in red, individual data points are displayed in grey to show data distribution. Difference of means are shown to the right of each group, with a 95% confidence interval to show effect size and significance. DKO (Δ mean = -0.84) and *panx1b*^{-/-} (Δ mean = -0.84) show a significant decrease in ATP with PTZ treatment. *Panx1a*^{-/-} (Δ mean = 0.1) and TL larvae with Pb (Δ mean = 0.07) show very low ATP concentrations, however, do show a slight increase in ATP with PTZ treatment that is not significant. *Panx1b*^{-/-} have the highest presence of ATP. **c** RT-qPCR of selected genes grouped into signal transduction and transport, or ATP signaling dynamic categories, showing significant up (red) or down (blue) regulation, with respect to non-treated controls, in response to PTZ treatment for TL, DKO and TLs treated with Pb. *p < 0.0001.

5.3.8. P2rx7 affects seizure-like activities but does not supersede *Panx1a*

The impact of P2rx7 on seizure activity in the presence of both *panx1* genes was tested in TL larvae. The treatment with A-438079 hydrochloride hydrate (100 μ M A43; n = 46) started 30min before PTZ application and did not alter the larvae's activity alone. PTZ-induced hyperactivity was reduced in A43 treated TL larvae compared to the activity induced in PTZ treated TLs (grey dotted line; n = 36) (**Figure 5.8a**). The AUC analysis corroborated that treatment with both A43 and PTZ significantly reduced the AUC when compared to PTZ treated larvae, with and without extracted baseline activity (**Figure 5.8b**). A43 treatment also significantly reduced Stage III counts (n = 18; **Figure 5.8c**), without influencing the onset and peak activity of stages II and III in the test period.

To isolate a potential role of *panx1a* in seizure-like activity, *panx1b*^{-/-} larvae which express *panx1a* and *p2rx7* mRNA were treated with A43 (n = 46). The A43 treatment alone did not affect the baseline locomotor activity in *panx1b*^{-/-} larvae. However, PTZ-induced activity was significantly reduced after 20min compared to activity in larvae treated with only PTZ (magenta dotted line; n = 31) (**Figure 5.8d**). The AUC analysis confirmed that A43 treated *panx1b*^{-/-} larvae had a reduced AUC compared to the PTZ treated, with and without extracted baseline activity (**Figure 5.8e**). A43 treatment also reduced Stage II and III event counts significantly (n = 18; **Figure 5.8f**). Our results demonstrated that the pharmacological targeting of P2rx7 in both TL and *panx1b*^{-/-} larvae improved outcomes of PTZ induced seizure-like swimming behavior. Furthermore, we concluded that *panx1a* appears to play a predominant role in seizure-like activity.

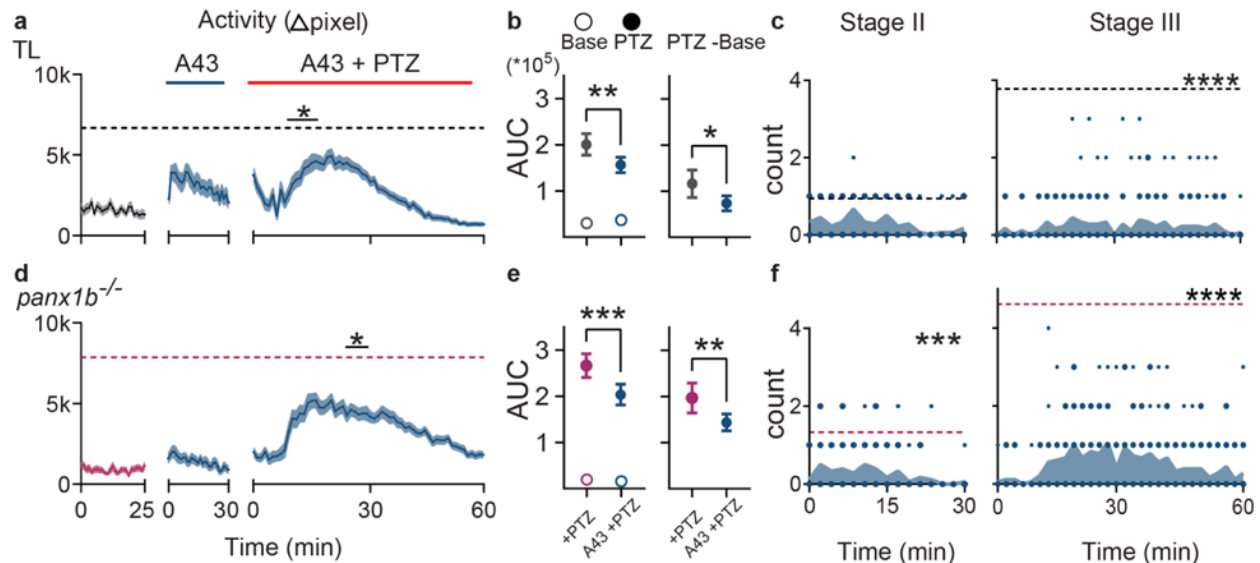


Figure 5.8. Blocking of *p2rx7* with A-438079 improves seizure-like behavior. a 100 μ M A-438079 (A43) treatment decreased hyperactivity in TL in the first 10min of PTZ treatment (Δ pixel \pm s.e.m.; n = 46). Dashed grey line indicates TL's max average activity score treated with only PTZ (n = 36). b AUCs for TL's baseline activity and A43 treatment did not differ (left, open points). A43 treatment significantly reduced the effect of PTZ without (left, filled points) and with (right) extracted baseline activity. c Stage III count (count/2min) was significantly reduced with A43 treatment in TL (n = 18). Dashed lines represent max average Stage II and Stage III counts for TL's PTZ-only group. d A43 treatment decreased PTZ-induced hyperactivity in *panx1b*^{-/-} (n = 46). Dashed magenta line indicates *panx1b*^{-/-}'s max average activity in the PTZ only group (n = 31). e A43 treatment significantly reduced the effect of PTZ in *panx1b*^{-/-} without (left, filled points) and with (right) extracted baseline activity. f Stage II and III counts were significantly reduced with A43 treatment in *panx1b*^{-/-} (n = 18). Dashed lines represent max average Stage II and Stage III counts for *panx1b*^{-/-}'s PTZ-only group. *p < 0.05, **p < 0.01, ***p < 0.001, ****p < 0.0001.

5.3.9. Molecular modeling of fish and human pannexins

High resolution cryo-EM structural studies of human and frog pannexins have provided an invaluable framework towards understanding the function of these channels⁴⁰⁻⁴³. One unanticipated outcome of this work was that pannexins form heptameric channels in contrast to the hexameric organization observed for connexins gap junctions and the octameric organization observed for innexin gap junctions. In each of the four pannexin structural studies, a carboxy-terminal region with known regulatory activity was not observed and thus, its structure-function relationship could not be determined. Furthermore, many mechanistic questions remain with respect to gating and selection of ions despite having a high-resolution view of the channel.

A sequence alignment, shown in **Figure 5.9a**, served a starting point for a structural comparison between human PANX1 and the two zebrafish pannexins. A high degree of sequence identity is evident, especially throughout the amino acids that line the channel (**Figure 5.9b**). Two

pairs of disulfide bonded cysteines in an extracellular facing domain of the channel are conserved in accordance with their established role in channel function ⁴⁴.

The pannexin channel has three gates each corresponding to a point of restriction (**Table 5.1**). Among these gates, a sequence comparison of zebrafish Panx1a and Panx1b with human PANX1 revealed that the first and most narrow gate had enough sequence diversity to be explored further by molecular modeling. In human PANX1, the extracellular gate is described by W74 and R75. The guanidino group of R75 is positioned to support a favorable cation- π interaction with the indole ring of W74 and an ionic bond with D81. Either or both interactions may be important for the function of the gate.

To produce models of the zebrafish Panx1a and Panx1b gates, the backbone of human PANX1 structure (PDB: 6LTO) was fixed in place, substitutions were made, and the side chains repacked. Before this was done, a control for the modeling study was performed by repacking the W74 and R75 side chains of human PANX1 according to the same protocol used to model the zebrafish Panx1a and Panx1b extracellular gates. The rotamer sampling method favored a wider gate due to an edge-to-edge packing of the indole ring of W74 (**Figure 5.9c**) versus a staggered packing observed in the original cryo-EM structure increasing the diameter of the gate from 8.1 to 10.9 Å. While the biological significance of these observed and modeled conformations are unknown, it demonstrates that side chain motions may limit the size of the extracellular facing gate in the absence of backbone conformational changes.

In zebrafish Panx1a, a cysteine (C75) replaces an arginine found in both human PANX1 and zebrafish Panx1b (**Figure 5.9d**). While the loss of a positive charge and a nearby ionic bond could affect anion selection at this gate, a cysteine is still poised to support hydrophobic interactions with W74. In zebrafish Panx1b, methionine (M74) substitutes for tryptophan and the adjacent arginine (R75) is preserved. The modeled diameter of M74 was determined to 8.3Å, comparable to W74 in the staggered conformation. To explain the reduced ATP transit that we have observed during our physiological experiments for Panx1b, we speculate that a methionine substitution may sample different conformations that either favor the closed state of the gate or simply create a gate that is smaller and thereby less permeable to ATP.

A W74A substitution is associated with increased channel activity, increased ATP release and a higher positive holding potential ⁴³. When we modeled an A74 variant of human PANX1, the diameter of Gate 1 was 11.2 Å (**Figure 5.9e**). The distance is comparable to the 10.9 Å

observed in wild type PANX1 protein when the indole ring of W74 is in its most open edge-to-edge conformation. If the A74 variant extracellular facing gate is incapable of closing like the wild type protein, we question whether that is sufficient to explain the functional differences, or if there is an alternate ATP-permeable state that the A74 variant is incapable of forming. Towards answering this question, other amino acid substitutions at position 74 may be required.

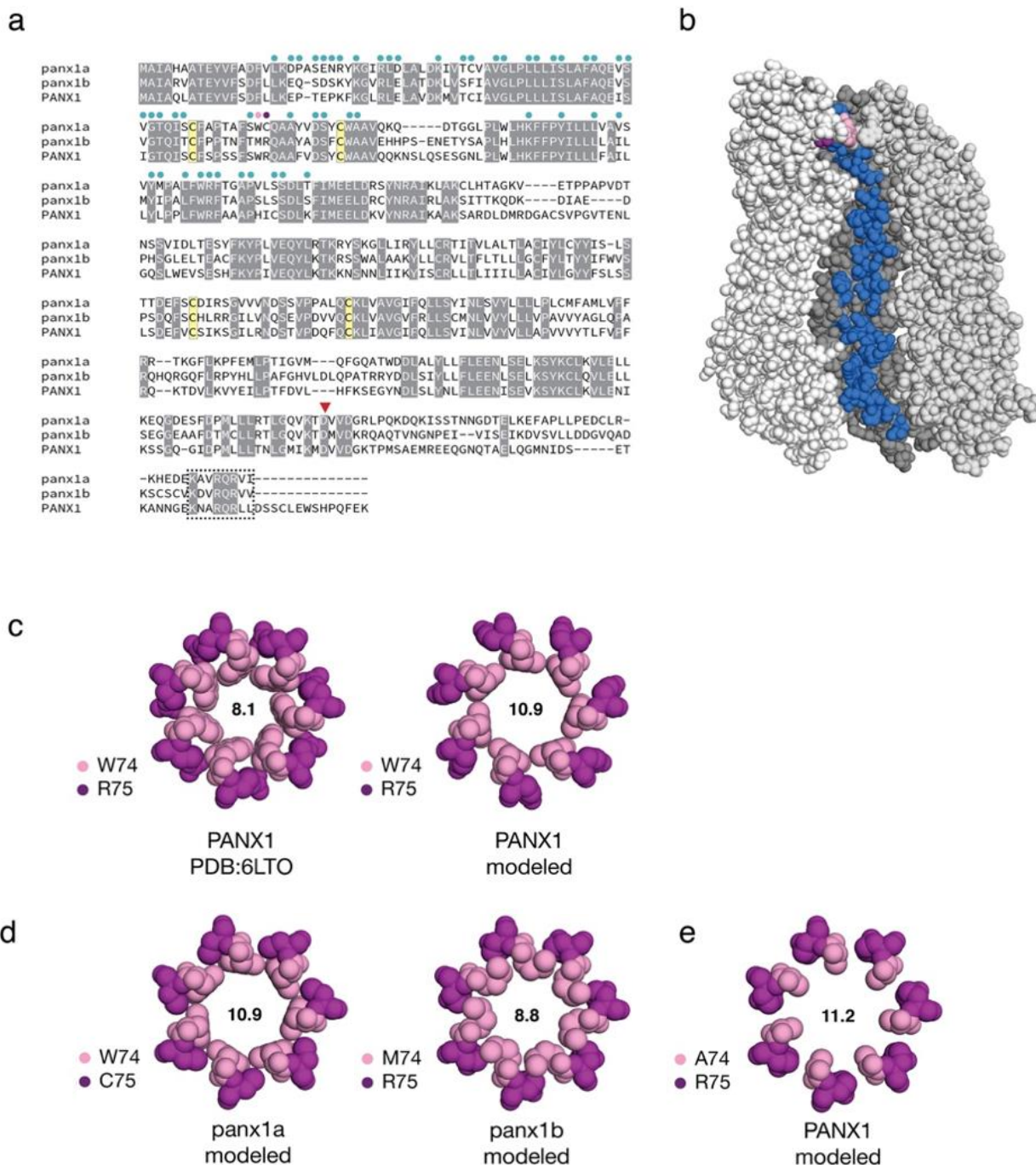


Figure 5.9. Sequence and structural attributes of the zebrafish pannexins. **a** Sequence alignment of human pannexin (PANX1) and zebrafish *panx1a/panx1b*. Amino acids that line the channel are indicated by circles above the sequence alignment. Two amino acids at positions 74 and 75 form an extracellular gate (in pink and purple, respectively). Four cysteines (in yellow) contribute two functionally important disulfide bonds. A caspase cleavage site is denoted by a red triangle. A box indicates a conserved carboxy-terminal segment of unknown significance. **b** Amino acids that line the inside of the channel are shown on one monomer of heptameric human PANX1 (PDB: 6LTO). The channel is oriented with the extracellular-facing side of the channel at the top. **c** The human PANX structure was used to model the extracellular gate of zebrafish *panx1a/panx1b* by making substitutions as required and repacking only amino acids 74/75 against a rigid

backbone. As a control, human PANX1 was subjected to the same refinement and repacking protocol, creating an extracellular gate that was larger than the original cryo-EM structure. Diameters of the respective gates (in angstroms) are shown. d Molecular models of the extracellular gates of zebrafish *panx1a/panx1b*. Each protein bears one substitution relative to human PANX1. e An alanine was modeled to mimic a constitutively ATP permeable state. Molecular graphics were produced with PyMOL v2.4.1 (Schrödinger, LLC).

Table 5.1. Proposed gates for panx1 structure.

	Human PANX1	<i>Panx1a</i>	<i>Panx1b</i>
Gate 1	W74-R75	W74-C75	M74-R75
Gate 2	I58	V58	V58
Gate 3	T21-E22-P23	S21-E22-N23	S21-D22-S23
CBX binding	I247-I258-F262	I247-V258-L262	L247-V258-V262

5.4. Discussion

The roles of Panx1 channels in neuronal excitability and experimental epilepsy models are controversial and incompletely understood^{45,46}. Here, the lower vertebrate zebrafish model was used to investigate pro-convulsant activities of *Panx1*. Our results demonstrate that a loss-of-function of the *panx1a* gene is the most discernable factor diminishing seizure susceptibility in gene-edited zebrafish by reducing extracellular ATP, and affecting biological processes related to transport and metabolism. In both gene-edited larvae and after acute blocking of *Panx1* channels, extracellular ATP and *P2rx7* were identified as factors contributing to seizure susceptibility. However, shared, and distinct outcomes of pharmacological and genetic models do not encourage a direct comparison of chronic and acute blocking of *Panx1* channels without caution.

To the best of our knowledge there is no direct evidence for Panx1 being epileptogenic and seizures are not a known comorbidity in patients with loss-of-function or gain-of-function mutations in human PANX1⁴⁷⁻⁴⁹. However, support for Panx1 contributing to seizures is from increased human PANX1 protein expression and seizure activity found in epileptic tissue^{8,11,12}. In rodents, activation of Panx1 augments aberrant bursting in the hippocampus and contributes to epileptiform seizure activities⁵⁰, meanwhile, inactivation leads to a reduction^{7-9,14}.

Here, blocking the gamma-aminobutyric acid (GABA)(A) receptor complex with PTZ evoked robust seizure-like events as reported previously in zebrafish²² and mouse models⁷. The two Panx1 orthologues show both pro- and anti-convulsant activities in the presence of PTZ. Similar opposing activities in mouse Panx1 are cell-type and brain region specific¹⁵. The genotype-specific differences described here are best explained by the distinct expression localizations and biophysical properties of Panx1a and Panx1b¹⁶⁻¹⁸. Like mammalian Panx1¹⁹⁻²¹,

Panx1a is broadly expressed throughout the zebrafish ^{16,17}. However, the expression of Panx1b is more restricted to the nervous system ¹⁷. The biophysical properties vary when comparing the complexity of subconductance stages, the cumulative open and closed times, and the unitary conductance of panx1a (≈ 380 pS) and panx1b (480-500pS) channels ¹⁷. These characteristics suggest that Panx1a channels copy characteristics of mammalian Panx1 and operate in different neuronal circuits of the brain to Panx1b.

Hypotheses regarding Panx1s' involvement in epileptic seizures vary, with evidence pointing towards the ability to release the neurotransmitter ATP ^{8,9 51}. Reports show extracellular ATP is reduced in brain tissue preparations deriving from mice with global loss of Panx1 ^{9,52,53}, or astrocytic deletion of Panx1 ¹⁴, and extracellular ATP concentrations increase during high levels of neuronal activity and seizure-like events ^{54,55}.

Since extracellular ATP levels depend on the rate of cellular release and enzymatic degradation, purinergic signaling, or the ratio between ATP and its metabolites ^{54,55}, we quantified extracellular ATP and expression of genes involved in the process. In line with observations in mice, zebrafish lacking Panx1a channels show reduced ATP release efficiency, extending previously reported differences in channel activation kinetics and open times ^{17,18}. Furthermore, RNA-seq analysis and a quantification of selected biomarkers provided evidence how ATP-related mechanism(s) contribute to pro-convulsant activities of Panx1a. The enriched biological processes and coordinated expression changes aligned with the opposite ATP release activities of *panx1a*^{-/-} and *panx1b*^{-/-} larvae, with DKO larvae representing mixed or bi-directional trends. Whether these opposing trends involve the differential expression of Panx1 channels in neurons and microglial cells known for protecting the mammalian brain from excessive activation that occurs during seizures ⁵⁶ remains to be demonstrated. However, our results suggest that changes of the transcriptome represent a broad impact of Panx1 channels in different brain regions tuning the neuronal circuits they support based on their cellular expression and biophysical properties.

The recent description of Panx1 structures ^{40,42,57} allowed us to inquire the relationship of the zebrafish Panx1 ohnologues and the human paralog by structural modeling. Previous work by the Dahl group identified that ATP permeates ⁵⁸ and activates mammalian Panx1 channels ⁵⁹, and that amino acids W74 and R75 play a critical role in the process ⁶⁰. Notable structural similarities and differences exist in the pore region of Panx1a, Panx1b, and human PANX1. However, the conservation of W74 at a critical gate in both human PANX1 and Panx1a suggests similar

permeability of ATP in an open state, We propose that this similarity enables Panx1a, like its mammalian paralogs to contribute to pro-convulsant activity via ATP signaling, as ATP release capabilities are reduced in the *panx1a*^{-/-} larvae, after probenecid treatment, and in the DKO. In turn, the lack of the conserved W74 could render Panx1b less competent for ATP signaling and seizure-like activities.

A functional interaction of the mammalian P2x7R-Panx1 complex is well established ²⁶. Moreover, like Panx1, mammalian P2x7R expression is upregulated in seizure conditions ⁶¹. Although, targeting P2x7R in mice reduces epileptic seizures in some but not all models ⁶²⁻⁶⁵. Here, the downregulation of *p2rx7* in *panx1a*^{-/-} larvae ²⁴ coincides with a significant reduction of SLEs, suggesting that these channels work together. However, when P2rx7 receptors were blocked in TL and *panx1b*^{-/-} larvae, only a moderate reduction of SLEs was observed, advocating for Panx1a and not P2rx7 as the principal driver of seizure-like activities.

Here we have taken important steps toward establishing Panx1 zebrafish models as a powerful system for studies of seizure mechanisms. We anticipate that the unique possibilities afforded by this behaving lower vertebrate model will play crucial roles in dissecting *in vivo* the mechanisms of how the brain can be guarded from excessive excitability and what functions require Panx1.

Additional Information

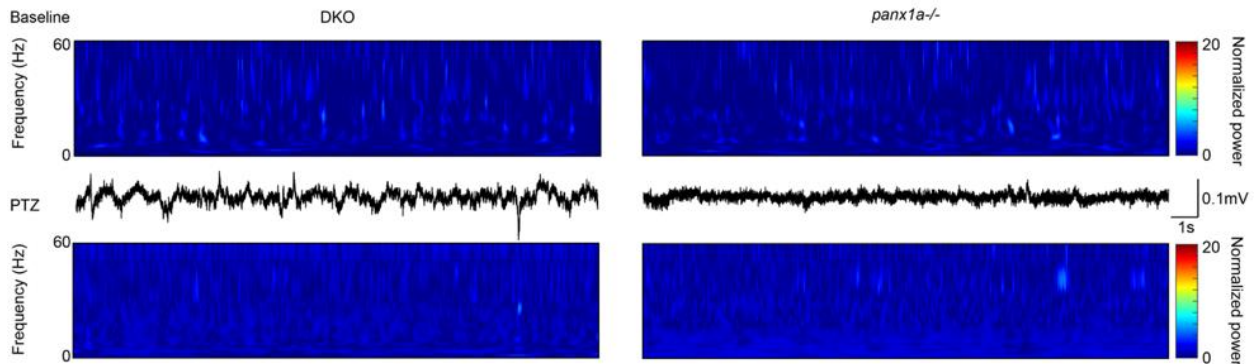
Acknowledgements

Acknowledgements: We wish to acknowledge Uilki Tufa (University of Toronto, ON, Canada) for kindly assisting in developing automated seizure detection. Special thanks to Janet Fleites-Medina and Veronica Scavo for zebrafish husbandry. This research was supported by a Natural Sciences and Engineering Research Council (NSERC) discovery grants RGPIN- 2018-05838 (LWD), RGPIN-2019-06378 (GRZ).

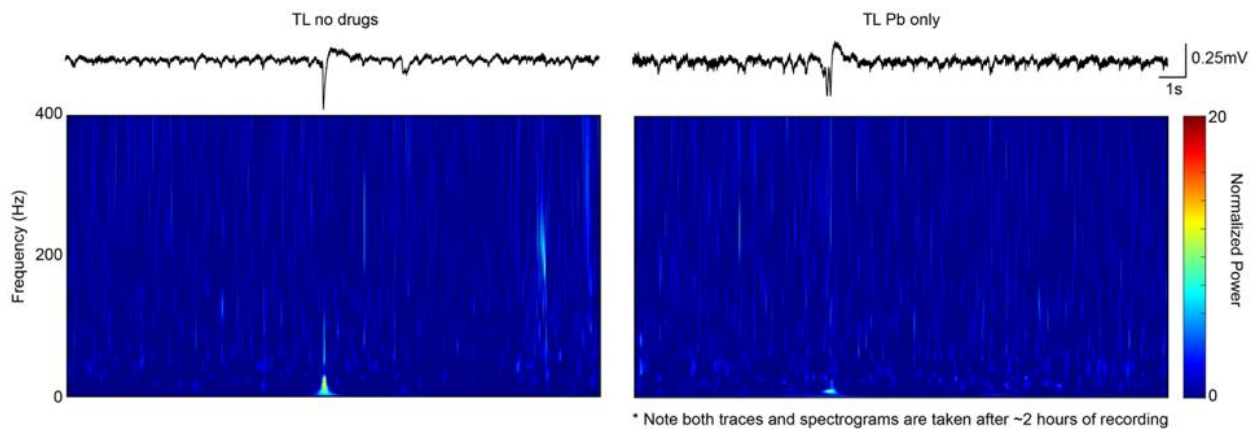
Conflict of Interest Statement

The authors declare no competing interests.

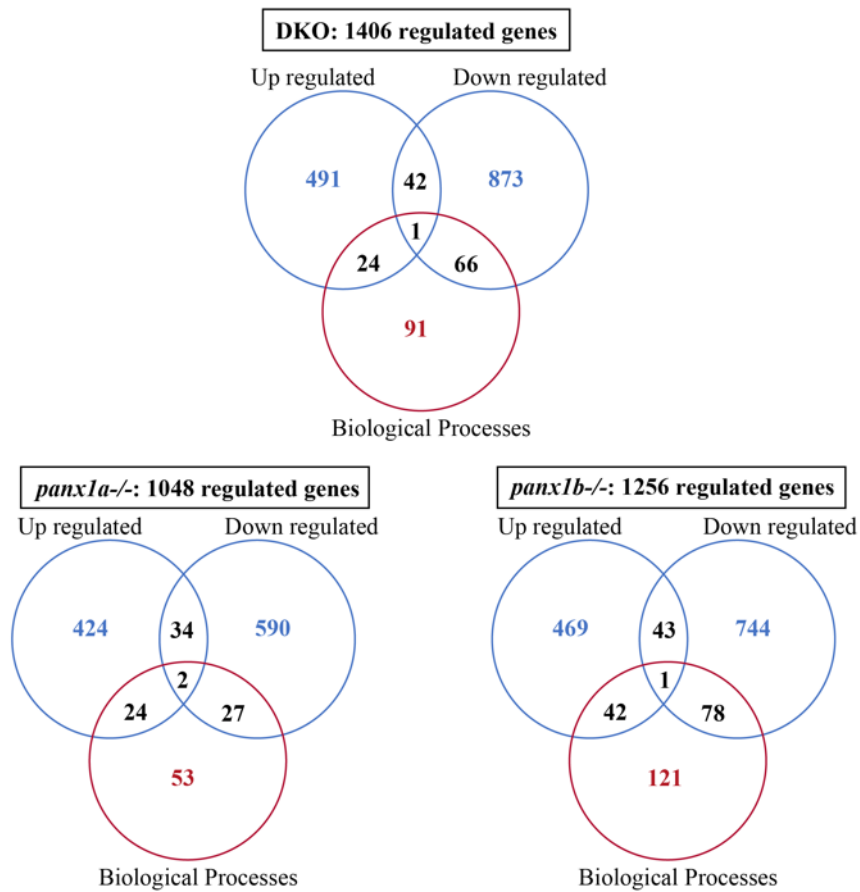
5.5. Supplementary Data – Included in published manuscript



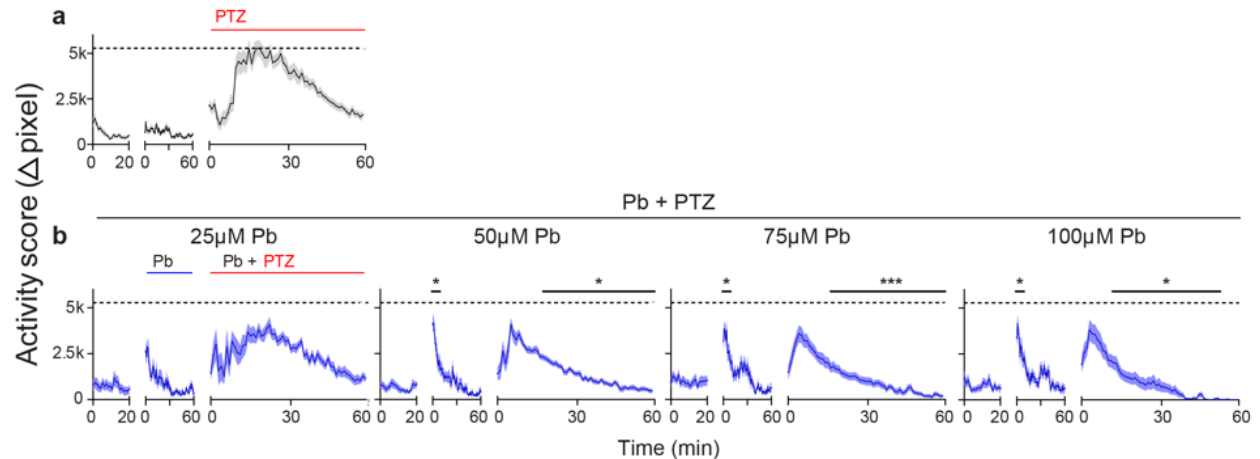
Supplementary Figure 5.1. Comparison of PTZ treatment to baseline activity is indistinguishable. Spectrograms of baseline activity (top) directly compared to recordings during PTZ treatment (bottom) for DKO (left) and *panx1a*^{-/-} (right) show that PTZ treatment does not affect neural activity in these genotypes. Sample traces from PTZ recordings at the 1hour mark are included for reference, revealing no major spiking activity.



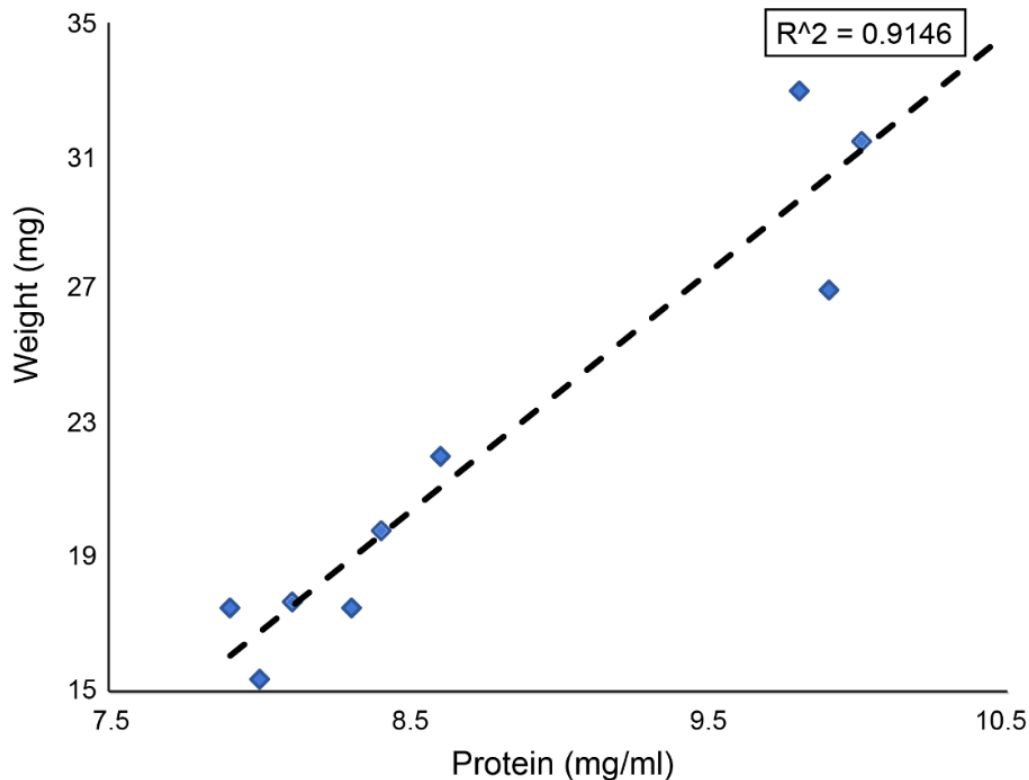
Supplementary Figure 5.2. Comparison of TL with and without Pb treatment only. Spectrograms of baseline activity taken after 2hours of recording from TLs with no drug treatment (left) at all and TLs treated with probenecid only (right). This comparison shows that Pb is not inducing a toxicity effect to prevent seizure-like events from occurring as these spectrograms look like baseline activity.



Supplementary Figure 5.3. Venn diagrams of differentially regulated genes and biological processes. Venn diagrams highlighting how many genes are regulated in each of our *panx1* genotypes and show how many genes fit into biological processes according to FishEnrichR ontology database. They also reveal the overlap in regulated genes.



Supplementary Figure 5.4. Concentration dependent reduction of PTZ-related hyperactivity in TL larvae by probenecid. 7dpf TL larvae were treated with 15mM PTZ (a), or incubated with 25μM, 50μM, 75μM, and 100μM Probenecid (Pb) one hour before treatment with PTZ (b). Pb significantly increased activity (Δ pixel; mean \pm S.E.M.) compared to baseline, and significantly reduced PTZ-induced activity above 50μM. Pb applied at 75μM reduced PTZ-induced activity, without the evidence of substantial toxicity (activity level 0 within one hour). Dashed lines indicate max average activity for PTZ treated TL. *** $p < 0.001$, * $p < 0.05$.



Supplementary Figure 5.5. Linear correlation of larval weight and protein content. Plotting the weight of pooled larvae ($n = 50$ larvae/sample) in mg against the amount of protein in mg/ml that was measured from the supernatant of the homogenate with a spectrophotometer demonstrates a clear linear relationship ($R^2 = 0.9146$). Therefore, ATP concentrations were plotted per protein content to account for biological variance of larval weight.

Supplementary Table 5.1. RT-qPCR values for Immediate early genes regulation in TL and *panx1* knockout larvae treated with PTZ for one hour (Figure 5.4f). Expression values, respective to non-treated controls are >1 for upregulated IEGs and <1 for downregulated IEGs. P-values in bold = $p < 0.05$.

Gene	TL	p-value	DKO	p-value	<i>panx1a</i> ^{-/-}	p-value	<i>panx1b</i> ^{-/-}	p-value
fosab	110.36	0	67.62	0	88.89	0	57.72	0
egr1	9.16	0.001	7.35	0	10.41	0	6.30	0
egr2a	21.42	0	44.20	0	17.28	0	7.98	0
egr2b	6.86	0	4.65	0.002	7.59	0	5.32	0
egr4	120.54	0	63.68	0	76.99	0	44.53	0
jun	4.17	0	4.57	0	9.38	0	5.34	0
bdnf	6.13	0	3.95	0	4.73	0	3.10	0
eif4ebp2	1.04	0.765	0.96	0.813	1.56	0.05	1.50	0.01

Supplementary Table 5.2. RT-qPCR values for Immediate early genes regulation in TL larvae treated with PTZ for one hour (+PTZ) or treated with Pb 30min prior to the PTZ treatment (Pb+PTZ; Figure 5.5i). Expression values, respective to non-treated controls are >1 for upregulated IEGs and <1 for downregulated IEGs. P-values in bold = $p < 0.05$.

Gene	TL (+PTZ)	p-value	TL (Pb + PTZ)	p-value
fosab	110.36	0	54.61	0
egr1	9.16	0.001	6.09	0.001
egr2a	21.42	0	39.38	0
egr2b	6.86	0	2.03	0
egr4	120.54	0	96.97	0
jun	4.17	0	1.44	0.073
bdnf	6.13	0	6.08	0
eif4ebp2	1.04	0.765	0.76	0.056

Supplementary Table 5.3. Gene ontology enriched biological processes from FishEnrichR.

DKO	Term from ZEBRAFISH ENRICHR with GO id	P-value	Log pvalue	Z-score	Combined Score	Genes
UP						
Transport	rRNA-containing ribonucleoprotein complex export from nucleus (GO:0071428)	0.01	1.87	-3.76	16.15	npml1a;ran
	nuclear import (GO:0051170)	0.05	1.31	-2.02	6.10	nup93;htatip2;ran
Signal transduction	regulation of calcium ion transmembrane transporter activity (GO:1901019)	0.02	1.65	-3.64	13.82	cacnb4b;cacnb4a
	regulation of voltage-gated calcium channel activity (GO:1901385)	0.04	1.41	-3.84	12.42	cacnb4b;cacnb4a
Metabolism	kynurenine metabolic process (GO:0070189)	0.01	2.00	-4.22	19.47	afmid;tdo2a
	GTP metabolic process (GO:0046039)	0.03	1.48	-2.96	10.08	ran;mbip
Cellular respiration	-					
	-					
Cell death	neuron apoptotic process (GO:0051402)	0.03	1.56	-3.03	10.87	pink1;siah1
	mitochondrial outer membrane permeabilization (GO:0097345)	0.02	1.75	-3.19	12.80	bnip3la;bnip3

	positive regulation of mitochondrial membrane permeability involved in apoptotic process (GO:1902110)	0.02	1.75	-3.06	12.31	bnip3la;bnip3
DOWN						
Transport	endosome transport via multivesicular body sorting pathway (GO:0032509)	0.01	1.92	-2.91	12.88	tmem50a;vcp;chmp3
	protein import (GO:0017038)	0.05	1.33	-2.14	6.58	nup155;ipo7;ran;nutf2l
	protein localization to nucleus (GO:0034504)	0.05	1.33	-2.14	6.57	nup155;ipo7;ran;nutf2l
Signal transduction	paraxial mesoderm development (GO:0048339)	0.05	1.31	-4.33	13.10	kmt2a;gadd45aa
Metabolism	-					
Cellular respiration	regulation of reactive oxygen species metabolic process (GO:2000377)	0.03	1.56	-3.31	11.87	mpx;acod1
Cell death	intrinsic apoptotic signaling pathway by p53 class mediator (GO:0072332)	0.01	1.92	-3.64	16.12	rps19;tp53;bag6l
	intrinsic apoptotic signaling pathway in response to endoplasmic reticulum stress (GO:0070059)	0.03	1.56	-7.08	25.40	bag6l;tp63
	intrinsic apoptotic signaling pathway	0.04	1.42	-5.65	18.54	tp53;bag6l

	in response to DNA damage by p53 class mediator (GO:0042771)					
panx1a-/-	Term from ZEBRAFISH ENRICHR with GO id	P-value	Log pvalue	Z-score	Combined Score	Genes
UP						
Transport	vesicle-mediated transport to the plasma membrane (GO:0098876)	0.02	1.77	-2.29	9.34	stxbp6l;arf2a;exoc1
	Golgi to plasma membrane transport (GO:0006893)	0.03	1.51	-1.18	4.10	stxbp6l;arf2a;exoc1
	post-Golgi vesicle-mediated transport (GO:0006892)	0.04	1.37	-1.56	4.94	stxbp6l;arf2a;exoc1
Signal transduction	response to axon injury (GO:0048678)	0.05	1.35	-2.37	7.33	cnp;lingo1a
	axon regeneration (GO:0031103)	0.05	1.29	-2.55	7.60	cnp;lingo1a
Metabolism	glutamine family amino acid catabolic process (GO:0009065)	0.03	1.53	-2.34	8.24	aspg;glsb
	nucleobase-containing compound catabolic process (GO:0034655)	0.05	1.35	-1.78	5.51	dnase1;raset2
	cellular macromolecule catabolic process (GO:0044265)	0.06	1.25	-1.79	5.13	dnase1;raset2
Cellular respiration	cellular response to oxidative stress (GO:0034599)	0.06	1.25	-2.18	6.25	pxmp2;prdx6
Cell death						

	neuron apoptotic process (GO:0051402)	0.02	1.68	-3.04	11.76	pink1;siah1
DOWN						
Transport	nuclear transport (GO:0051169)	0.01	1.87	-4.29	18.50	nxt2;nutf2l
	protein import (GO:0017038)	0.01	1.87	-2.19	9.43	ipo11;pttg1ipb;nxt2;nutf2l
	protein localization to nucleus (GO:0034504)	0.01	1.87	-2.19	9.41	ipo11;pttg1ipb;nxt2;nutf2l
	protein import into nucleus (GO:0006606)	0.05	1.32	-1.89	5.76	ipo11;pttg1ipb;nxt2;nutf2l
Signal transduction	paraxial mesoderm development (GO:0048339)	0.02	1.62	-4.38	16.35	kmt2a;gadd45aa
Metabolism	monocarboxylic acid catabolic process (GO:0072329)	0.01	1.98	-2.29	10.48	acot8;aspg;acot7
	fatty acid catabolic process (GO:0009062)	0.02	1.82	-2.69	11.28	acot8;acot7;aca2;zgc:174917
Cellular respiration	-					
Cell death	activation of cysteine-type endopeptidase activity involved in apoptotic process (GO:0006919)	0.02	1.76	-2.34	9.50	hip1;diabloa;caspbl
panx1b-/-	Term from ZEBRAFISH ENRICH with GO id	P-value	Log pvalue	Z-score	Combined Score	Genes
UP						
Transport	cytoskeleton-dependent intracellular	0.01	1.93	-2.59	11.48	kif1aa;ccdc88b;dync1i2a

	transport (GO:0030705) response to salt stress (GO:0009651)	0.02	1.68	-3.68	14.24	slc26a6;trpv6
Signal transduction	basement membrane organization (GO:0071711)	0.02	1.68	-3.80	14.73	col4a6;pxdn
	regulation of calcium ion transmembrane transporter activity (GO:1901019)	0.02	1.68	-3.64	14.10	cacnb4b;cacnb4a
	cytoplasmic microtubule organization (GO:0031122)	0.03	1.51	-2.03	7.07	camsap2b;ccdc88b;figln 1
	regulation of voltage-gated calcium channel activity (GO:1901385)	0.04	1.44	-3.83	12.70	cacnb4b;cacnb4a
	regulation of cation channel activity (GO:2001257)	0.05	1.32	-2.29	6.99	cacnb4b;cacnb4a;shank 3a
	divalent inorganic cation homeostasis (GO:0072507)	0.05	1.26	-3.23	9.36	trpv6;cnnm2b
Metabolism	GTP metabolic process (GO:0046039)	0.03	1.51	-2.96	10.30	ran;mbip
Cellular respiration	-					
Cell death	-					
DOWN						
Transport	nuclear import (GO:0051170)	0.01	2.17	-2.04	10.17	pttg1ipb;htatip2;ran;nup 621;nutf2l
	rRNA-containing ribonucleoprotein complex export from nucleus (GO:0071428)	0.03	1.55	-3.71	13.19	abce1;ran

	protein import into nucleus (GO:0006606)	0.03	1.55	-1.90	6.75	abraa;pttg1ipb;ran;nup62l;nutf2l
	protein import (GO:0017038)	0.03	1.54	-2.16	7.65	pttg1ipb;ran;nup62l;nutf2l
	protein localization to nucleus (GO:0034504)	0.03	1.54	-2.16	7.64	pttg1ipb;ran;nup62l;nutf2l
	establishment of protein localization to organelle (GO:0072594)	0.04	1.45	-2.12	7.08	pttg1ipb;ran;nup62l;nutf2l
	nucleocytoplasmic transport (GO:0006913)	0.04	1.43	-4.38	14.45	htatip2;nutf2l
	ammonium transmembrane transport (GO:0072488)	0.05	1.33	-3.60	11.05	rhcga;rhcgl1
Signal transduction	calcium ion homeostasis (GO:0055074)	0.05	1.31	-1.59	4.79	fhl1b;slc8a1a;atp2a2a;atp2b4;nr3c1
Metabolism	negative regulation of cellular amide metabolic process (GO:0034249)	0.01	2.16	-2.53	12.58	cnot7;fxr1;ormdl3;rpl13a
	gluconeogenesis (GO:0006094)	0.02	1.80	-1.99	8.22	fbp2;tpi1b;pck1
	glucose metabolic process (GO:0006006)	0.05	1.32	-2.22	6.75	fbp2;tpi1b;pck1
	cellular response to ketone (GO:1901655)	0.04	1.43	-3.71	12.25	hamp;pck1
Cellular respiration	regulation of reactive oxygen species metabolic process (GO:2000377)	0.02	1.68	-3.33	12.87	mpx;acod1
	mitochondrial electron transport, ubiquinol to cytochrome c (GO:0006122)	0.05	1.33	-3.58	11.01	uqcrb;uqcrh

Cell death	-					
------------	---	--	--	--	--	--

Supplementary Table 5.4. Clustergram genes according to each category and associated regulation values.

Transport			
Gene Name	DKO logFC value	panx1a-/- logFC value	panx1b-/- logFC value
<i>exoc3l2b</i>	-0.5841	-	-
<i>flot1b</i>	-0.5227	-	-
<i>fthl28</i>	-1.399	-	-
<i>gba</i>	-0.3936	-	-
<i>hmgn3</i>	0.4717	-	-
<i>hspa8</i>	-2.3201	-	-
<i>kcnc3a</i>	-7.5647	-	-
<i>kcnf1a</i>	-5.2609	-	-
<i>kcnk1a</i>	-2.3377	-	-
<i>kcnk5a</i>	-1.4174	-	-
<i>kdelr2a</i>	-0.5574	-	-
<i>ktn1</i>	-0.898	-	-
<i>lgals3b</i>	-1.0593	-	-
<i>loxl2a</i>	-1.1992	-	-1.1197
<i>lrrc6</i>	-6.2773	-	-
<i>mical3a</i>	-0.5704	-	-
<i>mfsd4aa</i>	-	-	0.781
<i>myo5b</i>	-3.1089	-	-
<i>ndel1b</i>	-0.5713	-	-
<i>ndufa10</i>	-0.497	-	-
<i>nlgn4xb</i>	-	-	-4.0171
<i>npm1a</i>	-0.3634	-	-
<i>nr3c1</i>	-8.2252	0.2801	0.3388
<i>nsfb</i>	-0.8964	-	-
<i>nutf2l</i>	-1.613	-	-
<i>oc90</i>	-	1.1787	-
<i>p2rx7</i>	-	-1.1265	-
<i>pafah1b1a</i>	-0.4651	-	-
<i>panx1a</i>	-2.4621	-2.7253	-
<i>panx3</i>	-5.3551	-	-
<i>pck1</i>	-	-	-1.0024
<i>pink1</i>	1.191	-	-
<i>pitpnaa</i>	-1.7653	-	-
<i>rab11bb</i>	-	-	-0.7261

<i>rab18a</i>	0.4016	-	-
<i>rab3ip</i>	-8.4318	-	-
<i>rock2b</i>	-	1.436	-
<i>rrbp1b</i>	-6.3568	-	-
<i>scn4bb</i>	-5.5241	-	-
<i>sdc2</i>	-0.4648	-	-
<i>sdha</i>	-	-	-0.2181
<i>sdhdb</i>	-	-	-0.5928
<i>selenbp1</i>	0.4764	-	-
<i>shtn1</i>	-0.6307	-	-
<i>slc12a4</i>	-	0.4625	-
<i>slc14a2</i>	-2.8632	-	-
<i>slc16a3</i>	-	-	-8.0358
<i>slc22a13a</i>	-	3.5978	-
<i>slc22a2</i>	-	-	-0.835
<i>slc25a55a</i>	-	-	0.5457
<i>slc26a3.1</i>	-3.0933	-	-
<i>slc26a6</i>	-	-	3.1939
<i>slc2a1a</i>	-0.861	-0.9445	-
<i>slc2a1b</i>	-1.0263	-	-
<i>slc2a2</i>	-	-	0.5076
<i>slc34a2b</i>	1.2019	5.3332	6.3308
<i>slc3a2b</i>	-0.6289	-	-1.0244
<i>slc40a1</i>	0.4478	-	-
<i>slc43a1a</i>	-0.7094	-	-
<i>slc43a2b</i>	-1.5258	-	-
<i>slc44a2</i>	-0.6071	-	-
<i>slc4a1a</i>	-7.9603	-	-
<i>slc5a8l</i>	-	-	-0.7408
<i>slc8a1b</i>	-	0.6127	1.0189
<i>slc8a2b</i>	-7.8466	-	-
<i>slc9a3r1a</i>	-	0.3518	0.392
<i>snap25b</i>	-7.059	-	-
<i>stim1a</i>	-1.2066	-	-
<i>stra6</i>	-0.5599	-	-
<i>tcnbb</i>	0.6342	-	-
<i>timm13</i>	-0.5591	-	-
<i>tmed9</i>	-0.5686	-	-
<i>trpv6</i>	-	-	1.7513
<i>typ23b</i>	-	-0.6821	-

<i>txnrd3</i>	-0.4692	-	-
<i>ucp2</i>	-	-	-0.7065
<i>ucp3</i>	-	-	-0.8651
<i>uqcrb</i>	-	-0.3278	-
<i>uqcrfs1</i>	-0.5015	-0.487	-
<i>vcp</i>	-8.8063	-	-
<i>vps39</i>	-1.4432	-	-
<i>yy1a</i>	0.2932	-	-
<i>zgc:92912</i>	-	-	-1.0469
Extracellular ATP			
Release			
Gene Name	DKO logFC value	panx1a-/- logFC value	panx1b-/- logFC value
<i>p2rx7</i>	-1.1265	-	-
<i>panx1a</i>	-2.7253	-	-2.4621
<i>panx3</i>	-	-	-5.3551
<i>panx3</i>	-	-	-5.3551
Degradation			
<i>enpp5</i>	-	-6.9338936	-
<i>enpp7.1</i>	-	-	-1.033231287
<i>entpd1</i>	-	-	-1.076657524
<i>entpd5a</i>	-	-	-1.1842079
<i>entpd5b</i>	-	-0.636278332	-
Metabolism			
Respirasome			
Gene Name	DKO logFC value	panx1a-/- logFC value	panx1b-/- logFC value
<i>higd1a</i>	-	-	-1.7325
<i>ndufa10</i>	-	-	-0.497
<i>sdha</i>	-	-0.2181	-
<i>sdhb</i>	-	-0.5928	-
<i>uqcrb</i>	-0.3278	-	-
<i>uqcrfs1</i>	-0.487	-	-0.5015
Oxidative phosphorylation			
<i>mrpl12</i>	-	-	-0.4597
<i>ndufa10</i>	-	-	-0.497
<i>sdha</i>	-	-0.2181	-
<i>sdhb</i>	-	-0.5928	-
<i>ucp2</i>	-	-0.7065	-

<i>ucp3</i>	-	-0.8651	-
<i>uqcrb</i>	-0.3278	-	-
<i>uqcrfs1</i>	-0.487	-	-0.5015
Solute Carriers			
Gene Name	DKO logFC value	panx1a-/- logFC value	panx1b-/- logFC value
<i>slc1a5</i>	-	-0.5517	-
<i>slc2a1a</i>	-0.9445	-	-0.861
<i>slc2a15a</i>	-	-	-1.7738
<i>slc3a2b</i>	-	-1.0244	-0.6289
<i>slc6a2</i>	-	-	-1.0484
<i>slc8a1b</i>	0.6127	1.0189	-
<i>slc8a2b</i>	-	-	-7.8466
<i>slc20a1a</i>	-	-0.7041	-
<i>slc22a2</i>	-	-0.835	-
<i>slc22a13a</i>	3.5978	-	-
<i>slc25a4</i>	-	-0.7764	-
<i>slc25a29</i>	0.9005	-	-
<i>slc25a36a</i>	-	0.5108	-
<i>slc25a40</i>	-	-0.7115	-
<i>slc35d1b</i>	-0.7702	-	-0.755

Supplementary Table 5.5. RT-qPCR values for gene regulation in PTZ treated (one hour) TL, DKO and Pb treated TL larvae compared to their respective controls (Figure 5.7c). Expression values are >1 for upregulated genes and <1 for downregulated genes. P-values in bold = P<0.05.

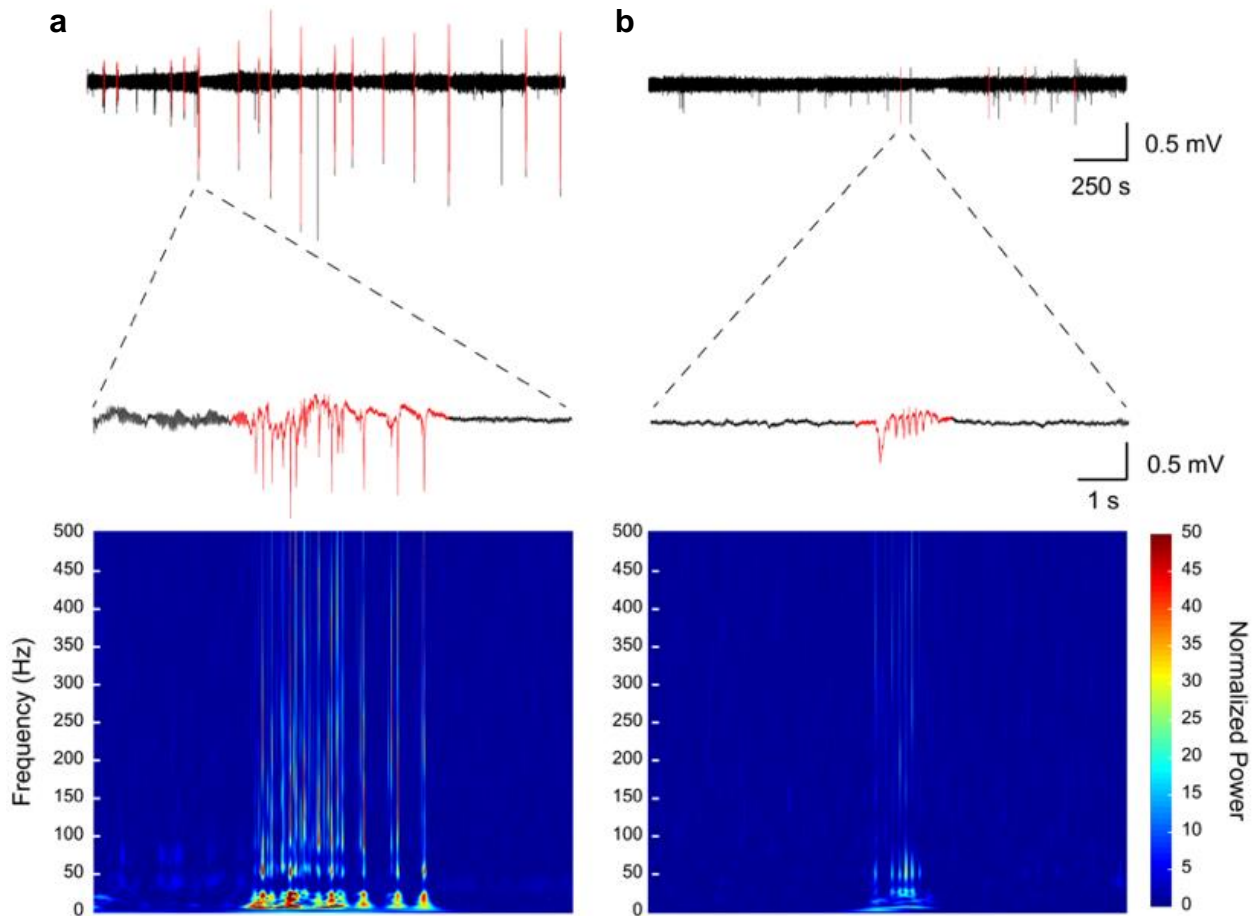
Gene	TL	p-value	DKO	p-value	TL + Pb	p-value
<i>kcnc3a</i>	1.18	0.319	0.65	0.311	3.70	0.001
<i>scn4bb</i>	0.92	0.632	0.86	0.128	1.02	0.936
<i>snap25b</i>	1.01	0.946	0.83	0.346	1.02	0.9
<i>sema6b</i>	1.34	0.204	1.21	0.461	1.22	0.277
<i>slc8a1b</i>	0.97	0.895	0.87	0.302	1.73	0
<i>slc8a2b</i>	0.66	0.159	0.79	0.029	2.00	0
<i>slco2b1</i>	0.88	0.268	1.06	0.505	0.73	0.008
<i>cacna1da</i>	1.03	0.859	0.96	0.582	0.77	0.091

<i>grin2bb</i>	1.08	0.803	0.75	0.091	1.79	0.02
<i>p2rx7</i>	0.80	0.004	0.79	0.378	1.10	0.645
<i>p2ry12</i>	1.83	0.187	0.84	0.526	1.52	0.12
<i>entpd1</i>	1.71	0	1.32	0.02	1.29	0.07
<i>nt5e</i>	1.16	0.184	1.07	0.628	0.88	0.499
<i>adora1b</i>	1.02	0.959	1.42	0.133	0.65	0.331

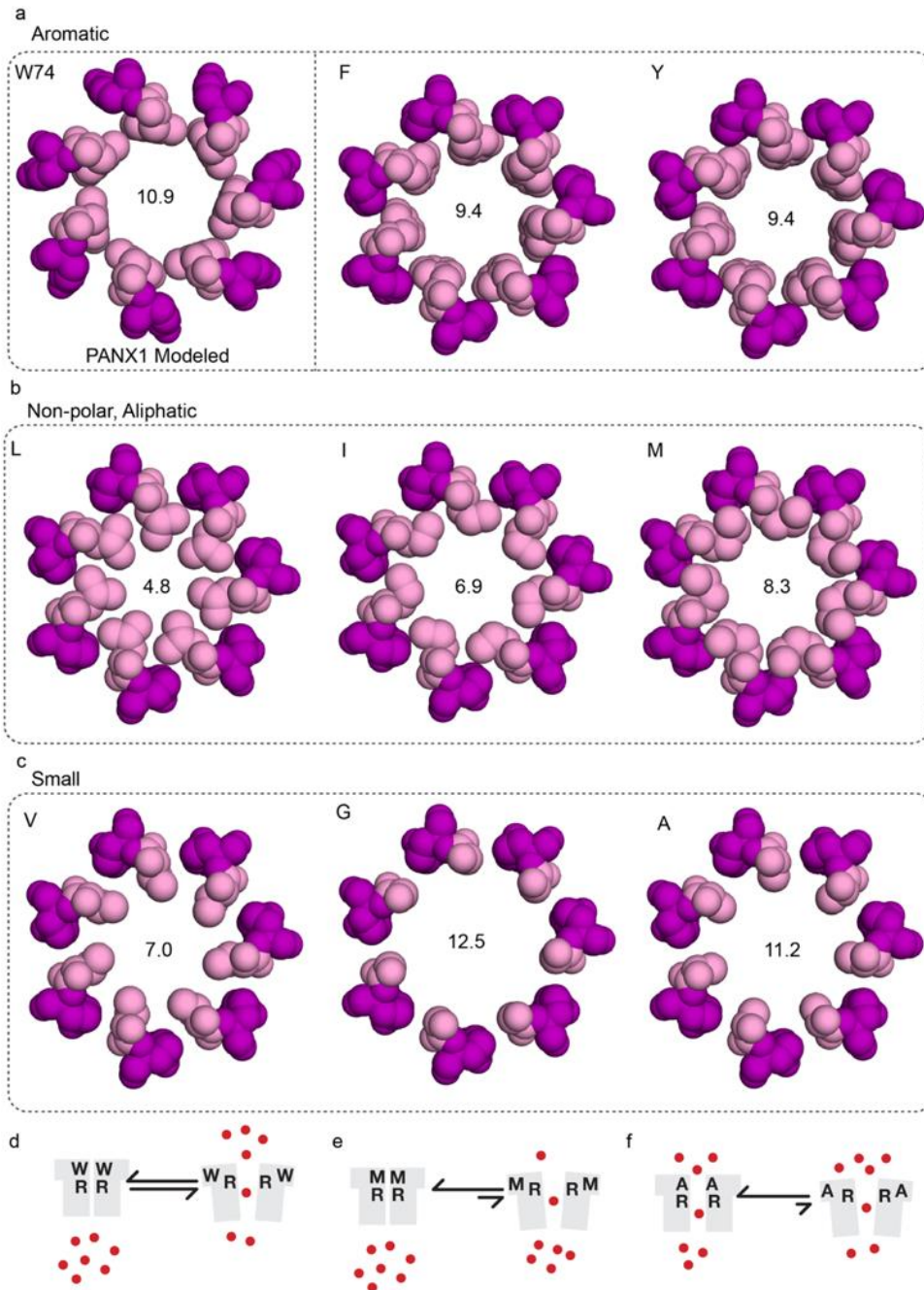
Supplementary Table 5.6. Primers for RT-qPCR.

Gene	Gene Accession Number	Forward Primer (5'-3')	Reverse Primer (5'-3')
<i>fosab</i>	NM_205569	GTGAACGAAACAAGATGGCTG	TTTCATCCTCAAGCTGGTCAG
<i>egr1</i>	NM_131248	TCAACATATCCCAGTGCCAAG	TGTGTCTGGATGGGTTTCTG
<i>egr2a</i>	NM_001328404	CTTCTCCTGTGACTTCTGCG	GCTTCTGTCCATTATGTCTCTGG
<i>egr2b</i>	NM_130997	GATGCGGAGAGGTCTATCAAG	AGGAGTAGGATGGCGGAG
<i>egr4</i>	NM_001114453	ACAGCACCTCAAAGACTACAG	ACGACAAGGTAAGACTGGAG
<i>jun</i>	NM_199987	CACAAGGCTCTGAAACACAAC	TGATGCCAGTTTGAGAAATCC
<i>bdnf</i>	NM_001308648	ACAAGCGGCACTATAACTCG	ACTATCTGCCCTCTTAATGG
<i>eif4ebp2</i>	NM_212803	AGTGACGGGCAAGAACATC	GTTGTCACGTAGGTTCTCTTC
<i>knc3a</i>	NM_001195240	CCATGATAGGGCCTGCTTC	AGAGATGTTATTGAGGCTGCG
<i>scn4bb</i>	NM_001077573	ACCTATGCCAGCTGTATTGG	CGCTCACGGTAAATTTGCAC
<i>snap25b</i>	NM_131434	TGAGAATTTGGAGCAGGTCG	TGTTGGAGTCAGCCATGTC
<i>sema6ba</i>	NM_001366315	TGATGGAGGGCTGTTTGTG	CGTTGCGTGTTTGGGATC
<i>slc8a1b</i>	NM_001039144	GGAGGGACCAGTTTATTGAGG	GGCACGAAAGCAAAGAGAAC
<i>slc8a2b</i>	NM_001123284	TCACCAATGACCAGACAATC	TGCACTCAACTGACCTTCTG
<i>slco2b1</i>	NM_001037678	AGATGGATTGGTGCTTGGTG	TTCTCAGTTGATGGCTCCAC
<i>cacna1da</i>	NM_203484	GGATGAGAAGGATAATGCCGAG	GGGTTTGTGTTGCTGAAGATG
<i>grin2bb</i>	NM_001128337	ATGAGGGACAGGGATAGAGG	AGGTTGGGATGAATGGGTTT
<i>p2rx7</i>	NM_198984	GTGTCATTTGTGGACGAGGAC	CACTCAACAGAGTCTTCATGCTG
<i>p2ry12</i>	NM_001308557	TCTTCGGTTTGATCAGCATCG	TCAGGATTACATTTGGGAGCG
<i>entpd1</i>	NM_001003545	ACCTGACCAACATGATTCCG	GCTGTTTTAGTAAAGCGACGG
<i>nt5e</i>	NM_200932	CAAACGGAAATGTGCTGGAG	GTCTGTCCCACTTGCTGAG
<i>adora1b</i>	NM_001128584	GGAACAATTTACACAGCCTGC	ACGAGCATGAAAAGCAGAGG
<i>tuba1a (ref)</i>	AF029250	GAGCGTCCTACTTACACCAAC	AGGGAAGTGGATACGAGGATAG
<i>actb2 (ref)</i>	NM_181601	GCCCCTAGCACAATGAAGATC	GACTCATCGTACTCCTGCTTG

5.6. Supplementary Data – Not included in published manuscript



Supplementary Figure 5.6. Comparison of TL and DKO seizure-like event detection and spectral analysis. a Sample recording from TL larvae under PTZ application with SLEs highlighted in red based upon automated seizure detection algorithm. SLE magnified below to show typical features of events including polyspiking and higher amplitudes, also shows accuracy of seizure detection from initiation to termination of events in red. Spectrogram associated with the event to show increased low frequency components within SLE as well as the high frequencies that are not present outside of the SLE. **b** Sample recording from one of the four DKO larvae that experienced a few SLEs under PTZ application. Again, SLEs are highlighted in red based upon automated seizure detection algorithm which reliably detected these events regardless of how different they appear in the LFPs. SLE magnified below reveal that these events in the DKO typically have much lower amplitudes, less polyspiking and are shorter in duration. Spectrogram associated with the event also shows that there is barely any high frequencies associated with these events and decreased low frequency components in comparison to TL.



Supplementary Figure 5.7. Structural models of W74 substitutions. a The extracellular facing pore opening of the human PANX1 modeled showing an opening of 10.9Å. When this critical amino acid is mutated to other aromatic amino acids (Phe - F or Tyr - Y) the opening remains quite similar. b By substituting W74 for non-polar, aliphatic amino acids (Leu - L, Ile - I, Met - M) there was no clear correlation between pore opening and these substitutions. c By substituting W74 for much smaller amino acids (Val - V, Gly - G, Ala - A) the simplest (G) and smallest ones (A) created a very large opening although it is undetermined whether these substitutions cause the channel to be more permeable. d A schematic demonstrating the closed (left) and open (right) state of the modeled Panx1 channel suggesting that in the open state there is a hydrophobic pocket favorable for the W to fit in and there is no preference for being in either state (indicated by the arrows). e Mutating this W to a M shows that this pocket is not favorable for the M and even though the pore is open at the same size as the published Panx1 structure (6LTO) this mutation (which is the substitution we see in the *panx1b* protein) does not appear to be as permeable as one would expect, favoring the closed state (arrow pointing left). f As the A

mutation provides one of the largest pores, here is a schematic demonstrating that the open state does not have a favorable hydrophobic pocket for the A but the close state is already permeable and is more favorable.

5.7. References

- 1 Burnstock, G. Introduction to Purinergic Signalling in the Brain. *Adv Exp Med Biol* **1202**, 1-12, doi:10.1007/978-3-030-30651-9_1 (2020).
- 2 Thompson, R. J. & Macvicar, B. A. Connexin and pannexin hemichannels of neurons and astrocytes. *Channels (Austin)* **2**, 81-86, doi:10.4161/chan.2.2.6003 (2008).
- 3 Orellana, J. A. Physiological Functions of Glial Cell Hemichannels. *Adv Exp Med Biol* **949**, 93-108, doi:10.1007/978-3-319-40764-7_5 (2016).
- 4 Ma, Z., Tanis, J. E., Taruno, A. & Foskett, J. K. Calcium homeostasis modulator (CALHM) ion channels. *Pflugers Arch* **468**, 395-403, doi:10.1007/s00424-015-1757-6 (2016).
- 5 Mulligan, S. J. & MacVicar, B. A. VRACs CARVe a path for novel mechanisms of communication in the CNS. *Sci STKE* **2006**, pe42, doi:10.1126/stke.3572006pe42 (2006).
- 6 Sabirov, R. Z. & Merzlyak, P. G. Plasmalemmal VDAC controversies and maxi-anion channel puzzle. *Biochim Biophys Acta* **1818**, 1570-1580, doi:10.1016/j.bbamem.2011.09.024 (2012).
- 7 Aquilino, M. S. *et al.* Pannexin-1 Deficiency Decreases Epileptic Activity in Mice. *Int J Mol Sci* **21**, doi:10.3390/ijms21207510 (2020).
- 8 Dossi, E. *et al.* Pannexin-1 channels contribute to seizure generation in human epileptic brain tissue and in a mouse model of epilepsy. *Sci Transl Med* **10**, doi:10.1126/scitranslmed.aar3796 (2018).
- 9 Santiago, M. F. *et al.* Targeting pannexin1 improves seizure outcome. *PLoS One* **6**, e25178, doi:10.1371/journal.pone.0025178 (2011).
- 10 Kim, J. E. & Kang, T. C. The P2X7 receptor-pannexin-1 complex decreases muscarinic acetylcholine receptor-mediated seizure susceptibility in mice. *J Clin Invest* **121**, 2037-2047, doi:10.1172/JCI44818 (2011).
- 11 Jiang, T. *et al.* Altered expression of pannexin proteins in patients with temporal lobe epilepsy. *Mol Med Rep* **8**, 1801-1806, doi:10.3892/mmr.2013.1739 (2013).
- 12 Li, S. *et al.* Expression of pannexin 1 and 2 in cortical lesions from intractable epilepsy patients with focal cortical dysplasia. *Oncotarget* **8**, 6883-6895, doi:10.18632/oncotarget.14317 (2017).
- 13 Mylvaganam, S. *et al.* Hippocampal seizures alter the expression of the pannexin and connexin transcriptome. *J Neurochem* **112**, 92-102, doi:10.1111/j.1471-4159.2009.06431.x (2010).
- 14 Scemes, E., Velisek, L. & Veliskova, J. Astrocyte and Neuronal Pannexin1 Contribute Distinctly to Seizures. *ASN Neuro* **11**, 1759091419833502, doi:10.1177/1759091419833502 (2019).
- 15 Obot, P., Velisek, L., Veliskova, J. & Scemes, E. The Contribution of Astrocyte and Neuronal Panx1 to Seizures Is Model and Brain Region Dependent. *ASN Neuro* **13**, 17590914211007273, doi:10.1177/17590914211007273 (2021).
- 16 Prochnow, N. *et al.* Pannexin1 in the outer retina of the zebrafish, *Danio rerio*. *Neuroscience* **162**, 1039-1054, doi:10.1016/j.neuroscience.2009.04.064 (2009).
- 17 Kurtenbach, S. *et al.* Pannexin1 channel proteins in the zebrafish retina have shared and unique properties. *PLoS One* **8**, e77722, doi:10.1371/journal.pone.0077722 (2013).
- 18 Bond, S. R., Wang, N., Leybaert, L. & Naus, C. C. Pannexin 1 ohnologs in the teleost lineage. *J Membr Biol* **245**, 483-493, doi:10.1007/s00232-012-9497-4 (2012).

- 19 Vogt, A., Hormuzdi, S. G. & Monyer, H. Pannexin1 and Pannexin2 expression in the developing and mature rat brain. *Brain Res Mol Brain Res* **141**, 113-120, doi:10.1016/j.molbrainres.2005.08.002 (2005).
- 20 Ray, A., Zoidl, G., Weickert, S., Wahle, P. & Dermietzel, R. Site-specific and developmental expression of pannexin1 in the mouse nervous system. *Eur J Neurosci* **21**, 3277-3290, doi:10.1111/j.1460-9568.2005.04139.x (2005).
- 21 Baranova, A. *et al.* The mammalian pannexin family is homologous to the invertebrate innexin gap junction proteins. *Genomics* **83**, 706-716, doi:10.1016/j.ygeno.2003.09.025 (2004).
- 22 Baraban, S. C., Taylor, M. R., Castro, P. A. & Baier, H. Pentylenetetrazole induced changes in zebrafish behavior, neural activity and c-fos expression. *Neuroscience* **131**, 759-768, doi:10.1016/j.neuroscience.2004.11.031 (2005).
- 23 Grone, B. P. & Baraban, S. C. Animal models in epilepsy research: legacies and new directions. *Nat Neurosci* **18**, 339-343, doi:10.1038/nn.3934 (2015).
- 24 Safarian, N., Whyte-Fagundes, P., Zoidl, C., Grigull, J. & Zoidl, G. Visuomotor deficiency in panx1a knockout zebrafish is linked to dopaminergic signaling. *Sci Rep* **10**, 9538, doi:10.1038/s41598-020-66378-y (2020).
- 25 Cenedese, V. *et al.* Pannexin 1 Is Critically Involved in Feedback from Horizontal Cells to Cones. *Front Mol Neurosci* **10**, 403, doi:10.3389/fnmol.2017.00403 (2017).
- 26 Iglesias, R. *et al.* P2X7 receptor-Pannexin1 complex: pharmacology and signaling. *Am J Physiol Cell Physiol* **295**, C752-760, doi:10.1152/ajpcell.00228.2008 (2008).
- 27 Baraban, S. C. Forebrain electrophysiological recording in larval zebrafish. *J Vis Exp*, doi:10.3791/50104 (2013).
- 28 Hunyadi, B., Siekierska, A., Sourbron, J., Copmans, D. & de Witte, P. A. M. Automated analysis of brain activity for seizure detection in zebrafish models of epilepsy. *J Neurosci Methods* **287**, 13-24, doi:10.1016/j.jneumeth.2017.05.024 (2017).
- 29 Colic, S., Wither, R. G., Zhang, L., Eubanks, J. H. & Bardakjian, B. L. Characterization of seizure-like events recorded in vivo in a mouse model of Rett syndrome. *Neural Netw* **46**, 109-115, doi:10.1016/j.neunet.2013.05.002 (2013).
- 30 de Curtis, M., Jefferys, J. G. R. & Avoli, M. in *Jasper's Basic Mechanisms of the Epilepsies* (eds th *et al.*) (2012).
- 31 Rakhade, S. N. *et al.* A common pattern of persistent gene activation in human neocortical epileptic foci. *Ann Neurol* **58**, 736-747, doi:10.1002/ana.20633 (2005).
- 32 Losing, P. *et al.* SRF modulates seizure occurrence, activity induced gene transcription and hippocampal circuit reorganization in the mouse pilocarpine epilepsy model. *Mol Brain* **10**, 30, doi:10.1186/s13041-017-0310-2 (2017).
- 33 Barkmeier, D. T. *et al.* Electrical, molecular and behavioral effects of interictal spiking in the rat. *Neurobiol Dis* **47**, 92-101, doi:10.1016/j.nbd.2012.03.026 (2012).
- 34 Dahl, G., Qiu, F. & Wang, J. The bizarre pharmacology of the ATP release channel pannexin1. *Neuropharmacology* **75**, 583-593, doi:10.1016/j.neuropharm.2013.02.019 (2013).
- 35 Turrini, L. *et al.* Optical mapping of neuronal activity during seizures in zebrafish. *Sci Rep* **7**, 3025, doi:10.1038/s41598-017-03087-z (2017).
- 36 Safarian, N., Zoidl, C., Zoidl, G. . Pannexin1b is a candidate for setting interactions between the circadian clock and the zebrafish visual system. (2021).

- 37 Chen, E. Y. *et al.* Enrichr: interactive and collaborative HTML5 gene list enrichment analysis tool. *BMC Bioinformatics* **14**, 128, doi:10.1186/1471-2105-14-128 (2013).
- 38 Kuleshov, M. V. *et al.* modEnrichr: a suite of gene set enrichment analysis tools for model organisms. *Nucleic Acids Res* **47**, W183-W190, doi:10.1093/nar/gkz347 (2019).
- 39 Klepper, J. *et al.* Glut1 Deficiency Syndrome (Glut1DS): State of the art in 2020 and recommendations of the international Glut1DS study group. *Epilepsia Open* **5**, 354-365, doi:10.1002/epi4.12414 (2020).
- 40 Deng, Z. *et al.* Cryo-EM structures of the ATP release channel pannexin 1. *Nat Struct Mol Biol* **27**, 373-381, doi:10.1038/s41594-020-0401-0 (2020).
- 41 Mou, L. *et al.* Structural basis for gating mechanism of Pannexin 1 channel. *Cell Res* **30**, 452-454, doi:10.1038/s41422-020-0313-x (2020).
- 42 Michalski, K. *et al.* The Cryo-EM structure of pannexin 1 reveals unique motifs for ion selection and inhibition. *Elife* **9**, doi:10.7554/eLife.54670 (2020).
- 43 Qu, R. *et al.* Cryo-EM structure of human heptameric Pannexin 1 channel. *Cell Res* **30**, 446-448, doi:10.1038/s41422-020-0298-5 (2020).
- 44 Bunse, S. *et al.* Single cysteines in the extracellular and transmembrane regions modulate pannexin 1 channel function. *J Membr Biol* **244**, 21-33, doi:10.1007/s00232-011-9393-3 (2011).
- 45 Aquilino, M. S., Whyte-Fagundes, P., Zoidl, G. & Carlen, P. L. Pannexin-1 channels in epilepsy. *Neurosci Lett* **695**, 71-75, doi:10.1016/j.neulet.2017.09.004 (2019).
- 46 Scemes, E. & Veliskova, J. Exciting and not so exciting roles of pannexins. *Neurosci Lett* **695**, 25-31, doi:10.1016/j.neulet.2017.03.010 (2019).
- 47 Sang, Q. *et al.* A pannexin 1 channelopathy causes human oocyte death. *Sci Transl Med* **11**, doi:10.1126/scitranslmed.aav8731 (2019).
- 48 Wang, W. *et al.* Homozygous variants in PANX1 cause human oocyte death and female infertility. *Eur J Hum Genet*, doi:10.1038/s41431-020-00807-4 (2021).
- 49 Shao, Q. *et al.* A Germline Variant in the PANX1 Gene Has Reduced Channel Function and Is Associated with Multisystem Dysfunction. *J Biol Chem* **291**, 12432-12443, doi:10.1074/jbc.M116.717934 (2016).
- 50 Thompson, R. J. *et al.* Activation of pannexin-1 hemichannels augments aberrant bursting in the hippocampus. *Science* **322**, 1555-1559, doi:10.1126/science.1165209 (2008).
- 51 Narahari, A. K. *et al.* ATP and large signaling metabolites flux through caspase-activated Pannexin 1 channels. *Elife* **10**, doi:10.7554/eLife.64787 (2021).
- 52 Kurtenbach, S. *et al.* Investigation of olfactory function in a Panx1 knock out mouse model. *Front Cell Neurosci* **8**, 266, doi:10.3389/fncel.2014.00266 (2014).
- 53 Whyte-Fagundes, P. *et al.* A Potential Compensatory Role of Panx3 in the VNO of a Panx1 Knock Out Mouse Model. *Front Mol Neurosci* **11**, 135, doi:10.3389/fnmol.2018.00135 (2018).
- 54 Beamer, E., Conte, G. & Engel, T. ATP release during seizures - A critical evaluation of the evidence. *Brain Res Bull* **151**, 65-73, doi:10.1016/j.brainresbull.2018.12.021 (2019).
- 55 Engel, T., Alves, M., Sheedy, C. & Henshall, D. C. ATPergic signalling during seizures and epilepsy. *Neuropharmacology* **104**, 140-153, doi:10.1016/j.neuropharm.2015.11.001 (2016).
- 56 Badimon, A. *et al.* Negative feedback control of neuronal activity by microglia. *Nature* **586**, 417-423, doi:10.1038/s41586-020-2777-8 (2020).

- 57 Ruan, Z., Orozco, I. J., Du, J. & Lu, W. Structures of human pannexin 1 reveal ion pathways and mechanism of gating. *Nature* **584**, 646-651, doi:10.1038/s41586-020-2357-y (2020).
- 58 Bao, L., Locovei, S. & Dahl, G. Pannexin membrane channels are mechanosensitive conduits for ATP. *FEBS Lett* **572**, 65-68, doi:10.1016/j.febslet.2004.07.009 (2004).
- 59 Locovei, S., Wang, J. & Dahl, G. Activation of pannexin 1 channels by ATP through P2Y receptors and by cytoplasmic calcium. *FEBS Lett* **580**, 239-244, doi:10.1016/j.febslet.2005.12.004 (2006).
- 60 Qiu, F. & Dahl, G. A permeant regulating its permeation pore: inhibition of pannexin 1 channels by ATP. *Am J Physiol Cell Physiol* **296**, C250-255, doi:10.1152/ajpcell.00433.2008 (2009).
- 61 Jimenez-Pacheco, A. *et al.* Increased neocortical expression of the P2X7 receptor after status epilepticus and anticonvulsant effect of P2X7 receptor antagonist A-438079. *Epilepsia* **54**, 1551-1561, doi:10.1111/epi.12257 (2013).
- 62 Fischer, W. *et al.* Critical Evaluation of P2X7 Receptor Antagonists in Selected Seizure Models. *PLoS One* **11**, e0156468, doi:10.1371/journal.pone.0156468 (2016).
- 63 Nieoczym, D., Socala, K. & Wlaz, P. Evaluation of the Anticonvulsant Effect of Brilliant Blue G, a Selective P2X7 Receptor Antagonist, in the iv PTZ-, Maximal Electroshock-, and 6 Hz-Induced Seizure Tests in Mice. *Neurochem Res* **42**, 3114-3124, doi:10.1007/s11064-017-2348-z (2017).
- 64 Amhaoul, H. *et al.* P2X7 receptor antagonism reduces the severity of spontaneous seizures in a chronic model of temporal lobe epilepsy. *Neuropharmacology* **105**, 175-185, doi:10.1016/j.neuropharm.2016.01.018 (2016).
- 65 Jimenez-Pacheco, A. *et al.* Transient P2X7 Receptor Antagonism Produces Lasting Reductions in Spontaneous Seizures and Gliosis in Experimental Temporal Lobe Epilepsy. *J Neurosci* **36**, 5920-5932, doi:10.1523/JNEUROSCI.4009-15.2016 (2016).
- 66 de Marchi, F. O. *et al.* P2X7R and PANX-1 channel relevance in a zebrafish larvae copper-induced inflammation model. *Comp Biochem Physiol C Toxicol Pharmacol* **223**, 62-70, doi:10.1016/j.cbpc.2019.05.012 (2019).
- 67 Donnelly-Roberts, D. L., Namovic, M. T., Han, P. & Jarvis, M. F. Mammalian P2X7 receptor pharmacology: comparison of recombinant mouse, rat and human P2X7 receptors. *Br J Pharmacol* **157**, 1203-1214, doi:10.1111/j.1476-5381.2009.00233.x (2009).
- 68 Sievers, F. *et al.* Fast, scalable generation of high-quality protein multiple sequence alignments using Clustal Omega. *Mol Syst Biol* **7**, 539, doi:10.1038/msb.2011.75 (2011).
- 69 Waterhouse, A. *et al.* SWISS-MODEL: homology modelling of protein structures and complexes. *Nucleic Acids Res* **46**, W296-W303, doi:10.1093/nar/gky427 (2018).
- 70 Kuhlman, B. *et al.* Design of a novel globular protein fold with atomic-level accuracy. *Science* **302**, 1364-1368, doi:10.1126/science.1089427 (2003).
- 71 Pellegrini-Calace, M., Maiwald, T. & Thornton, J. M. PoreWalker: a novel tool for the identification and characterization of channels in transmembrane proteins from their three-dimensional structure. *PLoS Comput Biol* **5**, e1000440, doi:10.1371/journal.pcbi.1000440 (2009).
- 72 Faul, F., Erdfelder, E., Lang, A. G. & Buchner, A. G*Power 3: a flexible statistical power analysis program for the social, behavioral, and biomedical sciences. *Behav Res Methods* **39**, 175-191, doi:10.3758/bf03193146 (2007).

Chapter 6. Discussion

“ I am never really satisfied that I understand anything; because, understand it well as I may, my comprehension can only be an infinitesimal fraction of all I want to understand about the many connections and relations which occur to me, how the matter in question was first thought of or arrived at, etcetera.”

- Ada Lovelace

Explanations for conflicting reports of Panx1 in health and disease do not appear immediately obvious. However, they reinforce the idea that Panx1 is a versatile and dynamic membrane channel protein that attracts significant attention as a potential therapeutic target for human disorders. With the discovery of germline human mutations of Panx1, this has further given us a glimpse of the importance of this channel within the human context. Identification of additional CNS disease causing mutations, and subsequent functional validation of their roles, will likely be important in decoding complex molecular dynamics of the Panx1 protein in health and disease in the future. However, the work from this thesis intends to shed a light towards highlighting possible Panx1 machineries underlying the shift in the function of the unchallenged protein from a physiological to a pathological state. This places an importance in studying Panx1 in the olfactory system to gain an understanding of how the protein functions contribute to physiology, as well as within an epilepsy context to determine which functional machinery becomes ‘hijacked’ during seizure activities. Here, connections will be drawn between the two investigations in order to speculate the synergistic element that elucidates the pathological transition of Panx1 at the core of disease.

Previous investigations regarding the developmental expression profiles of the Panxs suggests that Panx levels are dynamically regulated during differentiation in a variety of tissues and cells. In particular, Panx1 expression varies over the course of development, with expression peaking around birth and decreasing from postnatal day 15 in mice (Ardiles et al., 2014; Celetti et al., 2010; Penuela et al., 2012; Vogt et al., 2005; Wicki-Stordeur & Swayne, 2013). Panx3 expression levels appear unchanged with age (Celetti et al., 2010). However, their expression is induced early in osteoblast differentiation and decreases during maturation, taking on a new role in regulating growth plate development and bone formation (Ishikawa et al., 2011, 2016). Here, in the accessory olfactory system, expression was determined for Panx1 and Panx3 in the VNO of juvenile and adult mice. Although levels of expression for both of these proteins was not explicitly measured, the reorganization of Panx1, and Panx3 when it was upregulated in place of Panx1, was

observed when comparing expression patterns in juveniles to adults; where it was expressed in non-sensory epithelium and sensory epithelium respectively. This demonstration of age-related reorganization, together with the well-established characteristic of dynamic Panx1 expression, strongly suggests that the functions of Panx1 modify upon maturation. Although the exact responsibilities of the channel are unclear between juveniles and adults, it is particularly evident that Panx1 expression must decline with age and is a tightly regulated process required for maintaining physiology.

Differential regulation of Panx1 expression has also been linked to epilepsy, where increased Panx1 expression was found in adult human patient samples of temporal lobe epilepsy. However, in an adult mouse model of chemically induced epilepsy there are reports of anticonvulsant properties of Panx1 (Kim & Kang, 2011), possibly due to the timepoint of seizure induction and no evidence of increased Panx1 expression. Here, we presented two models that validate proconvulsant roles of Panx1 and *Panx1a* in juvenile mice and zebrafish larvae respectively. It is possible that Panx1 being proconvulsant in animal models of epilepsies are a result of them being conducted within juvenile stages where Panx1 expression is high. Based upon our zebrafish studies that suggest Panx1 participates in seizure activities by mediating P2X7 receptor signaling and ATP release, it is possible that the increased availability of Panx1 promotes excessive extracellular ATP concentrations in turn creating an excitable network that favours seizure dynamics. This potential age associated pattern of excitability may underlie the conflict that exists between reports of increased excitability and impaired learning in adult Panx1^{-/-} mice (Prochnow et al., 2012) compared to the reports suggesting juvenile Panx1 contributes to prolonged hyperexcitability (Santiago et al., 2011). Together, these studies suggest that although Panx1 is needed for early neuronal development, elevated levels in an adult brain can prime pathological outcomes.

This pattern of differential regulation in disease states expands beyond epilepsy (Davis et al., 2012; Zappalà et al., 2007; Y. Zhang et al., 2015), however, the molecular mechanism underlying the pathologically induced change in Panx1 expression has yet to be fully elucidated. It is probable that the regulatory machinery responsible for activating signaling pathways that control Panx1 gene expression is involved and should be a target of further investigations. Dufresne et al., began looking into transcriptional regulation via the Panx1 promoter, revealing binding sites for the ETS response element and CREB (cAMP-response element binding)

(Dufresne & Cyr, 2014). As a result, further research should be undertaken to investigate these transcription factors as they pose as potential regulators underlying the pathological expression of Panx1.

The investigation of Panx1 in physiological and pathological settings are intertwined as these outcomes convey a more complete picture of the roles of Panx1 in health and disease. Moving forward, particular interest should be paid to pathways associated with transcription and posttranslational regulation, as evidence mounting from OMICS studies suggest that they could be drivers of the multiple pathologies Panx1 is associated with. Furthermore, pathological expression levels of Panx1 must be considered, as its dynamic expression profile shows that it declines gradually with age in normal circumstances. This decline fits elegantly into studies of certain childhood epilepsies and Panx1 acting as a proconvulsant channel, since clinical reports exist for children ‘growing out’ of epilepsy. Albeit speculative, it is reasonable to test whether decreased Panx1 expression in adulthood can explain this phenomenon. In summary, as our understanding of Panx1 in CNS disorders advances and a Panx1 structure has become available for rational drug design, avenues will open for therapeutic targeting of Panx1 in epilepsy and beyond.

CONCLUSION

“ For a research worker, the unforgotten moments of one’s life are those rare ones which come after years of plodding work, when the veil over nature’s secret seems suddenly to lift and when what was dark and chaotic appears in a clear and beautiful light and pattern.”

- Gerty Cori

Despite clinical relevance in many physiological and pathological settings, precise links to Panx1 signaling pathways are largely unknown. Over the course of this thesis, I have experienced how the field of Panx1 research has transformed from fundamental, cell biological techniques and models to more translational models to address disease relevant outcomes. As such, my work began on olfaction using complimentary cell culture work to a Panx1^{-/-} mouse model. Upon completion of this line of inquiry, identifying that Panx3 upregulates and functionally compensates in the absence of Panx1, correlations of Panx1 with diseases continued to emerge and became of greater interest to the field. Therefore, this same mouse model permitted exploration of Panx1 into epilepsy research. Although we were able to provide evidence for Panx1 being proconvulsant, this model still left questions regarding a mechanism for Panx1 involvement in seizure activities, and in turn emphasized the need for alternative methods towards addressing them. This gave rise to our investigations of Panx1 in a zebrafish model of epilepsy. To the best of our knowledge, the study presented here, completed *in vivo*, using *panx1*^{-/-} zebrafish to determine the channels roles in seizures, is adding a new twist to the fast growing Panx1 field. With these innovations, we have been able to place Panx1 at the core of purinergic signaling alongside P2X7 receptors within the context of epilepsy in a complementary animal model. Overall, this thesis provides significant insight towards the understanding of Panx1 functions from health and disease perspectives using a variety of models including; mouse Panx1, and both zebrafish *Panx1a* and *Panx1b*, from genes to behavioural outcomes *in vitro* through to *in vivo*. As fundamental and clinical roles of Panx1 continue to emerge and others become more concrete, the work in this thesis has allowed me to contribute to the rapid paced advancements in an exciting field which Drs. Dahl and Keane imagined as “Pannexins: moving from discovery to bedside in 11±4 years?”

SIGNIFICANCE AND FUTURE DIRECTIONS

“ The more we know, the more we realize there is to know.”

- Jennifer Doudna

It is with great admiration for science, and the gap junction/Panx field, to observe that the research surrounding Panx1 has undergone fast progression since its discovery in the year 2000. Within this relatively short time span, Panx1 has undergone mis-annotation originally as a gap junction protein and misrepresentation structurally until its recent resolution. Involvement of Panx1 has been shown in diverse physiological and pathological functions; with research from this thesis contributing significantly to these ‘two faces’ of Panx1 by investigating its participation in olfaction and epilepsy. Although functions in olfaction have been temporarily dismissed based upon the upregulation of Panx3 in the mouse model, here exists an opportunity to expand Panx1 research beyond itself and embrace the idea of Panx family members coordinating their expression and function in order to maintain homeostatic conditions that support physiology.

A growing body of evidence also exists for the interaction of Panx1 with other proteins, like P2X7 receptors. Investigations into Panx1 mechanisms underlying seizure activities presented here, highlight an involvement of P2X7 receptors in mediating ATP release to facilitate seizure activity. This exemplifies the impact the Panx1 channel has beyond itself and implies the importance of its functions in a complex molecular network involving its signaling and possible protein-protein interactions. At this time no definitive conclusion can be drawn regarding whether or not Panx1 and P2X7 receptors are forming a physical complex in our model, and speculations arise regarding whether or not a direct interaction may occur only in cell or model specific contexts. Here, however, their coordinated down regulation was demonstrated *in vivo*; strongly favouring some manner of interconnectedness amongst the proteins and highlighting the need for Cryo-EM to model these possible interactions in the future.

As a whole, this thesis focused on the central idea of purinergic signaling via Panx1 in both physiological and pathological contexts. Although the ATP release property of Panx1 receives the most attention, recently, challenges were made regarding the ability of the protein to conduct this large signaling molecule. With efforts from the Dahl and Bayliss groups, in combination with the resolved structure, there is still strong support for the permeation of ATP through Panx1. Thus far,

point mutations *in vitro* identified critical residues, W74 and R75, that are required for channel gating and potential ATP release that have also been confirmed by structural modelling. However, upon the duplication of Panx1 in zebrafish, *Panx1a* retained only the W74 residue while *Panx1b* only retained R75. Although this appears perplexing, we demonstrate that the *panx1b* channel is unable to release ATP; providing a biological model that substantiates the importance of the W74 residue in particular for regulating native ATP release properties of Panx1.

Until now, the site for ATP coordination has not been exemplified *in vivo*. Interestingly, this same residue overlaps with the established target for carbenoxolone (CBX) inhibition of Panx1. Unfortunately, this blocker cannot be tested in a zebrafish model *in vivo* and selectivity for Panx1 is based upon tightly regulated concentrations of the drug. This raises questions regarding the generalization and efficiency of this blocker as a potential therapy for Panx1 involved pathologies, like epilepsy, and indicates a need for alternative drugs. Probenecid (Pb) has proven successful in blocking Panx1 in our fish model, and the tryptophan ring (W74) at the extracellular pore of the protein has been critically identified for channel pharmacology and ATP release properties. Together, with the resolved structure, the tools are in place for structure-based therapeutic drug design using a combination of the molecular makeup for CBX and Pb as a starting point for formulation. As proconvulsant activities of Panx1 have been established, and drug resistant epilepsies make up about one third of the epileptic patient population, there is a need for uncovering new molecular targets for seizure relief and Panx1 poses as a likely candidate. Our *Panx1* zebrafish model is in place with well-established protocols for monitoring seizure phenotypes. As such, we provide a feasible platform for future high throughput drug discovery with the hopes of uncovering a new drug designed to specifically target the critical sites in the Panx1 structure that will likely prove useful in other disease treatments beyond epilepsy.

BIBLIOGRAPHY

- Alberto, A. V. P., Faria, R. X., Couto, C. G. C., Ferreira, L. G. B., Souza, C. A. M., Teixeira, P. C. N., Fróes, M. M., & Alves, L. A. (2013). Is pannexin the pore associated with the P2X7 receptor? *Naunyn-Schmiedeberg's Archives of Pharmacology*, 386(9). <https://doi.org/10.1007/s00210-013-0868-x>
- Anumonwo, J. M. B., Taffet, S. M., Gu, H., Chanson, M., Moreno, A. P., & Delmar, M. (2001). The Carboxyl Terminal Domain Regulates the Unitary Conductance and Voltage Dependence of Connexin40 Gap Junction Channels. *Circulation Research*, 88(7). <https://doi.org/10.1161/hh0701.088833>
- Ardiles, A. O., Flores-Muñoz, C., Toro-Ayala, G., Cárdenas, A. M., Palacios, A. G., Muñoz, P., Fuenzalida, M., Sáez, J. C., & Martínez, A. D. (2014). Pannexin 1 regulates bidirectional hippocampal synaptic plasticity in adult mice. *Frontiers in Cellular Neuroscience*, 8. <https://doi.org/10.3389/fncel.2014.00326>
- Bao, L., Locovei, S., & Dahl, G. (2004). Pannexin membrane channels are mechanosensitive conduits for ATP. *FEBS Letters*, 572(1–3), 65–68. <https://doi.org/10.1016/j.febslet.2004.07.009>
- Baranova, A., Ivanov, D., Petrash, N., Pestova, A., Skoblov, M., Kelmanson, I., Shagin, D., Nazarenko, S., Geraymovych, E., Litvin, O., Tiunova, A., Born, T. L., Usman, N., Staroverov, D., Lukyanov, S., & Panchin, Y. (2004). The mammalian pannexin family is homologous to the invertebrate innexin gap junction proteins. *Genomics*, 83(4), 706–716. <https://doi.org/10.1016/j.ygeno.2003.09.025>
- Biechl, D., Tietje, K., Ryu, S., Grothe, B., Gerlach, G., & Wullimann, M. F. (2017). Identification of accessory olfactory system and medial amygdala in the zebrafish. *Scientific Reports*, 7(1). <https://doi.org/10.1038/srep44295>
- Bloomfield, S. A., Xin, D., & Persky, S. E. (1995). A comparison of receptive field and tracer coupling size of horizontal cells in the rabbit retina. *Visual Neuroscience*, 12(5). <https://doi.org/10.1017/S0952523800009524>
- Boassa, D., Ambrosi, C., Qiu, F., Dahl, G., Gaietta, G., & Sosinsky, G. (2007). Pannexin1 channels contain a glycosylation site that targets the hexamer to the plasma membrane. *The Journal of Biological Chemistry*, 282(43), 31733–31743. <https://doi.org/10.1074/jbc.M702422200>
- Boassa, D., Qiu, F., Dahl, G., & Sosinsky, G. (2008). Trafficking dynamics of glycosylated pannexin 1 proteins. *Cell Communication & Adhesion*, 15(1), 119–132. <https://doi.org/10.1080/15419060802013885>
- Bond, S. R., Wang, N., Leybaert, L., & Naus, C. C. (2012). Pannexin 1 Ohnologs in the Teleost Lineage. *The Journal of Membrane Biology*, 245(8). <https://doi.org/10.1007/s00232-012-9497-4>
- Bruzzone, R., Hormuzdi, S. G., Barbe, M. T., Herb, A., & Monyer, H. (2003). Pannexins, a family of gap junction proteins expressed in brain. *Proceedings of the National Academy of Sciences of the United States of America*, 100(23), 13644–13649. <https://doi.org/10.1073/pnas.2233464100>
- Burnstock, G. (2006). Historical review: ATP as a neurotransmitter. *Trends in Pharmacological Sciences*, 27(3). <https://doi.org/10.1016/j.tips.2006.01.005>
- Burnstock, G. (2018). Purine and purinergic receptors. *Brain and Neuroscience Advances*, 2. <https://doi.org/10.1177/2398212818817494>
- Burnstock, G. (2020). *Introduction to Purinergic Signalling in the Brain*. https://doi.org/10.1007/978-3-030-30651-9_1

- Carlen, P. L. (2012). Curious and contradictory roles of glial connexins and pannexins in epilepsy. *Brain Research*, *1487*, 54–60. <https://doi.org/10.1016/j.brainres.2012.06.059>
- Celetti, S. J., Cowan, K. N., Penuela, S., Shao, Q., Churko, J., & Laird, D. W. (2010). Implications of pannexin 1 and pannexin 3 for keratinocyte differentiation. *Journal of Cell Science*, *123*(8). <https://doi.org/10.1242/jcs.056093>
- Cenedese, V., de Graaff, W., Csikós, T., Poovayya, M., Zoidl, G., & Kamermans, M. (2017). Pannexin 1 Is Critically Involved in Feedback from Horizontal Cells to Cones. *Frontiers in Molecular Neuroscience*, *10*. <https://doi.org/10.3389/fnmol.2017.00403>
- Chiu, Y.-H., Jin, X., Medina, C. B., Leonhardt, S. A., Kiessling, V., Bennett, B. C., Shu, S., Tamm, L. K., Yeager, M., Ravichandran, K. S., & Bayliss, D. A. (2017). A quantized mechanism for activation of pannexin channels. *Nature Communications*, *8*(1). <https://doi.org/10.1038/ncomms14324>
- Chuah, M. I., & Zheng, D. R. (1992). The human primary olfactory pathway: fine structural and cytochemical aspects during development and in adults. *Microscopy Research and Technique*, *23*(1), 76–85. <https://doi.org/10.1002/jemt.1070230107>
- Coppi, E., Cellai, L., Maraula, G., Pugliese, A. M., & Pedata, F. (2013). Adenosine A2A receptors inhibit delayed rectifier potassium currents and cell differentiation in primary purified oligodendrocyte cultures. *Neuropharmacology*, *73*. <https://doi.org/10.1016/j.neuropharm.2013.05.035>
- Cotrina, M. L., Lin, J. H.-C., & Nedergaard, M. (1998). Cytoskeletal Assembly and ATP Release Regulate Astrocytic Calcium Signaling. *The Journal of Neuroscience*, *18*(21). <https://doi.org/10.1523/JNEUROSCI.18-21-08794.1998>
- Dahl, G. (2015). ATP release through pannexon channels. *Philosophical Transactions of the Royal Society B: Biological Sciences*, *370*(1672), 20140191. <https://doi.org/10.1098/rstb.2014.0191>
- Davis, L. K., Gamazon, E. R., Kistner-Griffin, E., Badner, J. A., Liu, C., Cook, E. H., Sutcliffe, J. S., & Cox, N. J. (2012). Loci nominally associated with autism from genome-wide analysis show enrichment of brain expression quantitative trait loci but not lymphoblastoid cell line expression quantitative trait loci. *Molecular Autism*, *3*(1). <https://doi.org/10.1186/2040-2392-3-3>
- Deng, Z., He, Z., Makshev, G., Bitter, R. M., Rau, M., Fitzpatrick, J. A. J., & Yuan, P. (2020). Cryo-EM structures of the ATP release channel pannexin 1. *Nature Structural & Molecular Biology*, *27*(4). <https://doi.org/10.1038/s41594-020-0401-0>
- Dourado, M., Wong, E., & Hackos, D. H. (2014). Pannexin-1 Is Blocked by Its C-Terminus through a Delocalized Non-Specific Interaction Surface. *PLoS ONE*, *9*(6). <https://doi.org/10.1371/journal.pone.0099596>
- Dufresne, J., & Cyr, D. G. (2014). Regulation of the Pannexin-1 Promoter in the Rat Epididymis 1. *Biology of Reproduction*, *91*(6). <https://doi.org/10.1095/biolreprod.114.122168>
- Dvorianchikova, G., Ivanov, D., Pestova, A., & Shestopalov, V. (2006). Molecular characterization of pannexins in the lens. *Molecular Vision*, *12*, 1417–1426. <http://www.ncbi.nlm.nih.gov/pubmed/17149368>
- Ekstrom, A. D. (2015). Why vision is important to how we navigate. *Hippocampus*, *25*(6). <https://doi.org/10.1002/hipo.22449>
- Engel, T., Alves, M., Sheedy, C., & Henshall, D. C. (2016). ATPergic signalling during seizures and epilepsy. *Neuropharmacology*, *104*. <https://doi.org/10.1016/j.neuropharm.2015.11.001>
- Gulbransen, B. D., Bashashati, M., Hirota, S. A., Gui, X., Roberts, J. A., MacDonald, J. A., Muruve, D. A., McKay, D. M., Beck, P. L., Mawe, G. M., Thompson, R. J., & Sharkey, K. A. (2012).

- Activation of neuronal P2X7 receptor–pannexin-1 mediates death of enteric neurons during colitis. *Nature Medicine*, 18(4). <https://doi.org/10.1038/nm.2679>
- Halpern, M. (1987). The Organization and Function of the Vomeronasal System. *Annual Review of Neuroscience*, 10(1). <https://doi.org/10.1146/annurev.ne.10.030187.001545>
- Housley, G. D., Bringmann, A., & Reichenbach, A. (2009). Purinergic signaling in special senses. *Trends in Neurosciences*, 32(3). <https://doi.org/10.1016/j.tins.2009.01.001>
- Iglesias, R., Locovei, S., Roque, A., Alberto, A. P., Dahl, G., Spray, D. C., & Scemes, E. (2008). P2X7 receptor-Pannexin1 complex: pharmacology and signaling. *American Journal of Physiology. Cell Physiology*, 295(3), C752-60. <https://doi.org/10.1152/ajpcell.00228.2008>
- Ishikawa, M., Iwamoto, T., Nakamura, T., Doyle, A., Fukumoto, S., & Yamada, Y. (2011). Pannexin 3 functions as an ER Ca²⁺ channel, hemichannel, and gap junction to promote osteoblast differentiation. *Journal of Cell Biology*, 193(7). <https://doi.org/10.1083/jcb.201101050>
- Ishikawa, M., Williams, G. L., Ikeuchi, T., Sakai, K., Fukumoto, S., & Yamada, Y. (2016). Pannexin 3 and connexin 43 modulate skeletal development via distinct functions and expression patterns. *Journal of Cell Science*. <https://doi.org/10.1242/jcs.176883>
- Jia, C; Doherty, P; Crudgington, S; Hegg, C. (2009). Activation of purinergic receptors induces proliferation and neuronal differentiation in swiss webster mouse olfactory epithelium. *Neuroscience*, 163, 102–128.
http://journals2.scholarsportal.info/pdf/03064522/v163i0001/120_aopripiswmoe.xml
- Jiang, T., Long, H., Ma, Y., Long, L., Li, Y., Li, F., Zhou, P., Yuan, C., & Xiao, B. (2013). Altered expression of pannexin proteins in patients with temporal lobe epilepsy. *Molecular Medicine Reports*. <https://doi.org/10.3892/mmr.2013.1739>
- Kamkin, A., Kiseleva, I., Lozinsky, I., & Scholz, H. (2005). Electrical interaction of mechanosensitive fibroblasts and myocytes in the heart. *Basic Research in Cardiology*, 100(4). <https://doi.org/10.1007/s00395-005-0529-4>
- Kawamura, M., Ruskin, D. N., & Masino, S. A. (2010). Metabolic Autocrine Regulation of Neurons Involves Cooperation among Pannexin Hemichannels, Adenosine Receptors, and KATP Channels. *Journal of Neuroscience*, 30(11). <https://doi.org/10.1523/JNEUROSCI.0055-10.2010>
- Kim, J.-E., & Kang, T.-C. (2011). The P2X7 receptor–pannexin-1 complex decreases muscarinic acetylcholine receptor–mediated seizure susceptibility in mice. *Journal of Clinical Investigation*, 121(5). <https://doi.org/10.1172/JCI44818>
- Kurtenbach, S., Whyte-Fagundes, P., Gelis, L., Kurtenbach, S., Brazil, É., Zoidl, C., Hatt, H., Shestopalov, V. I., & Zoidl, G. (2014). Investigation of olfactory function in a Panx1 knock out mouse model. *Frontiers in Cellular Neuroscience*, 8. <https://doi.org/10.3389/fncel.2014.00266>
- Kurtenbach, Sarah, Prochnow, N., Kurtenbach, S., Klooster, J., Zoidl, C., Dermietzel, R., Kamermans, M., & Zoidl, G. (2013). Pannexin1 Channel Proteins in the Zebrafish Retina Have Shared and Unique Properties. *PLoS ONE*, 8(10). <https://doi.org/10.1371/journal.pone.0077722>
- Lee, C.-Y. (1992). On the activation-inactivation coupling in *Shaker* potassium channels. *FEBS Letters*, 306(2–3). [https://doi.org/10.1016/0014-5793\(92\)80976-N](https://doi.org/10.1016/0014-5793(92)80976-N)
- Li, S., Zang, Z., He, J., Chen, X., Yu, S., Pei, Y., Hou, Z., An, N., Yang, H., Zhang, C., & Liu, S. (2017). Expression of pannexin 1 and 2 in cortical lesions from intractable epilepsy patients with focal cortical dysplasia. *Oncotarget*, 8(4). <https://doi.org/10.18632/oncotarget.14317>
- Locovei, S., Bao, L., & Dahl, G. (2006). Pannexin 1 in erythrocytes: Function without a gap. *Proceedings of the National Academy of Sciences*, 103(20). <https://doi.org/10.1073/pnas.0601037103>

- Locovei, Silviu, Scemes, E., Qiu, F., Spray, D. C., & Dahl, G. (2007). Pannexin1 is part of the pore forming unit of the P2X7 receptor death complex. *FEBS Letters*, *581*(3), 483–488. <https://doi.org/10.1016/j.febslet.2006.12.056>
- Locovei, Silviu, Wang, J., & Dahl, G. (2006). Activation of pannexin 1 channels by ATP through P2Y receptors and by cytoplasmic calcium. *FEBS Letters*, *580*(1), 239–244. <https://doi.org/10.1016/j.febslet.2005.12.004>
- Lohman, A. W., Weaver, J. L., Billaud, M., Sandilos, J. K., Griffiths, R., Straub, A. C., Penuela, S., Leitinger, N., Laird, D. W., Bayliss, D. A., & Isakson, B. E. (2012). S-Nitrosylation Inhibits Pannexin 1 Channel Function. *Journal of Biological Chemistry*, *287*(47). <https://doi.org/10.1074/jbc.M112.397976>
- Lopatář, J., Dale, N., & Frenguelli, B. G. (2015). Pannexin-1-mediated ATP release from area CA3 drives mGlu5-dependent neuronal oscillations. *Neuropharmacology*, *93*. <https://doi.org/10.1016/j.neuropharm.2015.01.014>
- McBride, T. A., Stockert, B. W., Gorin, F. A., & Carlsen, R. C. (2000). Stretch-activated ion channels contribute to membrane depolarization after eccentric contractions. *Journal of Applied Physiology*, *88*(1). <https://doi.org/10.1152/jappl.2000.88.1.91>
- Mendoza-Fernandez, V., Andrew, R. D., & Barajas-López, C. (2000). ATP inhibits glutamate synaptic release by acting at P2Y receptors in pyramidal neurons of hippocampal slices. *The Journal of Pharmacology and Experimental Therapeutics*, *293*, 172–179.
- Michalski, K., & Kawate, T. (2016). Carbenoxolone inhibits Pannexin1 channels through interactions in the first extracellular loop. *Journal of General Physiology*, *147*(2). <https://doi.org/10.1085/jgp.201511505>
- Michalski, K., Syrjanen, J. L., Henze, E., Kumpf, J., Furukawa, H., & Kawate, T. (2020). The Cryo-EM structure of pannexin 1 reveals unique motifs for ion selection and inhibition. *ELife*, *9*. <https://doi.org/10.7554/eLife.54670>
- Mim, C., Perkins, G., & Dahl, G. (2021). Structure versus function: Are new conformations of pannexin 1 yet to be resolved? *Journal of General Physiology*, *153*(5). <https://doi.org/10.1085/jgp.202012754>
- Miras-Portugal, M. T., Sebastián-Serrano, Á., de Diego García, L., & Díaz-Hernández, M. (2017). Neuronal P2X7 Receptor: Involvement in Neuronal Physiology and Pathology. *The Journal of Neuroscience*, *37*(30). <https://doi.org/10.1523/JNEUROSCI.3104-16.2017>
- Moreno, A. P., Chanson, M., Anumonwo, J., Scerri, I., Gu, H., Taffet, S. M., & Delmar, M. (2002). Role of the Carboxyl Terminal of Connexin43 in Transjunctional Fast Voltage Gating. *Circulation Research*, *90*(4). <https://doi.org/10.1161/hh0402.105667>
- Mou, L., Ke, M., Song, M., Shan, Y., Xiao, Q., Liu, Q., Li, J., Sun, K., Pu, L., Guo, L., Geng, J., Wu, J., & Deng, D. (2020). Structural basis for gating mechanism of Pannexin 1 channel. *Cell Research*, *30*(5). <https://doi.org/10.1038/s41422-020-0313-x>
- Mylvaganam, S., Ramani, M., Krawczyk, M., & Carlen, P. L. (2014). Roles of gap junctions, connexins, and pannexins in epilepsy. *Frontiers in Physiology*, *5*(172), 1–12. <https://doi.org/10.3389/fphys.2014.00172>
- Mylvaganam, S., Zhang, L., Wu, C., Zhang, Z. J., Samoilova, M., Eubanks, J., Carlen, P. L., & Poulter, M. O. (2010). Hippocampal seizures alter the expression of the pannexin and connexin transcriptome. *Journal of Neurochemistry*, *112*(1). <https://doi.org/10.1111/j.1471-4159.2009.06431.x>

- Panchina, Y., Kelmanson, I., Matz, M., Lukyanov, K., Usman, N., & Lukyanov, S. (2000). A ubiquitous family of putative gap junction molecules [2]. *Current Biology*, *10*(13), 473–474. [https://doi.org/10.1016/S0960-9822\(00\)00576-5](https://doi.org/10.1016/S0960-9822(00)00576-5)
- Pelegri, P., & Surprenant, A. (2006). Pannexin-1 mediates large pore formation and interleukin-1 β release by the ATP-gated P2X₇ receptor. *The EMBO Journal*, *25*(21), 5071–5082. <https://doi.org/10.1038/sj.emboj.7601378>
- Penuela, S., Bhalla, R., Gong, X.-Q., Cowan, K. N., Celetti, S. J., Cowan, B. J., Bai, D., Shao, Q., & Laird, D. W. (2007). Pannexin 1 and pannexin 3 are glycoproteins that exhibit many distinct characteristics from the connexin family of gap junction proteins. *Journal of Cell Science*, *120*(Pt 21), 3772–3783. <https://doi.org/10.1242/jcs.009514>
- Penuela, S., Gehi, R., & Laird, D. W. (2013). The biochemistry and function of pannexin channels. *Biochimica et Biophysica Acta (BBA) - Biomembranes*, *1828*(1), 15–22. <https://doi.org/10.1016/j.bbamem.2012.01.017>
- Penuela, S., Gyenis, L., Ablack, A., Churko, J. M., Berger, A. C., Litchfield, D. W., Lewis, J. D., & Laird, D. W. (2012). Loss of Pannexin 1 Attenuates Melanoma Progression by Reversion to a Melanocytic Phenotype. *Journal of Biological Chemistry*, *287*(34). <https://doi.org/10.1074/jbc.M112.377176>
- Pérez-Gómez, A., Stein, B., Leinders-Zufall, T., & Chamero, P. (2014). Signaling mechanisms and behavioral function of the mouse basal vomeronasal neuroepithelium. *Frontiers in Neuroanatomy*, *8*, 135. <https://doi.org/10.3389/fnana.2014.00135>
- Prochnow, N., Hoffmann, S., Vroman, R., Klooster, J., Bunse, S., Kamermans, M., Dermietzel, R., & Zoidl, G. (2009). Pannexin1 in the outer retina of the zebrafish, *Danio rerio*. *Neuroscience*, *162*(4). <https://doi.org/10.1016/j.neuroscience.2009.04.064>
- Prochnow, N., Abdulazim, A., Kurtenbach, S., Wildförster, V., Dvorianchikova, G., Hanske, J., Petrasch-Parwez, E., Shestopalov, V. I., Dermietzel, R., Manahan-Vaughan, D., & Zoidl, G. (2012). Pannexin1 Stabilizes Synaptic Plasticity and Is Needed for Learning. *PLoS ONE*, *7*(12). <https://doi.org/10.1371/journal.pone.0051767>
- Puthussery, T., Yee, P., Vingrys, A. J., & Fletcher, E. L. (2006). Evidence for the involvement of purinergic P2X₇ receptors in outer retinal processing. *European Journal of Neuroscience*, *24*(1). <https://doi.org/10.1111/j.1460-9568.2006.04895.x>
- Qiu, F., & Dahl, G. (2009). A permeant regulating its permeation pore: inhibition of pannexin 1 channels by ATP. *American Journal of Physiology-Cell Physiology*, *296*(2). <https://doi.org/10.1152/ajpcell.00433.2008>
- Qu, R., Dong, L., Zhang, J., Yu, X., Wang, L., & Zhu, S. (2020). Cryo-EM structure of human heptameric Pannexin 1 channel. *Cell Research*, *30*(5). <https://doi.org/10.1038/s41422-020-0298-5>
- Rahman, S. (2015). Pathophysiology of mitochondrial disease causing epilepsy and status epilepticus. *Epilepsy & Behavior*, *49*. <https://doi.org/10.1016/j.yebeh.2015.05.003>
- Ray, A., Zoidl, G., Weickert, S., Wahle, P., & Dermietzel, R. (2005). Site-specific and developmental expression of pannexin1 in the mouse nervous system. *European Journal of Neuroscience*, *21*(12). <https://doi.org/10.1111/j.1460-9568.2005.04139.x>
- Ruan, Z., Orozco, I. J., Du, J., & Lü, W. (2020). Structures of human pannexin 1 reveal ion pathways and mechanism of gating. *Nature*, *584*(7822). <https://doi.org/10.1038/s41586-020-2357-y>
- Rummery, N. M., Brock, J. A., Pakdeechote, P., Ralevic, V., & Dunn, W. R. (2007). ATP is the predominant sympathetic neurotransmitter in rat mesenteric arteries at high pressure. *The Journal of Physiology*, *582*(2). <https://doi.org/10.1113/jphysiol.2007.134825>

- Salazar, I., Sánchez-Quinteiro, P., Alemañ, N., & Prieto, D. (2008). Anatomical, immunohistochemical and physiological characteristics of the vomeronasal vessels in cows and their possible role in vomeronasal reception. *Journal of Anatomy*, *212*(5). <https://doi.org/10.1111/j.1469-7580.2008.00889.x>
- Sandilos, J. K., Chiu, Y.-H., Chekeni, F. B., Armstrong, A. J., Walk, S. F., Ravichandran, K. S., & Bayliss, D. A. (2012). Pannexin 1, an ATP Release Channel, Is Activated by Caspase Cleavage of Its Pore-associated C-terminal Autoinhibitory Region. *Journal of Biological Chemistry*, *287*(14). <https://doi.org/10.1074/jbc.M111.323378>
- Santiago, M. F., Veliskova, J., Patel, N. K., Lutz, S. E., Caille, D., Charollais, A., Meda, P., & Scemes, E. (2011). Targeting Pannexin1 Improves Seizure Outcome. *PLoS ONE*, *6*(9). <https://doi.org/10.1371/journal.pone.0025178>
- Sosinsky, G. E., Boassa, D., Dermietzel, R., Duffy, H. S., Laird, D. W., MacVicar, B., Naus, C. C., Penuela, S., Scemes, E., Spray, D. C., Thompson, R. J., Zhao, H. B., & Dahl, G. (2011). Pannexin channels are not gap junction hemichannels. *Channels (Austin, Tex.)*, *5*(3), 193–197. <https://doi.org/10.4161/chan.5.3.15765>
- Storan, M. J., & Key, B. (2006). Septal organ of Grüneberg is part of the olfactory system. *The Journal of Comparative Neurology*, *494*(5), 834–844. <https://doi.org/10.1002/cne.20858>
- Swayne, L. A., Sorbara, C. D., & Bennett, S. A. L. (2010). Pannexin 2 Is Expressed by Postnatal Hippocampal Neural Progenitors and Modulates Neuronal Commitment. *Journal of Biological Chemistry*, *285*(32). <https://doi.org/10.1074/jbc.M110.130054>
- Takigami, S. (2000). Projection Pattern of Vomeronasal Neurons to the Accessory Olfactory Bulb in Goats. *Chemical Senses*, *25*(4). <https://doi.org/10.1093/chemse/25.4.387>
- van Gelder, N. M., & Sherwin, A. L. (2003). Metabolic Parameters of Epilepsy: Adjuncts to Established Antiepileptic Drug Therapy. *Neurochemical Research*, *28*(2). <https://doi.org/10.1023/A:1022433421761>
- Vogt, B. A., Vogt, L., Farber, N. B., & Bush, G. (2005). Architecture and neurocytology of monkey cingulate gyrus. *The Journal of Comparative Neurology*, *485*(3). <https://doi.org/10.1002/cne.20512>
- Vroman, R., Klaassen, L. J., Howlett, M. H. C., Cenedese, V., Klooster, J., Sjoerdsma, T., & Kamermans, M. (2014). Extracellular ATP Hydrolysis Inhibits Synaptic Transmission by Increasing pH Buffering in the Synaptic Cleft. *PLoS Biology*, *12*(5). <https://doi.org/10.1371/journal.pbio.1001864>
- Wang, J., Ambrosi, C., Qiu, F., Jackson, D. G., Sosinsky, G., & Dahl, G. (2014). The membrane protein Pannexin1 forms two open-channel conformations depending on the mode of activation. *Science Signaling*, *7*(335), ra69. <https://doi.org/10.1126/scisignal.2005431>
- Wang, J., Ma, M., Locovei, S., Keane, R. W., & Dahl, G. (2007). Modulation of membrane channel currents by gap junction protein mimetic peptides: size matters. *American Journal of Physiology. Cell Physiology*, *293*(3), C1112-9. <https://doi.org/10.1152/ajpcell.00097.2007>
- Wei, L., Sheng, H., Chen, L., Hao, B., Shi, X., & Chen, Y. (2016). Effect of pannexin-1 on the release of glutamate and cytokines in astrocytes. *Journal of Clinical Neuroscience*, *23*. <https://doi.org/10.1016/j.jocn.2015.05.043>
- Whyte-Fagundes, P., Kurtenbach, S., Zoidl, C., Shestopalov, V. I., Carlen, P. L., & Zoidl, G. (2018). A Potential Compensatory Role of Panx3 in the VNO of a Panx1 Knock Out Mouse Model. *Frontiers in Molecular Neuroscience*, *11*. <https://doi.org/10.3389/fnmol.2018.00135>
- Whyte-Fagundes, P., Siu, R., Brown, C., & Zoidl, G. (2019). Pannexins in vision, hearing, olfaction and taste. *Neuroscience Letters*, *695*. <https://doi.org/10.1016/j.neulet.2017.05.010>

- Wicki-Stordeur, L. E., & Swayne, L. (2013). Panx1 regulates neural stem and progenitor cell behaviours associated with cytoskeletal dynamics and interacts with multiple cytoskeletal elements. *Cell Communication and Signaling*, *11*(1). <https://doi.org/10.1186/1478-811X-11-62>
- Xia, J., Lim, J. C., Lu, W., Beckel, J. M., Macarak, E. J., Laties, A. M., & Mitchell, C. H. (2012). Neurons respond directly to mechanical deformation with pannexin-mediated ATP release and autostimulation of P2X₇ receptors. *The Journal of Physiology*, *590*(10). <https://doi.org/10.1113/jphysiol.2012.227983>
- Yeung, A. K., Patil, C. S., & Jackson, M. F. (2020). Pannexin-1 in the CNS: Emerging concepts in health and disease. *Journal of Neurochemistry*, *154*(5). <https://doi.org/10.1111/jnc.15004>
- Zappalà, A., Li Volti, G., Serapide, M. F., Pellitteri, R., Falchi, M., la Delia, F., Cicirata, V., & Cicirata, F. (2007). Expression of pannexin2 protein in healthy and ischemized brain of adult rats. *Neuroscience*, *148*(3). <https://doi.org/10.1016/j.neuroscience.2007.06.028>
- Zhang, C. (2011). Expression of connexin 57 in the olfactory epithelium and olfactory bulb. *Neuroscience Research*, *71*(3), 226–234. <https://doi.org/10.1016/j.neures.2011.07.1832>
- Zhang, Y., Laumet, G., Chen, S.-R., Hittelman, W. N., & Pan, H.-L. (2015). Pannexin-1 Up-regulation in the Dorsal Root Ganglion Contributes to Neuropathic Pain Development. *Journal of Biological Chemistry*, *290*(23). <https://doi.org/10.1074/jbc.M115.650218>
- Zoidl, G., Kremer, M., Zoidl, C., Bunse, S., & Dermietzel, R. (2008). Molecular Diversity of Connexin and Pannexin Genes in the Retina of the Zebrafish *Danio rerio*. *Cell Communication & Adhesion*, *15*(1–2). <https://doi.org/10.1080/15419060802014081>

APPENDICES

Appendix A: Plasmid maps

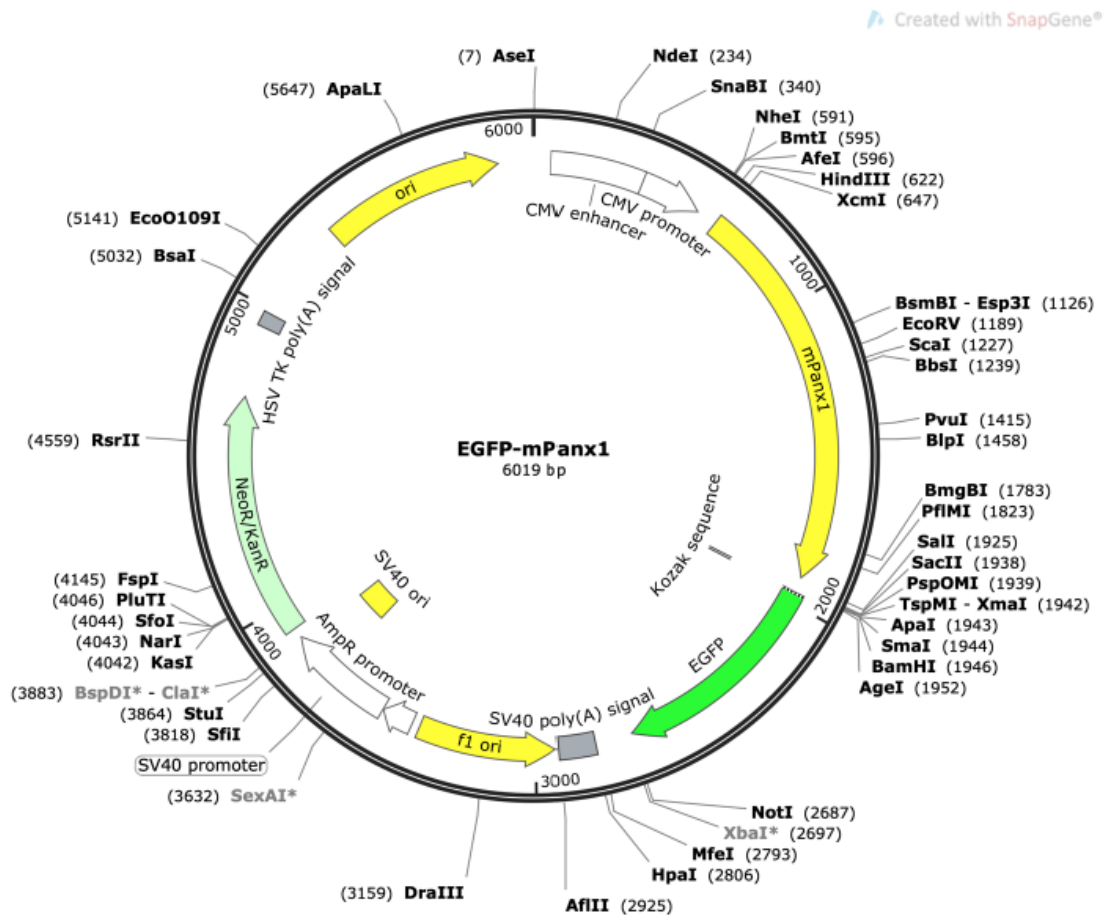


Figure A.3.4: Gene map of pEGFP-mPax1 indicating insert and various regions of expressions.

Appendix B: Phase Amplitude Coupling (PAC) for Pax1^{-/-} and pharmacological blocking compared to WT

PAC was quantified further by examining the median PAC across slices. WT slices treated with 4-AP demonstrated several frequency pairings of increased coupling (**Figure 6.1a**). From these pairings, delta-gamma (Alvarado-Rojas et al., 2015; Buzsáki & Wang, 2012) and delta-HF (Guirgis et al., 2013) PAC are relevant to epilepsy. However, for KO slices, median PAC did not exceed

thresholds above the baseline mean; as such, no coupling was present (**Figure 6.1b**). A similar absence of coupling was observed in WT mice pretreated with BB (**Figure 6.1c**) or Pb (**Figure 6.1d**) prior to 4-AP application. Taken together, these findings suggest that Panx1 activity contributes to the presence of delta-gamma or delta-HF cross-frequency coupling associated with hyperexcitability (Grigorovsky et al., 2020). This analysis was completed by Mark Aquilino from Dr. Peter Carlens lab, figure was adapted by PW-F to show only relevant portions for this thesis.

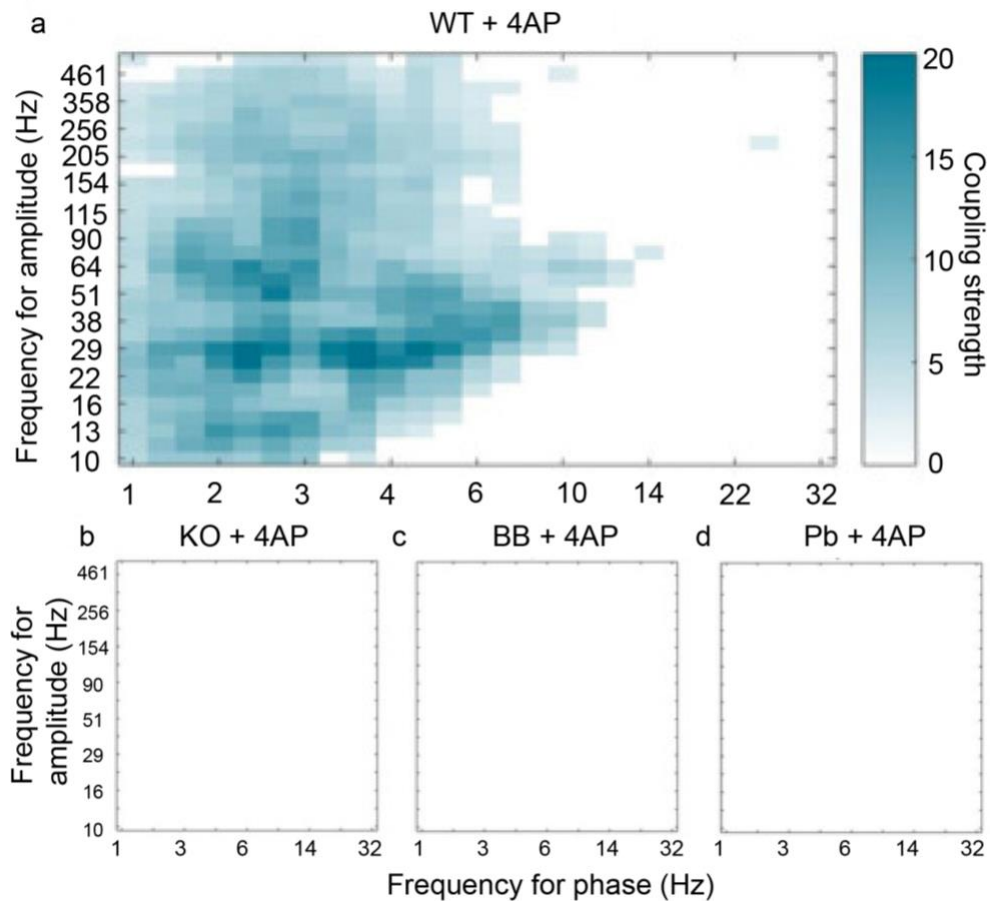


Figure 6.1. Median phase-amplitude cross frequency coupling comodulograms for the in vitro 4-AP slice model following z-score normalization to baseline conditions. a Cortical slices from WT mice incubated with 4AP showed a phase-amplitude coupling of delta to high frequency. **b** Cortical slices from Panx1 KO incubated with 4AP demonstrated reduced phase-amplitude coupling compared to WT counterparts. Coupling of delta phase to high frequency amplitude was also absent in WT slices pretreated with Panx1 blockers **c** BB-FCF and **d** probenecid. This finding is indicative of reduced epileptiform activity in the absence of functional Panx1. Coupling strength indicated to the right of comodulogram. Figure adapted from Aquilino et al., 2020.

Table 6: Multialignment sequencing showing residues of conservation for the entire Panx1 sequence.

human	MAIAQLATEYVFSDFLLKE-PTEPKFKGLRLELAVDKMVTICIAVGLPLLLISLAFQAQEIS	59
chimpanzee	MAIAHLATEYVFSDFLLKE-PTEPKFKGLRLELAVDKMVTICIAVGLPLLLISLAFQAQEIS	59
pongo	MAIAHLATEYVFSDFLLKE-PTEPKFKGLRLELAVDKMVTICIAVGLPLLLISLAFQAQEIS	59
bos	MAIAHLATEYVFSDFLLKE-PSEAKFKGLRLELAVDKMVTICIAVGLPLLLVSLAFQAQEIS	59
sheep	MAIAHLATEYVFSDFLLKE-PSEPKFKGLRLELAVDKMVTICIAVGLPLLLISLAFQAQEIS	59
dolphin	MAIAHLATEYVFSDFLLKE-PSEPKFKGLRLELAVDKMVTICIAVGLPLLLISLAFQAQEIS	59
mus	MAIAHLATEYVFSDFLLKE-PTEPKFKGLRLELAVDKMVTICIAVGLPLLLISLAFQAQEIS	59
rabbit	MAIAHLATEYVFSDFLLKE-PAEPKFKGLRLELAVDKMVTICIAVGLPLLLISLAFQAQEIS	59
gallus	-----E-PPETRYKGLRLELALDKIVTCIAVGLPLLLISLAFQAQEV	41
xenopus	MAIAHIAATEYVFSDFLLKD-PPESKYKGLRLELAVDKLVSCIAVGLPLLLISLAFQAQEIT	59
fishA	MAIAHAATEYVFADFVLDPAENRYKGIKIRLDLALDKIVTCVAVGLPLLLISLAFQAQEV	60
fishB	MAIARVATEYVFSDFLLKE-QSDSKYKGVRLATDKLVSFIAVGLPLLLISLAFQAQEV	59
	: .: :*:**:*:* **:*::*****:*****::	
human	IGTQISCFSPSSFSWRQAAFVDSYCWAAVQQKNSLQSESGNLPWLHKFFPYILLFAIL	119
chimpanzee	IGTQISCFSPSSFSWRQAAFVDSYCWAAVQQKNSLQSESGNLPWLHKFFPYILLFAIL	119
pongo	IGTQISCFSPSSFSWRQAAFVDSYCWAAVQQKNSLQSESGNLPWLHKFFPYILLFAIL	119
bos	IGTQISCFSPSSFSWRQASFVDSYCWAAVQQKDSLQGDGSGNLPCLHKFFPYILLVAIL	119
sheep	IGTQISCFSPSSFSWRQASFVDSYCWAAVQQKDSLQGDGSGNLPCLHKFFPYILLVAIL	119
dolphin	IGTQISCFSPSSFSWRQASFVDSYCWAAVQQKDSLQGDGSGNLPCLHKFFPYILLVAIL	119
mus	IGTQISCFSPSSFSWRQAAFVDSYCWAAVQQKSSLQSESGNLPWLHKFFPYILLFAIL	119
rabbit	IGTQISCFSPSSFSWRQAAFVDSYCWAAVQQKESLRSDSGNLPWLHKFFPYILLFAIL	119
gallus	PRAQISCFAPSSFSWRQAAVDSYCWAAVQQKQPAYNNPENIPLWLHKFFPYILLVAIL	101
xenopus	LGSQISCFAPTSFSWRQAAVDSYFCWAAVQQKHLSDSGNVPLWLHKFFPYILLVAVL	119
fishA	VGTQISCFAPTAFSWCQAAVDSYCWAAVQKQ----DTGGLPLWLHKFFPYILLVAVS	115
fishB	VGTQITCFPPTNFTMRQAAVADSFCAAVEHHPSE-ENETYSAPLHLHKFFPYILLLAIL	118
	:**:*:*.*: * : **::**:*:*:*::: . . ** *****.*:	
human	LYLPPLFWRFAAAPHICSDLKFIMEELDKVYNRAIKAAKSARDLDMRDGACSV---PGVT	176
chimpanzee	LYLPPLFWRFAAAPHICSDLKFIMEELDKVYNRAIKAAKSVRDLDMRDGAACSV---PGVT	176
pongo	LYLPPLFWRFAAAPHICSDLKFIMEELDKVYNRAIKAAKSARDLDMRDGACSV---PGVT	176
bos	LYLPPLFWRFAAAPHVCSLDKFIMEELDKVYNRAIKAAKSMHDLDLRDGACPA---PEVN	176
sheep	LYLPPLFWRFAAAPHVCSLDKFIMEELDKVYNRAIKAAKSMHDLDLRDGACPV---PEVN	176
dolphin	LYLPPLFWRFAAVPHLCSLDKFIMEELDKVYNRAIKAAKSVRDLDLRDGAACPA---QEVN	176
mus	LYLPALFWRFAAAPHLCSLDKFIMEELDKVYNRAIKAAKSARDLDLRDGPGP----PGVT	175
rabbit	LYLPPLFWRFAAAPHLCSLDKFIMEELDKVYNRAIKAAKSARNLDLTDGVCAPGFPVVK	179
gallus	LYLPCLFWRFTAAPHLSSDLKFIMEELDKAYNRAIKAANSVRSRDPDPADSI---PAAN	158
xenopus	LYLPNLFWRFTAAPHLSSDLKFIMEELDKCYNRDIKDIKAANNLNSSDKRDGLN-SPVVS	178
fishA	VYMPALFWRFTGAPVLSDDLTFIMEELDRSYNRAIKLAKCLHTAGKVETPPAP-----	168
fishB	MYIPALFWRFTAAPSLSSDLKFIMEELDRCYNRAIRLAKSITTKQDKDIAEDP-----	171
	:*:* *****:.* :.*:*:*:*:*:*: ** * : . . :	

human	ENLGQSLWEVSESHFKYPIVEQYLKTKKNSNNLI IKYISCRLLTLII IILLACIYLGYYFS	236
chimpanzee	ENLGQSLWEVSDSHFKYPIVEQYLKTKKNSNNLI IKYISCRLLTLII IILLACIYLGYYFS	236
pongo	ENLRQSLWEVSESHFKYPIVEQYLKTKKNSNNLI IKYISCRLLTLII IILLACIYLGYYFS	236
bos	ENMRQS---SQESHFRYPIVEQYLRTKKASRH LIVKYMSCRVLSTILLASLYLGYYS	233
sheep	ENMQS---SQESHFRYPIVERYLRTKKASRH LIVKYMSCRVLSTILLASIYLGYYLS	233
dolphin	ENLGQSLWEISESHFKYPIVEQYLKTKKNSKNLIVKY ISCRVLSLSI ILLAGVYLGYYFS	236
mus	ENVGQSLWEISESHFKYPIVEQYLKTKKNSHLMKY ISCRVTFV VILLACIYLSYYFS	235
rabbit	ENVGQSLWEISESHFKYPIVEQYLKTKKNSHRLIAEYLGCRLLTLAIVLVACVYLGYYFS	239
gallus	ENLTQSLWEISDSHFYPIVEQYLKTKKNSKCLII KYIFCRLLTLV IIFIACLYLGYYIS	218
xenopus	ENLQQSLWEIPLSHYKYPIVEQYLKTKNNSYGLII KYLICRVVTLII VFTACIYLGYYIS	238
fishA	VDTNSSVIDLTESYFKYPLVEQYLRTKRYSKGLLIRYLLCRTITVLALTLACIYLCYYIS	228
fishB	HSG----LELTEACFKYPLVEQYLKTKRSSWALAAKYLLCRVLTFLTLLLGCFYLTYYIF	227
	. : : ** : ** : ** : ** . * * . * : * * : . : . . ** * * :	
human	LSSLSDEFVCSIKSGILRNDSTVPDQFQCKLI AVGIFQLLSVINLVVYVLLAPVVVYTLF	296
chimpanzee	LSSLSDEFVCSIKSGILRNDSTVPDQFQCKLI AVGIFQLLSVINLVVYVLLAPVVVYTLF	296
pongo	LSSLSGEFVCSIKSGILRNDSTVPDQFQCKLI AVGIFQLLSVINLVVYVLLAPVVVYTLF	296
bos	LSSLSDEFVCSIKSGILKNDSTVPDKFQCKLI AVGIFRLLSF INLVVYVMLVPVVVYSLF	293
sheep	LSSLSDEFVCSIKSGILKNDSTVPDKFQCKLI AVGIFRLLSF INLVVYVMLVPVVVYSLF	293
dolphin	LSSLSDEFICNIKSGILKNDSTVPDRFQCKLI AVGIFQLLSFINLVVYVLLAPLVVYTLF	296
mus	LSSLSDEFVCSIKSGVLRNDSTIPDRFQCKLI AVGIFQLLSINLIVYALLIPVVVYTF	295
rabbit	LSSLSDEFVCSVKSILRNDSSVPDQFQCKLI AVGVFQLLSLMNLLVYVLLAPVLVYTLF	299
gallus	LSSLSDEFVCSIKSGILRNDSTVPDQFQCKLI AVGVFQLLSINLIVYLLVMPVVYAMF	278
xenopus	LFSLTDEFVCSIKSGILRNDSTVPDQFQCKLI AVGVFQLLSINLIIYVLIIMPFI IYAML	298
fishA	-LSTTDEFVCSIKSGVLRNDSSVPDQFQCKLI AVGVFQLLSINLIVYLLVMPVVYAMF	287
fishB	WVSPDQFVCSIKSGILRNDSTVPDQFQCKLI AVGVFQLLSINLIVYLLVMPVVYAMF	287
	* : . : * * : : * : : * : : * * . * * * : * * : * * : * * : * * : : * : : :	
human	VPFRQKTD--VLKVYEILPTFD-VLHFKSEG-YNDLSLYNLFLEENI SEVKSYPKCLKVL	351
chimpanzee	VPFRQKTD--VLKVYEILPTFD-VMHFKSEG-YNDLSLYNLFLEENI SEVKSYPKCLKVL	351
pongo	VPFRQKTD--VLKVYEILPTFD-VLHFKSEG-YNDLSLYNLFLEENI SEVKSYPKCLKVL	351
bos	VPFQKMD--VLKVYEILPTFD-ILHLKLEG-YNDLSLYVLFLEENI SELKSYKCLKVL	348
sheep	VPFQKPD--VLKVYEILPTFD-VLHLKLEG-YNDLSLYVLFLEENI SELKSYKCLKVL	348
dolphin	VPFRQKTD--VLKVYEILPTFD-VLHFKSEG-YNDLSLYILFLEENI SELKSYKCLKVL	351
mus	IPFRQKTD--ILKVYEILPTFD-VLHFKSEG-YNDLSLYNLFLEENI SELKSYKCLKVL	350
rabbit	VPCRQKTD--VLKVYEILPTFD-VLQFQSEG-YNDLSLYNLFLEENVSELKSYKCLRVL	354
gallus	VPFWRNSG--ILKVYEILPTFD-VLKLKSKS-LDDLSIYLLFLEENVSELKSYKCLKVL	333
xenopus	VPFRTAN--VLKVYEVLPFTS-VQQAPSKT-YDDHSLFLLFLEENVSELKSYKFLKVL	353
fishA	VPFRTKG--FLKPFEMLPFTS-VMQFGQAT-WDDLALYLLFLEENLSELKSYKCLKVL	342
fishB	QPARQHQRGQFLRPYHLLPAFGHVLDLQPATRYDDLSIYLLFLEENLSELKSYKCLQVL	347
	* : . : * * : : * : : * : : * * . * * * : * * : * * : * * : * * : : * : : :	

human	ENIKSSG-QGIDPMLLLTNLGMKMDVVDGK----TP-MSAEM-REEQGNQTAELQGMN-	403
chimpanzee	ENIKSSG-QGIDPMLLLTNLGMKMDVVDGK----TP-MSAEM-REEQGNQTAELQAMN-	403
pongo	ENIKSSG-QGIDPMLLLTNLGMKMDVVDGK----TA-MSAET-REEHGNQTAELQAMN-	403
bos	ENIKSSC-QDVPMLLLTNFGMIKMDMVDGK----NP-EPVEMMVEELGDQTTELQDLN-	401
sheep	ENIKSSC-QDVPMLVLLTNLGMKMDMVDGK----NP-EPVEMTAEELGDQTTKLQDLN-	401
dolphin	ENIKSSC-QGIDPMLLLTNLGMKMDVVDGK----NP-EPAEM-AEEQGDQTADLKDLN-	403
mus	ENIKSNG-QGIDPMLLLTNLGMKMDIIDGK----IP-TSLQTKGEDQGSQRVEFKDLD-	403
rabbit	ENIKSSS-EGIDPMLLLTNLGMKMDVIDGK----TP-RPAEMTGEEPGSRVAELTVLTD	308
gallus	ENIAVS--EKFDVMQLLINLGTIKTDTVDGKPGTAVPGKPEETAVEELEKDATELQDRD-	390
xenopus	ENIKNTG-ENFDTIQYLTSGLTVKTDVVDGK----LAFKCTSEVPNNTEQNEVELTVQP-	407
fishA	ELLKEQGDESFDPMLLLRTLGQVKTDVVDGRLPQKDQKISSTNNGDTELKEFAPLLPED-	401
fishB	ELLSEGGEAAFDTMCLLRTLGQVKTDVVDKRRQAQTVN--GNPEIIVISEIKDVSVLLDDG-	404
	* : . * : * . : * : * * : * :	
human	--IDSETKANNGEKNARQRLLDSSC	426
chimpanzee	--IDSETKANNGEKNARQRLLDSSC	426
pongo	--IDGETKANNGEKNARQRLLNSSC	426
bos	--VHSETKISNREKNARQRLLDTSC	424
sheep	--VHSETKISNREKNARQRLLDTSC	424
dolphin	--GHSGTKINNGEQNARQRLLDTSC	426
mus	--LSSEAAANNGEKNSRQRLNPPSC	426
rabbit	FAEQSGAKATNGDKHARQRLLNSSC	433
gallus	---ASGHVSPKEDKCLRQRLIDSSC	412
xenopus	----SSDNAKTEEKVQRLLDSSC	428
fishA	---CLRKHED--EKAVRQRVI----	417
fishB	---VQADKSCSCVKDVRQRVV----	422
	: ***::	

PUBLICATIONS, PRESENTATIONS & CONFERENCES

“ A good designer has a lot in common with a good researcher. Both hunt for excellence and perfection. You have to really focus on the details, and you don't really know what the final result will be before you have it .”

- May-Britt Moser

Publications

- [1] **Whyte-Fagundes, P.**, Taskina, D., Safarian, N., Zoidl, C., Carlen, P., Donaldson, L., Zoidl, G. (2021) Panx1 channels promote both anti- and pro-seizure-like activities in the zebrafish via p2rx7 receptors and ATP signaling. *bioRxiv*; doi:<https://doi.org/10.1101/2021.06.03.446992>
• Preprint, open access
- [2] Aquillino, M., **Whyte-Fagundes, P.**, Lukewich, M., Zhang, L., Bardakjian, B., Zoidl, G., Carlen, P. (2020). Pannexin-1 deficiency decreases epileptic activity in mice. *International Journal of Molecular Sciences*. <https://doi.org/10.3390/ijms21207510>
• Peer reviewed, open access
- [3] Safarian, N., **Whyte-Fagundes, P.**, Zoidl, C., Grigull, J., Zoidl, G. (2020) Visuomotor deficiency in *panx1a* knockout zebrafish is linked to dopaminergic signaling. *Scientific Reports*. <https://doi.org/10.1038/s41598-020-66378-y>
• Peer reviewed, open access
- [4] **Whyte-Fagundes, P.**, Siu, R., Brown, C., Zoidl, G. (2019). Pannexins in vision, hearing, olfaction and taste. *Neuroscience Letters*. <https://doi.org/10.1016/j.neulet.2017.05.010>.
• Peer reviewed
- [5] Aquilino, M*, **Whyte-Fagundes, P***, Zoidl, G., Carlen, P. (2019). Pannexin-1 channels in epilepsy. *Neuroscience Letters*. <https://doi.org/10.1016/j.neulet.2017.09.004>.
* **Denotes equal contributions**
• Peer reviewed
- [6] **Whyte-Fagundes, P.**, Kurtenbach, S., Zoidl, C., Shestopalov, V., Carlen, P., Zoidl, G. (2018). A potential compensatory role of Panx3 in the VNO of a Panx1 knockout mouse model. *Frontiers in molecular neuroscience*. doi: 10.3389/fnmol.2018.00135.
• Peer reviewed, open access
- [7] **Whyte-Fagundes, P.**, Zoidl, G. (2018). Mechanisms of pannexin1 channel gating and regulation. *BBA Biomembranes*. <https://doi.org/10.1016/j.bbamem.2017.07.009>.
• Peer reviewed

[8] Kurtenbach, S., **Whyte-Fagundes, P.**, Gelis, L., Kurtenbach, S., Brazil, E., Shestopalov, I., Hatt, H., Zoidl, G. (2014). Investigation of olfactory function in a Panx1 knock out mouse model. *Frontiers in Cellular Neuroscience*. <https://doi/10.3389/fncel.2014.00266>.

- Peer reviewed; open access

Presentations & Conferences

[1] **Whyte-Fagundes, P.**, Taskina, D., Saffarian, N., Zoidl, C., Donaldson, L., Carlen, P., Zoidl, G. (2021) Pannexin1 knockout zebrafish as a model for seizure investigation.

- This work was presented at: SfN Jan 13; international, oral presentation, selected by invitation, competitive.

[2] Taskina, D., **Whyte-Fagundes, P.**, Taskina, D., Saffarian, N., Zoidl, C., Carlen, P., Zoidl, G. (2020) Pannexin1 knockout zebrafish as a model for seizure investigation.

- This work was presented at: Neuromatch 3.0 Oct 26 – 30; international, oral presentation, selected by invitation, competitive.

[3] **Whyte-Fagundes, P.**, Taskina, D., Saffarian, N., Grigull, J., Zoidl, C., Carlen, P., Zoidl, G. (2019) Panx1 knockout fish as a model to investigate seizure activity.

- This work was presented at: The Zebrafish Precision Medicine Conference Sept 18-20; international, oral presentation, selected by invitation, competitive.

[4] **Whyte-Fagundes, P.**, Saffarian, N., Taskina, D., Zoidl, C., Carlen, P., Zoidl, G. (2019). Panx1 knockout fish as a model to investigate seizure activity using *in vivo* electrophysiology.

- This work was presented at: The International Gap Junction Conference July 27-31; international, research poster presentation, selected by invitation, competitive.

[5] **Whyte-Fagundes, P.**, Saffarian, N., Taskina, D., Zoidl, C., Carlen, P., Zoidl, G. (2019). Panx1 knockout fish as a model to investigate seizure activity.

- This work was presented at: Canadian Association of Neuroscience May 22-25; international, research poster presentation, selected by invitation, competitive.

[6] **Whyte-Fagundes, P.**, Saffarian, N., Taskina, D., Zoidl, C., Carlen, P., Zoidl, G. (2019). Panx1 knockout fish as a model to investigate seizure activity.

- This work was presented at: University Health Network: Krembil Research Day May 15; regional, oral presentation, selected by invitation, competitive.

[7] **Whyte-Fagundes, P.**, Zoidl, C., Carlen, P., Zoidl, G. (2018). Forebrain electrophysiological recording of seizure activity in genetically modified zebrafish larvae.

- This work was presented at: University Health Network: Krembil Research Day May 23; regional, oral presentation, selected by invitation, competitive.

[8] **Whyte-Fagundes, P.**, Zoidl, C., Carlen, P., Zoidl, G. (2018). Forebrain electrophysiological recording of seizure activity in genetically modified zebrafish larvae.

- This work was presented at: The Graduate Student Symposium; institutional, oral presentation, selected by invitation, competitive.

[9] **Whyte-Fagundes, P.**, Kurtenbach, S., Zoidl, C., Carlen, P., Zoidl, G. (2017). Pannexin3 compensates for pannexin1 in the vomeronasal organ of a knockout mouse model.

- This work was presented at: The International Gap Junction Conference; international, research poster presentation, selected by invitation, competitive.

[10] **Whyte-Fagundes, P.**, Kurtenbach, S., Zoidl, C., Carlen, P., Zoidl, G. (2017). Pannexin3 compensates for pannexin1 in the vomeronasal organ of a knockout mouse model.

- This work was presented at: University Health Network: Krembil Research Day; regional, oral presentation, selected by invitation, competitive.

[11] **Whyte-Fagundes, P.**, Kurtenbach, S., Zoidl, C., Carlen, P., Zoidl, G. (2017). Pannexin3 compensates for pannexin1 in the vomeronasal organ of a knockout mouse model.

- This work was presented at: York University 43rd Biology Symposium: From Micro to Macro; institutional, research poster presentation, selected by invitation, competitive.

[12] **Whyte-Fagundes, P.**, Kurtenbach, S., Zoidl, G. (2016). Panx channel expression and function in the olfactory system of a knock out panx1 mouse.

- This work was presented at: The Canadian Association of Neuroscience; regional, research poster presentation, selected by invitation, competitive.

[13] **Whyte-Fagundes, P.**, Kurtenbach, S., Zoidl, G. (2016). Panx channel expression and function in the olfactory system of a knock out panx1 mouse.

- This work was presented at: York University 42nd Biology Symposium: Science and Society; institutional, research poster presentation, selected by invitation, competitive.

[14] **Whyte-Fagundes, P.**, Kurtenbach, S., Zoidl, G. (2016). Panx channel expression and function in the olfactory system of a knock out panx1 mouse.

- This work was presented at: York University Biology Day; institutional, research poster presentation, selected by invitation, competitive.

[15] **Whyte-Fagundes, P.**, Zoidl, G. (2015). Decoding Gating Properties of the Panx1 Channel: pH sensitivity and the potential role in health and disease.

- This work was presented at: The Graduate Student Symposium; institutional, oral presentation, selected by invitation.

[16] **Whyte-Fagundes, P.**, Zoidl, G. (2015). Decoding Gating Properties of the Panx1 Channel: pH sensitivity and the potential role in health and disease.

- This work was presented at: Neuroscience Association at York Symposium; institutional, oral presentation, selected by invitation, competitive.